Magnesium alloy for next generation of biologically-informed biodegradable orthopaedic implants

Magnesium alloy for next generation of biologically-informed biodegradable orthopaedic implants

by

Diana Maradze

A thesis submitted to
Loughborough University
for the degree of

DOCTOR OF PHILOSOPHY

Centre of Biological Engineering
Department of Mechanical and Manufacturing Engineering
Loughborough University
November 2017

Abstract

Although magnesium alloys have been explored intensively for application as biodegradable metal implants, there is lack of understanding of the biological response to its corrosion products and the correlation between corrosion behaviour and local tissue repair process at the implantation site. The aim of the study was to develop a reliable *in vitro* testing method for biodegradable implants that closely emulates the *in vivo* environment and to investigate the response of mesenchymal stem cells, osteoclasts, skeletal muscle cells and monocytes to both soluble (Mg ions) and insoluble (corrosion granule) corrosion products. This study has revealed that the presence of the corrosion products significantly altered the cells' metabolic and proliferative activities. This influence on metabolic activities also affected cell fusion/differentiation. A high Mg^{2+} concentration was shown to indirectly inhibit bone healing by interfering with the differentiation process of MSCs. Osteoclastogenesis and myotube formation was significantly affected by the presence of high Mg corrosion products, it was shown that a high Mg^{2+} concentration was required for accelerating cell proliferation but the availability of Ca^{2+} was crucial for cell fusion. The effect of Mg corrosion products varied depending on the state of differentiation of cells, concentration and length of exposure. Cells tolerated the presence of Mg concentration higher than the physiological range; however concentrations below 10mM were beneficial for cell growth. The outcomes of this study on the biological response of cells involved in bone regeneration to the corrosion behaviour of Mg biomaterials are important as they can be used to inform standardisation of regulatory requirements for the testing of biodegradable materials to reduce the discrepancies seen between *in vitro* and *in vivo* studies.

Acknowledgements

Firstly, I would like to give all my gratitude to God; to him I owe everything, for without his love and grace nothing would have been possible.

I would like to thank my supervisors Yang Liu and Mark Lewis for guiding me through this journey. To Yang, thank you for supporting me through throughout my doctoral training and for opening doors for me to experience new opportunities. I also want to thank everyone from the CBE and Doctoral Training Centre for their support and for the opportunity to pursue my doctoral training. I would also like to take this opportunity to acknowledge the Engineering and Physical Sciences Research Council (EPSRC) for funding this research.

Lastly I would like to thank my family and friends for supporting me, and encouraging me throughout this journey. Specifically, I would like to thank my mother, Ruth Nyamadzawo for her love, guidance, sacrifice and for being a blessing; no words can express my gratitude. To my dearest Clive Chibaya thank you for believing in me, for always being there and for being a great support system.

Table of Contents

List of Figures

List of Tables

List of Abbreviations

ALP	Alkaline phosphatase
ARS	Alizarin red S
BMP	Bone morphogenic protein
cDNA	Complementary DNA
Cbfa1	Transcription factor
Ca^{2+}	Calcium
COL1	Collagen type 1
CO_2	Carbon dioxide
ΔΔCt	Comparative Ct method
Ct-	Cycle-threshold
cST	Salmon calcitonin
DC-STAMP	Dendrocyte expressed seven transmembrane protein
DDSA	Dodecenyl Succinic Anhydride
DNA	Deoxyribonucleic acid
DMEM	Dulbecco's Modified Eagle Medium
ECM	Extracellular matrix
EDX	Energy dispersive X-ray
ER	Endoplasmic reticulum
FGF	Fibroblast growth factor
FBS	Foetal bovine serum
GAPDH	Glyceraldehyde-3-phosphate-dehydrogenase
HA	Hydroxyapatite

HCL	Hydrochloric acid
HESCs	Human embryonic stem cells
HMSCs	Human mesenchymal stem cells
ICP-OES	Inductively coupled plasma optical emission spectrometry
IL	Interleukin
IGF	Insulin-like growth factor
LIF	Leukaemia inhibitory factor
MCSF	Macrophage colony stimulating factor
MEM	Minimum essential medium
MIDAS	Metal ion dependent adhesion sites
Mg^{2+}	Magnesium ion
MMP	Matrix metalloproteinase
mRNA	Messenger ribonucleic acid
MuRF1	Muscle RING-finger protein-1
MO	Mature osteoclast
NFATc-1	Nuclear factor of activated T-cells 1
OC	Osteocalcin
OPG	Osteoprotegerin
PDGF	Platelet-derived growth factor
PBS	Phosphate buffered saline
PCL	Poly-caprolactone
PCR	Polymerase chain reaction
PLA	Polylactic acid

PNP	P-nitrophenol
RAW	Cell line murine macrophage from blood
RLT buffer	Lysis buffer
RPE buffer	Lysis buffer
SBF	Simulated body fluid
TBS	Tris-buffered saline
TEM	Transmission electron microscopy
THP-1	Human monocytic cell line
TNF	Tumour necrosis factor
TRAP	Tartrate-resistant acid phosphatase
TGF	Transforming growth factor
UV	Ultra-violet
VEGF	Vascular endothelial growth factor
Y	Yttrium
qRT- PCR	Quantitative real time PCR
RE	Rare earth
RNA	Ribonucleic acid
RPMI	Roswell Park Memorial Institute
SERCA2	Sarcoplasmic/endoplasmic reticulum calcium ATPase 2
SLC20a1	Solute carrier family 20 phosphate transporter, member 1
Zn	Zinc
Zr	Zirconium

CHAPTER 1: Introduction and Literature Review

1.1. Introduction

The main cause of physical disability in the United States (2005) was largely contributed by the 15 million diagnoses of musculoskeletal disorders and trauma-related injuries. The cost of treating these conditions has been estimated to be around $127 billion US dollars (Woolf & Pfleger, 2003). Current treatment modalities for musculoskeletal conditions include the use of metallic biomaterials, bio-resorbable ceramics and biodegradable polymers. However, there are limiting factors associated with these methods that render them inadequate for orthopaedic applications. Currently approved metallic biomaterials include stainless steel and titanium based alloys. Limitations of using these materials include possible release of toxic wear particles to the surrounding tissues. The elastic moduli of these metals are not matched with that of bone, leading to stress shielding effects and ultimately end in reduction of bone formation and remodelling (Staiger *et al*., 2006). Stress shielding refers to the reduction in bone density caused by an implant bearing part of the stress load, subjecting bone to reduced stress. Under normal conditions healthy bone remodels in response to its bearing load. Furthermore, the use of inert materials requires a second surgery resulting in pain and increased cost for the patients. Biodegradable polymers such as polylactic acid (PLA), poly-caprolactone (PCL) are used in clinics for different applications; however, they are not suitable for load bearing applications due to their low mechanical strength, wear and breakdown of the bulk material (Tan *et al.*, 2013).

1.1.1. Why Biodegradable Magnesium

Biodegradable magnesium has been shown to overcome the limitations associated with inert materials. Magnesium plays an important role in a number of biological functions: it is involved in bone and mineral homeostasis, (Beyenbach, 1990; Grubbs & Maguire, 1987; Saris et al., 2000) promotion of DNA replication and transcription (Beyenbach, 1990; Wacker & Parisi, 1968) and regulation of opening and closing of ion channels (Agus & Morad, 1991; Flatman, 1991; Romani & Scarpa, 2000). The normal physiological range of magnesium is between 0.8mM and 1.0mM, of which approximately 60-65% is stored in bone and homeostasis is maintained by the kidneys and intestines (Belluci *et al*., 2013). Magnesium metal has an elastic modulus closer to that of bone, and as such its use as biomaterial for orthopaedic implant reduces the likelihood of stress shielding (Table.1). As Mg corrodes *in vivo* it aids biological repair and simultaneously becomes less important as a constituent for mechanical support. Furthermore, magnesium is biocompatible, non-toxic and has been shown to enhance bone formation (Castellani *et al*., 2011).

Table.1-1. Mechanical properties of natural bone and biomaterials used in orthopaedic applications

Material	Compressive yield strength (Mpa)	Elastic modulus (Gpa)	Yield strength (Mpa)	Ultimate tensile strength (Mpa)	Density (g/cm^3)	References
Natural bone	164-240	5-23	105-114	35-283	1.8-2.0	(Kirkland et al., 2012)
Magnesium	40-140	5-45	19-100	66	1.74	(Zhao et al., 2017)
Mg-Ca alloy		40-50	130	239.63	1.70-1.80	(Kirkland, 2012)
Mg alloy (As-drawn AZ31)	105	55	202	268	1.78	(Rho et al., 1993)
Titanium alloy		114	760-1103	830-1172	4.4	(Witte et al., 2005)
Stainless steel		193	170-310	480-620	8.0	(Oyen et al., 2008)
PLA		1.9-2.4	15-75	29-35	1.26	(Witte et al., 2008)
						(Miyazaki et al., 1994)
						(Honget al., 2013)

1.1.2. Magnesium based orthopaedic implants: current status

There have been improvements in the development of novel Mg-based orthopaedic implants since the 19th century. Studies have been published showing the successful use of Mg-based implants in clinical trials (Windhagen *et al.,* 2013; D. Zhao *et al.,* 2016; Lee *et al.,* 2016). A randomized clinical trial by Zhao *et al* (2016) that used high purity Mg screws for fixing vascularized bone flaps during surgery for osteonecrosis of the femoral head revealed the following:

- The use of Mg screws resulted in a stable fixation on bone flaps.
- No adverse effects were reported following corrosion of Mg screws, indicating high biocompatibility.

- More neovascularisation was observed around the implantation site in the presence of Mg.
- No loosening and deformation of Mg screws was reported during the 12 month follow up period.

These high purity Mg screws have been named as an innovative medical device by the Chinese FDA (CFDA) in 2015 (D. Zhao et al., 2017). Another clinical study (J.-W. Lee et al., 2016) using Mg-Ca-Zn alloy screws for hand and wrist fractures reported that patients were able to heal without any signs of pain and discomfort. The findings from this study have contributed to the approval of Mg-Ca-Zn screws for clinical use by the Korea Food and Drug Administration (KFDA) in 2015 (D. Zhao et al., 2017). Windhagen et al., 2013 reported good clinical and radiographic outcomes with no adverse effects when magnesium-yitrium-rare earth-zirconium (Mg-Y-RE-Zr) screws were used in hallux valgus surgery. Data from this clinical trial led to the approval of Mg-Y-RE-Zr as a medical device in 2013 and has since been used for the treatment of Madelung deformity and scaphoid fractures (D. Zhao et al., 2017).

1.2. Corrosion mechanism of magnesium

During fracture healing the biomaterial implant should have the ability to sustain mechanical strength until the formation of new bone bridges the gap of the fracture. For this to happen, the biodegradable material should degrade gradually to allow for tissue implant integration. Pure magnesium has a high corrosion rate in the physiological environment, thereby limiting its use in load bearing applications. It is therefore important to understand the changes in mechanical properties of magnesium metal during the corrosion process.

Exposure of materials to certain environments and interaction with that environment can lead to the deterioration of the mechanical properties of the material. In metals, the deterioration results in material loss through corrosion (Callister & Rethwisch, 2010). When magnesium is exposed to the environment, the metal goes through physical and chemical changes. While there are different types of corrosion, the focus is going to be on galvanic and localized corrosion. When magnesium is exposed to the environment a partially protective film protects the surface of magnesium from corrosion. Magnesium and magnesium alloys degrade in aqueous environment via an electrochemical reaction releasing hydrogen gas (H_2) and magnesium hydroxide ($Mg(OH)_2$) (Eq. 1). The overall reaction also includes partial reactions (Eq. 2, 3 and 4). The standard electrode potential (E_p) of magnesium is -2.37V, and this represents the driving force for the electrochemical oxidation-reduction reaction (Gu & Zheng, 2010).

Overall reaction

$$Mg + 2H_2O \rightarrow Mg(OH)_2 + H_2 \quad (1)$$

Partial reactions

$$Mg \rightarrow Mg^{2+} + 2e^- \text{ (Anodic reaction)} \quad (2)$$

$$2H_2O + 2e^- \rightarrow H_2 + 2OH^- \text{ (Cathodic reaction)} \quad (3)$$

Precipitation reaction

$$Mg^{2+} + 2OH^- \rightarrow Mg(OH)_2 \text{ (Corrosion product)} \quad (4)$$

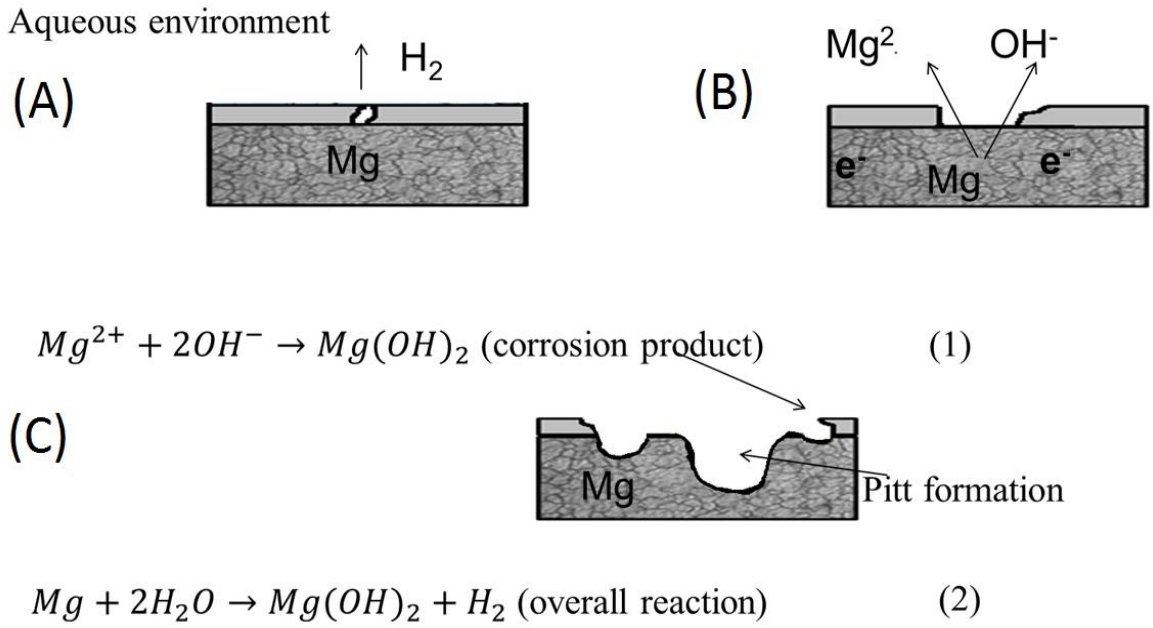

(Adapted from Song & Atrens, 2003)

Fig.1-1. Corrosion of magnesium. (**A**) Magnesium corrosion is initiated when magnesium is exposed to aqueous environment. Corrosion starts from the surface, hydrogen gas is released and a corrosion layer is formed. (**B**) Mg^{2+} are released into the surrounding environment and OH^- is formed leading to increase in pH in the surrounding environment, this increase in pH favours the formation of Mg $(OH)_2$. The corrosion layer acts to slow down the corrosion process but at a potential above the Ep, corrosion layer becomes partially protective, exposing the magnesium metal to the aqueous environment. (**C**) Pitting corrosion is initiated which eventually leads to the destruction of magnesium metal (Song & Atrens, 2003).

1.2.1. Localized corrosion

The corrosion of single-phase magnesium in immersed conditions begins as localised corrosion. Pitting is a form of localised corrosion that results in the formation of irregular pits (Fig.1-1). The pit formation starts from the top of a horizontal surface and continues downward in a vertical direction. During pitting, corrosion oxidation occurs within the pit, with complementary reduction occurring on the top surface (Song & Atrens, 1999). Gravity then pulls the pits downward as the pits growth progresses covering the surface of the metal. The release of hydrogen gas and OH^- ions results in an increase in pH in the surrounding environment. This increase in pH stabilises the hydroxide layer thus preventing further corrosion. Localised corrosion eventually leads to the undermining and falling out of magnesium particles. Polishing surfaces of metals allows them to have a better resistance to pitting corrosion (Song & Atrens, 1999).

1.2.2. Galvanic corrosion

Poor resistance to corrosion in magnesium alloys is enhanced by the presence of second phases or impurities. During galvanic corrosion, there is extensive localised corrosion of magnesium that is adjacent to a cathode. The impurities act as internal cathodes in the corroding media, forming micro-cells with the anodic magnesium matrix (Song & Atrens, 1999). Other metals such as nickel and iron can act as external cathodes when in close contact with magnesium, resulting in severe galvanic corrosion. A number of factors increase the galvanic corrosion rate for example: high potential difference between anode and cathode and medium with high conductivity (Song & Atrens, 1999).

1.3. Effect of environment on magnesium corrosion

When magnesium is immersed in an aqueous solution a number factors affect the corrosion rate. These factors include: volume of the medium, composition of the medium, pH, humidity, flow rate, temperature, microstructure and production process. The reaction of magnesium with water results in the formation of a protective insoluble film of magnesium hydroxide at pH above 10.5 (Song & Atrens, 2003). High concentrations of chloride ions increase the corrosion rate of magnesium in neutral aqueous solutions. The magnesium hydroxide layer is not very stable and the presence of chloride ions leads to the breakdown of the protective layer and pitting corrosion. Nitrates, phosphates and sulphates attack magnesium but to a lesser extent than chloride ions (Song & Atrens, 2003). With respect to humidity, the rate of corrosion is very low at low humidity but increases significantly above a relative humidity of 90% (Song & Atrens, 2003). The higher the temperature the higher the corrosion rate and this effect is more pronounced in magnesium alloy compared to pure magnesium. This is because high temperatures increase the activity of impurities in the magnesium alloy. High flow rate or agitation results in high corrosion rate because these conditions can destroy or prevent formation of the protective layer (Song & Atrens, 2003).

1.4. Magnesium alloy used as orthopaedic implants

Studies have shown the addition of alloying elements to pure magnesium improves the mechanical properties of magnesium. Some of the alloying elements that have been studied for magnesium-based implants are aluminium, zinc, calcium and yttrium. Alloying with elements such as lithium results in better mechanical strength and slower corrosion rate compared to alloying with calcium. However these elements have been found to be toxic to

biological tissue especially at high concentrations (Feyerabend et al., 2010; Krause et al., 2010). Therefore, a compromise between the strength of the alloying elements and the cytotoxic effects should be considered in order to have a clinically safe and stable alloy. Zinc and calcium are well tolerated by the body; they are essential minerals that play important roles in the body. Zinc plays numerous roles in cellular metabolism; it supports the immune system and is required for DNA synthesis. Calcium is a structural component in bone and is involved in cell signalling (Ilich & Kerstetter, 2000). Furthermore calcium can improve mechanical properties by acting as a grain refining agent. Grain refining results in the formation of fine, uniform and equiaxed grain structure, leading to the formation of more boundaries and hence grain boundary strengthening (Feyerabend et al., 2010). Furthermore it decreases corrosion rate in trace amounts (Feyerabend et al., 2010).

1.4.1. Magnesium-zinc-zirconium alloys (Mg-Zn-Zr)

Adding alloying elements such as zinc (4%) and zirconium (0.5%) in small amounts to pure magnesium results in the improvement of mechanical properties such as increased Young's modulus and ultimate strength. The improvement in mechanical properties can be attributed to the strong refinement efficacy of zirconium (Hong *et al.*, 2013). *In vitro* studies using Mg-Zn-Zr alloy showed that the alloy was stable in physiological environment and positively influenced cell viability of a murine osteoblast-like cell line when compared to pure magnesium. In addition implantation of the alloy in mice showed no adverse effects (Hong *et al.*, 2013). Surface coating can be used as a method to improve corrosion resistance. Studies have shown that the coating of Mg-Zn-Zr alloy with hydroxyapatite results in better corrosion resistance compared to uncoated alloy (Lu et al., 2012). Hydroxyapatite is used as a coating agent because it is a derivative of calcium phosphate; it is non-toxic and has similar chemical

properties to natural bone. Hydroxyapatite coating can decrease corrosion rate of Mg by slowing down the diffusion of water to the surface of magnesium, which in turn improves implant stability by slowing down pitting corrosion (Guan *et al.*, 2012; Iskandar *et al*., 2013). Hydroxyapatite has also been shown to have osteo-conductive properties (B. Wang, Gao, Wang, Zhu, & Guan, 2012).

1.4.2. Magnesium-zinc-calcium (Mg-Zn-Ca) alloys

As mentioned earlier, corrosion of pure magnesium in physiological conditions results in the formation of magnesium hydroxide. However, it has been noted that the corrosion of Mg-Zn-Ca alloy results in the formation of an extra product, zinc hydroxide. The formation of both magnesium hydroxide and zinc hydroxide results in improved corrosion resistance (X. Gu et al., 2010). Furthermore the use of magnesium-bulk metallic glasses has been reported to have superior mechanical properties and better corrosion potential (Cao *et al*., 2012) when compared to crystalline magnesium.

Studies using Mg-Zn-Ca bulk metallic glasses have reported better corrosion resistance, slower rate of release of magnesium ions into the media, reduced hydrogen evolution and improved biocompatibility (Zberg *et al*., 2009; Gu *et al.*, 2010; Cao *et al.*, 2012). This is due to their single phase, homogenous microstructure and lack of impurities/second phases; and therefore not susceptible to galvanic corrosion (Gebert *et al.*, 2001; Song & Atrens, 2003; Scully, Gebert & Payer, 2007; Gu *et al.*, 2010). Moreover, the elastic modulus of Mg-Zn-Ca bulk metallic glass is closer to that of bone compared to other Mg alloys (Song & Atrens, 2003; Gu *et al*., 2010). Gu et al., 2010 have shown that murine fibroblast cells were able to attach and proliferate on the surface of Mg-Zn-Ca bulk metallic samples, and cell viability was improved when compared to pure crystalline magnesium. However, another study (Cao et al.,

2012) showed that culture of fibroblast cells in direct contact with the Mg-Zn-Ca bulk metallic glass resulted in areas of minimal cell growth and no cell attachment was observed. Even though Mg-Zn-Ca had a lower corrosion rate, cell viability was lower compared to pure crystalline magnesium. Gu *et al*., 2010 performed both direct and indirect cytotoxicity assays and found that cell viability obtained in the indirect assay was higher than that obtained in the direct assay. The reduction in cell viability in the direct cell assay could be attributed to the fluctuating environment caused by the corrosion process resulting in hydrogen evolution, pH changes and release of corrosion products. The effect of these factors would be enhanced when cells are cultured directly onto the magnesium alloy sample. No significant difference in ion concentration and pH changes from the indirect and direct assay was detected. Another study using a sensitive model of human embryonic stem cells (hESCs) showed that alkaline media (pH 8.1) and Mg ion concentration below 10mM had no adverse effects on cell viability and morphology (Nguyen *et al*., 2013). Therefore, hydrogen gas evolution could be the major factor responsible for reduced cell viability in direct contact tests. It has been suggested (X. Gu et al., 2010) that the evolution of hydrogen from the surface of sample could disrupt cell adhesion and growth.

1.4.3. Magnesium-calcium (Mg-Ca) alloy

The addition of calcium to magnesium results in the formation of second phases (Mg_2Ca). The amount of the Mg_2Ca phases present controls the mechanical properties and corrosion behaviour of Mg-Ca alloys (Wan et al., 2008). The higher the calcium content, the higher the amount of Mg_2Ca phase. High amounts of the Mg_2Ca phase results in the reduction in compressive strength, bending strengths and corrosion resistance (Wan et al., 2008). The optimum amount of calcium in magnesium-calcium alloys should be between 0.6-1% (Wan *et*

al., 2008; Li *et al.*, 2008). Wan et al., 2008 reported enhanced mechanical properties and better corrosion resistance when using Mg-0.6%Ca alloy. Furthermore the modulus (15.4) and bending strength (143.4MPa) of Mg-0.6%Ca was comparable to that of bone (17.5 and 180MPa respectively) (Wan et al., 2008).

Li et al., 2008 have also shown that the use of calcium content at 1% improved ultimate tensile strength, corrosion resistance and enhanced bone formation. Mg-1%Ca alloy promoted cell growth in an *in vitro* study and it is thought that the release of Mg ions increases cell viability through the stimulation of integrin-mediated osteoblast response (Zreiqat et al., 2002). Furthermore, magnesium is required for calcium incorporation into the bone (Serre et al., 1998), therefore the co-release of magnesium and calcium might be beneficial for bone formation and healing. Magnesium has been reported to have a direct effect on cellular function; acting as a mitogenic factor for osteoblast cells in culture. Moreover, the restriction of magnesium concentration in *in vitro* culture resulted in inhibition of cell growth and bone formation (Belluci et al., 2013). Li *et al*., 2008 reported that the implantation of Mg-1%Ca alloy facilitated bone formation *in vivo*, whilst there was no evidence of bone formation with the control sample (titanium).

1.4.4. Magnesium-yttrium (Mg-Y) alloy

Addition of yttrium to magnesium has both corrosion promoting and inhibiting activities depending on the environment (Johnson & Liu 2013; Johnson *et al.*, 2012). Like any other alloying element, yttrium is used because it enhances the mechanical properties of magnesium alloys (Aghion *et al.*, 2008; Zhang *et al.*, 2009; Johnson & Liu, 2013). When Mg-Y alloy is exposed to physiological environment, yttrium migrates to the surface of the alloy to be oxidised resulting in the formation of yttrium-oxide (Hänzi *et al.*, 2009; Gunde *et al.*, 2010;

Johnson & Liu, 2013). The presence of yttrium oxide in the corrosion layer slows down corrosion, but when the layer becomes unstable yttrium promotes micro-galvanic corrosion (Hänzi *et al.*, 2009; Johnson & Liu, 2013). The study by Johnson & Liu 2013 revealed the following:

- Polishing of Mg surfaces did not influence corrosion behaviour.
- Addition of yttrium promoted corrosion of magnesium in water regardless of surface treatment.
- When Mg-Y alloy was immersed in phosphate buffered saline, the presence of yttrium temporary inhibited corrosion only when metallic layer was present. In contrast when oxide layer was present yttrium promoted corrosion in phosphate buffered saline.

The oxide layer is rich in oxygen which makes the surface vulnerable to ions and furthermore rough surfaces reduce the effectiveness of passivation and encourage surface pitting (Johnson *et al*., 2012). Conclusions to be drawn from the study by Johnson *et al*., 2012 are: environment, alloy composition, microstructure and the interaction of these factors influence the corrosion behaviour of magnesium. Secondly, corrosion medium has a vital role in the corrosion of Mg than surface conditions (polished vs oxidised surfaces). In agreement with Johnson *et al*., 2013, a study by Lui *et al*., 2011 also revealed the following:

- Even though oxidised and polished Mg surfaces had different morphology, topography and composition they did not affect cell adhesion properties.
- Effect on cell adhesion on polished and oxidised surfaces was only seen when yttrium was added to magnesium.

- Polished Mg-Y surfaces allowed for better cell attachment compared to Mg-Y oxidised surface.

- Exposure of both surfaces to biological ions and proteins resulted in surface pitting corrosion.

The studies above show important factors for consideration when designing magnesium-based implants for load bearing applications.

1.5. Bridging *in vitro* and *in vivo* studies

While studies look at the degradation behaviour of magnesium in static conditions, this is not a true reflection of the degradation behaviour of magnesium *in vivo*. The ultimate goal is to use magnesium based alloys as implants in the body to aid the healing process of bone. *In vivo* the implant would be subjected to compressive stress, bending stress and fluid flow. These factors also contribute to the degradation rate of Mg alloys. Compressive stress can change the degradation behaviour of magnesium by initiating the propagation of microcracks, removing any protective layers present and allowing for continuous corrosion (B. Wang et al., 2012). Shear stress also contributes to the corrosion behaviour of magnesium alloys, magnesium alloys degrade rapidly in a dynamic environment compared to a static environment (Chen et al., 2010).

Studies have shown that the surface morphology and composition of magnesium samples in *in vivo* corrosion differ from those seen in *in vitro* corrosion, suggesting different corrosion behaviour of the magnesium alloys in the two environments (S. Zhang et al., 2010). *In vivo* corrosion showed high levels of nitrogen suggesting the adherence of cells and proteins on the alloy might have influenced corrosion (S. Zhang et al., 2010). In addition, the corrosion

rate of magnesium alloys in contact with blood vessel and body fluids is higher compared to implants located in cortical bone (Erdmann et al., 2011; Huehnerschulte et al., 2011; von der Höh et al., 2009).

Li *et al*., 2008 reported a much faster corrosion rate of Mg-Ca alloy implant in *in vitro* electrochemical test compared to that observed *in vivo*. Also high activity of osteoblasts was observed around the Mg-Ca alloy pin *in vivo*, but still an unfilled void was left at implantation site when the Mg pin was totally degraded at the end of 3months (Li *et al.*, 2008). Thus, there is a lack of correlation of *in vitro* and *in vivo* corrosion and, of an understanding of the effects of Mg corrosion products on stem cells responsible for bone tissue regeneration. It is also of interest to understand the response of immune cells to Mg alloys. A study (Erdmann et al., 2010) looking at the host's reaction to Mg-Ca implant showed that inflammatory host reaction was only seen during times of intense corrosion; however, the response was not severe. Humoral immune response was detected for Mg-Ca implant indicating the presents of soluble antigens such as the wear products of the corrosion process (Erdmann et al., 2010). The production of hydrogen gas resulted in the formation of cavities within the peri-implant fibrous tissue, but did not influence the extent of host response (Erdmann et al., 2010).

It is important to understand the consequences of implanting Mg and Mg alloys in the body. The reaction of magnesium in physiological environment results in high pH, hydrogen evolution and release of corrosion products; this environment has a profound effect on cells. Magnesium alloys reviewed in this report have been shown to be biocompatible, but *in vivo* studies reveal that the corrosion environment may affect local cells and therefore hinder total regeneration of bone tissue. It is therefore important to understand the effect of both soluble

(Mg^{2+}) and insoluble (corrosion granule) corrosion products on the cells involved in bone regeneration.

1.6. Bone structure and organization

Bone is a highly vascularised connective tissue that can be classified based on anatomy and structure. The bone is composed of long bones (e.g. femur, tibia, and humerus), short bones (e.g. sesamoid bone, carpal bone), irregular bones (e.g. vertebrae, sacrum) and flat bones (e.g. skull, shoulder blade, hip bone). The structure of bone can be divided into three levels; macroscopic (cortical, trabecular bone), microscopic (lamella, osteons) and nanostructure (collagen fibrils, bone crystals) (Rho *et al.*, 1998; Kalb *et al.*, 2013). Fig.1-2 shows the hierarchical structural organization of bone.

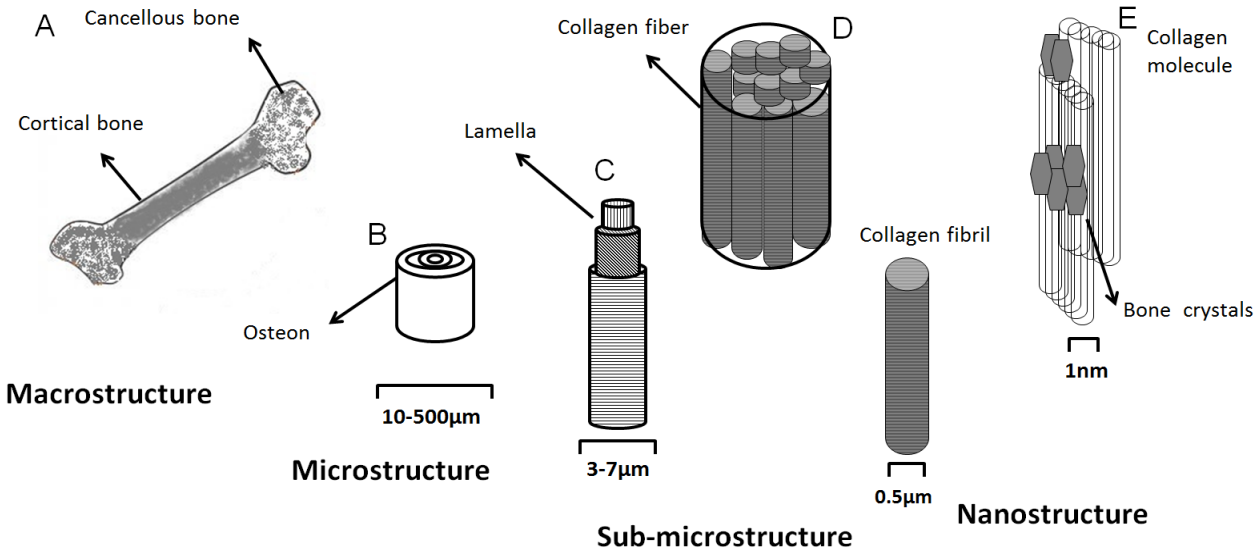

(Adapted from Rho et al, 1998)

Fig.1-2. Hierarchical structural organization of bone (**A**) cortical and cancellous bone, (**B**) osteon, (**C**) lamella, (**D**) collagen fibre, (**E**) bone mineral crystals and collagen molecules (Rho *et al.*, 1998)**.**

1.7. Macroscopic level

1.7.1. Cortical bone

Cortical bone is located at the outer structure of bone and accounts for 80% of bone mass. It has high density, high Young's modulus, low porosity and is highly mineralised (Brown *et al*., 2013). Cortical bone is highly organized and is made up of concentric osteons or Harversian systems separated by interstitial lamellae (Bayliss *et al*., 2012). Blood supply to osteons is through the Harversian canal and the Volkmann canals connect the osteons and supplies blood between them (Rho et al., 1998; Rao & Stegemann, 2013).

1.7.2. Trabecular bone

Trabecular bone (also known as spongy or cancellous bone) is located in the inner core of the bone and accounts for 20% of bone mass. It is highly porous (80%), highly elastic, has low density and low Young's modulus. It has a high turnover rate to allow for bone remodelling. It has a high surface area for homeostatic function and metabolic regulation (Brown et al., 2013). The structure is irregular, consisting of struts (trabeculae) arranged in a loose network. Red and yellow bone marrow is located in the pores within the centre of the trabecular bone (Kalb *et al.*, 2013). The red marrow is vascularised and provides nutrients to the bone; it is also a source of hematopoietic progenitor cells and mesenchymal stem cells (Rao & Stegemann, 2013).

1.8. Microstructure and Nanostructure

The lamellae are formed of mineralized collagen fibres, which wrap around the Haversian canal in concentric layers thereby forming the Harversian system or osteon. The fibres within

the lamellae are arranged in a parallel formation, with fibre orientation alternating from one lamella to another (Rho et al., 1998). At nanostructure level, collagen fibrils have bone crystals embedded within their structure.

Osteoblasts synthesize and deposit type 1 collagen in two forms, woven and lamellar, and thus both cortical and trabecular bone is formed from woven and lamellar bone (Doblaré *et al*., 2004). In an environment where there is no pre-existing bone matrix, osteoblasts secrete collagen fibrils to form a woven matrix. Woven bone is associated with bone formation in foetal, neonatal, early bone healing process and pathological states (osteogenesis imperfecta). Woven bone is structurally weak and its main purpose is to serve as a template for stronger lamellar bone. Once sufficiently woven bone has been deposited, osteoblasts deposit new matrix in lamellar orientation (Rho *et al*., 1998).

1.9. Anatomic level: long bones and flat bones

There are three regions in long bones, namely the diaphysis, metaphysis and epiphysis. The diaphysis is a hollow shaft composed of cortical bone. The metaphysis is a thin cortical layer between epiphysis and diaphysis. The epiphyseal region is located at the ends of the bone that forms the articular surface. The epiphysis and metaphysis are composed of trabecular bone surrounded by a thin layer of cortical bone (Rho *et al*., 1998). The periosteum covers the bone surface and is divided into a fibrous outer layer and inner cellular layer, which houses mesenchymal stem cells. The endosteum (mature osteoblast as lining cells) covers endocortical and trabecular surfaces, thereby enclosing the marrow (Weatherholt *et al*., 2012). Flat bones are made of thick cortical layers on the outside and thin trabecular bone

between the layers. In some cases the bone structure is composed of just cortical bone (Rho *et al*., 1998).

1.10. Bone Extracellular Matrix (ECM)

1.10.1. Organic matrix

Bone is made up of one third organic matrix, and two thirds mineralized matrix. Mineralized matrix provides strength to the bone and the organic matrix provides flexibility and elasticity (Clarke, 2008).

The organic matrix is 95% type 1 collagen structured in the form of a triple helix consisting of three alpha chains twisted together to give bone strength and stability (Bayliss *et al*., 2012; Kalb *et al.*, 2013). The remainder of the organic matrix consists of proteoglycans, glycoproteins, matrix proteins (osteocalcin, osteonectin, ostepontin), collagen 5, cytokines and growth factors (Rho *et al*., 1998; Bayliss *et al*., 2012; Newman *et al.*, 2013). Proteoglycans bind sulphate and uronic acid on binding sites throughout the matrix (Newman et al., 2013). Hyaluronan, chondroitin-sulphate, biglycan and decorin are proteoglycan molecules involved in different stages of bone formation. Glycoproteins attach to chemical mediators and are involved in cell adhesion, signalling and matrix organization (Newman et al., 2013). Fibronectin is a member of the glycoprotein family and is involved in the binding of integrin proteins with the matrix allowing for cell communication. Interaction between cells and the matrix is important in that the matrix provides an environment for the cells to attach and grow, whilst the cells releases proteins that build, degrade and remodel the ECM (Newman et al., 2013). Matrix proteins promote mineralization; osteocalcin (OC) is the most abundant non-collagen protein, accounts for 15% of the total proteins and is used as a bone biomarker

(Fernandez-Tresguerres-Hernandez-Gil et al., 2006). OC is produced by mature osteoblasts and requires vitamin K for its synthesis (Fernandez-Tresguerres-Hernandez-Gil et al., 2006). Osteonectin is produced by osteoblasts and platelets; it has affinity for calcium, collagen type 1 and hydroxyapatite. Osteonectin also plays a role in regulating cellular adhesion on matrix and organizing mineral in the matrix. Alkaline phosphatase (ALP) provides inorganic phosphates (Orimo, 2010). Glycoproteins such as osteopontin, bone sialoprotein, fibronectin and thrombospondin act as surface receptors, allowing binding of cells to matrix and are involved in bone regeneration (Rho et al., 1998; Fernandez-Tresguerres-Hernandez-Gil *et al.*, 2006). Growth factors and cytokines such as BMPs, IGF, TGF-β, are involved in cell differentiation and proliferation of bone cells (Rao & Stegemann, 2013).

1.10.2. Mineralised matrix

The inorganic component of the matrix (accounting for two thirds of the matrix) consists of calcium phosphates in the form of hydroxyapatite crystals (Fernandez-Tresguerres-Hernandez-Gil et al., 2006). This mineralised matrix is reactive and soluble. It provides compressive strength to bone and allows for bone remodelling and turnover, releasing essential ions into the blood system. Bone is a reservoir for ions such as calcium which is an essential component in bone metabolism and homeostatic regulation (Rao & Stegemann, 2013).

1.11. Mechanical properties of bone

The properties of solid materials fall under six categories: mechanical, electrical, thermal, magnetic, optical and chemical. Materials have been grouped into three categories: metals, ceramics and polymers. In this section the focus is on mechanical properties of bone material.

Mechanical properties relate to the deformation of a material in response to applied force or load, and a stress-strain curve is used to illustrate this relationship. The load could be compressive, tensile or shear stress. Hooke's law states that the degree to which a material deforms is dependent on the magnitude of stress imposed; this deformation where stress and strain are proportional is known as elastic deformation (Callister & Rethwisch, 2010). The slope of the stress-strain curve is equal to the Young's modulus/modulus of elasticity (Fig.1-3). The Young's modulus of elasticity represents the stiffness or material's resistance to elastic deformation whereby the higher the modulus the stiffer the material (Callister & Rethwisch, 2010). Elastic deformation is reversible; once the load is removed the material will revert back to its original shape. However, for most materials, beyond a certain stress level, the relationship between stress and strain becomes nonlinear. Deformation beyond this point (yield point) results in permanent deformation referred to as plastic deformation (Fig.1-3) (Callister & Rethwisch, 2010). The yield strength of a material is a measure of the material's resistance to plastic deformation. The ultimate tensile strength is the maximum stress that can be sustained by the material in tension; deformation is uniform until this point where subsequent deformation is confined to one point leading to fracture (Callister & Rethwisch, 2010). Ductility is the ability of the material to withstand plastic deformation without fracturing; a ductile material can change form without breaking, whereas a brittle material experiences very little plastic deformation before fracture. The ability of the material to absorb energy and plastically deform before fracture is known as fracture toughness; tough materials can resist fracture even in the presence of a crack (Callister & Rethwisch, 2010).

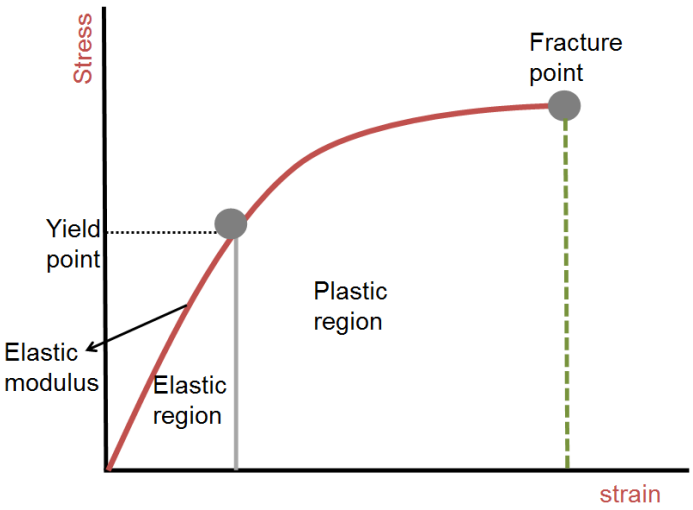

Fig.1-3. Stress-Strain curve of a typical metal alloy

Bone experiences high percentage of tensile strain compared to other strains, and is also weaker under tensile strain compared to compression (Currey, 2004; Rubin & Rubin, 2006). When bone is subjected to tensile strain beyond the yield point, it is pulled apart and cracks form along tension within the bone. The accumulation of damage is a normal response of composite materials to mechanical loading; the damage allows these materials to be tough. The formation of cracks in bone tissue provides a way for energy to be released. During loading, energy is transferred to the bone, and if the energy is above the level that bone can absorb, energy is released when the bone fractures (Ritchie, 2011). The composite anisotropic structure of bone (Fig.1-2) allows bone to be light weight but strong enough to withstand compressive, tensile, bending and torsional stress (Rubin & Rubin, 2006). By design, the microstructure of bone provides optimal toughness. Mineralization of collagen fibrils gives bone the ability to resist plastic deformation, increase fracture strength and a high Young's modulus (Buehler, 2007). Orientation of the collagen between adjacent lamellae can rotate up to 90° to allow tissue to resist forces and moments from different directions (Rubin &

Rubin, 2006). Collagen fibrils dissipate energy/yield by intermolecular slip allowing the mineralised collagen fibrils to tolerate cracks without causing macroscopic failure of bone (Buehler, 2007; Ritchie *et al*., 2009). Microstructure of bone influences fracture toughness through a number of mechanisms such as microcracking, crack bridging and crack deflection (Fig.1-4). Microcracking leads to extrinsic toughening where the crack tip is shielded by reducing stress intensity at or behind the crack tip (Nalla, Stolken, Kinney, & Ritchie, 2005). Furthermore, microcracks exist in healthy bone and are known to play a role in bone remodelling. It has been suggested that the presence of microcracks activates osteoclasts to remove damaged bone whilst osteoblasts form new bone (Herman, Cardoso, Majeska, Jepsen, & Schaffler, 2010). During crack deflection, the crack is deflected around osteons to move along the weak cement line (outer border of an osteon) (Yeni & Norman, 2000). Collagen fibrils also contribute to toughening by crack bridging (Nalla et al., 2005).

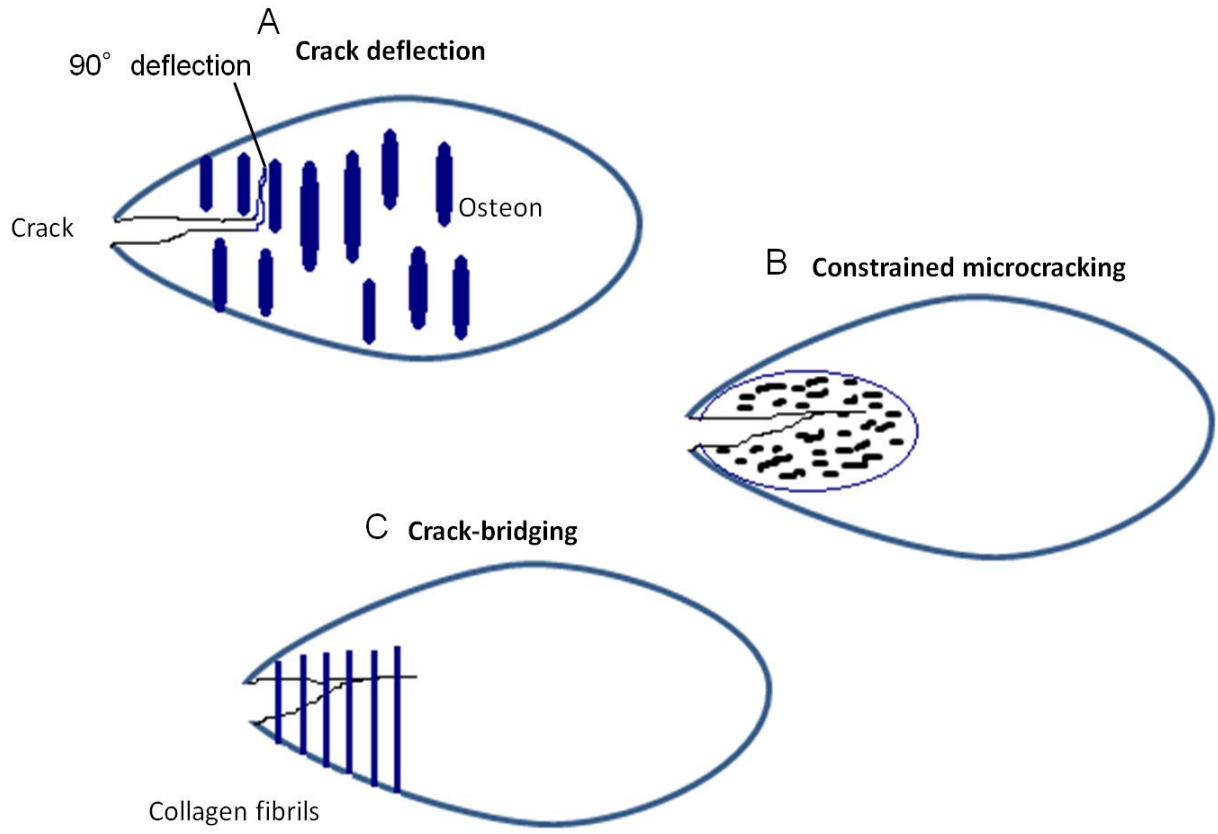

(Adapted from Ritchie et al., 2009)

Fig.1-4. Bone toughening mechanisms (**A)** The growth of a crack is deflected as it encounters an osteon. Crack growth is retarded as the crack deviates from direction of maximal tensile strength and moves along weak cement-line, thereby increasing bone toughness. (**B**) Microcracks cause dilation and compliance of the region surrounding the crack, which compresses the crack. (**C**) Collagen fibrils inhibit crack propagation by bridging the gap formed by the crack. The fibrils carry the load that would otherwise be used to propagate the crack (Ritchie *et al.*, 2009).

1.12. Bone development and bone healing

There are two stages of bone formation in the developing foetus; endochondral ossification (vertebrae) and intramembranous ossification (craniofacial skeleton). During intramembranous ossification mesenchymal stem cells (MSCs) can differentiate directly into osteoblast cells (Ortega *et al.*, 2004). Osteoblasts lay down organic matrix (collagen type1) on a pre-existing fibrous layer followed by mineralization resulting in trabecular bone formation (Kular, Tickner, Chim, & Xu, 2012). During endochondral ossification MSCs differentiate into cartilage that acts as a template for bone formation (Ortega *et al.*, 2004).

1.12.1. Embryonic Development

During embryonic development, MSCs differentiate into chondrocytes, forming a cartilaginous template (soft callus) similar to the structure of long bones (Gerber & Ferrara, 2000; Ortega *et al.*, 2004). The proliferative chondrocytes differentiate further into hypertrophic chondrocytes (Deschaseaux *et al*., 2009). ECM production by surrounding hypertrophic chondrocytes is calcified. Initial vascularization of the cartilage occurs concurrently with the hypertrophic differentiation of chondrocytes. The hypertrophic chondrocytes undergo apoptosis and woven bone is formed by osteoblasts (Ortega *et al*., 2004).

1.12.2. Postnatal Growth Development

Growth plate is formed between the diaphysis and epiphysis. The epiphyseal growth plate has several zones; namely the resting zone, the proliferative zone and the vascular ingrowth zone. Chondrocyte differentiation and matrix production results in the enlargement of cartilage. The enlargement of the cartilage allows for the bone to grow. The hypertrophic

chondrocytes direct mineralization of matrix and attract blood vessel formation through expression of vascular endothelial growth factor (VEGF). The newly formed blood vessels provide access for cells involved in the regulation of bone formation. Chondrocytes undergo apoptotic death and are replaced by osteoblasts (Gerber & Ferrara, 2000; Deschaseaux *et al*., 2009). At the end of puberty, growth plates regions of long bones cease to grow (Gerber & Ferrara, 2000). Hyaline cartilage remains on epiphyseal surfaces forming articular cartilage (Kular et al., 2012).

1.13. Cells involved in bone development

1.13.1. Osteoblast Cells

Osteoblasts are formed from mesenchymal mono-nucleated cells (Fig.1-5). Precursor cells express markers that are specific to their function on the cell membrane. For example, the first indication of osteogenic differentiation is through the expression of Cbfa1, ALP, collagen type 1 (COL1) and osteopontin. Bone sialoprotein and OC are expressed in the final stages of differentiation; they appear at the beginning of mineralization (Fernandez-Tresguerres-Hernandez-Gil et al. 2006).

Osteoblasts play various roles in bone formation, remodelling and mineralization. Bone matrix production occurs through the synthesis of collagen type 1 and non-collagenous proteins such as OC, osteopontin and bone sialoprotein. After matrix production osteoblasts differentiate into bone lining cells known as osteocytes (Aubin & Heersche, 2003; Bayliss *et al*., 2012). More than 80% of trabecular bone surfaces are covered by lining cells and the rest is occupied by osteoblasts or osteoclasts (Aubin & Heersche, 2003). Bone lining cells can re-differentiate into osteoblasts upon mechanical or hormone stimulation. These cells are

involved in the transportation of mineral ions into and out of the extracellular matrix (Clarke, 2008).

Osteocytes also act as mechano-sensors and they are involved in converting mechanical loading stimulus into biochemical signals. They communicate with neighbouring osteoblasts through cytoplasmic processes running through a canalicular network. Gap junction proteins allow cellular communication via intercellular signals such as nitric oxide, calcium, cytokines and prostaglandins (Fernandez-Tresguerres-Hernandez-Gil *et al.*, 2006; Bayliss et al, 2012).

1.13.2. Osteoclast cells

Osteoclasts are multinucleated, phagocytic cells of haematopoietic origin, (derived from mononuclear cells) (Aubin & Heersche, 2003). These mononuclear cells first differentiate into pre-osteoclasts which then fuse together to form multinucleated osteoclasts (Fig.1-6). Cytokines such as RANK-L and macrophage CSF (M-CSF) are responsible for the proliferation, differentiation and survival of pre-osteoclasts (Clarke, 2008). Osteoclasts have receptors for calcitonin (a calcium regulating hormone) and they stain positive for tartrate-resistant acid phosphatase (TRAP) (Aubin & Heersche, 2003). Calcitonin is secreted by cells in the thyroid gland in response to increasing levels of calcium; it binds to receptors on osteoclast cells to inhibit osteoclast cell activity (Bayliss *et al*., 2012). Osteoclast cells express cathepsin K and matrix metalloproteinase-9 (MMP-9), enzymes involved in the degradation of matrix proteins (Kalb et al., 2013). Osteoclast cells are rare in the bone and exist either as motile osteoclasts or resorptive osteoclasts. Motile osteoclasts are flattened, non-polarised cells with membrane protrusions known as lamellipodia (Kular et al., 2012). Resorptive cells are dome shaped with no lamellipodia. Motile osteoclasts move through lamellipodia formation and become polarized once they reach the resorptive site (Kular et al., 2012).

1.13.3. Interaction of osteoblasts and osteoclasts

Cytokines and growth factors play important roles in bone regulation by influencing the activities and signalling interaction of osteoblasts and osteoclasts (Table.1-2). The ligand RANK-L binds to the receptor RANK on pre-osteoclast cells resulting in differentiation and activation into mature osteoclast cells (Miyamoto et al., 2001). On the other hand, Osteoprotegerin, a factor secreted by osteoblasts, inhibits osteoclast formation by binding to the receptor RANK on pre-osteoclast cells (Fig.1-6) (Udagawa et al., 2014). Polarization of osteoclasts through cytoskeletal reorganisation leads to the formation of four domains: a ruffled border, sealing zone, functional secretory domain and basolateral membrane (Kular et al., 2012). Osteoclast cells attach to the bone matrix through integrin proteins and the attachment results in the formation of a compartment between ruffled ends of the osteoclast and bone surface (Aubin & Heersche, 2003; Weatherholt *et al*., 2012). This leads to the formation of a sealing zone that separates the acidic resorptive environment from extracellular environment (Vaananen & Horton, 1995; Kular *et al.*, 2012; Weatherholt *et al*., 2012). Acidified vesicles containing proteolytic enzymes fuse with the membrane and the ruffled ends of the osteoclast release hydrogen ions and proteolytic enzymes *(*Teitelbaum *et al*., 1995; Clarke, 2008). The acidified compartment exposes the matrix to the activity of the enzymes thereby initiating resorption process (Fernandez-Tresguerres-Hernandez-Gil *et al.*, 2006; Clarke, 2008; Weatherholt *et al*., 2012).

1.13.4. Muscle cells

Skeletal muscle comprises around 40% of the body and is involved in generating forces for movement and locomotion. Skeletal muscle tissue regeneration depends on a stem cell population known as satellite cells; these are mononuclear cells located underneath mature

myofibres (Karalaki et al., 2009). They are activated to proliferate during regeneration and upon relevant cues the cells will differentiate into myoblast cells (Karalaki et al., 2009). Myoblast cells will then migrate to the reparative site and differentiate to become myotubes.

Contractile forces caused by muscle activity and release of myokins by muscle cells regulate bone mass and bone formation (Hamrick, 2012). Skeletal muscle and bone have a common mesodermal origin (Fig.1-5) and there is evidence showing cross-talk between bone and muscle throughout development and healing (Kunert-Keil et al., 2014; Tagliaferri et al., 2015). This cross talk is important for the function of both tissues. Skeletal muscle adjacent to bone fractures interacts with the periosteum leading to the release of osteogenic/chrondogenic factors and growth factors involved in bone regeneration (Abou-Khalil et al., 2015). Furthermore muscle stem cells can differentiate into osteoblast and chrondogenic lineage (Herzog *et al*., 2003; Orbay *et al*, 2012).

1.13.5. Vascularization during bone development

There are three different stages of cartilage vascularization in bone during development. The first process is known as quiescent angiogenesis, where vascular structures invaginate from the connective tissue surrounding the bone into the cartilage. The second stage occurs postnatal during periods of rapid skeletal growth where capillary structures invade the long bones. The third stage is switched on in adults during bone remodelling in response to injury or disease (Gerber & Ferrara, 2000). The vascular network not only supplies nutrients and oxygen to the bone, but removes waste products. A reliable and constant supply of oxygen is very important in energy production, regulation of calcium homeostasis and enzyme function. Restricted blood supply to bone is associated with the formation of non-unions, decreased bone mass and decreased bone formation (Axelrad et al., 2007; Deschaseaux *et al*, 2009).

Lack of oxygen also hampers efficient cell proliferation as well as production of collagen from osteoblasts (Kular et al., 2012; Utting et al., 2006).

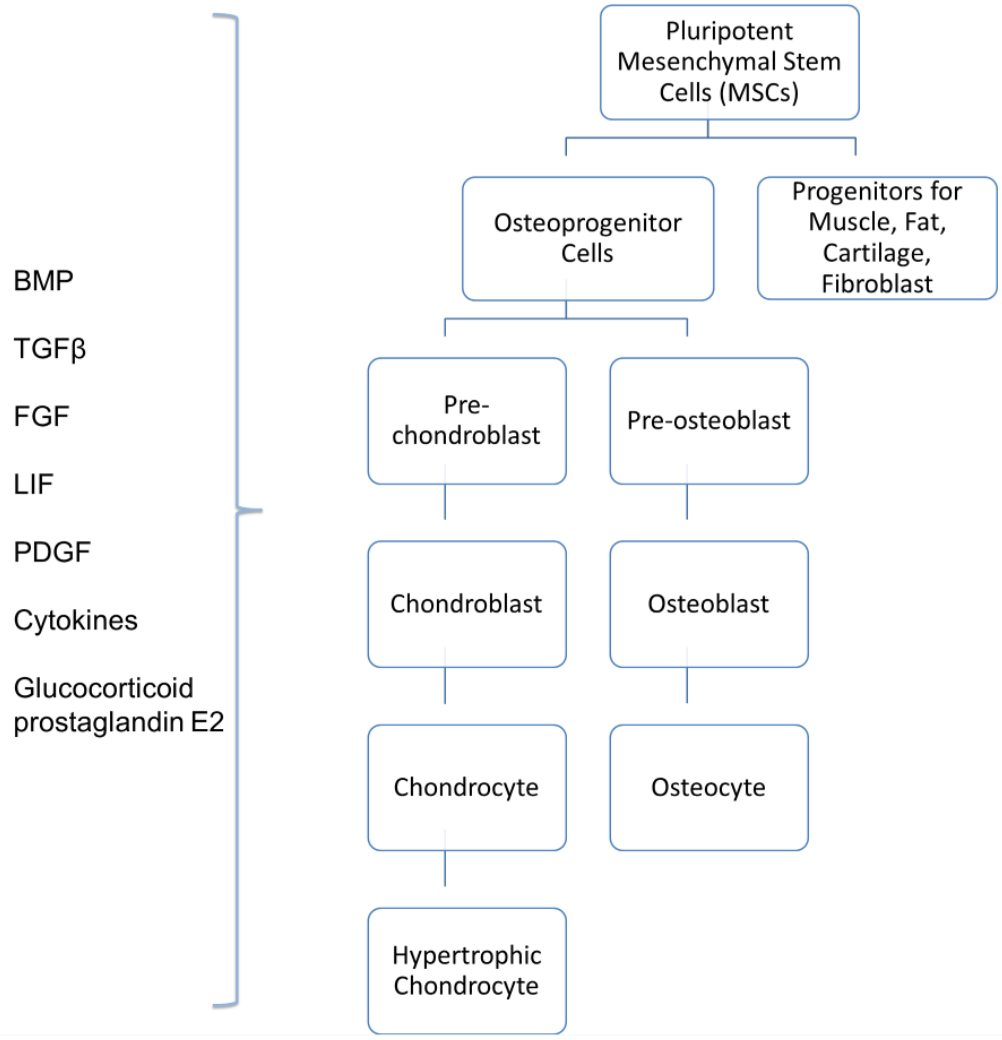

Fig.1-5. Osteoblast and chondrocyte lineage. Osteoblasts are multipotent cells that can be induced to differentiate into specific cell lineages (bone, muscle, fat and cartilage) under specific conditions.

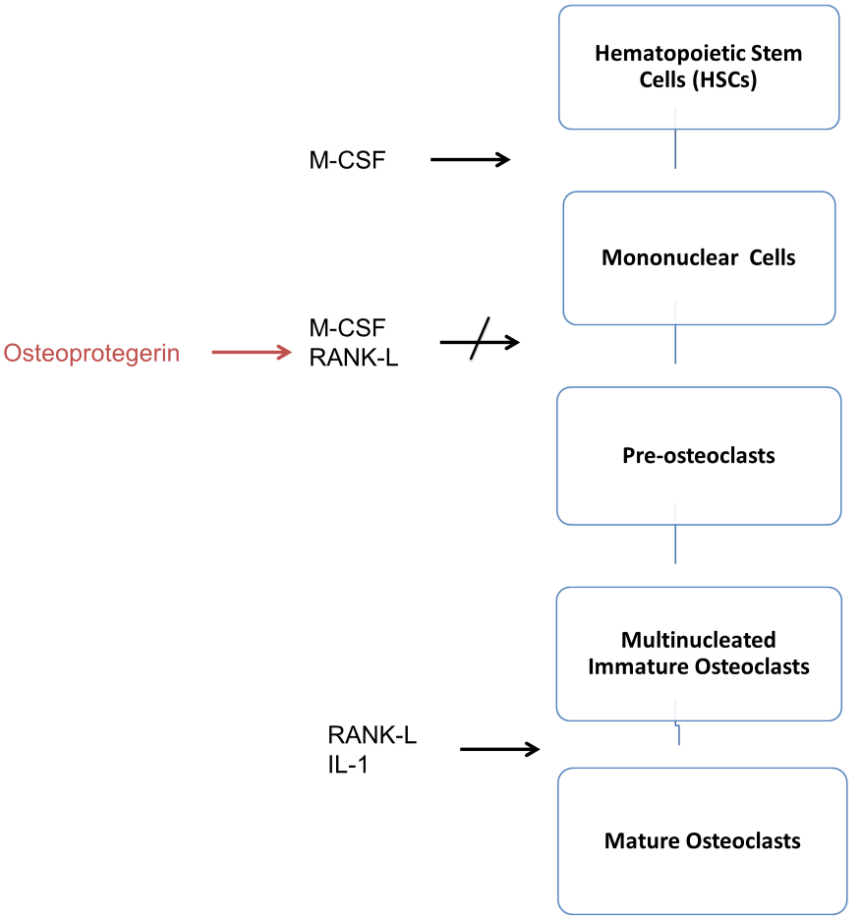

Fig.1-6. Osteoclastogenesis. In the presence of M-CSF and RANK-L mononuclear cells differentiate into pre-osteoclasts. In addition to RANK-L and M-CSF, IL-1 also plays a part in the maturation of osteoclast cells. Osteoprotegerin inhibits osteoclast formation by preventing RANK-L to RANK binding.

Table.1-2. Factors involved in the regulation of bone formation

Factor	Source	Function	References
IL-1 IL-2 Rank-L OPG MCSF TNF-α	▪ Macrophages ▪ Cells of mesenchymal origin	▪ Initiates repair cascade ▪ Chemotactic effect on other inflammatory cells ▪ Promotes extracellular matrix formation ▪ Stimulates angiogenesis ▪ Recruits fibrogenic cells to injury site ▪ Involved in endochondral bone formation and remodelling ▪ Promotes recruitment and differentiation of MSCs ▪ Induces apoptosis of hypertrophic chondrocytes ▪ Stimulates osteoclast function	(Kon et al., 2001) (Cho et al., 2002)
BMP	▪ Osteoprogenitors in the Matrix ▪ MSCs ▪ Osteoblasts ▪ Chondrocytes	▪ Bind to serine/threonine kinase receptors on target cells leading to intracellular signalling which affects gene expression in the nucleus ▪ Regulates growth, differentiation, apoptosis of osteoblasts and chondroblasts ▪ Involved in angiogenesis and matrix synthesis during osteogenesis	(Ducy & Karsenty, 2000) (Dimitriou et al., 2005)
TGF-β1, β2, β3	▪ Platelets ▪ Osteoblasts ▪ Chondrocytes	▪ Released in inflammatory phase of bone healing ▪ Chemotactic stimulator of MSCs ▪ Promotes MSCs, osteoblasts, chondrocytes proliferation. ▪ Stimulates production of collagen and alkaline phosphatase	(Lieberman et al., 2002)
PDGF	▪ Platelets ▪ Monocytes ▪ Macrophages ▪ Endothelial cells ▪ Osteoblast	▪ Released during the early phase of fracture healing ▪ Enhances mitogenic activity of fibroblasts, osteoblasts, MSCs and endothelial cells ▪ Stimulates angiogenesis and aggregation of platelets	(Barnes et al., 1999)
FGF	▪ Monocytes ▪ Macrophages ▪ MSCs ▪ Osteoblasts ▪ Chondrocytes	▪ Active in the early stages of fracture healing ▪ Plays crucial roles in angiogenesis and MSC mitogenesis ▪ Involved in chondrocyte maturation	(Canalis, 1980)
IGF	▪ Bone matrix ▪ Endothelial cells ▪ Osteoblasts ▪ Chondrocytes	▪ Promotes bone matrix formation by osteoblasts ▪ Stimulation of collagen synthesis ▪ Cartilage synthesis ▪ Regulation of proliferation and differentiation of MSCs during chondrogenesis	(Ortega et al., 2004)
MMP	▪ Extracellular matrix	▪ Degradation of cartilage during final stages of bone formation to allow invasion of blood vessels	(Gerstenfeld et al., 2003)
VEGF	▪ Endothelial cells ▪ Osteoblasts	▪ Mediator of neo-angiogenesis and endothelial-cell specific mitogens ▪ Couples angiogenesis to cartilage remodelling and bone formation in bones	
Angiopoietin 1 and 2		▪ Regulates vascular molecules involved in larger blood vessel formation	

1.14. Bone remodelling

Bone modelling is a process that leads to bone changing its structure due to physiological and mechanical stimuli to accommodate stress placed on them (Wolff's law)(Clarke, 2008). Bone is remodelled to maintain strength and mineral homeostasis. This process begins in the developing foetus and continues until death (Clarke, 2008). During remodelling old bone is removed and replaced by new mineralised bone to prevent accumulation of micro-damage (defects in matrix due to skeletal loadings or pathological conditions) (Clarke, 2008; Kular *et al.*, 2012). The turnover rate for cortical bone (2 to 3 years) is lower compared to that of trabecular bone. Trabecular bone turnover is important for mineral metabolism (Clarke, 2008). Remodelling process allows for the formation of new bone with low mineral content, which allows for mineral exchange with extracellular fluid (Clarke, 2008).

Activation of remodelling is initiated when the endosteum (containing bone lining cells) separates to expose bone and recruitment of pre-osteoclast cells. The resorption process takes between 2 to 4 weeks in each remodelling cycle (Clarke, 2008). Following the resorption process, osteoblasts release membrane bound matrix vesicles that concentrate calcium and phosphate and digest mineralization inhibitors such as proteoglycans (Clarke, 2008). Osteoblasts take between 4 to 6 months to form new bone through matrix production and mineralization (Clarke, 2008).

1.15. Regeneration after Injury

The process of bone formation is reinitiated following injury. Bone tissue has the ability to regenerate itself after injury without scar formation (Deschaseaux *et al.*, 2009). During fracture healing both endochondral and intramembranous ossification take place. Bone Morphogenic Proteins (BMPs) have been shown to be involved in the promotion of these processes during fracture healing (Cho et al., 2002). There are two types of fracture healing: primary and secondary healing.

1.15.1. Primary healing

Primary fracture healing occurs when there is an anatomic reduction of the fracture fragments and stability is established (Dimitriou *et al.*, 2005). Healing occurs by direct synthesis of lamellar bone without the need for callus formation (Weatherholt *et al.*, 2012). This is achieved by the formation of remodelling units known as "cutting cones" which establish new Harversian systems (Dimitriou *et al.*, 2005). The osteoclasts (in cutting cones) resorb the damaged tissue from the bone fragments, followed by lamellar bone formation by osteoblasts (Shapiro, 2008).

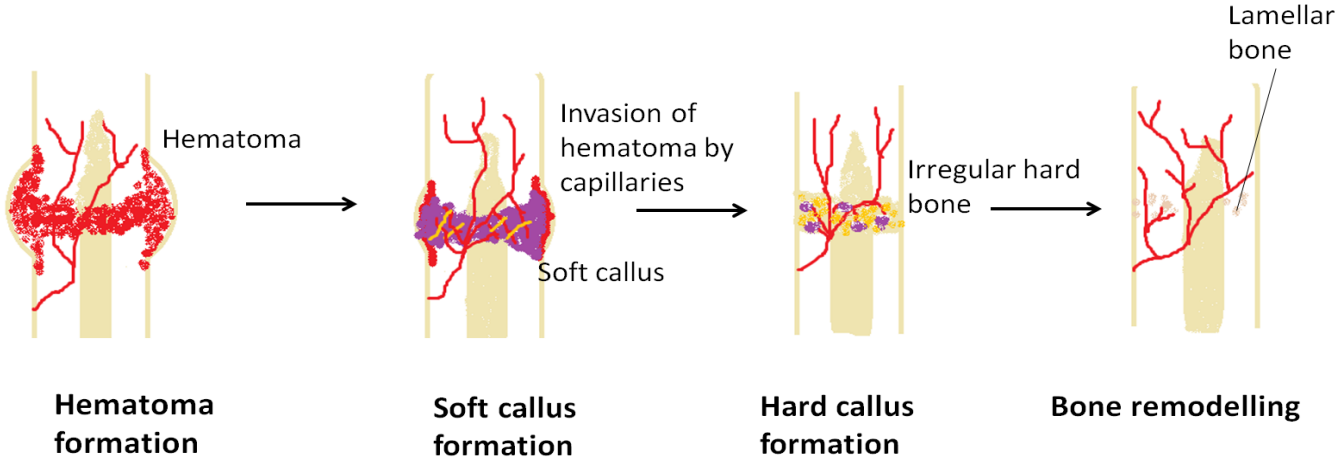

(Adapted from Marieb, 2004)

Fig.1-7. Stages of secondary healing. Healing is initiated by the formation of a hematoma at the fracture site. Growth factors and cytokines promote the formation of a soft callus through collagen production by fibroblasts. The soft callus is mineralised and differentiation of osteoblasts leads to hard callus formation. The hard callus is then remodelled in the last stage to form lamellar bone.

1.15.2. Secondary healing

Regeneration after injury results in an inflammatory response and formation of a hematoma (Gerstenfeld *et al.*, 2003; Hutchison *et al.*, 2007). There are four distinct, overlapping stages of fracture repair, namely 1) inflammation 2) soft callus formation 3) hard callus formation and 4) bone remodelling (Fig.1-7).

Inflammation: the disruption of blood vessels results in the formation of a blood clot at the fracture site during the first few days. Platelets, macrophages and other inflammatory cells (granulocytes, lymphocytes and monocytes) infiltrate the hematoma to fight infection by secreting cytokines and growth factors (Table.1-2) (Schindeler et al., 2008). The platelets release granules that convert the clot into a fibrin rich hematoma. Macrophages and phagocytic cells are recruited to the area to remove debris and degenerated tissue (Schindeler et al., 2008). The hematoma is invaded by capillaries; this is followed by the conversion of the hematoma into granulation tissue formed by fibroblasts through production of collagen (Bayliss *et al*., 2012). During this early process, oxygen and nutrients are supplied by the exposed cancellous bone and muscle. The use of anti-inflammatory drugs during this first week may alter the inflammatory response and inhibit bone healing (Kalfas, 2001).

Soft callus formation: Chondrocytes and fibroblasts are the main cells involved in the formation of the soft callus (fibrocartilage). Chondrocytes synthesize a cartilage rich matrix which gradually replaces the granulation tissue; fibroblasts synthesize fibrous tissue to fill out spaces lacking cartilage. The net result is an avascular fibro-cartilage callus which bridges the

fracture ends of the bone to provide mechanical stability to allow for bone formation process to continue (Marsell & Einhorn, 2011). The callus is very weak in the first 4-6 weeks and requires some fixation for protection. Furthermore improper immobilization may prevent callus ossification resulting in an unstable fibrous union (Kalfas, 2001). In the final stage of soft callus formation, chondrocytes become hypertrophic and mineralise the cartilaginous matrix, followed by apoptosis of the chondrocytes. Angiogenic factors such as VEGF and BMPs (Deckers et al., 2002; Gerstenfeld et al., 2003; Kalfas, 2001; Schindeler et al., 2008) promote angiogenesis and neovascularisation of the soft callus (Bayliss *et al*., 2012).

Hard callus formation: Osteogenesis dominates this stage; revascularisation and conversion of soft callus to irregular hard bone occurs simultaneously. Vascularization allows for the release of chrondoclasts and osteoblasts that are involved in the replacement of woven bone with lamellar bone (Mehta et al., 2012; Schindeler et al., 2008). During osteogenesis, osteoblasts replace the cartilage formed during primary callus formation with new bone via endochondral ossification (Bayliss *et al*., 2012; Weatherholt *et al.*, 2012).

Bone remodelling: Irregular woven bone is converted into lamellar bone through the action of osteoclast and osteoblasts. Osteoclasts resorb the woven bone and osteoblast lay down lamellar bone (Schindeler *et al.*, 2008; Bayliss *et al*, 2012). Adequate strength for bone is achieved in 3 to 6 months (Fig. 1-8) (Kalfas, 2001).

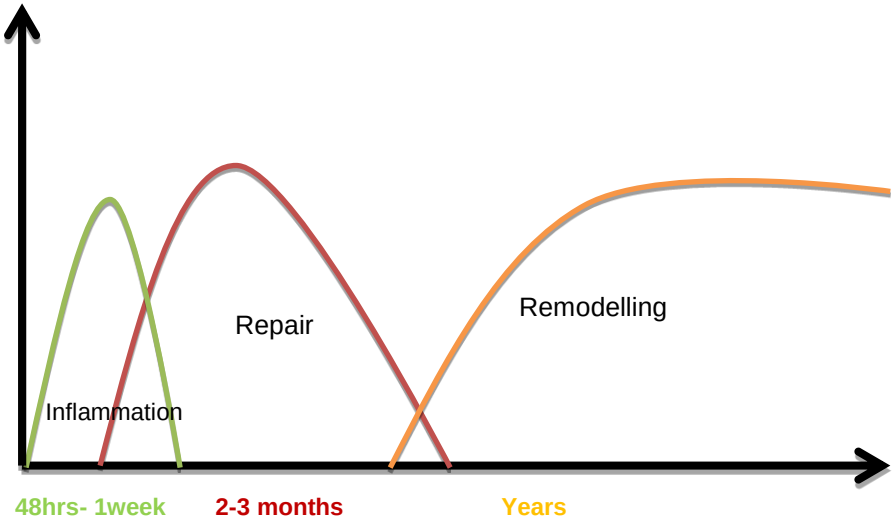

(Adapted from Cruess & Dumont, 1975)

Fig.1-8. Duration of secondary healing phase

1.16. Focus of study

In the draft of the new American Society of Testing and Materials standard (ASTM WK52640), it has been clearly pointed out that the experimental approaches informing development of standards for application of Mg as biodegradable metal implants must control the corrosion test environment through standardization of conditions and utilization of physiologically relevant electrolyte fluids. One of the most important steps in *in vitro* testing is the preparation of extracts from the implants. The current testing standards requires the removal of the granule formed during the corrosion process and in most cases, only simulated body fluid (SBF) is used. However, in this study, to emulate the biological response to the corrosion products in the *in vivo* environment, the use of complete extracts from Mg metal conditioned medium containing both the Mg^{2+} and corrosion granule was used. As magnesium degrades at the implantation site, there is a subsequent release of large particulate matter and smaller corrosion products. Relatively few studies have detailed effects of Mg corrosion on progenitor cells at the implantation site. The ability of the body to clear the granule from the implantation site is crucial for local inflammation response and tissue implant integration. Although studies (Castellani et al., 2011; Janning et al., 2010; J. Wang et al., 2016) have reported enhanced bone formation near the implantation site, other studies reported (Zhang *et al*. 2010; Li *et al*. 2008) the presence of cavities after the Mg implant had degraded. At present, the cause of these cavities remains unknown. The presence of the granule might be involved in attracting the migration of osteoclasts to the implantation site, whereby increased osteoclast activity could result in the formation of cavities (T A Huehnerschulte et al., 2012). Titanium metal particles have been shown to trigger osteolytic activities in osteoblasts and osteoclasts through the expression of RANK-L (Choi et al., 2005). It is possible that the

presence of Mg metal particles in the corrosion granule could elicit the same response as the metal particles *in vivo*. Therefore, it is crucial to understand how Mg corrosion products affect osteoclast activity and function. Alterations in the functions of osteoblast and osteoclasts can offset bone homeostasis leading to the impairment of bone healing and development of bone diseases.

Muscle, bone and tendon are integral components of the musculoskeletal system and collectively these tissues work together to provide the framework of the body and determine movement and degree of flexibility. Damage to skeletal muscles can be caused by trauma, contusions and strains during sports activities. Trauma injuries can result in bone fractures. The severity of the surrounding soft tissue damage and type of fracture influences the method of treatment. Bone fractures may also involve soft tissue injuries and these can cause significant clinical complications such as infection, soft tissue loss or non-union. Increase in delayed union and non-union have been reported when there is damage to skeletal muscle (Sen & Miclau, 2007; Abou-Khalil *et al.*, 2015). During fracture healing, the lack of intact muscle was shown to affect the healing process resulting in delayed bone deposition and callus remodelling, impaired release of the factors and cells required for bone healing and reduced vascularisation (Abou-Khalil et al., 2014). A study by Tagliaferri et al., 2015 also concluded that loss of a large amount muscle tissue impaired fracture healing, whilst molecules released from intact muscle enhanced bone healing. Therefore, proper grasp of fracture healing also requires understanding of the mechanism of soft tissue injury and healing. While there is considerable research on the impact of Mg alloy corrosion products on bone forming cells, the effect of on muscle cells is lacking. This is important as bone regeneration is negatively impacted by a pathologic and inflammatory muscle environment.

Furthermore, muscle stem cells may be as important as mesenchymal stem cells in the reparative process of bone. Magnesium also plays an important role in muscle function; it has been shown that magnesium deficiency can inhibit muscular growth (Furutani *et al*., 2011) and negatively affect structural and functional properties of skeletal muscle (Astier et al., 1996).

1.17. Aims of the current study

The aim was to develop a reliable *in vitro* testing method for Mg-based biodegradable materials that closely emulates the *in vivo* environment, considering the different cell types of skeletal tissue. Specifically, the study aimed to:

- Understand the biological response of human mesenchymal stem cells, monocytes, osteoclasts and skeletal muscle cells to the corrosion products of pure Mg and Mg-Ca alloy.
- Understand the concentration effects following corrosion by simulating the concentration gradients in the tissue surrounding the implantation site
- Compare the effect of the different degradation behaviour of pure Mg and Mg-Ca alloy on cells of the skeletal tissue.
- Investigate the immune response of pure Mg or Mg-Ca corrosion products by looking at the expression of inflammatory markers from immune cells.

CHAPTER 2: Materials and Methods

2.1. Mg sample preparation

In the previous study by Li *et al*., 2008, high activity of osteoblasts and osteocytes were observed around a Mg-Ca alloy implant, however after the implant had degraded a void was left in the implant position. Furthermore, as the implant degraded no regeneration occurred, thus this study was designed to investigate the effect of pure Mg and Mg-Ca alloy corrosion products on cells of the skeletal tissue. Mg-Ca alloy manufactured in a similar manner to the one used by Li *et al*., 2008 was supplied by a partner from Peking University, Beijing, China and the procedures used to prepare the Mg samples are presented here: Mg-Ca alloy with a nominal composition of 1 wt. % Ca was prepared from commercially pure Mg (99.9%) and Ca (99.8%). Mg ingots were melted in a high purity graphite crucible under the protection of high purity argon (99.99%) atmosphere at about 670°C. After the addition of the alloy elements, the temperature of the mixture was increased to 720°C for 40mins before being poured into a steel mould preheated to 250°C. During the whole melting procedure, mechanical stirring was applied. The as-cast ingots of Mg-Ca alloys were solid solution treated at 340°C for about 4hrs, followed by quenching in water. Finally, the alloy samples were hot extruded at a temperature of about 320°C with an extrusion speed of 2 mm min^{-1}. The melting process of commercial pure Mg was the same as that of Mg-Ca. Pure Mg was solid solution treated at 340°C for about 4hrs, followed by quenching in water and hot extrusion at a temperature of about 320°C with an extrusion speed of 2 mm min^{-1}.

Both Mg and Mg-Ca disks were supplied in the form of cylindrical ingots. Before cell culture use, the disks were polished with 1200 grit paper to clean the surface, sterilised by soaking

them in 100% (v/v) ethanol for 5mins and were subsequently irradiated under ultraviolet light (UV) for 3hrs each side.

Alloy preparation was included here even though it was not performed in this study because it is important to understand processing or manufacturing effects on metal structure and elemental distribution. These factors influence the corrosion behaviour of Mg and Mg alloys and hence also the biological response of cells exposed to these biomaterials. A review by Song & Atrens 1999 revealed the following information: Different elements have different influences on the corrosion behaviour of Mg alloys, some elements act to inhibit corrosion and other act to accelerate the corrosion rate. The presence of critical contaminants in high concentrations such as nickel, iron and copper can increase the corrosion rate by a factor of 100 (Fig.2-1). Contamination by iron can come from the use of steel melting pots during the manufacturing process. The microstructure (grain size and phase distribution) of Mg alloys can also influence the corrosion behaviour of these biomaterials, for example:

- Fine and uniformly dispersed cathodic phases can accelerate the corrosion of Mg alloys.
- High density porosity can increase the amount of corrosion per unit area of the material.
- Micropores can provide active sites for corrosion reaction leading to a greater tendency towards severe localized corrosion.

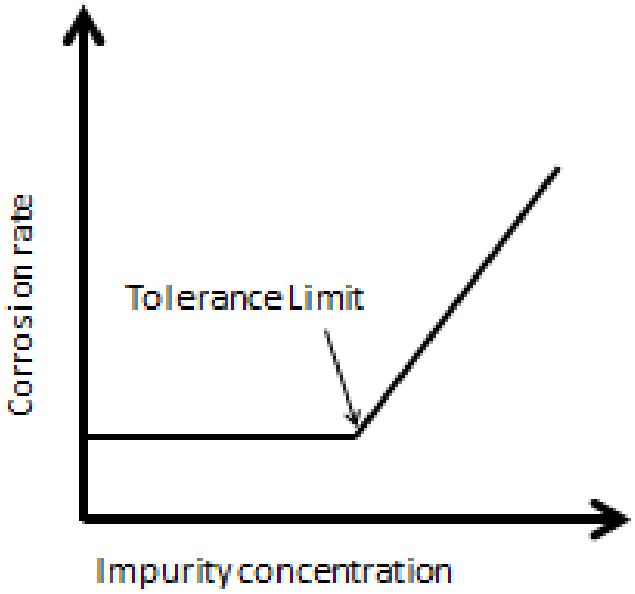

Adapted from Song & Atrens (1999)

Fig.2-1. Curve on the influence of impurities on the corrosion rate of magnesium. When the impurity concentration of impurities such as copper, nickel and iron exceeds the tolerance limit, the corrosion rate of magnesium is accelerated (Song & Atrens, 1999).

Experimental procedures were carried at two different institutes. The work on hMSCs and muscle cells was carried out at Loughborough University, UK. However the work on osteoclast cells and immune response was carried out at the University of Auckland, New Zealand. The work in New Zealand was part of an exchange activity, SkelGen under Marie Skłodowska-Curie Research and Innovation Staff Exchange programme. As a result of the two different environments the PCR procedures used were different, Two-step PCR was used at the University of Auckland and a One-step PCR process was used at Loughborough University. For all experimental procedures the number of replicates for each specific experiment is represented by n.

2.2. Conditioned Media Preparation

Mg disk (1g) with the following dimensions: 12.0mm (diameter) x 5.0mm (depth) or Mg-Ca1% disk (1.5g) with dimensions: 16.0mm (diameter) x 3.5mm (depth) were immersed in 400 ml of appropriate cell culture medium for the specific cell type and kept in a humidified atmosphere with 5% CO_2 for 72hours. In order to distinguish between the effects of released corrosion products presented as insoluble granule and soluble ions, part of the conditioned medium was filtered using a 0.22µm sterile filter (Millipore, UK) to prepare a conditioned medium free of particulate (filtered medium), while the other half was left unfiltered (non-filtered medium). The stock conditioned medium (100) was diluted 1:2 (50), 1:4 (25) and 1:10 (10) with fresh culture medium and then supplemented with growth supplements as required for culture of specific cell types.

2.3. Chemical Quantification of Major Ions in Corrosion Products

Following corrosion, the concentration of Mg^{2+} and Ca^{2+} ions in the conditioned media were analysed using inductively coupled plasma optical emission spectrometry (ICP-OES), (iCAP 6000 series, ThermoFisher Scientific) and ITEVA analyst software (iCAP, ThermoFisher). Mg/Mg-Ca conditioned media were diluted and ICP-OES analysis was conducted as follows: 0.2 g, of the different concentrations of Mg/Mg-Ca filtered conditioned media was weighed and transferred into a tube, 0.4g of 2% v/v nitric acid and 9.5g of deionized water were also added to the tube. Calibration standards required for the construction of a standard curve covering the range of analyte concentration were prepared as follows: 28 element standard (100ppm) (Fisher Scientific) was serially diluted in 2% v/v nitric acid resulting in the following concentrations, 50ppm, 5ppm, 0.5ppm and 0.05ppm. 2% v/v nitric acid was used as the blank control and ICP-OES machine was used as per manufacturers' instructions. The measurement for Mg^{2+} and Ca^{2+} were measured at 279.5 and 317.9 wavelengths respectively. Each sample was measured in triplicate. Every time the conditioned medium was prepared the ion concentration for Mg^{2+} and Ca^{2+} were measured.

2.4. Analysis of corrosion granules

A separate analysis was performed to measure the concentration of corrosion granules present following corrosion in DMEM. After a 72hour immersion in DMEM, the resultant conditioned media was centrifuged at 500g. The supernatant was removed and the corrosion granule was allowed to dry in a drying oven at 40°C before the weight was measured. The concentration of the corrosion granule formed was measured at approximately 1.5mg/ml for the non-filtered undiluted concentration (Mg100) and the pH was measured at 8.5 using a pH

meter (Mettler Toledo, UK). The corrosion granule formed when Mg-Ca disk corroded was not measured because the disk had a much slower corrosion rate and less corrosion granule was released. The amount released was difficult to accurately measure, as some of the granule was lost during the collection procedure. Energy dispersive X-ray (EDX) was then conducted for chemical analysis of the corrosion granule.

2.5. EDX Analysis of Corrosion Granule

Scanning electron microscopy (SEM) and EDX analysis on uncoated Mg corrosion granule was performed using SEM Cambridge 360 stereoscan equipped with a secondary electron detector, running at 15kV with a tungsten source. Interaction of the electrons with the corrosion granule resulted in the formation of x-rays which are characteristic of the elements in the corrosion granule. The inbuilt analytical system analysed the x-rays resulting in the formation of general composites. A random area on the composite of the corrosion granule was chosen and analysed to give a general idea of the elements present, 3 points were also randomly chosen and an intense beam was directed at these points for a quantitative analysis of the elements. A spectrum with elemental compositions of the corrosion granule was obtained for each time point and area analysis.

2.6. Cell Resuscitation, Seeding and Counting

The following procedures were applied to resuscitate and expand the various cell types, unless specified. Cryopreserved cells were thawed quickly in 37°C water bath; cells were transferred to a tube with pre-warmed growth medium. Cells were counted using a haemocytometer per manufacturers' instructions. 200µL cell suspension was transferred from the tube to a small vial, equal volume of trypan blue solution was added to the solution

and mixed. 20µL of cell suspension + trypan blue was added to the haemocytometer. Haemocytometer was placed under a light microscope and living cells (non-stained) were counted. The cell suspension was then transferred into a flask taking into account the concentration of viable cells previously assessed and the cell density required for seeding. Warm medium was added (1ml/5cm^2) before incubation in a humidified atmosphere at 37°C, 5% CO_2.

Table.2-1. Seeding parameters used

Cell type	Procedure	Density
hMSCs		5000-6000 cells/cm^2
C2C12		10 000cells/cm^2
RAW cells	Expansion	3000-5000cells/cm^2
	Differentiation assay	2000-2500 cells/cm^2
THP-1 cells	Expansion	40 000 cells/ cm^2
	Immune assay	750 000- 1x10^6 cells/mL

2.7. Cell Culture Media Formulations

Different media formulations were used for the different cell types; complete growth medium was stored at 2 to 8°C and used within one month of preparation. Tissue culture flasks and plated were bought from Fisher Scientific unless stated otherwise.

2.7.1. hMSC culture medium

MSC growth medium comprised of Dulbecco's Modified Eagle's Medium (DMEM) (Lonza, UK) supplemented with 10% (v/v) foetal bovine serum (FBS) (Sigma-Aldrich, UK), L-glutamine final media concentration 2 mM (ThermoFisher Scientific, UK), and 100 units/ml penicillin-streptomycin (ThermoFisher Scientific, UK).

MSC osteogenic medium comprised of MSC growth media supplemented with 100nM dexamethasone (Sigma Aldrich, UK), 10mM glycerolphosphate (Sigma Aldrich, UK) and 50µg/ml L-ascorbic acid (Sigma Aldrich, UK). Fresh osteogenic medium was made up every week.

2.7.2. C2C12 culture medium

C2C12 growth medium comprised of HyClone Dulbecco's High Glucose Modified Eagles Medium with L-glutamine (GE Healthcare, UK) supplemented with 20% (v/v) FBS (Dutscher Scientific, UK) and 100units/ml penicillin-streptomycin.

C2C12 differentiation medium comprised of HyClone Dulbecco's High Glucose Modified Eagles Medium with L-glutamine supplemented with 2% (v/v) horse serum (Life Technologies, UK) and 100units/ml penicillin-streptomycin.

C2C12 maintenance medium comprised HyClone Dulbecco's High Glucose Modified Eagles Medium with L-glutamine supplemented with 7% (v/v) FBS and 100units/ml penicillin-streptomycin.

2.7.3. RAW growth medium

RAW growth medium comprised of α-MEM (Life Technologies, NZ) supplemented with 10% (v/v) FBS (Life Technologies, NZ), L-glutamine final media concentration 2mM (Life Technologies, NZ) and 100units/ml penicillin-streptomycin (Life Technologies, NZ).

RAW cell differentiation medium comprised of growth media supplemented with (10ng/ml) RANK-L (Amgen).

2.7.4. THP-1 cell growth medium

THP-1 growth medium comprised of Roswell Park Memorial Institute (RPMI) 1640 medium supplemented with 10% (v/v) FBS, 100 units/ml penicillin-streptomycin and 1mM sodium pyruvate.

2.7.5. Mature osteoclast (MO) growth medium

Earle's MEM (ThermoFisher Scientific, NZ) supplemented with 10% (v/v) FBS, 100units/ml penicillin-streptomycin and 0.1% 12 M HCL.

2.8. Cell Culture

2.8.1. Human bone marrow derived mesenchymal stem cells (hMSCs)

Cryopreserved hMSCs (from a specific donor, Lonza, USA) were thawed quickly in 37°C water bath, and then centrifuged at 200g for 5mins. After centrifugation supernatant was aspirated and cell pellet was resuspended in pre-warmed MSC growth media. The cells were counted and $5x10^5$ cells were seeded in a T75 flask for expansion. Medium was refreshed every 3 days

and cells were allowed to grow until 70% confluent before being passaged. Cells were washed with Ca^{2+} and Mg^{2+} free phosphate buffered saline (PBS) (Lonza, UK). Trypsin (Lonza, UK) was used to detach the cells from the surface, it was inactivated by the addition of fresh MSC growth medium equivalent to three times the volume of the trypsin solution used for cell detachment. The cell suspension was then centrifuged at 200g for 5mins; supernatant containing trypsin was removed and cells were resuspended in fresh MSC growth medium before being cultured in a humidified atmosphere at 37˚C under 5% CO_2. Cells below passage 5 were used for experimental procedures.

2.8.2. Mouse C2C12 myoblasts

C2C12 cell line from European Collection of Authenticated Cell Cultures (ECACC) supplied through Sigma Aldrich, UK was used for experimental procedures. The cell line is a subclone from myoblast cell line established from normal C3H mouse leg muscle.

Cryopreserved C2C12 cells were thawed quickly in 37°C water bath, and then centrifuged at 200g for 5mins. The cell pellet was resuspended in C2C12 growth medium and counted before $1x10^6$ cells were seeded in a T75 flask. Medium was refreshed every 3 days and cells were allowed to grow until 70% confluent before being passaged. For passaging, cells were washed with Ca^{2+} and Mg^{2+} free PBS and trypsin was used to detach the cells from the surface. The cell suspension was then centrifuged at 200g for 5mins; supernatant containing trypsin was removed and cells were resuspended in fresh C2C12 growth medium before being cultured in a humidified atmosphere at 37˚C under 5% CO_2.

2.8.3. Mouse RAW cells

RAW 264.7 from ATCC (The Global Bioresource Centre) supplied through In vitro technologies, NZ were used for experimental procedures. This is an adherent cell line from macrophage; Abelson murine leukaemia virus transformed.

Cryopreserved RAW cells were thawed quickly in 37°C water bath, and then centrifuged at 200g for 5mins. The cell pellet was resuspended in RAW growth medium and counted before $1x10^6$ cells were seeded in a T75 flask. Medium was refreshed every 3 days and cells were allowed to grow until 70% confluent before being passaged. For passaging, cells were washed with Ca^{2+} and Mg^{2+} free PBS and detached from the surface using a cell scrapper. The cell suspension was then centrifuged at 200g for 5mins; supernatant was removed and cells were resuspended in fresh RAW growth medium before being cultured in a humidified atmosphere at 37˚C under 5% CO_2.

2.9. Exposure of cultured cells to the corrosion products

2.9.1. hMSCs

hMSCs were seeded onto a 24 well plate at density of $1x10^4$ cells/well in triplicate. Cells were incubated in MSC growth medium for 24 hours to allow for attachment. The MSC growth medium was then replaced with Mg/Mg-Ca filtered medium or non-filtered medium (DMEM) supplemented with 10% (v/v) FBS, L-glutamine final media concentration 2mM and 100units/ml penicillin-streptomycin. Cells cultured in MSC growth medium were used as the standard control. Viability assay was performed after cells were cultured with conditioned medium on day 1, 3 and 7 using AlamarBlue reagent (Invitrogen, Life Technologies), please refer to section 2.10 for further details on the AlamarBlue assay.

2.9.2. Mouse C2C12 myoblasts

C2C12 were seeded onto 24 well plate at a density of $2x10^4$ cells/well in triplicate. Cells were cultured in C2C12 growth medium for 24 hours. After 24 hours C2C12 growth medium was switched to C2C12 differentiation medium for the fusion of myoblasts into myotubes. After 3 days in differentiation medium mature myotubes were formed and then cells were cultured in Mg/Mg-Ca filtered medium or non-filtered medium (Hyclone DMEM) supplemented with 7% (v/v) FBS, L-glutamine final media concentration 2mM and 100units/ml penicillin-streptomycin for a further 3 days. Cells cultured in C2C12 maintenance medium were used as the standard control. Viability assay was performed after cells were cultured with conditioned medium on day 1, 2 and 3 using AlamarBlue reagent.

2.9.3. Mouse RAW cells

RAW cells were seeded onto a 24 well plate at density of $1x10^4$ cells/well in triplicate. Cells were incubated in RAW growth medium for 24 hours to allow for attachment. RAW growth medium was then replaced with Mg/Mg-Ca filtered medium or non-filtered medium (α-MEM) supplemented with 10% (v/v) FBS, L-glutamine final media concentration 2mM and 100units/ml penicillin-streptomycin. Cells cultured in RAW growth medium were used as the control. Viability assay was performed after cells were cultured with conditioned medium on day 1, 2 and 3 using AlamarBlue reagent.

2.10. AlamarBue assay

AlamarBue assay was performed following manufacturer's protocol. 10% v/v AlamarBlue reagent in the appropriate culture medium was added to the cells and incubated for 4 hours. After the 4hour incubation, 200µL of AlamarBlue solution from each well was transferred into

a 96well plate. FLUOstar Omega plate reader (BMG Labtech) was used to measure fluorescence level of the supernatant at excitation: emission 530:590nm and normalised to DNA concentration (PicoGreen assay) (refer to section 2.11). Fluorescence of growth medium without cells was used as the background. Fluorescence from the background was subtracted from the fluorescence of the treated and the control sample. In general, cell viability ≥70% in relation to the control was defined as a non-toxic effect; this is in accordance to the ISO standard for biological evaluation of medical devices (ISO, 10993-15, 2009).

2.11. DNA Quantification

DNA was quantified using the Quant-iT PicoGreen Kit (Invitrogen USA) following manufacturer's protocol. Briefly, cells were lysed with trypsin and 0.1% Triton X at a ratio of 1:1. 100µL of cell lysate solution and 100µL of Quanti-iT PicoGreen reagent (Life Technologies, UK) were added to a black 96well plate. The plate was incubated in the dark for 5 minutes. Fluorescence intensity was read using the plate reader (VaioSkan Flash, ThermoFisher Scientific) at excitation: emission wavelength of 480nm:520nm.

2.12. Gene expression analysis

2.12.1. hMSCs

hMSCs were seeded onto a 6well plate at density of $6x10^4$ cells/well in triplicate. Cells were incubated in MSC growth medium until 90% confluent. The MSC growth medium was then replaced with Mg/Mg-Ca filtered or non-filtered medium (DMEM) supplemented with 10% (v/v) FBS, L-glutamine final media concentration 2mM (Life Technologies, NZ) and 100units/ml penicillin-streptomycin and cultured for a period of 12 days. Cells cultured in MSC

growth medium were used as the standard control and cells cultured in osteogenic medium were used as positive control. RNA was extracted at day 2, 4, 8 and 12 (see section 2.13). The quantity and purity of RNA was measured using a Nanodrop spectrophotometer (see section 2.13.1). The RNA produced was used for quantitative real time PCR (qRT-PCR) to amplify the primers of osteogenesis-related genes: Runx-2, COL1 and OC (Quantitect primer assays, QIAGEN, UK) using a one-step real time PCR machine (ViiA 7, Applied Biosystems) and QuantiFast SYBR Green RT-PCR Kit (QIAGEN, UK). House-keeping gene GAPDH was used as the internal control. Table.2-2 is showing information on primer assay design.

Table.2-2: Quantitect Primer Assay Design

Gene	Species	Accession number
Collagen type 1	Human	NM_000088 XM_005257058 XM_005257059 XM_006721703
GAPDH	Human	NM_002046 NM_001289745
Osteocalcin	Human	NM_199173 NM_000711
Runx-2	Human	NM_001015051

2.12.2. Osteoclastogenesis of RAW cells

RAW cells were seeded onto a 48well plate at density of 4000 cells/well, 8 wells were used for each sample. Cells were incubated in RAW growth medium for 3 hours. After 3hours, RAW growth medium was then replaced with Mg/Mg-Ca filtered or non-filtered medium (α-MEM) supplemented with 10% (v/v) FBS, L-glutamine final media concentration 2mM and 100units/ml penicillin-streptomycin and 10ng/mL RANK-L. The cells were allowed to

differentiate over a culture period of 5 days; medium was changed once on day 3 and on day 5 RNA was extracted. Cells cultured in RAW growth medium were used as the control and cells cultured in RAW differentiation medium were used as the positive control. The quantity and quality of RNA was measured using a Nanodrop spectrophotometer. The cDNA produced (see section 2.14.2) was used for a two-step PCR process to amplify osteoclastogenesis related genes using a real-time PCR machine (QuantStudio 12K, Applied Biosystems). FAM-labelled TaqMan assays specific for NFATc-1 and TRAP and VIC-labelled 18S rRNA endogenous control were used per manufacturers' instructions. The predesigned TaqMan gene assays were supplied by Applied Biosystems (ThermoFisher Scientific) (Table.2-3).

Table.2-3: TaqMan Primer Assay Design

Gene	Species	Accession number
NFATc-1	House mouse	NM_001164109.1
TRAP	House mouse	NM_001102404.1

2.12.3. Myogenic genes expressed by C2C12 myoblasts

Cells were cultured in C2C12 growth medium for 24 hours until confluent. Once the cells were confluent C2C12 growth medium was switched to C2C12 differentiation medium for the fusion of myoblast into myotubes. After 3 days in differentiation medium, mature myotubes were formed and cells were cultured in Mg/Mg-Ca conditioned media (Hyclone DMEM) supplemented with 7% (v/v) FBS and 100units/ml penicillin-streptomycin for a further 3 days. Cells cultured in C2C12 maintenance medium were used as the control. After treatment with Mg/Mg-Ca conditioned media RNA was extracted and used for qRT-PCR to amplify expression

of muscle related genes, myogenin, MAFbx and MuRF1, using a one-step real time PCR machine (ViiA 7), QuantiFast SYBR Green RT-PCR Kit and reverse and forward primers designed and validated by School of Sport, Exercise and Health Sciences (University of Loughborough) (Table.2-4). RP2-β was used as the control house-keeping gene.

Table.2-4: Primer Assay Design

Species	Gene of interest	Forward Primer (5'-3')	Reverse Primer (5'-3')
House mouse	Myogenin	CCA ACT GAG ATT GTC TGT C	GGT GTT AGC CTT ATG TGA AT
	MuRF-1	CCA AGG AGA ATA GCC ACC AG	CGC TCT TCT TCT CGT CCA G
	MAFbx	CTG AAA GTT CTT GAA GAC CAG	GTG TGC ATA AGG ATG TGT AG
	RP2-β	GGT CAG AAG GGA ACT TGT GGT AT	GCA TCA TTA AAT GGA GTA GCG TC

2.13. RNA Extraction

Cell suspensions were centrifuged for 5mins at 5000g, supernatants were removed and lysis buffer was added to the cells. Cells in the buffer solution were passed through a 1mL syringe with a 21gauge needle (BD Microlance), this was repeated 5x, followed by vortexing for approximately 30secs. Lysate was transferred to a genomic DNA eliminator column and centrifuged for 30secs at 8000g. The column was discarded and 70% ethanol was added to the flow through and mixed well by pipetting. The sample was then transferred to an RNeasy spin column and centrifuged for 30s at 10 000g. The flow through was discarded, RWI buffer (washing buffer) was added to the RNeasy spin column, centrifuged for 1min at 10 000g and

flow through was discarded. Another washing buffer (RPE buffer) was added to the RNeasy spin column, centrifuged for 2mins at 10 000g and flow through was discarded. Each washing step was repeated three times. Water was added to the RNeasy spin column, centrifuged for 1 min at 8000g to elute the RNA. RNA was stored at -80°C; gene expression analysis was usually performed within one week of RNA extraction. RNA can be stored in nuclease free water for up to year with no risk of degradation. RNA quantity and quality was measured each time the samples were used and no significant changes were detected.

2.13.1. Determination of RNA Quantity and Purity

The quantity and quality of RNA was measured using a NanoDrop spectrophotometer (ThemoFisher Scientific). Briefly, the NanoDrop was blanked using nuclease free water. 1µL of RNA sample was transferred onto the NanoDrop and the machine was able to give readings for RNA concentration (ng/µL) and A260/A280nm ratio. A260/A280nm ratio was used as an assessment of RNA purity, pure RNA has A260/A280 nm ratio between 1.8 and 2.

2.14. Polymerise chain reaction (PCR)

2.14.1. One-step quantitative PCR

One-step quantitative PCR was used to synthesise and amplify cDNA from RNA (C2C12 cells and hMSCs). The volume of the components required for PCR were set up as shown in Table.2-5. This set up was used for RNA extracted from C2C12 cells. For the amplification of genes related to osteogenesis (RNA extracted from hMSCs) the set up in Tabe.2-6 was used. There was a slight adjustment in the PCR mix set up because with the Quantitect primer assay (osteogenesis related genes) the reverse and forward primers were combined, whereas for muscle related genes the forward and reverse primers were separate. 10µl of the master mix

containing RNA was transferred into a 384well plate before being loaded onto the PCR machine. Amplification was performed for 40 cycles, consisting of reverse transcription at 50°C for 10 minutes, DNA polymerase activation at 95°C for 5 minutes, denaturation at 95°C for 10 seconds and annealing/extension at 60°C for 30 seconds. Melting curves were generated to distinguish and exclude non-specific amplifications and primer dimers. Cycle-threshold (Ct) values were analysed by the comparative Ct (ΔΔCt) method. Ct value of each sample was normalised with the average Ct value of the housekeeping gene.

Table.2-5. Components of PCR mix (C2C12 cells)

Reagent	**Volume per reaction (µl)**
2x Quantifast SYBR green	4.7
Forward primer (100µM stock)	0.1
Reverse Primer (100µM stock)	0.1
Quantifast RT mix	0.1
RNA diluted in water (µl)	5
Total	10

Table.2-6. Components of PCR mix (hMSCs)

Reagent	Volume per reaction (µl)
2x Quantifast SYBR green	4.7
Quantitect primer assay	0.1
Quantifast RT mix	0.2
RNA diluted in water(µl)	5
Total	10

2.14.2. Two-step quantitative PCR

Two-step quantitative PCR was used to first synthesize and amplify cDNA (RAW and THP-1 cells). Briefly, RNA and water were transferred into a 0.2mL PCR tube and then loaded to the PTC-100TM (MJ Research INC.) cycling machine. SuperScript III first-strand synthesis system (Invitrogen, Life Technologies) was used for the reverse transcription of RNA into cDNA per manufacturer's protocol. Briefly, the cycler was heated up to 65^{o}C for 5mins (denaturing), then down to 25^{o}C. cDNA synthesis mix was then added to the tubes containing RNA and cycler was held at 25^{o}C for 5mins (annealing). The cDNA was then synthesized at 50^{o}C for 60mins followed by an increase to 70^{o}C for 15mins to terminate the reaction and the resultant cDNA was stored at -20°C. The cDNA samples were diluted 1:20 with Milli Q water (Merk Millipore) and added to a 384well plate. TaqMan universal master mix (ThermoFisher Scientific) was also added to the plate (see Table.2-7). The plate was spun at 200g for 1min and then loaded on to the real-time PCR machine (QuantStudio 12K Flex). Amplification was performed for 40 cycles, DNA polymerase activation at 95°C for 10mins, denaturation at 95°C for 15 seconds and annealing/extension at 60°C for 1min. Ct values were analysed by using

the ΔΔCt method. Ct value of each sample was normalised with the average Ct value of the housekeeping gene. The PCR run was repeated twice.

Table.2-7. Components of PCR mix (RAW and THP-1 cells)

Reagent	Volume per reaction (µl)
Taqman master mix	5
18S (endogenous control)	0.5
Gene of interest	0.5
MilliQ water	2
cDNA (1:20)	2
Total:	10

2.15. Alkaline phosphatase activity assay

hMSCs were seeded onto a 24well plate at density of $1x10^4$ cells/well. Cells were incubated in MSC growth medium until 90% confluent. The MSC growth medium was then replaced with Mg/Mg-Ca filtered medium or non-filtered medium (DMEM) supplemented with 10% (v/v) FBS, L-glutamine final media concentration 2mM and 100units/ml penicillin-streptomycin and cultured for a period of 12 days. Cells cultured in MSC growth medium were used as the standard control and cells cultured in osteogenic medium were used as the positive control. ALP assay was performed at day 2, 7 and 12 using p-Nitrophenyl Phosphate (pNPP) Liquid Substrate System, (Sigma Aldrich, UK). Briefly, cells were lysed in 0.1% v/v Triton X-100; pNPP solution was added to each well and the plate was incubated in the dark for approximately 30 minutes at room temperature. The production of p-nitrophenol (PNP) was quantified at an

absorbance of 405 nm using a plate reader (VaioSkan Flash, ThermoScientific) and normalised to DNA concentration, using the PicoGreen assay.

2.16. Mature Myotube Actin Filament Staining

Glass cover slips were treated with gelatin (Sigma Aldrich, UK) for 30 minutes before cell culture, to allow for attachment of cells to the surface. Cells were seeded on the cover slips in a six well plate at a seeding density of 100 000 cells/well. Cells were cultured in C2C12 growth medium until confluent. Once the cells were confluent C2C12 growth medium was switched to C2C12 differentiation medium for the fusion of myoblast into myotubes. After 3 days in differentiation medium mature myotubes were formed then medium was changed and cells were cultured in Mg/Mg-Ca filtered and non-filtered medium (Hyclone DMEM) supplemented with 7% (v/v) FBS and 100units/ml penicillin-streptomycin for a further 3 days. After 3 days in Mg/Mg-Ca conditioned media cells were fixed with 2% formaldehyde (Sigma Aldrich, UK) for 30 minutes. Fixed cells were washed with PBS 3x and then treated with 0.2% Triton-X-100 and 5% goat serum in tris-buffered saline (TBS) for 5mins. Fixed cells were washed 3 times in PBS and then treated with rhodamine phalloidin (Life Technologies) diluted 1:40 in PBS. 0.1% DAPI was also added to the phalloidin working solution and cells were incubated for 60mins at room temperature in the dark. After incubation, the fixed cells on cover slips were mounted on glass slides for image analysis. The cells were visualised with a fluorescence microscope to determine degree of differentiation.

2.16.1. Quantitative analysis of myotubes

For analytical purposes, a myotube was defined as a cell that stained positive for phalloidin and containing at least 3 nuclei. 21 images for each sample from 3 biological repeats were

analysed. Myotubes treated with Mg/Mg-Ca conditioned media were organized into 4 groups: 3-10 nuclei/myotube (small), 11-50 nuclei/myotube (medium), 51-100 nuclei/myotube (large) and 101-300 nuclei/myotube (extra-large).

2.17. TRAP Staining Assay

TRAP fixative formulation:

- Sodium citrate (0.01 M) 25 mL
- Acetone 65 mL
- 37% v/v formaldehyde 8 mL

RAW cells were seeded onto a 48well plate at density of 2000 cells/well, 8 wells were used for each sample. Cells were incubated in RAW growth medium for 3hours. After 3hours, RAW growth medium was then replaced with Mg/Mg-Ca filtered medium or non-filtered medium (α-MEM) supplemented with 10% (v/v) FBS, L-glutamine final media concentration 2mM and 100units/ml penicillin-streptomycin and 10ng/mL RANK-L. The cells were allowed to differentiate over a culture period of 5 days; medium was changed once on day 3, on day 5 cells were fixed using 200µL of TRAP fixative for 30 seconds and then washed with distilled water. The culture plate was allowed to air dry. Cells were stained for TRAP using a Leukocyte Acid Phosphatase kit (Sigma Aldrich). Briefly, 50µL sodium nitrate and 50µL fast garnet solution were mixed together and left for 2mins at room temperature. The mixture was then transferred to a tube containing 4.5 ml water. 50µL of naphol phosphoric acid solution, 200µL acetate solution and 100µL of tartrate solution were also added to the water to make up the TRAP staining solution. 200µL of the TRAP staining solution was added to each well and cells

were incubated for 5-10mins in a humidified atmosphere at 37˚C under 5% CO_2. Cells were washed 3x with distilled water and allowed to air dry. Cells from 3 biological repeats were analysed, all cells in each well were counted using an inverted light microscope. Cells that had more than 3 nuclei and stained positive for TRAP were counted as osteoclast cells.

2.18. Immune Response

Human THP-1 cells are monocytic cells derived from peripheral blood of a donor with monocytic leukaemia. These cells can be activated to form mature macrophages. (ATCC, In vitro Technologies, NZ). The cells were resuscitated from cryopreservation in a 37°C water bath and then the cell suspension was transferred into a tube. Cells were centrifuged at 200g for 2mins, supernatant was removed and cells were resuspended in fresh THP-1 growth medium. Cell culture was established with subsequent re-suspension at $4x10^5$ cells/ml. Cells were then subcultured when cell concentration reached $8x10^5$ cells/ml using T75 flask and cultured in a humidified atmosphere at 37˚C under 5% CO_2 for 5 days. 1.5 x 10^6 cells/ml were seeded in each well in triplicate in a 24well plate; 3cm polyglycolic acid suture material (Starmedix, USA), Mg and Mg-Ca pieces were placed in each well. Mg or Mg-Ca disks were cut into four equal smaller pieces before being placed into the 24well plate. Cells cultured without biomaterial contact (untreated cells) were used as the control. Cells were cultured in the presence of biomaterial for 24 hours in a humidified atmosphere at 37˚C under 5% CO_2. After 24hours biomaterials were removed and the cell suspension was transferred into tubes. The tubes were centrifuged and supernatant was removed. RNA was extracted using RNeasy Kit as per manufacturers' instructions for PCR analysis. The cDNA (see section 2.14.2) produced was used for a two-step qRT-PCR process to amplify genes that code for cytokines involved in inflammatory response using a real-time PCR machine (QuantStudio 12K). FAM-labelled

TaqMan assays specific for IL-8, TNF-α and IL-1β and VIC-labelled 18S rRNA endogenous control were used per manufacturers' instructions. The predesigned TaqMan gene assays were supplied by Applied Biosystems. Table.2-8 shows the information on assay design.

Table.2-8: TaqMan Primer Assay Design

Gene name	Species	Accession number
TNF-α	Human	NM_000594.3
IL-1β	Human	NM_000576.2
IL-8	Human	NM_000584.3

2.19. Mature Osteoclast Assay

32 dentin bone slices (supplied by the University of Auckland) were sonicated in distilled water in a sonicator (Wave Energy System, Newtown, PA) for 5-10 min, after air drying the bone slices were numbered using a pencil. The bone slices were sterilized with 70% ethanol for 10mins followed by a rinse in PBS and then RAW growth medium. The slices were placed into 96well plate and 50µl RAW growth medium was added to each of the wells. 2.5ml/well Mg non-filtered medium (RPMI 1640) supplemented with 10% (v/v) FBS, L-glutamine final media concentration 2mM and 100units/ml penicillin-streptomycin at the following concentrations: Mg100, Mg50 and Mg25 was added to a 12 well plate and 2ml of RAW growth medium was added to a glass homogenizer. 96well plate with the bone slices and the 12well plate with Mg non-filtered medium were placed in a humidified atmosphere at 37˚C under 5% CO_2.

2.19.1. Mature osteoclast isolation

Six 2-day-old rats were sacrificed; this was performed at the University of Auckland by an experienced staff member. All the animal work had the approval of the University of Auckland animal ethical committee. The animals were rinsed with 70% ethanol followed by PBS and placed in a clean petri dish. The legs were removed above the hip joint followed by limbs on the shoulder joint. Each limb was rinsed in PBS and placed in a clean petri dish. The skin was gently peeled away from the muscle of each limb. In a separate dish using a scalpel and forceps, the muscle was scraped away to expose the length of bone. Each bone was cut near the epiphyses and then split in half lengthwise and carefully placed inside the glass cell homogeniser containing 2 mL of RAW growth medium. In a sterile cabinet, the bone was crushed with a homogenizer and then chopped up in a 35-mm dish using a scalpel. The osteoclast-rich cell suspension was then transferred to a 15-ml tube. This was repeated 3x to make up the cell suspension to 6mL. The cell suspension was then loaded (150-180µl/well) onto the 96well plate with the bone slices (~9mm^2) in the wells (one bone slice/well) and incubated for 20-30 min in a humidified atmosphere at 37˚C under 5% CO_2. After 30mins the bone slices were rinsed twice with PBS to remove any contaminating non-osteoclast cells and once with the RAW growth medium and then transferred to the previously incubated 12well plate containing various concentrations of Mg non-filtered medium. Cells cultured in MO growth medium were used as the control and cells cultured in MO growth medium with the presence of 9M salmon calcitonin (sCT-9M), (Bachem, Inc. Torrance, CA) were used as the positive control. Salmon calcitonin was used as the positive control because it is an inhibitor of osteoclast resorption activity. The bone slices were incubated for 24hrs in a humidified atmosphere at 37˚C under 5% CO_2. After 24hours, media was removed from the wells, 0.6mL

of formaldehyde fixative was added to each of the wells and left for 30 seconds. Fixative was removed and bone slices rinsed twice with distilled water. The bone slices were stained for TRAP as previously described (2.17). TRAP positive cells were counted and after counting, the cells were removed from the bone slice by gently brushing with a small paint brush to assess the pits excavated by the osteoclasts.

2.19.2. Pit staining

Drops (10µl) of 1% toluidine blue in 1% sodium borax were used to stain the resorption pits on the dentin bone slices. The drops were placed on parafilm, and then bone slices were gently placed on top of the drop floating. The slices were stained for 30 seconds, washed with water and left to air dry. The stained pits were counted using reflected light microscopy and metallurgic lenses (Olympus BH2). Osteoclast activity was calculated: number of pits/number of cells. There were 6 bone slices for each condition and the experiment was repeated three times.

2.20. Live imaging

Live imaging of cells cultured in Mg/Mg-Ca non-filtered medium was performed using the Cell 1Q imagen, a live cell observation and analysis system equipped with a Nikon microscope (TAP Biosystems). Cells were monitored continuously via the Imagen program, whilst the Analyser software was used for cell analysis and quantification. Cells were seeded in a 6 well plate at a density of 60 000 cells/well. The cells were cultured in MSC growth medium for 24 hours to allow for attachment. After 24 hours MSC growth medium was replaced with Mg/Mg-Ca non-filtered medium (DMEM) supplemented with 10% (v/v) FBS, L-glutamine final media concentration 2mM and 100units/ml penicillin-streptomycin. The cells were incubated

in the Cell IQ system at 37°C, and 5% CO_2, under humidified conditions. 3hrs after the cells were placed in the Cell IQ incubator; the images were refocused due to the formation of condensation in the plate. Live imaging was checked often; at least every 3hrs and refocused when necessary. Images were taken at 7 different locations of each well every 10 minutes for 48 hours. Video files were extracted from the images taken and they can be played with any media player application that supports the .wmv file format.

2.21. Transmission electron microscopy (TEM)

TEM analysis was performed to understand the effect of corrosion granule on hMSCs and to verify the presence of Mg at subcellular level. Contrast in electron microscopy depends on the differences in electron density of organic molecules in cells that are being analysed. The atomic weight of the stain attached to the organic structures in the cells determines the efficiency of the stain (Ruwin, 2013). Therefore, heavy metals such as uranium and lead are used as stains in TEM. High contrast TEM images are obtained when uranyl acetate (UA) and lead citrate are used in sequence; this is known as double staining. Uranyl ions bind to proteins, lipids and nucleic acids in the cell, this leads to high contrasting results of membrane, nucleic acids and ribosomes (Ruwin, 2013). Lead citrate enhances contrasting effects for structures such as glycogens, lipid membranes and cytoskeleton; this enhancement effect is also dependant on the interaction with osmium tetroxide (Ruwin, 2013). Osmium tetroxide facilitates the attachment of lead ions to polar groups of molecules, lead citrate also interacts with UA and therefore cells are stained with UA first followed by lead citrate (Ruwin, 2013).

2.21.1. Resin Preparation

Resin was used to embed stained cell pellet for sectioning, the resin was prepared by mixing 25ml Araldite CY212 resin (TAAB Laboratories, UK), 15ml Agar 100 resin (Agar Scientific, UK), 55ml Dodecenyl Succinic Anhydride (DDSA), (TAAB Laboratories, UK), 2ml Dibutyl phthalate (TAAB Laboratories, UK) and 1.5ml Tri-Dimethylaminomethyl Phenol (DMP 30), (TAAB Laboratories, UK) in a fume hood.

2.21.2. Sample preparation

hMSCs were seeded in a 6well plate at a density of 60 000 cells/well. The cells were cultured in MSC growth medium for 24 hours to allow for attachment. After 24 hours MSC growth medium was replaced with Mg/Mg-Ca non-filtered medium (DMEM) supplemented with 10% (v/v) FBS, L-glutamine final media concentration 2mM and 100units/ml penicillin-streptomycin. After 24 and 48 hours, cells were harvested using trypsin and transferred into Eppendorf tubes. 500µL of 3% glutaraldehyde (TAAB Laboratories, UK) in 0.1M cacodylate buffer (fixative) was added to the cell suspension and cells were spun at 200g in a microcentrifuge (Fisher Scientific) for 5mins. After centrifugation, supernatant was removed and cell pellet was resuspended in 1ml fixative and left for 2 hours. After 2 hours, cell suspension was centrifuged as before, fixative was removed and pellet was resuspended in 0.1M cacodylate buffer (TAAB Laboratories, UK), this washing step was repeated 3x. After the washing step, supernatant was removed and pellet was resuspended in 1% v/v aqueous osmium tetroxide for 30 mins (TAAB Laboratories, UK). After osmium tetroxide was removed the pellet was centrifuged as before and resuspended in distilled water for 1min, this step was repeated 5x. On the last washing step, the water was removed after centrifugation and the cell pellet was dehydrated in graded ethanol (TAAB laboratories, UK) series as follows:

- 2 x 10mins 50% v/v ethanol
- 2 x 10mins 70% v/v ethanol
- 2 x 10mins 90% v/v ethanol
- 3 x 15mins 100% ethanol
- 2 x 15mins 100% Propylene Oxide (propox) (TAAB laboratories, UK)

Following dehydration the pellet was infiltrated with resin as follows:

- 2hours in 1:3 resin : propox mix
- Overnight in 1:1 resin : propox mix
- In fresh bottles, 3 x 1.5hours in pure resin

The pellet was then embedded in a BEEM capsule and left in the embedding oven at 60°C for at least 48hours. After 48hours the embedded cell pellet was cut into slices of 500µm using a LeicaUC6-ultramicrotome. The cut samples were then transferred onto water drops held on top of a glass slide. The slide was dried on a hot plate and the 500µm samples on the slide were stained with toluidine blue (Sigma Aldrich, UK) to establish cell presence and quality. Once the presence of cells was established, 90nm thick samples were cut using the ultramicrotome. The samples were then placed on TEM support mesh grids (3mm in diameter) (Agar Scientific) and stained with UA (TAAB laboratories, UK) saturated in 50% v/vethanol for 5mins followed by Reynold's lead citrate (TAAB laboratories, UK) for 5mins. Samples were washed with water followed by 50% v/v ethanol. The grids were placed on sodium hydroxide

pellets (TAAB laboratories, UK) for the absorption of CO_2 (to prevent precipitation of lead carbonate). Samples were left at room temperature until imaging.

2.22. TEM imaging

For TEM analysis two instruments were used, 2000 FX TEM (JEOL, USA) (Loughborough University) *and* Tecnai BioTwin-12 TEM (FEI, USA) (Nottingham University). JEOL 2000FX TEM was accelerated at 100kV and bright field images were recorded in conventional TEM mode. Tecnai BioTwin-12 TEM was accelerated at 100kV and bright field images were taken using gatan SIS megaview IV digital camera. Three grids containing cell samples from each condition were analysed. Individual hexagons within the grid were chosen randomly and cells within the hexagon were analysed (Fig.2-1). At least 9 images were taken for each condition at different magnifications. The images represent general subcellular features for each condition.

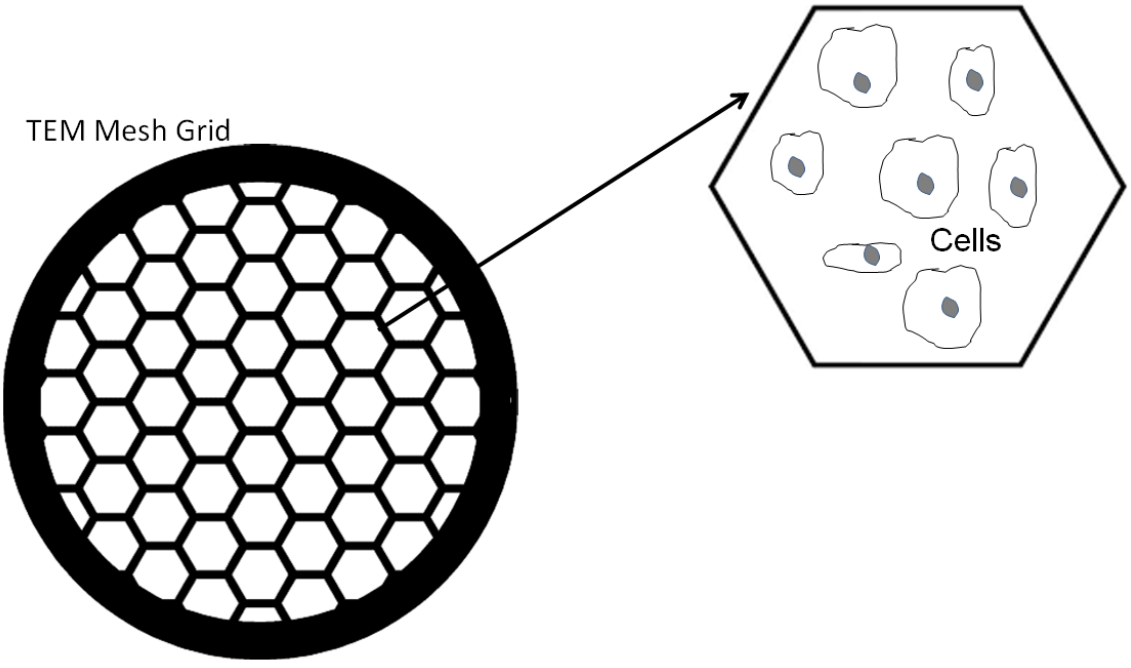

Fig.2-2. Stained cells on a TEM mesh grid. The above figure is showing how cells were prepared for TEM imaging and analysis.

2.23. Fluorescence Microscopy

A Leica DMIRB inverted microscope was used in conjunction with COHU CCD camera and Leica imaging software to capture images of stained myotubes. 7 images for each of the concentrations for Mg/Mg-Ca conditioned medium were taken.

2.24. Light Microscopy

Cell cultures were viewed using an inverted microscope (Olympus CKX41) in conjunction with QIMAGING system and QC capture Pro 6.0 to capture and analyse images of cells. Furthermore, the microscope was used to assess the degree of confluency and confirm the absence of bacterial and fungal contaminants.

2.25. Statistical Analysis

Statistical analysis was performed using SPSS software (IBM,USA), multivariate analysis of variance and One-way ANOVA, including Tukey's post hoc tests, were performed to detect significant ($p<0.05$) effects of the experimental variables.

2.26. Chemical analysis of magnesium corrosion products

2.26.1. ICP-OES analysis of Mg and Mg-Ca conditioned media

ICP-OES was used to measure the amount of Mg and Ca ions following the degradation of Mg and Mg-Ca disks in culture medium. As indicated in Table 2-9 and 2-10, the concentration of calcium ions in Mg100 conditioned media was depleted during the corrosion process. As a result, the concentration of calcium ions in Mg100 conditioned media was half the amount present in the control. But as the conditioned media was diluted to Mg50, Mg25 and Mg10

the calcium ions were replenished by the addition of fresh medium and the Ca/Mg ratio also increased. The dilution of the conditioned media also resulted in the reduction of Mg ion concentration. It is believed that during the corrosion of Mg metal or Mg alloys, calcium phosphates are formed through the consumption of calcium and phosphate ions from the surrounding medium, resulting in a calcium depleted medium. The formation of calcium phosphates such as hydroxyapatite from Mg corrosion processes is established, with previous studies highlighting the importance of the oxide phase in hydroxyapatite formation (Witte *et al.*, 2005; Li, Z *et al.*, 2008; Li *et al.*, 2014).

Table.2-9: Concentration of calcium and magnesium ions in the conditioned media following the corrosion of pure magnesium in DMEM for the culture of hMSCs and mature myotubes.

Ion concentration (mean ±SD)			
Sample	**Ca (mM)**	**Mg (mM)**	**Ca: Mg**
Mg100	0.8±0.2	16. 9±1.1	0.05
Mg50	1.2±0.2	10.8±1.2	0.1
Mg25	1.5	4.9±0.4	0.3
Mg10	2.1±0.7	3.1±0.7	0.7
Control	2.2±0.6	0.9±0.2	2.0

Table.2-10: Concentration of calcium and magnesium ions in the conditioned media following the corrosion of pure magnesium in α-MEM for the culture of RAW cells and mature osteoclast cells.

Ion concentration			
Sample	**Ca (mM)**	**Mg (mM)**	**Ca: Mg**
Mg100	1.0	11.0	0.1
Mg50	2.0	6.4	0.3
Mg25	1.7	3.0	0.6
Mg10	2.0	1.7	1.0
Control	3.2	1.4	2.0

The alloying of pure Mg with 1% calcium results in a slower corrosion rate (Li *et al.*, 2008; Harrison *et al.*, 2014); Mg-Ca alloy corrodes slower than pure Mg leading to less Mg ions being released into the medium. Table 2-11 shows that after 72 hours of corrosion in culture medium, the highest concentration of Mg ions detected in Mg-Ca100 conditioned medium (3.9mM) was 4x less the concentration detected in Mg100 conditioned medium (16.9mM). As observed with pure Mg corrosion, the corrosion of Mg-Ca also resulted in the depletion of calcium from the medium. The Ca/Mg ratio of Mg100 conditioned medium (0.05) was 10x less compared to Mg-Ca100 conditioned medium (0.5). However, when Mg-ca disk was immersed in α-MEM for osteoclast culture, the corrosion behaviour was similar to that of pure Mg disk resulting in similar amounts of corrosion products (Mg ion and corrosion granule) being released from both Mg and Mg-Ca (Table 2-10 and 2-12). For most of the studies the metal disks used came from the same batch and their corrosion behaviour was consistent each time. However, for one part of the study a new batch of Mg and Mg-Ca were used, although they were prepared using the same method as the previous batches, it's not clear

why the batch of Mg-Ca disk used in the particular study behaved as observed, possibly this was due to contamination with impurities during the manufacturing process. As mentioned in section 1.2, the presence of impurities can lead to the formation of second phases that act as internal cathodes with the ability to form micro-cells with the anodic magnesium matrix, resulting in severe galvanic corrosion.

Table.2-11: Concentration of calcium and magnesium ions in the conditioned media following the corrosion of Mg-Ca in DMEM for the culture of hMSCs and mature myotubes.

Ion concentration (mean ±SD)			
Sample	**Ca (mM)**	**Mg (mM)**	**Ca:Mg**
MgCa100	1.9±0.3	3. 9±0.7	0.5
MgCa50	1.7±0.1	2.4±0.6	0.7
MgCa25	1.7±0.3	1.6±0.5	1.0
MgCa10	2.2±0.4	1.2±0.2	2.0
Control	2.2±0.6	0.9±0.2	2.0

Table.2-12: Concentration of calcium and magnesium ions in the conditioned media following the corrosion of Mg-Ca in α-MEM for the culture of RAW cells and mature osteoclast cells.

Ion concentration			
Sample	**Ca (mM)**	**Mg (mM)**	**Ca:Mg**
Mg-Ca 100	0.7	14.4	0.05
Mg-Ca 50	1.4	6.8	0.2
Mg-Ca 25	1.9	4.2	0.5
Mg-Ca 10	2.1	2.1	1.0
Control	3.2	1.4	2.0

2.26.2. SEM and EDX analysis of Mg corrosion granule

To gain a better understanding of the corrosion process methods of chemical and elemental analysis were applied. Fig 2-3 is showing the EDX analysis of Mg corrosion granule after 72hours corrosion in culture medium. EDX analysis reveals the elemental composition of the sample which was found to be C-16%, O-57%, Mg-14%, P-5%, Ca-8%. A ratio of 1.61 Ca/P was derived from the EDX data (Table 2-13). A Ca/P ratio between 1.5 and 1.67 is indicative of calcium deficient hydroxyapatite (Ca/P ratio =1.67) (Wang & Nancollas, 2009; Berzina-Cimdina & Borodajenko, 2012).

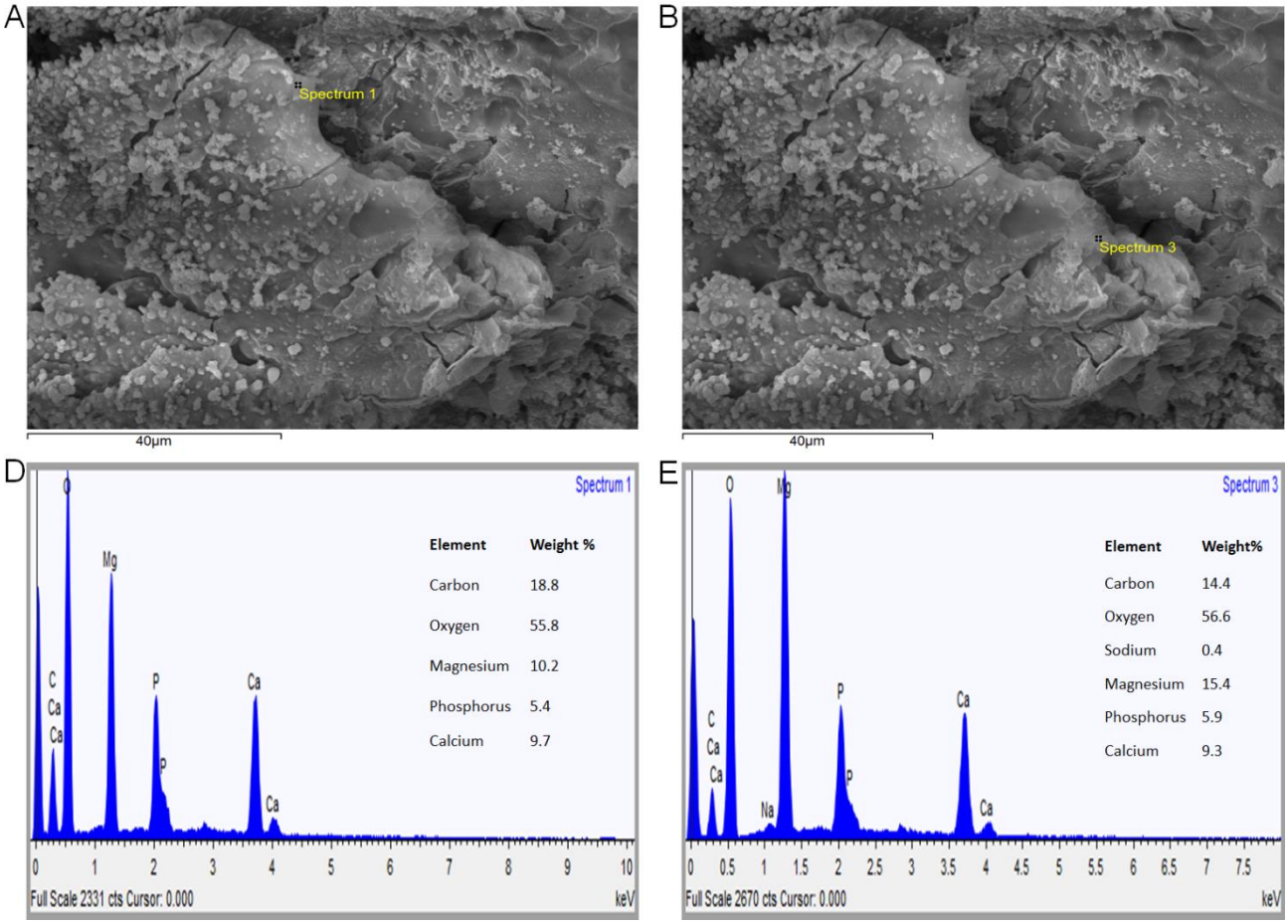

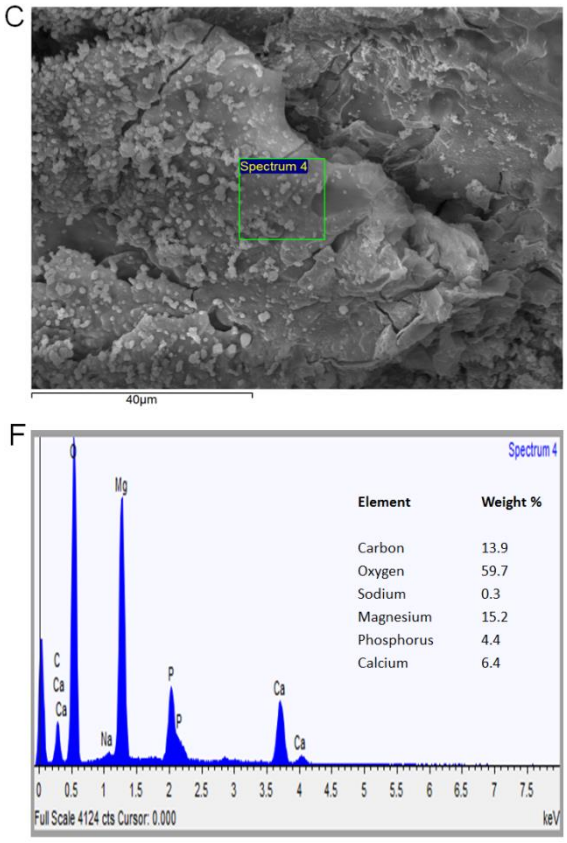

Fig.2-3. Chemical analysis of the Mg corrosion granulae after 3 days of corrosion in growth medium under culture conditions. (**A-C**) SEM analysis of Mg corrosion granule and (**D-F**) corresponding EDX spectra of Mg corrosrion granule.

Table 2-13: Average EDX spectra (Spectra 1, 3 and 4) for the chemical analysis of Mg corrosion products.

EDX spectra (mean±SD)	
Element	Weight %
Carbon	16±3
Oxygen	57±2
Magnesium	14±3
Phosphorus	5±0.7
Calcium	8±2

CHAPTER 3: Magnesium corrosion products and the *in vitro* effects on hMSCs metabolic activities

3.1. The response of hMSCs to media conditioned with pure Mg metal

AlamarBlue assay was used to measure hMSCs viability following exposure to Mg/Mg-Ca conditioned media. The assay measured metabolic activity of cells and was performed over a period of 7 days (section 2.10). Pico green assay was also performed to measure the DNA concentration/cell number over a period of 7 days (section 2.11). The assay was performed following culture in Mg/Mg-Ca conditioned media. AlamarBlue and Pico green assay were performed on days 1, 3 and 7.

Fig.3-1 is showing the metabolic activity of cells following culture in the presence of various concentrations of Mg conditioned media. Metabolic activity was above 70% in comparison to the control for all the concentrations (filtered and non-filtered medium) at each time point. Thus it was identified that hMSCs were able to tolerate Mg concentrations up to 17 times greater (16.9mM) than those typically found in serum (0.70-1.0mM). Even in the presence of corrosion granules (non-filtered medium) metabolic activity was ≥ 70%; however, a decrease in metabolic activity on day 3 and day 7 was observed when cells were cultured in Mg100 non-filtered medium compared to the control. On the other hand, cells cultured in Mg25 filtered medium showed an increase in metabolic activity compared to control on day 7.

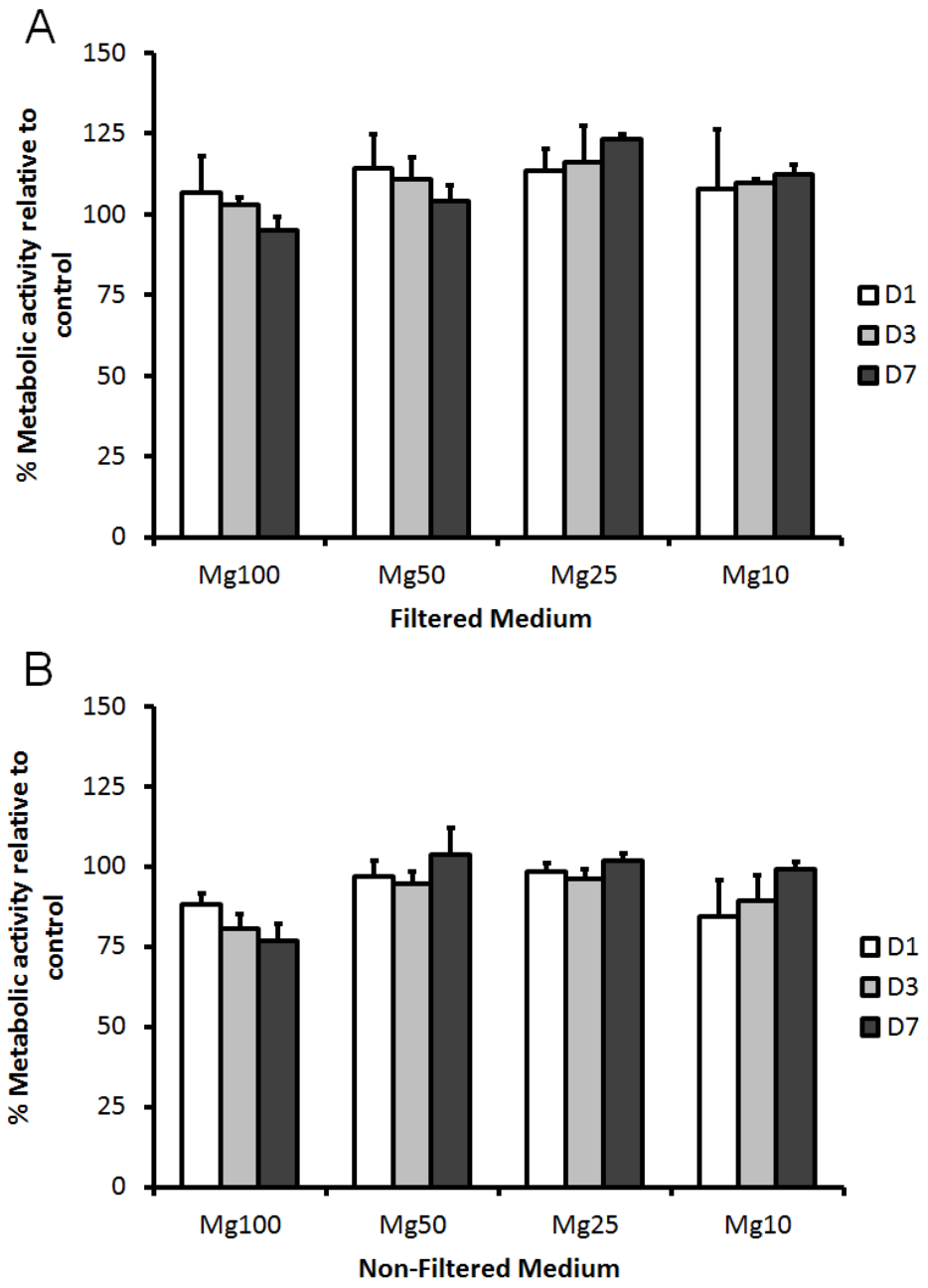

Fig.3-1. **Effect of Mg conditioned media on hMSCs metabolic activity.** The effect of varying Mg conditioned media concentration on hMSCs was investigated over a period of 7 days. Alamar blue reduction was used as an indication of metabolic activity for cells cultured in (**A**) filtered medium and (**B**) non-filtered medium. Metabolic activity was above 75% for all the conditions with the exception of Mg100 condition, where it proved to be highly toxic. The metabolic activity was normalised to the control condition (100% viability). The bars

represent the mean and standard deviation in the positive orientation of three independent experiments, each with n=3.

To further understand the effect of conditioned media on cell proliferation, DNA concentration analysis was also performed to quantify the change of cell number and hence, cell death or growth (Fig 3-2). When cells were cultured in filtered medium they were able to proliferate over time (day1 -7), no cytotoxicity effects were detected. DNA concentration was ≥70% when cells were cultured in filtered media over the 7-day culture period. On the other hand, the presence of corrosion granules significantly affected cell proliferation. Furthermore, DNA concentration of cells cultured in Mg100 non-filtered medium significantly dropped ($p<0.001$) from day 1 in relation to the control to below the cytotoxicity threshold by day 7 (Fig 3-2); an indication that longer exposure to high concentrations of corrosion granules is detrimental to cells. Indeed, the dilution of Mg100 non-filtered medium to Mg25 and Mg10 alleviated the cytotoxicity effects, resulting in a significant ($p<0.001$) increase in DNA concentration.

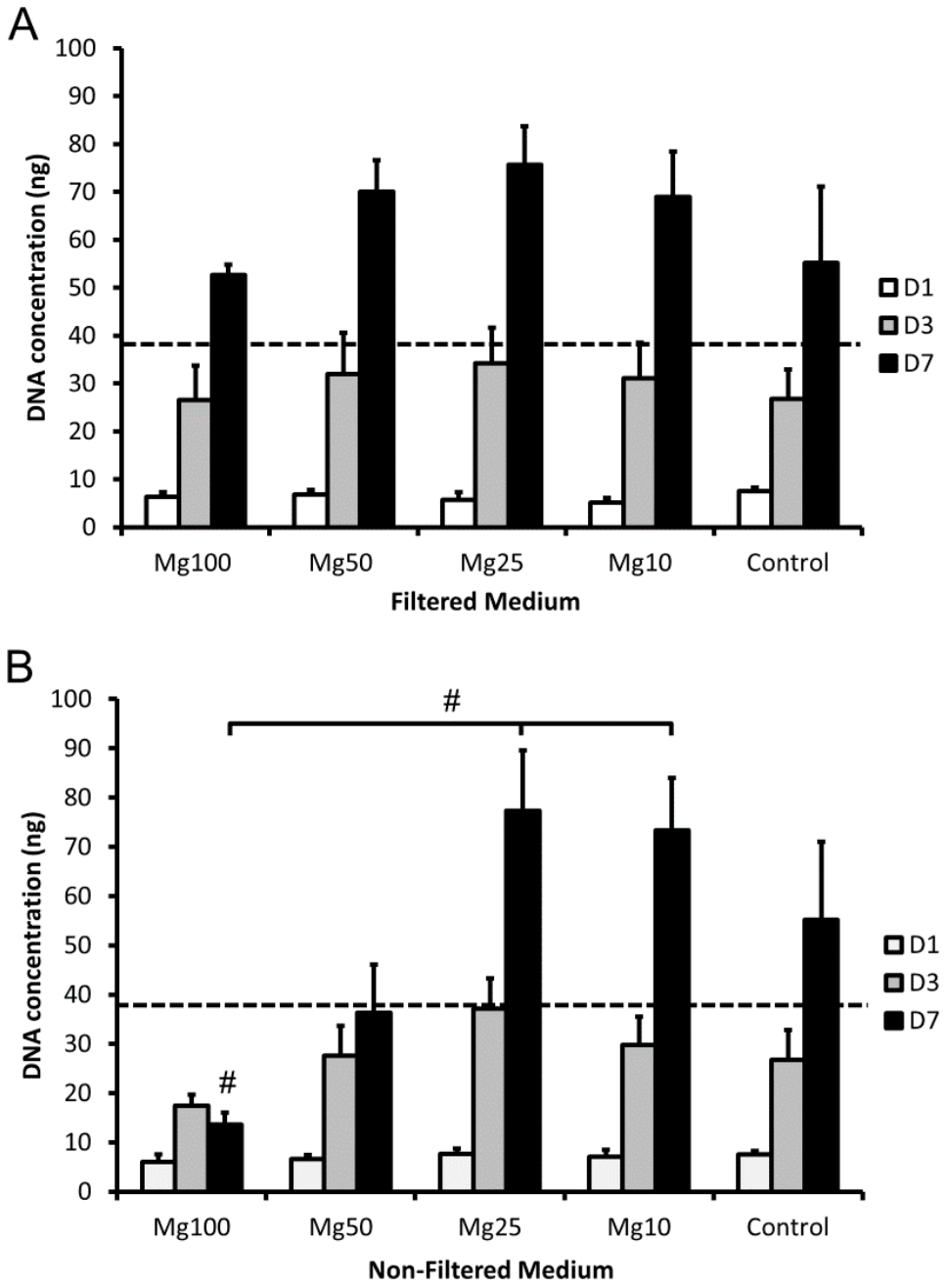

Fig.3-2. **Effect of Mg conditioned media on hMSCs DNA concentration.** DNA concentration was measured using Pico green assay and was used as an indication of cell proliferation. (**A**) Cells cultured in filtered were able to proliferate over time and no evidence of cytotoxicity effects was detected. (**B**) When cells were cultured in Mg100 non-filtered medium there was a significant decrease (#, $p < 0.001$) in DNA concentration at day 7 compared to the control. However dilution of Mg100 non-filtered medium to Mg25 and Mg10 non-filtered medium

resulted in a significant increase (#, $p < 0.001$) in DNA concentration. The dotted line represents the DNA concentration equivalent to 70% viability at day 7 (cytotoxicity threshold). The bars represent the mean and standard deviation in the positive orientation of three independent experiments, each with n=3.

The effect of Mg conditioned media on individual cells was also investigated; this meant evaluating the metabolic activity relative to the DNA concentration. When cells were cultured in filtered medium, metabolic activity/DNA concentration decreased over time relative to control. Metabolic activity/DNA was higher than the control on day 1 but by day 7 the activity reduced to levels lower than the control. Moreover, on day 7 a reduction in metabolic activity/DNA concentration was observed when cells were cultured in Mg100 and Mg50 filtered medium compared to the control (Fig.3-3A). On the other hand, when cells were cultured in non-filtered medium, metabolic activity/DNA concentration remained constant over time with the exception of Mg100 and Mg50 on day 7. Interestingly, an increase in metabolic activity/DNA concentration in the presence of Mg100 and Mg50 non-filtered medium was observed on day 7 compared to the control (Fig.3-3B).

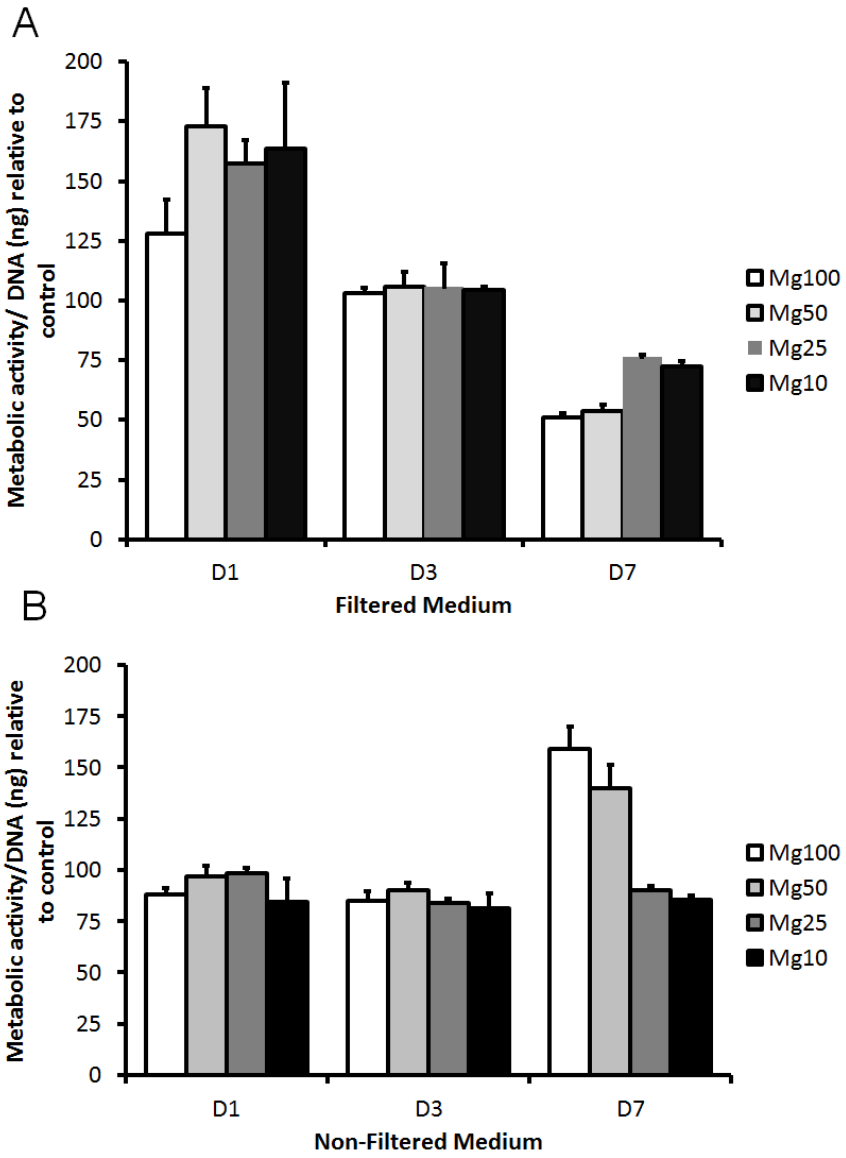

Fig.3-3. **Effect of Mg conditioned media on metabolic activity/DNA concentration.** The effect of varying Mg conditioned media concentration on metabolic activity relative to DNA concentration over a period of 7 days: (**A**) cells cultured in filtered medium and (**B**) cells cultured in non-filtered medium. Metabolic activity/DNA concentration represented relative to the control (100%). The bars represent the mean and standard deviation in the positive orientation of three independent experiments, each with n=3

To further understand the effect of non-filtered medium on cell behaviour, live imaging was performed. Representative images of the cells exposed to medium containing corrosion granules are presented in (Fig.3-4). In the presence of Mg corrosion granules (Mg50), cells were seen migrating to the granules and forming nodules (Fig.3-4 A-C). The cells were still able to maintain viability and proliferate over time in the presence of the corrosion granule. However, high concentrations of corrosion granule (Mg100) resulted in a lower proliferation rate compared to Mg50; no formation of cell nodules was observed at 48 hours (Fig.3-8D-F). Cells cultured in the presence of Mg50 non-filtered appeared to have typical MSC morphology. The cells had a small cell body with thin and long cell processes. On the other hand, the cells cultured in Mg100 non-filtered medium appeared to have thinner cell processes compared to control. At 48hrs, Mg50 non-filtered medium had the highest cell density followed by control with Mg100 non-filtered medium having the lowest cell density.

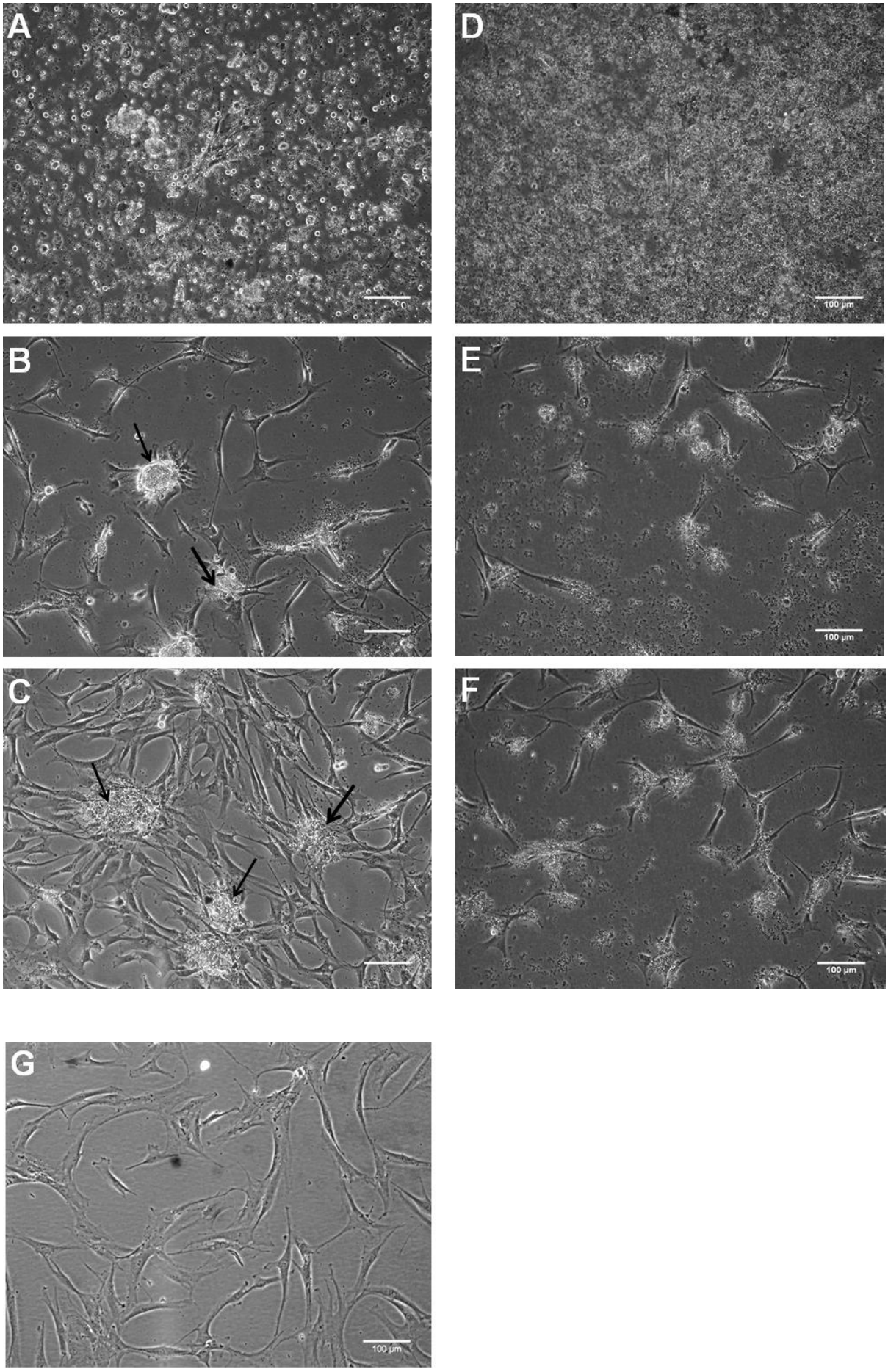
A
D
100 µm
B
E
100 µm
C
F
100 µm
G
100 µm

Fig.3-4. **Effect of Mg conditioned media on cell viability.** Representative images taken using Cell IQ live imaging system showing cells cultured in non-filtered medium (Mg50) at (**A**) 0hrs (**B**) 24hrs and (**C**) 48 hrs and (Mg100) at (**D**) 0hrs (**E**) 24hrs and (**F**) 48 hrs. (**G**) Image shows cells cultured in standard growth medium (control) at 48hrs. Scale bar=100µm arrows indicate the presence of cell nodules.

3.2. The response of hMSCs to media conditioned with Mg-Ca alloy

When cells were cultured in Mg-Ca conditioned media, no evidence of cytotoxicity was seen, metabolic activity was above the cytotoxic threshold (70%) for all the conditions (Fig.3-5). The low concentration of corrosion granules in Mg-Ca conditioned media did not have any adverse effects on metabolic activity. In fact, an increase in metabolic activity was observed when cells were cultured in the presence of MgCa50 and MgCa25 non-filtered medium compared to control (Fig.3-5B). There were no differences between the various Mg-Ca conditioned media (filtered and non-filtered) concentrations.

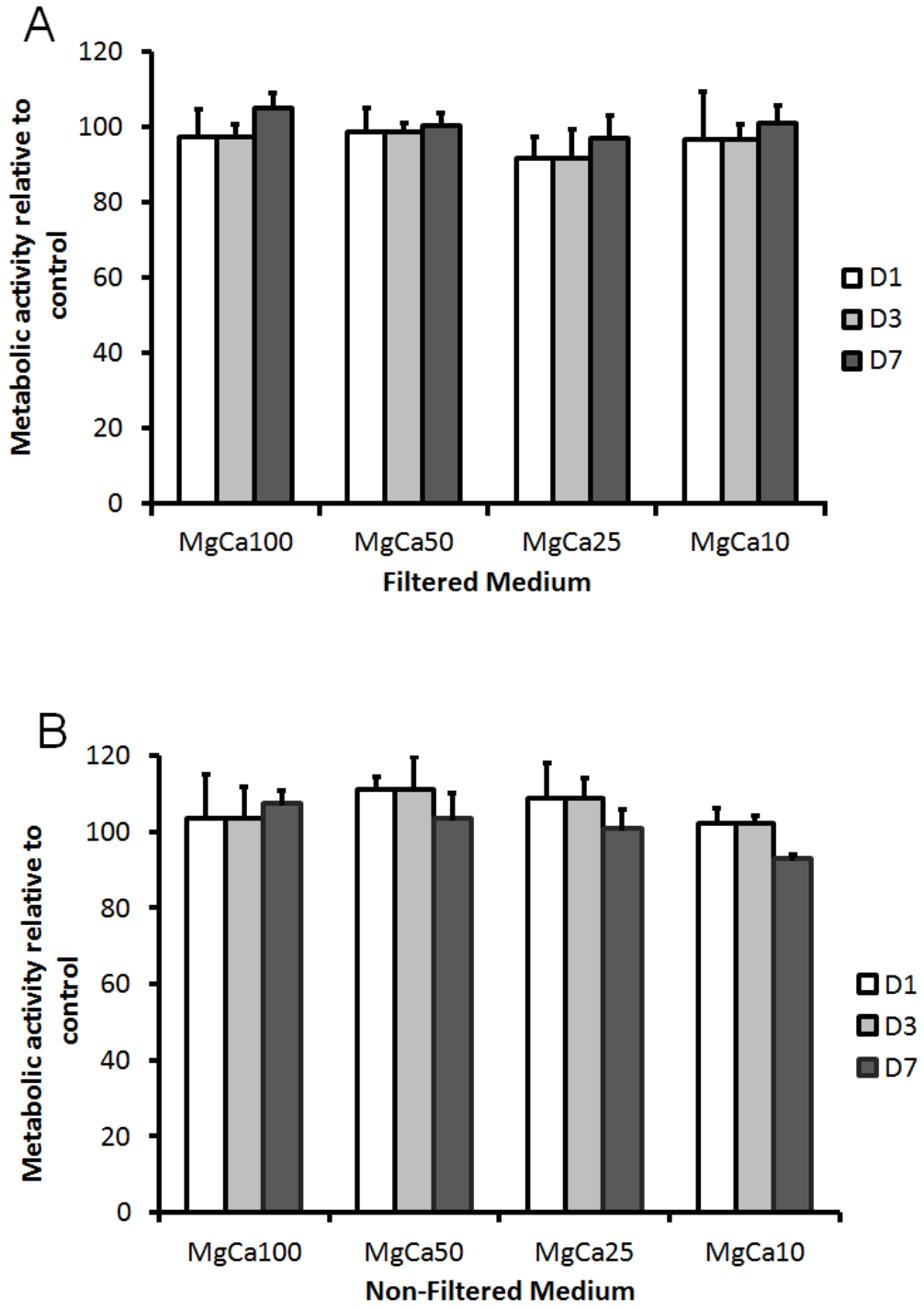

Fig.3-5. Effect of Mg-Ca conditioned media on hMSCs metabolic activity. The effect of varying Mg-Ca conditioned media concentration on hMSCs metabolic activity was investigated over a period of 7 days. Alamar blue reduction was used as an indication of metabolic activity for cells cultured in (**A**) filtered medium and (**B**) non-filtered medium. The

metabolic activity was normalised to the control condition (100% viability). The bars represent the mean and standard deviation in the positive orientation of three independent experiments, each with n=3

Cells were also able to proliferate over time in the presence of Mg-Ca conditioned media (filtered and non-filtered), DNA concentration levels were above 70% the level of the control (cytotoxicity threshold) (Fig.3-6). DNA concentration was higher than the control for most of the conditions throughout the culture period, with the exception of MgCa10 non-filtered medium on day 7. On day 7, a significant reduction ($p < 0.05$) in DNA concentration was observed with MgCa10 compared to MgCa100 non-filtered medium, however DNA concentration was still above the cytotoxicity threshold and no significant difference was detected between Mg-Ca10 non-filtered medium and control (Fig.3-6).

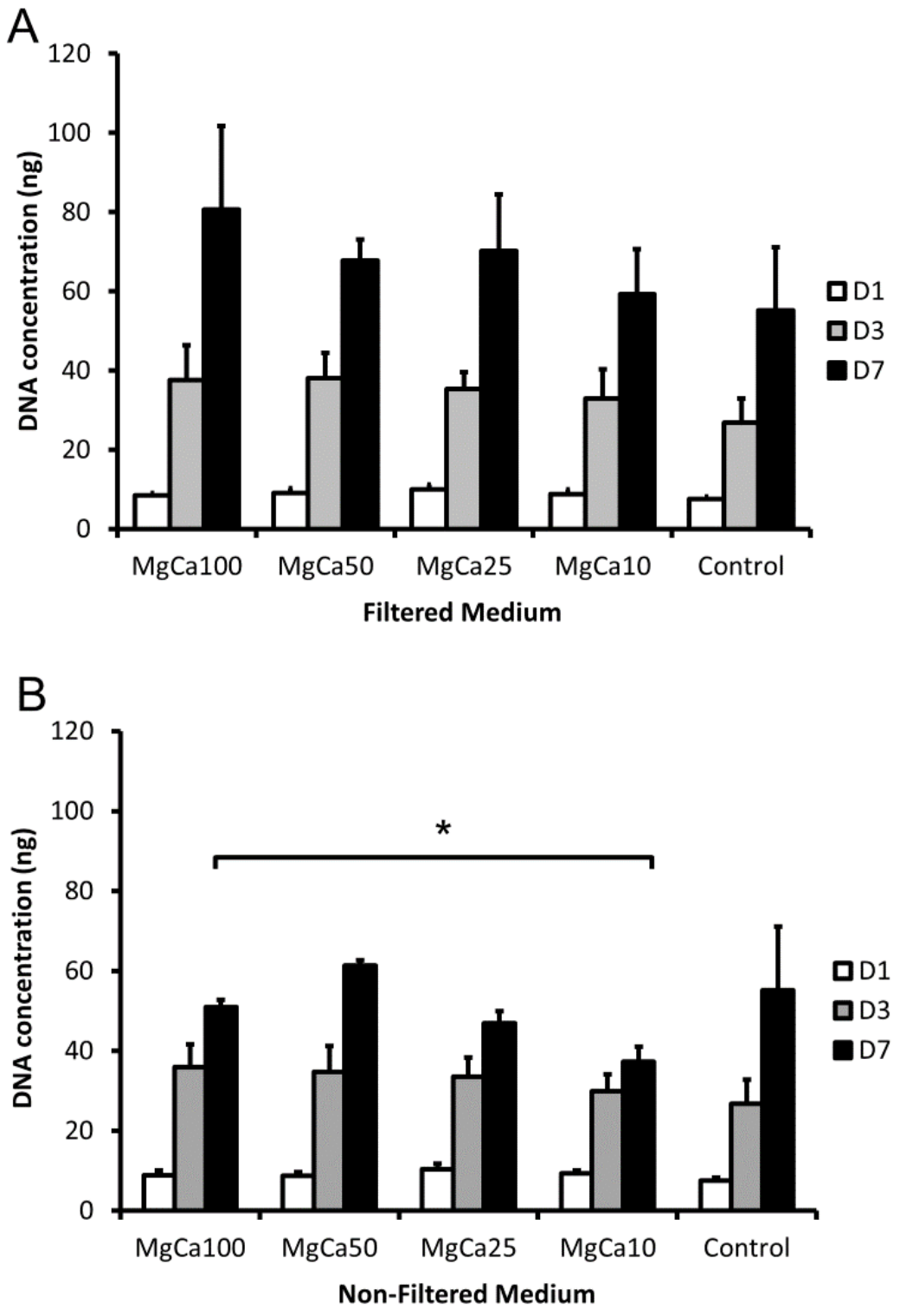

Fig.3-6. Effect of Mg-Ca conditioned media on hMSCs DNA concentration. DNA concentration was measured using Pico green assay and was used as an indication of cell proliferation. (**A**) Cells cultured in filtered were able to proliferate over time and no evidence

of cytotoxicity effects was detected. (**B**) When cells were cultured in MgCa100 non-filtered medium there was a significant decrease (*, $p < 0.05$) in DNA concentration at day 7 compared to MgCa10 non-filtered medium, however DNA concentration was still above the cytotoxic threshold. The bars represent the mean and standard deviation in the positive orientation of three independent experiments, each with n=3.

In the presence of Mg-Ca filtered medium the metabolic activity/DNA concentration was comparable to the control on day 1 for all concentrations. There were no significant differences between the different concentrations. By day 3, the metabolic activity had reduced for all concentrations in comparison to the control and remained reduced until day 7. However, an increase in metabolic activity/DNA concentration was observed when cells were cultured in MgCa10 filtered medium compared to MgCa100 filtered medium on day 7 (Fig.3-7A). This suggests that small changes in Mg ion concentration significantly affect the metabolic activity/DNA concentration. The metabolic activity/DNA concentration was also reduced over time for all concentrations when cells were cultured in the presence of Mg-Ca non-filtered medium. It was noted that on day 7 the dilution of MgCa100 non-filtered medium to MgCa50 resulted in a reduction in metabolic activity/DNA concentration.

Formation of cell nodules was also observed similar to those observed when cells were cultured in Mg conditioned media (Fig 3-8). In the presence of low corrosion granules (MgCa100), cells were also able to migrate to the corrosion granules and were still able to proliferate over time. Cells appeared to have typical MSC morphology and at 48hrs density was higher for Mg-Ca treated cells compared to control.

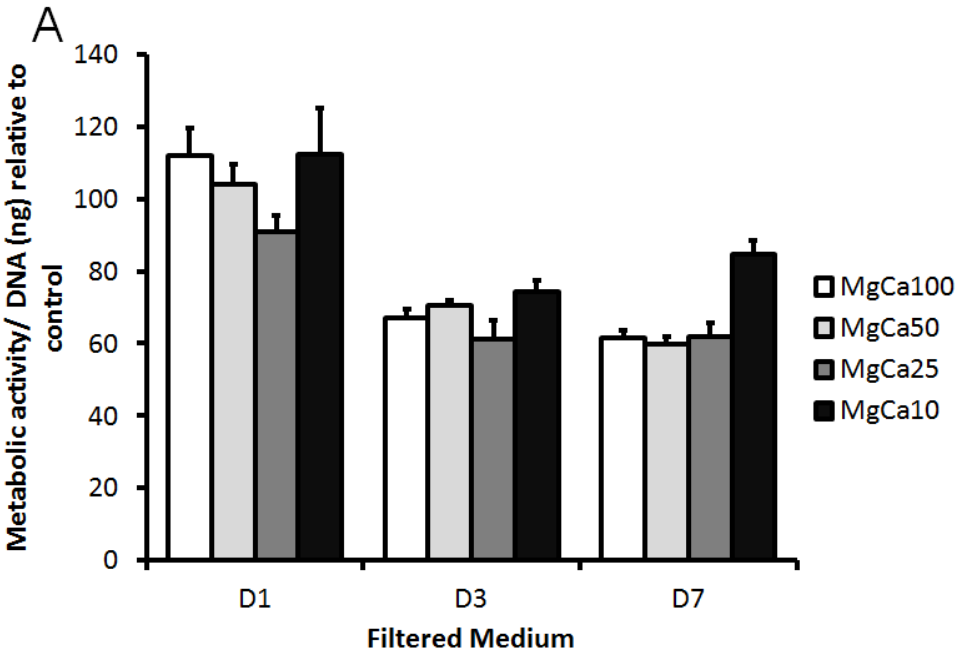
A
Metabolic activity/ DNA (ng) relative to control
140
120
100
80
60
40
20
0
D1
D3
D7
Filtered Medium
MgCa100
MgCa50
MgCa25
MgCa10

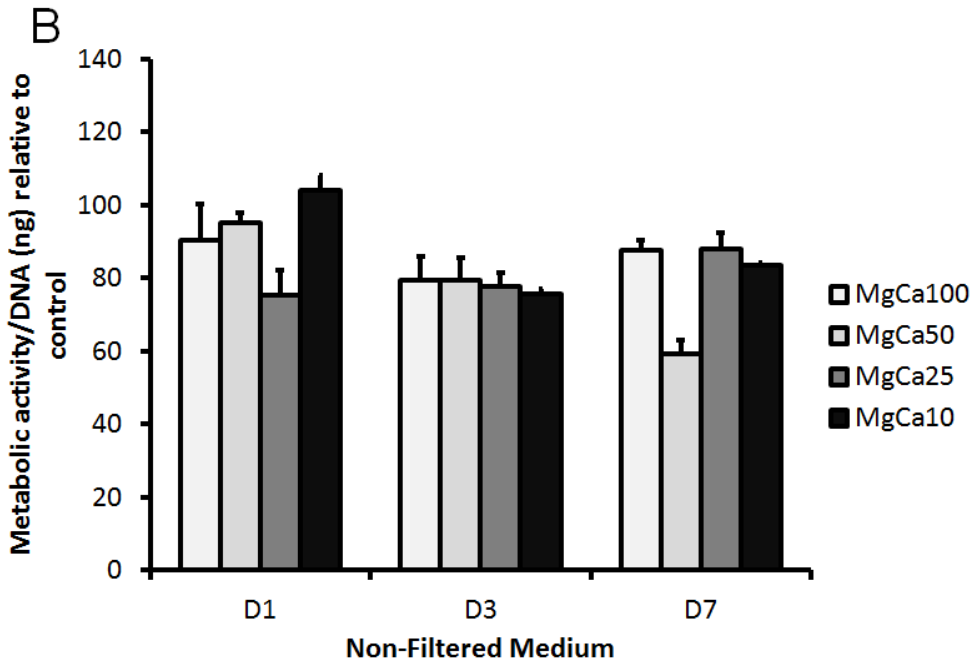
B
Metabolic activity/DNA (ng) relative to control
140
120
100
80
60
40
20
0
D1
D3
D7
Non-Filtered Medium
MgCa100
MgCa50
MgCa25
MgCa10

Fig.3-7. Effect of Mg-Ca conditioned media on metabolic activity/DNA concentration. The effect of varying Mg-Ca conditioned media concentration on metabolic activity relative to DNA concentration over a period of 7 days: (**A**) cells cultured in filtered medium and (**B**) cells cultured in non-filtered medium. Metabolic activity/DNA concentration represented relative to the control (100%). The bars represent the mean and standard deviation in the positive orientation of three independent experiments, each with n=3.

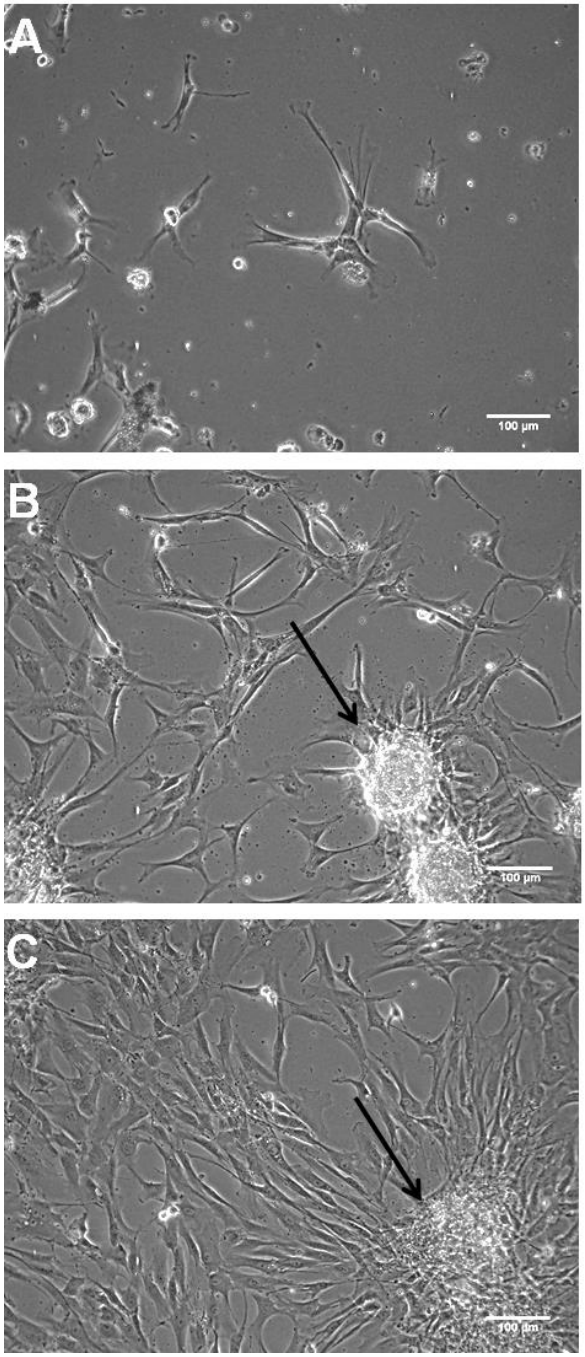
A
100 µm
B
100 µm
C
100 µm

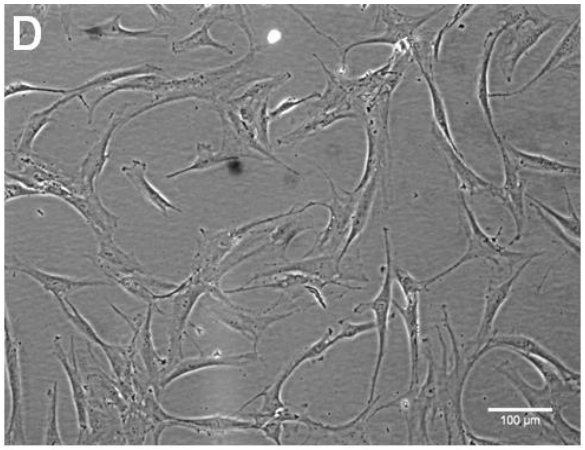

Fig.3-8. Effect of Mg-Ca conditioned media on cell viability. Representative images taken using the Cell IQ live imaging system showing cells cultured in non-filtered medium (MgCa100) at (**A**) 0hrs, (**B**) 24hrs and (**C**) 48 hrs. (**D**) Image shows cells cultured in standard growth medium (control) at 48hrs. Scale bar=100µm, arrows indicate the presence of cell nodules.

3.3. TEM analysis of cells treated with Mg and Mg-Ca conditioned medium

TEM analysis was performed to understand the effect of corrosion granules on hMSCs and to verify the presence of Mg at subcellular level. hMSCs were cultured in the presence of Mg/Mg-Ca non-filtered medium for 24 and 48 hours; following culture cells were fixed and prepared for TEM analysis. Fig.3-9A shows cells cultured in standard growth medium (the control), the cells appeared to have normal morphology; cell membrane appeared intact, mitochondria and rough endoplasmic reticulum (ER) structures were not altered. After treatment with Mg-Ca100 non-filtered conditioned media for 24 hours, significant blebbing at the surface of the cell was observed. A lot of elongated and round mitochondria filled with electron dense material and clear cristae, and ER with moderately dilated cisternae were also present within the treated cell compared to the control (Fig.3-9B). After 48 hours the nucleus was still intact but with an irregular shape and deep invaginations. The cells became more vacuolated with electron dense filled vacuoles scattered within the cytoplasm (Fig.3-10A). More mitochondria were visible and appeared to be located near the vacuoles (Fig.3-10B). Similar morphology was also seen when cells were cultured in the presence of Mg50 non-filtered conditioned medium, the nucleus shape was irregular, there was a lot of vacuoles scattered within the cell (Fig.3-12A). Following treatment with Mg/Mg-Ca non-filtered medium the nucleus of the cells appeared more irregular with deep invaginations.

In this study different types autolysosomes were observed; at 48 hours the presence of these lysosomes was higher compared to the control cells (Fig.3-11A). Cup-shaped autolysosomes that were possibly derived from the endoplasmic reticulum were seen when cells were treated with corrosion granule (Fig.3-11B). These types of lysosomes appeared towards the periphery of the cell and near mitochondria and ER. Cup-shaped autolysosomes appeared to

be wrapping around organelles such as the mitochondria and forming a pocket containing cytoplasmic organelles and cytoplasmic material (Fig.3-11B). In addition to lysosomes with partially digested material, autolysosomes containing what could be glycogen or lipid bodies were also seen in treated cells (Fig.3-11B). Features with a stacked or whorled appearance were observed after cells had been treated with corrosion granule (Fig.3-11A). These features appeared to be scattered towards the periphery of the cell. A lot of mitochondria and dilated ER cisternae were also observed around or near these features.

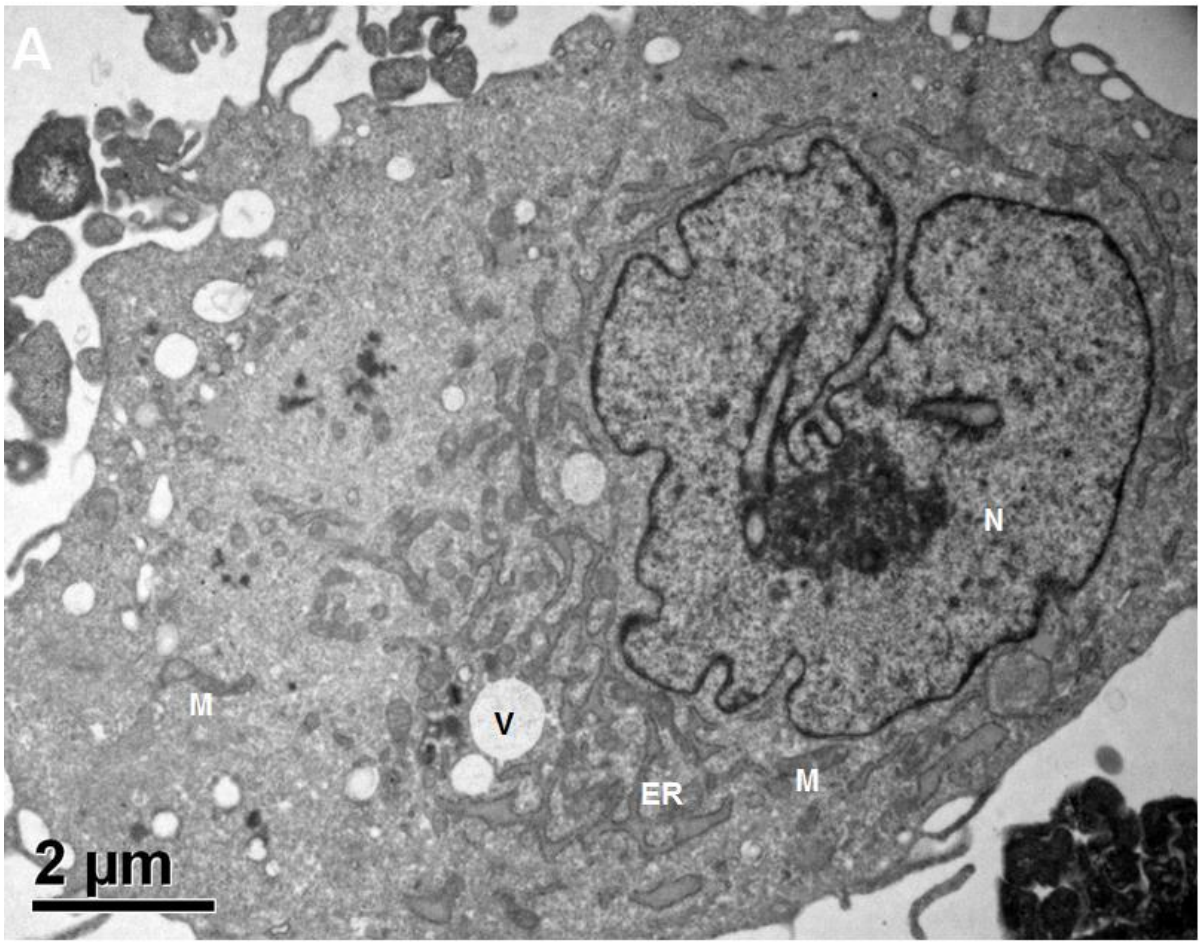

Fig.3-9A. hMSCs cultured in normal growth media (control) for 48 hours. Cell is showing normal cellular components, this includes: a defined nucleus, vacuoles, mitochondria and

cisternae of the endoplasmic reticulum scattered within the cytoplasm and an intact membrane. Scale bar=2µm.

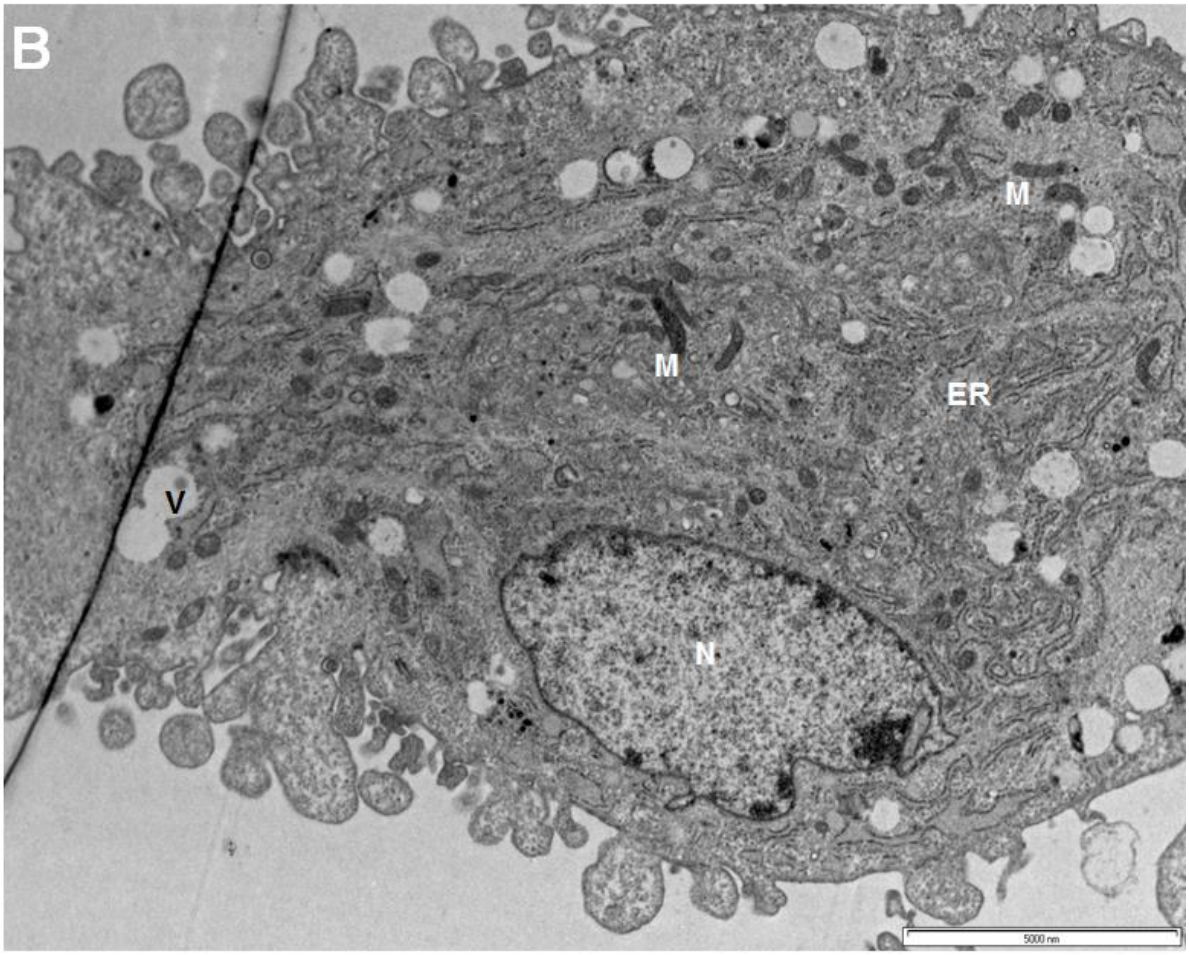

Fig.3-9B. hMSCs cultured in Mg-Ca100 non-filtered medium for 24 hours. By comparison with the control, there was a lot more mitochondria present after culture in the presence of the corrosion products. There was also significant blebbing than in the control cells and a few vacuoles were scattered towards the periphery of the cell. ER with moderately dilated cisternae was also observed. Scale bar = 5µm. M-mitochondria, V--vacuole, N-nucleus, ER-endoplasmic reticulum.

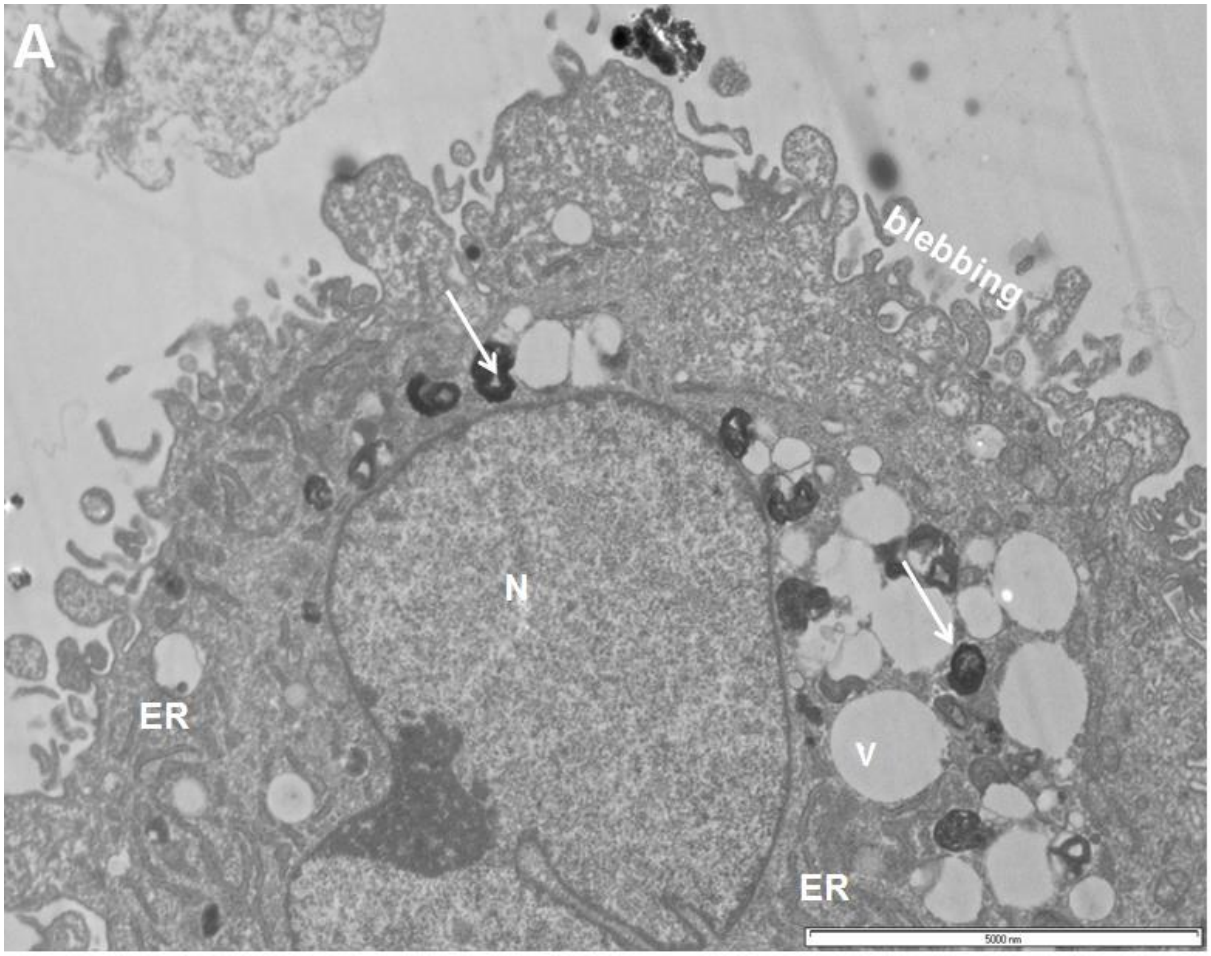
A
blebbing
N
ER
V
ER
5000 nm

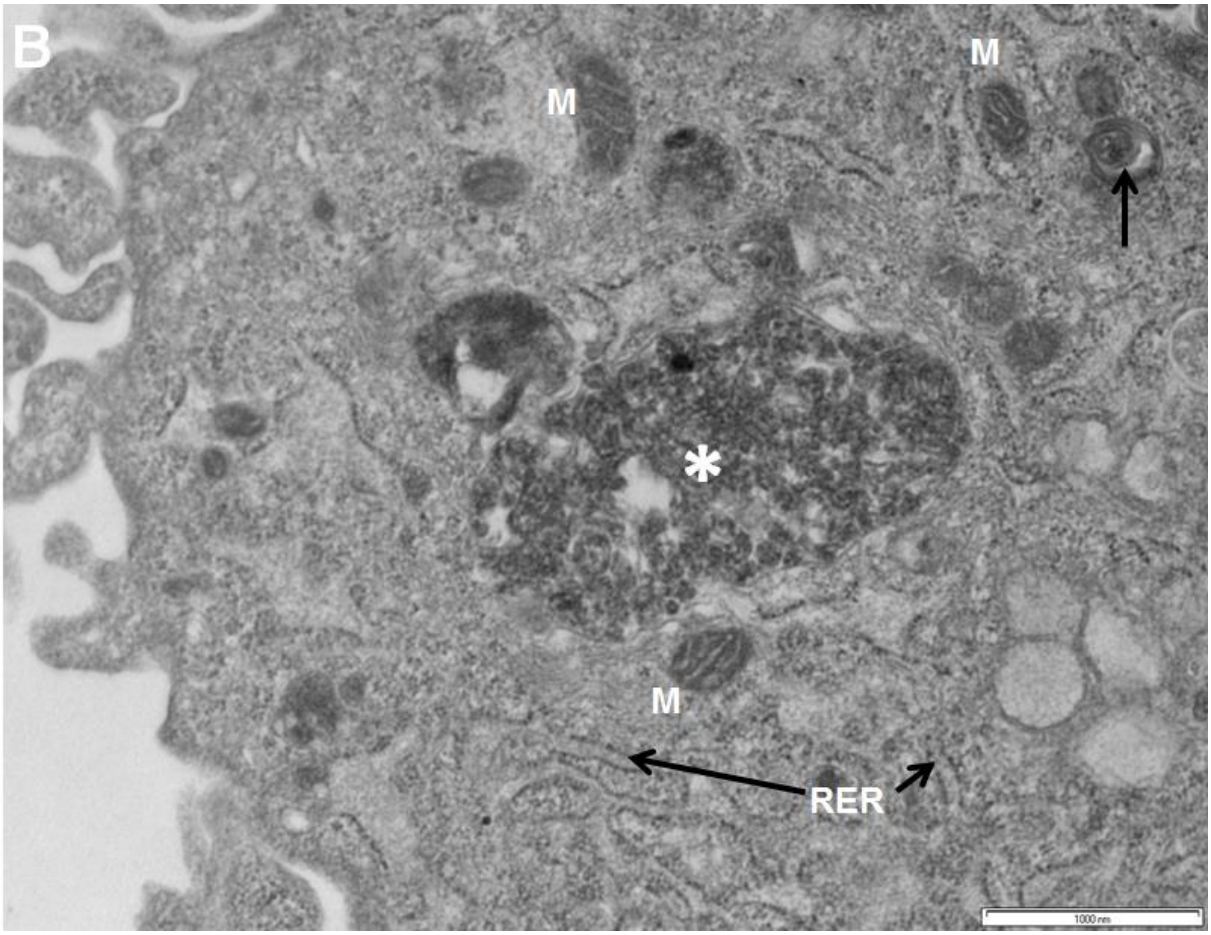

Fig.3-10. hMSCs cultured in Mg-Ca100 non-filtered conditioned medium for 48 hours. (**A**) After 48 hours the cell appeared to be more vacuolated, the vacuoles were larger in comparison to the ones seen in the control cells. There was also a co-localisation of these vacuoles with organelles filled with electron dense material (autolysosomes) (**B**) A large electron dense material (*) that could be identified as glycogen or lipid bodies was present in treated cells. An autolysosome appeared to be wrapping around a mitochondrion (arrow) towards the right top corner of the image. RER with moderately dilated cisternae was also observed. Scale bar for image **A**=5µm and image **B**=1µm. M-mitochondria, V- vacuole, N-nucleus, RER-rough endoplasmic reticulum.

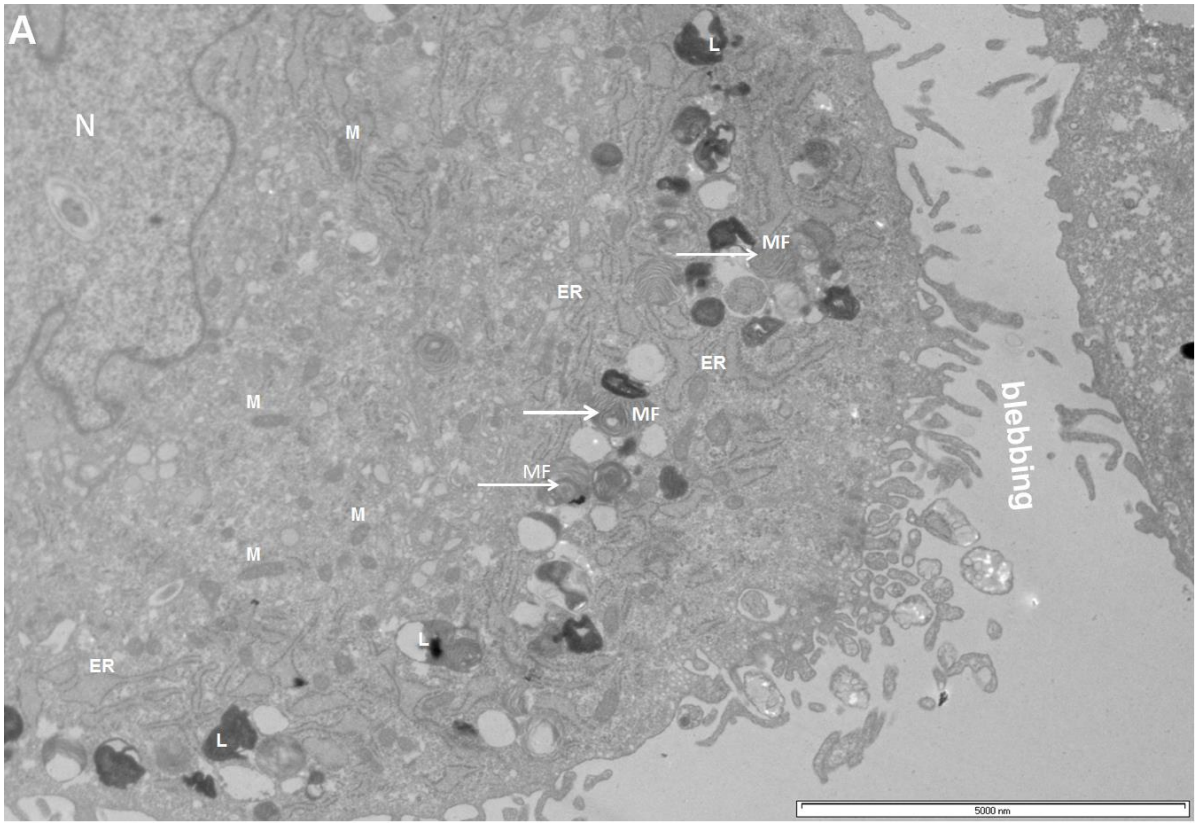
A
N
M
L
MF
ER
ER
M
MF
MF
M
M
L
ER
L
blebbing
5000 nm

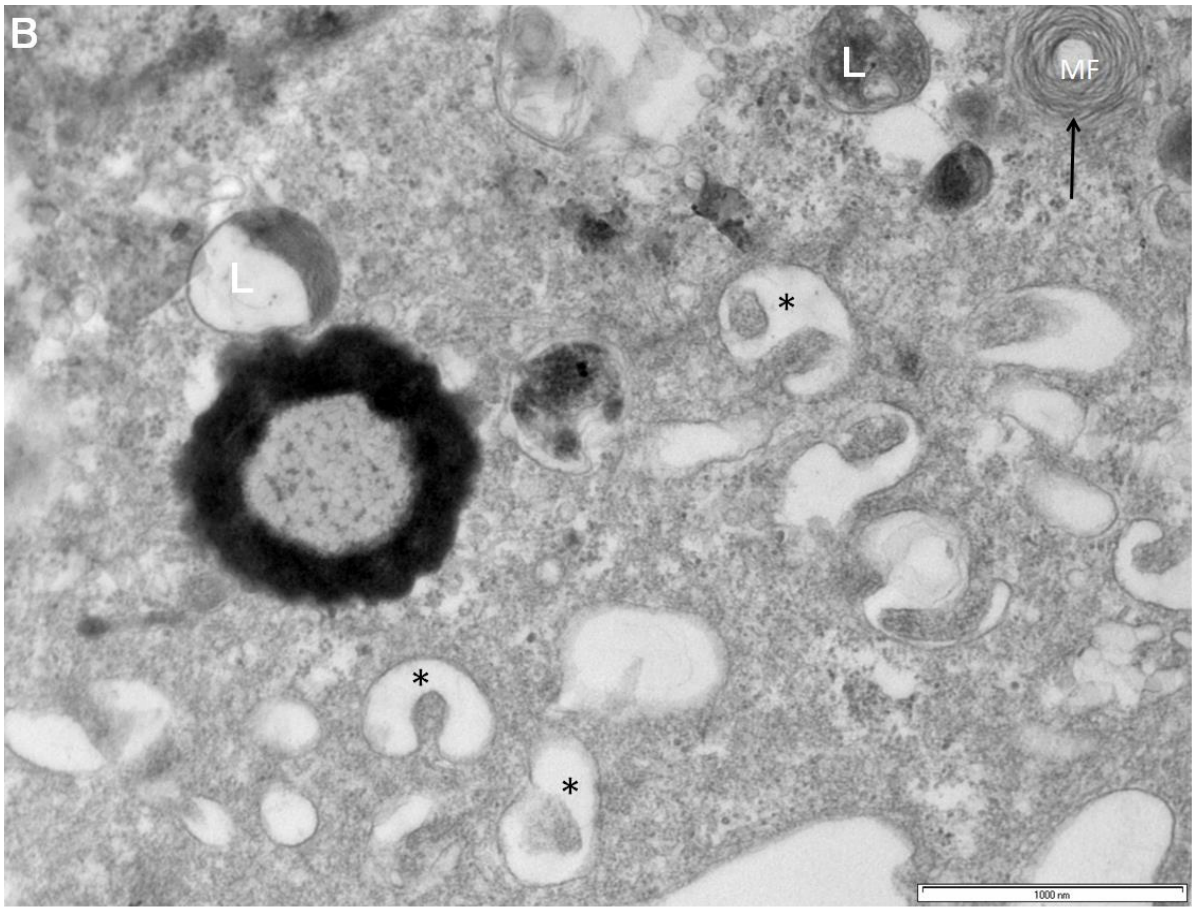
B
L
MF
L
*
*
*
1000 nm

Fig.3-11. hMSCs cultured in Mg-Ca100 non-filtered conditioned medium for 48 hours. (**A**) The treatment with corrosion products resulted in the formation of different types of autolysosomes. The arrows are showing the presence of a few autolysosomes within the cell. Some of the autolysosomes were filled with partially degraded material (L), some were filled with electron dense material and some were filled with figures that had a whorled appearance (myelinosome). Lot of mitochondria were present within the cytoplasm compared to the control. Mitochondria were also present in close proximity to the lysosomes. Cisternae of the endoplasmic reticulum near the lysosomes appeared to be dilated. (**B**) Cup shaped features were observed wrapping around cytoplasmic materials (*) and the arrow shows the presence of myelinosome. Scale bar for image **E**= 5µm and image **F**=1µm. M-mitochondria, V- vacuole, N-nucleus, RER-rough endoplasmic reticulum, MF-myelinosome.

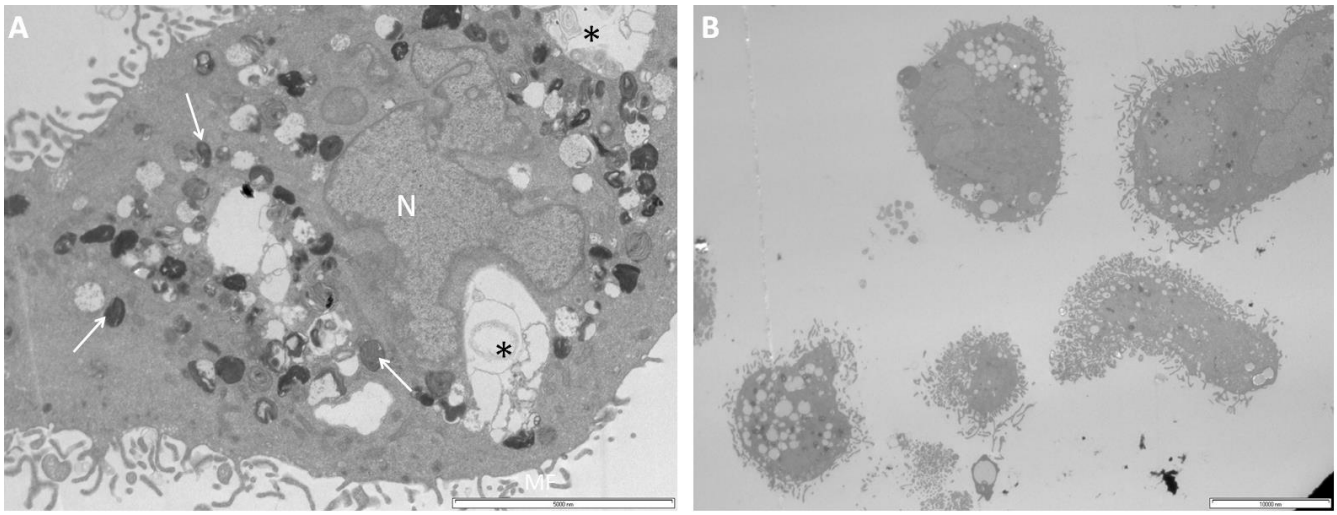

Fig.3-12. hMSCs cultured in Mg50 non-filtered conditioned medium for 48 hour. The treatment with Mg conditioned medium had similar effect to the treatment with Mg-Ca conditioned medium. Different types of autolysosomes were seen in the image (**A**). The nucleus was irregular and the presence of late stage lysosomes (*) was observed. (**B**) Image showing a lower magnification of the cell population, some cells do not appear to have as

many vacuoles as seen in image (**A**)**.** Scale bar for image **A** = 5µm and image **B**=10µm. N-nucleus.

3.4. Summary

- MSC were able to tolerate Mg ion concentration up to 17mM, however concentration below 10mM were beneficial for cell growth.
- The presence of corrosion granules especially in high concentrations reduced cell viability, furthermore longer exposure to the corrosion products also affected cell viability.
- In the presence of corrosion granules metabolic activity was focused on removing/digesting the corrosion granule.
- Cells tolerated Mg-Ca conditioned media more than Mg conditioned media because the slow degrading Mg-Ca alloy produced fewer corrosion products.
- When cells were exposed to corrosion product, interaction with corrosion products was observed at the intercellular level, this interaction also altered the morphology of the cells.
- Different types of autolysosomes were observed when cells were presented with Mg corrosion products. Highly vacuolated cells were observed as the cells dealt with the corrosion products.

CHAPTER 4: Magnesium corrosion product and the in vitro effects on hMSCs osteogenic behaviour

4.1. The effect of Mg conditioned media on hMSCs on gene and protein level

Gene and protein studies were performed to investigate the effect of the corrosion products on osteogenic lineage differentiation. Quantitative real time PCR was used to amplify the primers of osteogenesis-related genes: Runx-2, COL1A1 and osteocalcin following treatment of hMSCs with corrosion products over a period of 12 days. ALP assay was also performed at day 2, 7 and 12 using pNPP liquid substrate system to investigate the effect of corrosion products on ALP protein levels. Expression of the master regulator of osteogenesis, Runx-2, was upregulated for all conditions compared to cells cultured in standard growth medium on day 2. On day 2 expression of Runx-2 was significantly higher ($p<0.05$) in cells cultured in osteogenic medium compared to cells cultured in Mg100 non-filtered medium (Fig 4-1A). For all conditions Runx-2 expression was downregulated from day 4 until day 12. On the other hand, OC gene expression was significantly enhanced when cells were cultured in non-filtered medium compared to cells cultured in osteogenic growth medium and filtered medium on days 4, 8 and 12 (Fig 4-1B). On day 4, a significant ($p<0.01$) fold change (3x fold) in OC expression was observed when cells were cultured in non-filtered medium compared to osteogenic medium and filtered medium. Again, on day 8 and 12 OC expression of cells cultured in non-filtered medium was significantly higher ($p<0.05$) compared to cells cultured in filtered medium and osteogenic medium. It was also observed that the effect of non-filtered medium started to diminish by day 12.

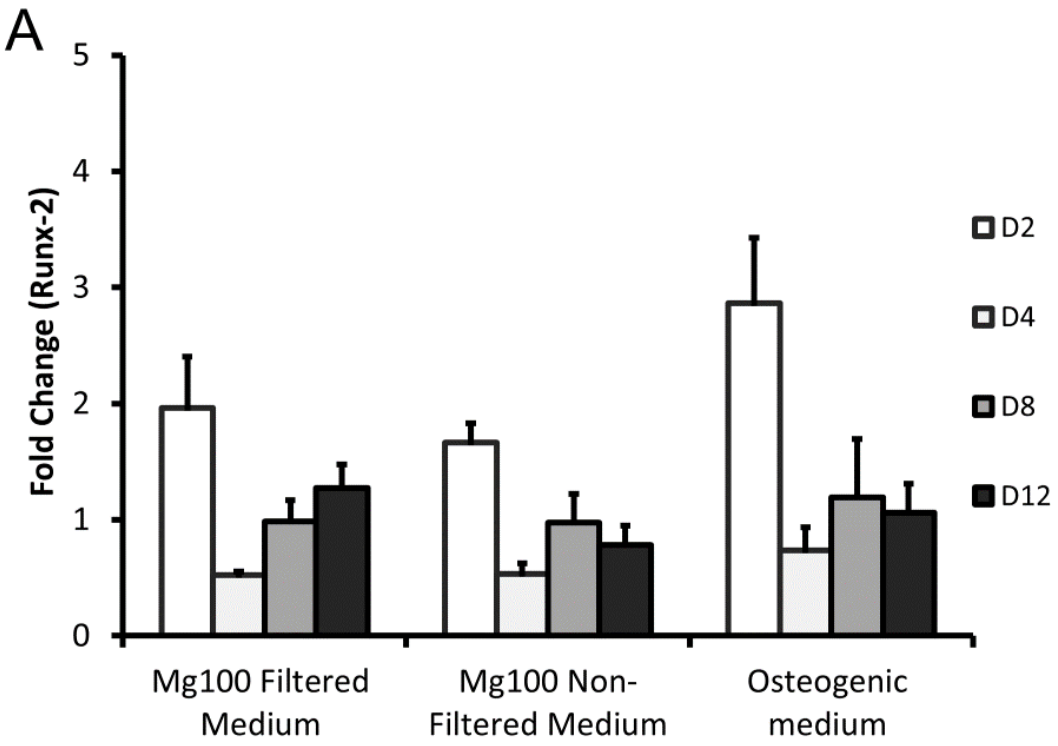
A
Fold Change (Runx-2)
5
4
3
2
1
0
D2
D4
D8
D12
Mg100 Filtered Medium
Mg100 Non-Filtered Medium
Osteogenic medium

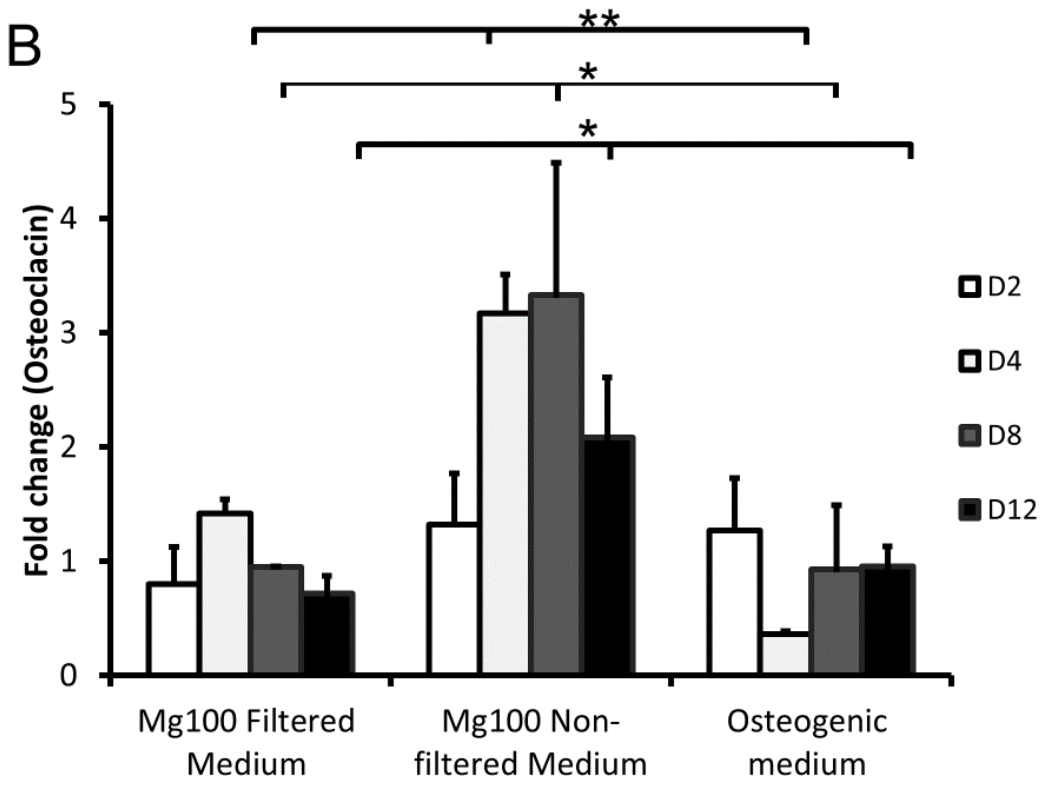
B
**
*
*
Fold change (Osteoclacin)
5
4
3
2
1
0
D2
D4
D8
D12
Mg100 Filtered Medium
Mg100 Non-filtered Medium
Osteogenic medium

Fig.4-1. The effect of Mg100 conditioned media on the expression of osteoblast related genes was investigated using qRT-PCR. (A) Fold change in the gene expression of Runx-2 and (**B**) osteocalcin in cells cultured in filtered or non-filtered medium over a period of 12 days. A significant fold change (*, $p < 0.05$) in the gene expression of Runx-2 was observed when cells were cultured in Mg100 non-filtered medium compared to osteogenic medium on day 2. A significant fold change in osteocalcin expression was also observed when cells cultured in Mg100 non-filtered medium compared to Mg100 filtered medium and osteogenic medium on day 4 (**, $p < 0.01$) and on day 8 and 12 (*, $p < 0.05$) a similar trend was also observed. The fold change is relative to the control sample, represented by a fold change of 1. Osteogenic medium was used as positive control. The bars represent the mean and standard deviation in the positive orientation of three independent experiments, each with n=3.

The culture of cells in the presence of Mg conditioned media showed that COL1 was downregulated in the presence of non-filtered medium on day 4, however by day 8 expression started to increase (Fig.4-2). Expression of COL1 was 3x fold higher in cells cultured in osteogenic medium compared to filtered and non-filtered medium. Overall it appears culture of cells in Mg conditioned media did not have any effects on COL1 expression.

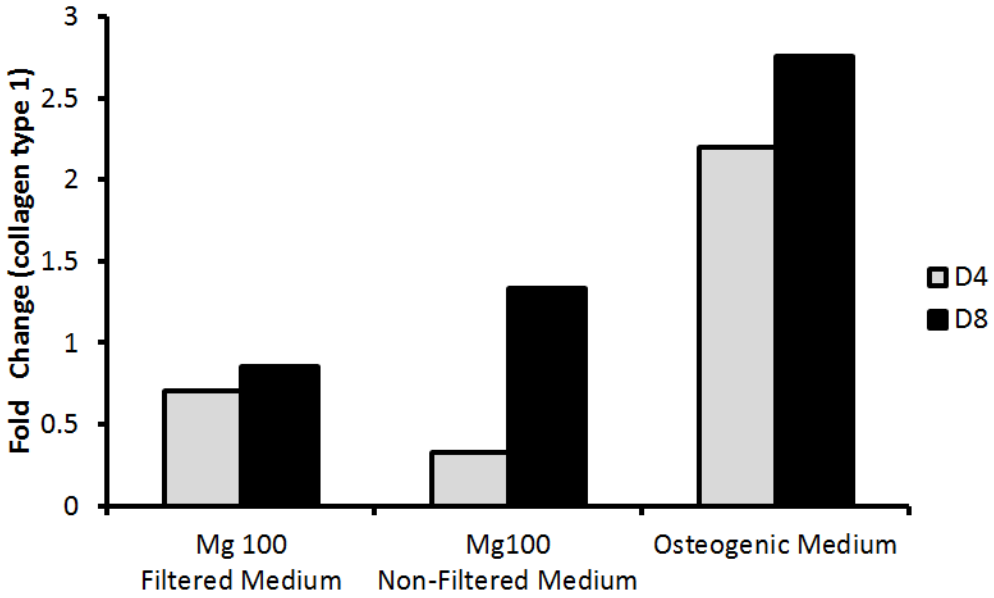

Fig.4-2. The effect of Mg conditioned media on the expression of osteoblast related genes was investigated using qRT-PCR. Fold change in the gene expression of COL1 on days 4 and 8 in cells cultured in filtered or non-filtered medium. The fold change is relative to the control sample, represented by a fold change of 1. Osteogenic medium was used as the positive control.

The effect of Mg50 filtered and non-filtered medium on the expression of osteoblast related markers was also investigated. The expression of Runx-2 was not significantly altered when cells were cultured in the presence of conditioned media from day 4 to 12 (Fig 4-3A). However, on day 4 OC expression was significantly enhanced ($p<0.01$) when cells were cultured in the presence on Mg50 non-filtered medium compared to osteogenic medium (Fig 4-3B).

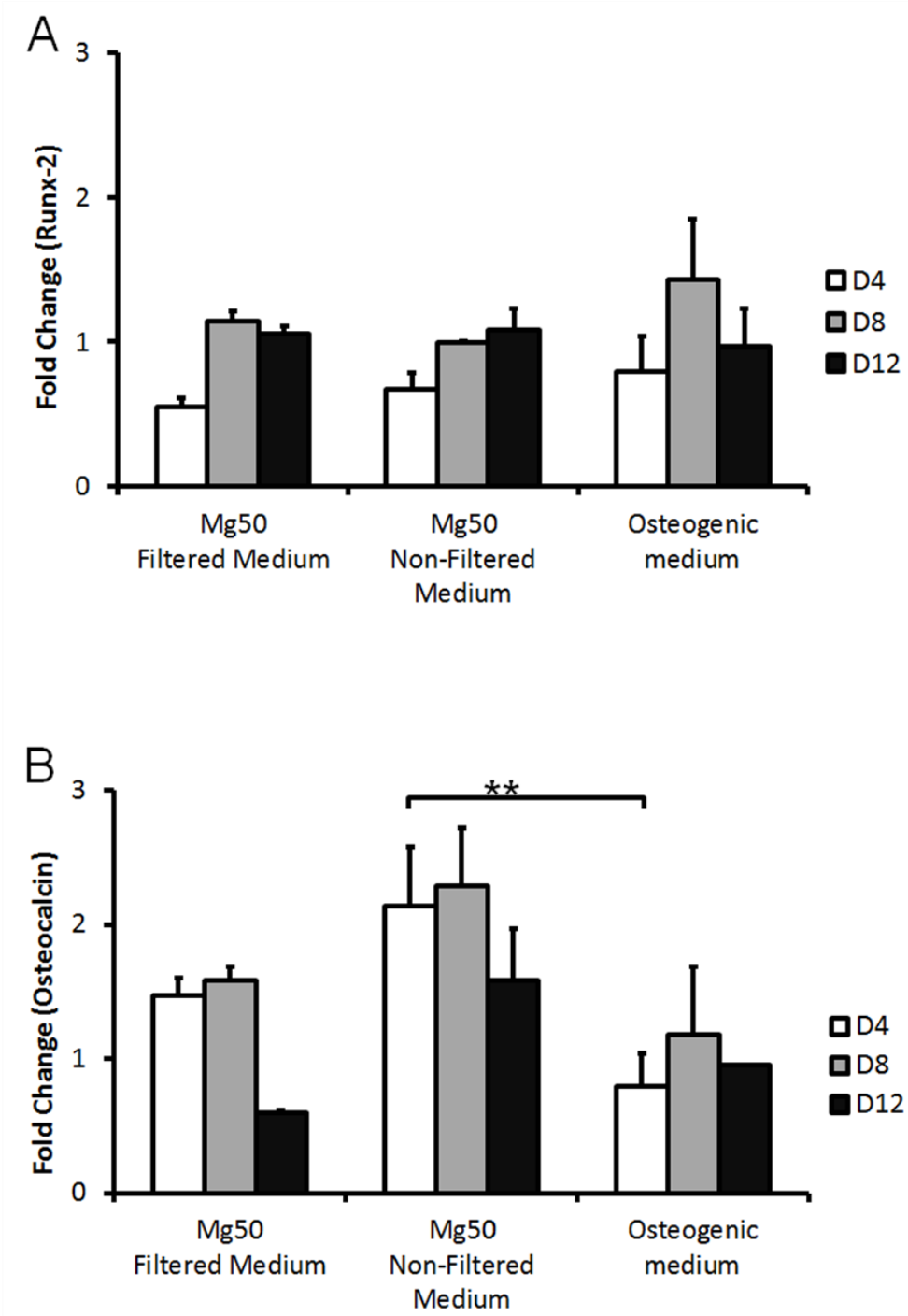

Fig.4-3. The effect of Mg50 conditioned media on the expression of osteoblast related genes was investigated using qRT-PCR. (A) Fold change in the gene expression of Runx-2 and (**B)** OC in cells cultured in filtered or non-filtered medium over a period of 12 days. A significant increase (**, $p<0.01$) in OC expression was observed in cells cultured in Mg50 non-filtered medium compared to osteogenic medium. The fold change is relative to the control sample, represented by a fold change of 1. Cells cultured in osteogenic medium were used as positive control. The bars represent the mean and standard deviation in the positive orientation of three independent experiments, each with n=3.

Levels of ALP, a hydrolase enzyme with an integral role in providing free phosphates for the synthesis of calcium phosphate were significantly higher ($p<0.05$) in cells treated in the presence of Mg corrosion granules (non-filtered medium) compared to filtered medium and standard growth medium (control) on day 7 (Fig 4-4). No significant difference between cells cultured in Mg100 non-filtered medium and the positive control (osteogenic medium) was detected on day 7. On day 12 ALP levels were also significantly higher ($p<0.001$) in cells cultured in Mg non-filtered medium compared to filtered medium and the control. However expression was significantly lower ($p<0.001$) compared to cells cultured in osteogenic medium (Fig 4-4).

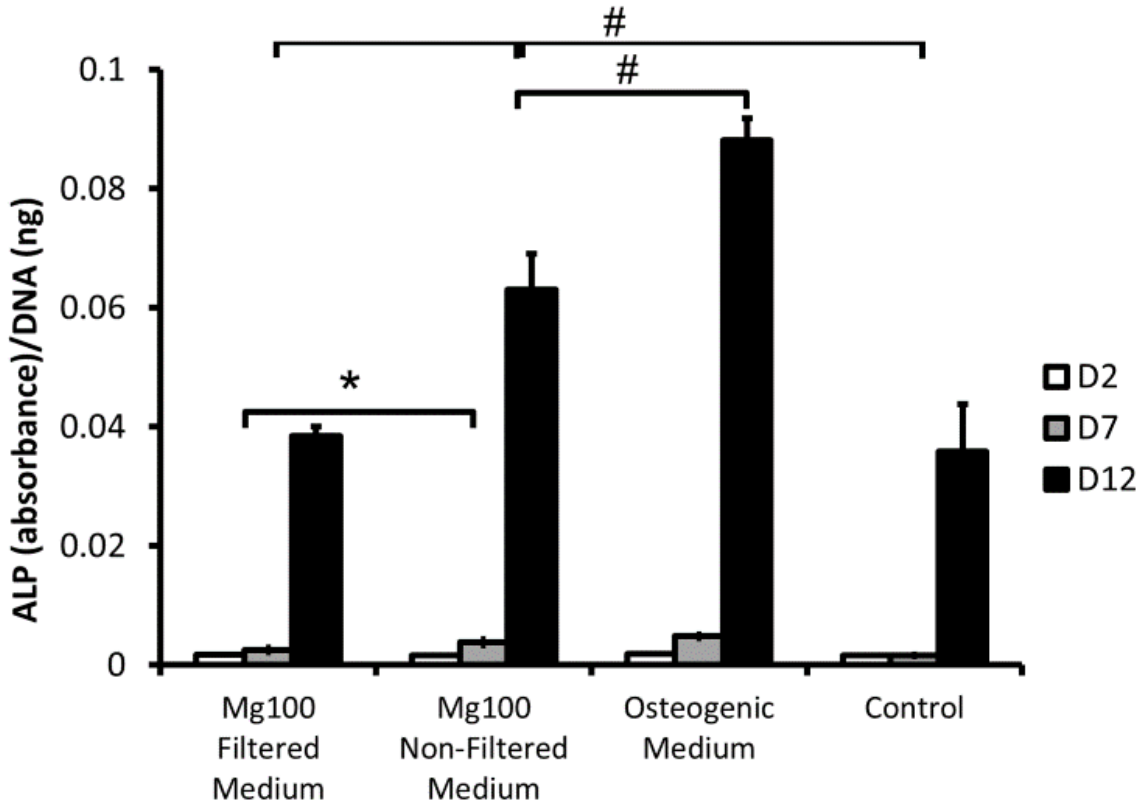

Fig.4-4. The effect of Mg100 conditioned media on ALP protein was investigated using the pNPP liquid substrate system. Cells were cultured in the presence of Mg100 conditioned medium over a period of 12 days; the presence of ALP protein was evaluated at different time points (day 2, 7, 12). On day 7 a significant increase (*, $p < 0.05$) in the presence of ALP was observed in Mg100 non-filtered medium compared to Mg100 filtered medium. A significant increase (#, $p < 0.001$) in the presence of ALP was observed when cells were cultured in Mg100 non-filtered medium compared to Mg100 filtered and control. However, a significant reduction (#, $p < 0.001$) in ALP presence was also observed when cells were cultured in Mg100 non-filtered medium compared to osteogenic medium. ALP protein was normalised to DNA concentration. Osteogenic medium was used as the positive control. The bars represent the mean and standard deviation in the positive orientation of three independent experiments, each with n=3.

4.2. The effect of Mg-Ca conditioned media on hMSCs on gene and protein level

In the presence of Mg-Ca non-filtered medium Runx-2 expression was reduced compared to osteogenic medium on day 2; there was a 3x fold increase in the expression Runx-2 when cells were cultured in osteogenic medium. After day 2, in the presence of osteogenic medium, expression of Runx-2 was downregulated until day 12. Mg-Ca conditioned media did not enhance the expression of Runx-2; the level of Runx-2 expression was similar to control throughout the 12 day culture period, with a slight increase on day 8 (1.5x fold change) (Fig.4-5A). In contrast, to Mg conditioned media, in the presence of Mg-Ca non-filtered medium the expression of OC was lower than the control (untreated) on day 4. However, on day 8, expression of OC increased but the level of expression was still lower than the one observed when cells were cultured in the presence of Mg conditioned medium (Fig.4-5B).

ALP protein quantification was significantly higher ($p<0.001$) in cells cultured in the presence of osteogenic medium compared to Mg-Ca non-filtered medium and control following culture for 12 days. A significant reduction ($p<0.05$) in ALP protein was also observed when cells were cultured in the presence of Mg-Ca non-filtered medium compared to the control (Fig.4-6).

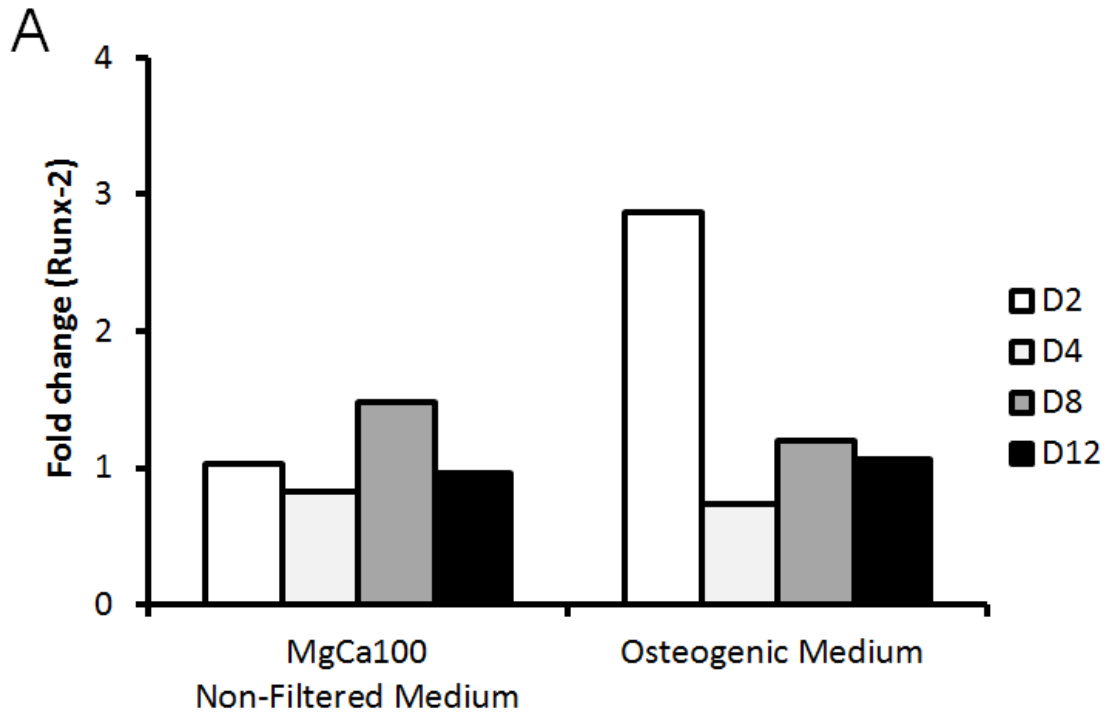

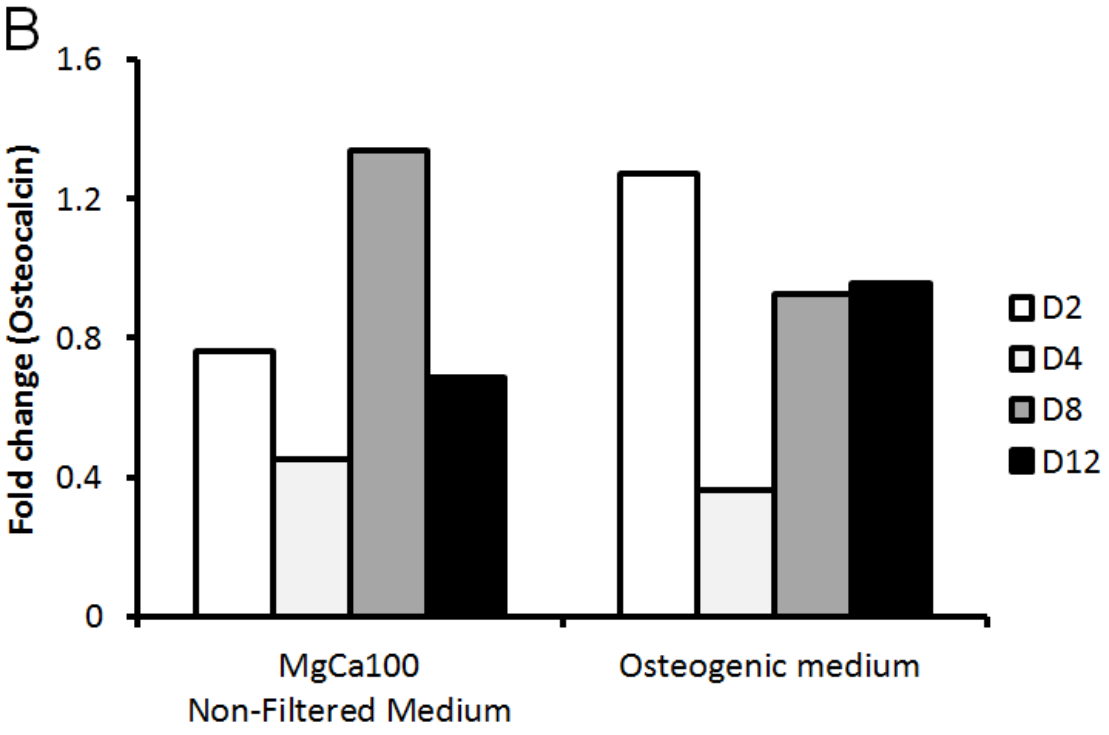

Fig.4-5. The effect of Mg-Ca100 conditioned media on the expression of osteoblast related genes was investigated using qRT-PCR. Gene expression of **(A)** Runx-2 and (**B**) OC in cells

cultured in Mg-Ca100 filtered or non-filtered medium was investigated over a period of 12 days. The fold change is relative to the control sample, represented by a fold change of 1. Osteogenic medium was used as positive control.

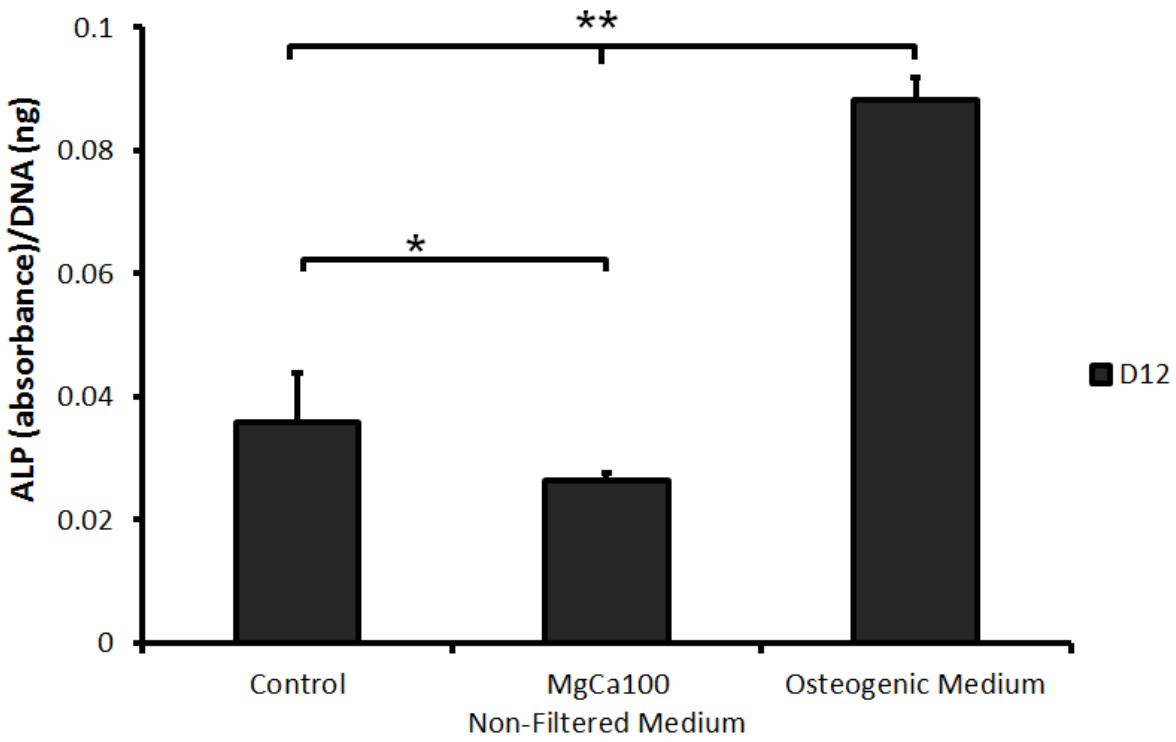

Fig.4-6. The effect of MgCa100 conditioned media on ALP protein level was investigated using the pNPP Liquid Substrate System. Cells were cultured in the presence of MgCa100 non-filtered medium over a period of 12 days. ALP protein analysis was performed on day 12 following treatment with Mg-Ca100 filtered or non-filtered medium. ALP protein level was significantly reduced (*, $p<0.05$) when cells were cultured in MgCa100 non-filtered medium compared to control. When cell were treated with osteogenic medium ALP protein level was significantly higher (**, $p<0.01$) compared to Mg-Ca100 non-filtered medium and control. ALP protein was normalised to DNA concentration. Osteogenic medium was used as positive control. The bars represent the mean and standard deviation in the positive orientation of three independent experiments, each with n=3.

4.3. Summary

- The presence of corrosion granules (Mg100 non-filtered medium) resulted in enhanced OC gene expression at day 4.
- The effect of corrosion granules on OC expression was concentration dependant. Culture of cells in Mg50 non-filtered medium enhanced OC expression but not to the same level as Mg100 non-filtered medium.
- On day 12, ALP expression was significantly enhanced when cells were cultured in the presence of Mg non-filtered medium compared to filtered medium and standard growth medium; however expression was significantly lower compared to osteogenic medium.
- Mg conditioned media did not affect the expression of COL1.
- In the presence of Mg-Ca conditioned no significant increases in gene or protein expression were observed.

CHAPTER 5: The response of osteoclasts and monocytes to the corrosion of Mg and Mg-Ca alloy

5.1. The effect of Mg conditioned media on RAW cell metabolic activity

AlamarBlue assay was used to measure response of pre-osteoclast cells (RAW cells) to the presence of Mg and Mg-Ca conditioned. The assay measured metabolic activity of cells and was performed over a period of 3 days. Fig.5-1 shows that the effect of Mg conditioned media on RAW cell metabolic activity was dose dependant. The reduction of Mg conditioned media concentration (filtered and non-filtered media) resulted in increased metabolic activity. A reduction in metabolic activity was observed when cells were cultured in Mg100 filtered medium at day 1, 2 and day 3 compared to the control. When cells were cultured in Mg50 filtered medium a reduction in metabolic activity was also observed at day 1 and 2 compared to the control. Treatment duration and concentration of Mg conditioned media significantly affected the behaviour of RAW cells. Over time cells were able to adapt to the presence of Mg conditioned media, thereby restoring the metabolic activity of cells to levels comparable to the control. In the presence of corrosion granule (Mg100 non-filtered medium), the metabolic activity of cells was also reduced in comparison to the control. In contrast to what was observed when cells were cultured in Mg100 filtered medium over the 3 day culture period the metabolic activity of cells cultured in Mg100 non-filtered medium decreased in comparison to the control. However, the dilution of Mg100 non-filtered medium concentration to Mg50 non-filtered medium resulted in a recovery in metabolic activity at all the time points of the culture period. In the presence of corrosion granule, time did not restore the metabolic activity of cells cultured in Mg100 non-filtered medium (Fig.5-1B).

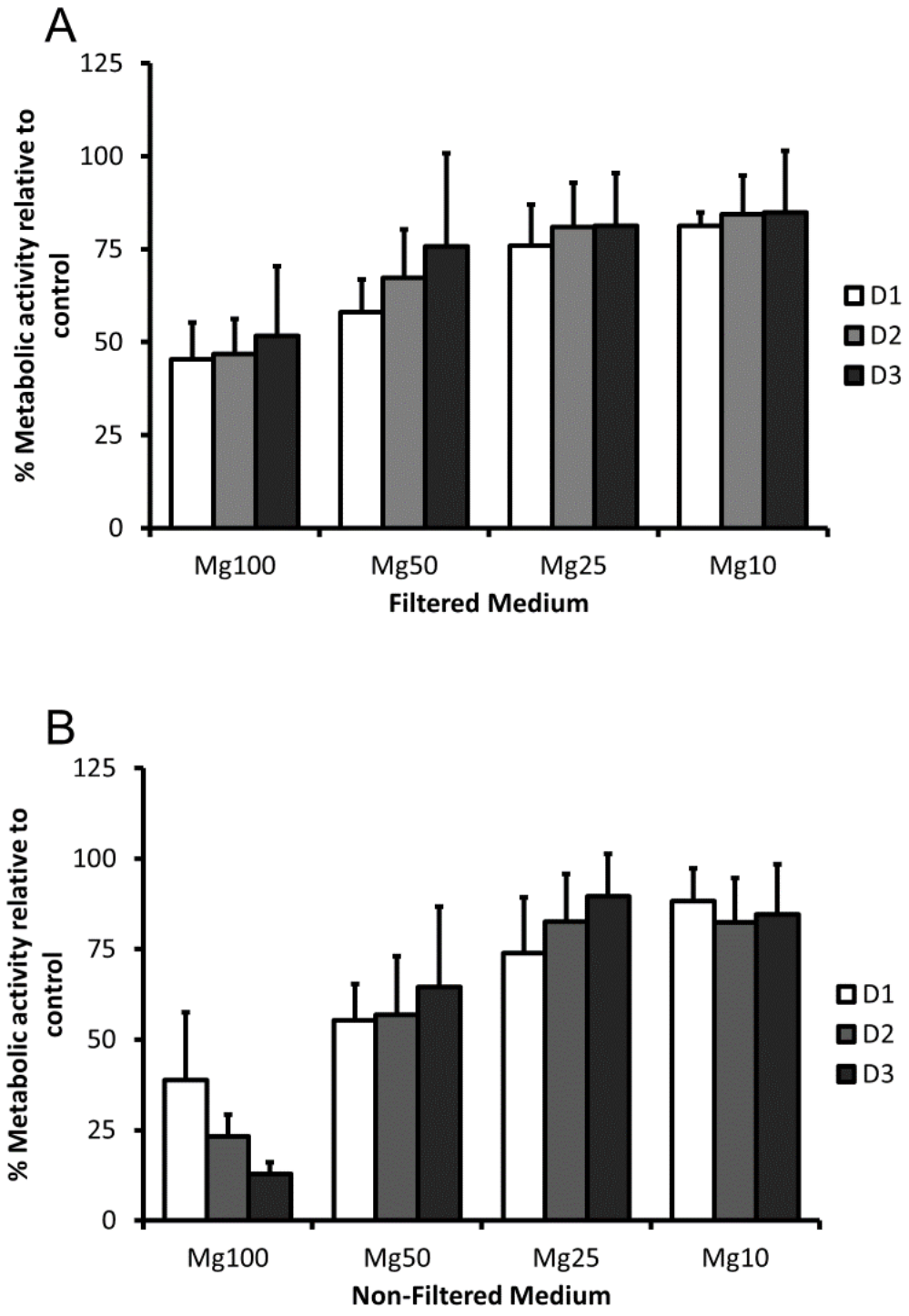

Fig.5-1. The effect of Mg conditioned medium on RAW cell metabolic activity was investigated using AlamarBue assay. RAW cells were cultured in the presence of various concentrations of Mg conditioned medium, **(A)** filtered medium and **(B)** non-filtered medium. A reduction in metabolic activity was observed when cells were cultured in Mg100 filtered

medium over the 3 day culture period compared to the control. Culture in Mg50 filtered and non-filtered medium also resulted in a reduction in metabolic activity at day 1 and 2 compared to the control. When cells were cultured in Mg100 non-filtered medium metabolic activity was reduced over the 3 day culture period compared to the control. The data is presented relative to the control (100%). The bars represent the mean and standard deviation in the positive orientation of three independent experiments, each with n=3.

5.2. The effect of Mg-Ca conditioned media on RAW cell metabolic activity

The initial investigation of the metabolic activity of cells treated with various concentrations of Mg-Ca conditioned media showed acceptable biocompatibility (Fig.5-2). The metabolic activity of cells increased over time for all conditions for both filtered and non-filtered media. The metabolic activity of cells treated with Mg-Ca100 filtered medium (Fig. 5-2A) were above the cytotoxicity threshold (>70%). As the culture prolonged to day 3, the dilution of Mg-Ca filtered medium to concentrations ≤50% resulted in metabolic activity higher than the control. When cells were treated with Mg-Ca100 non-filtered medium the metabolic activity was around 70% in relation to the control throughout the culture period. The dilution of Mg-Ca non-filtered medium resulted in increased metabolic activity and over time the metabolic activity was similar to the control. For both filtered and non-filtered media the decrease in the concentration of conditioned media resulted in increased cell metabolic activity.

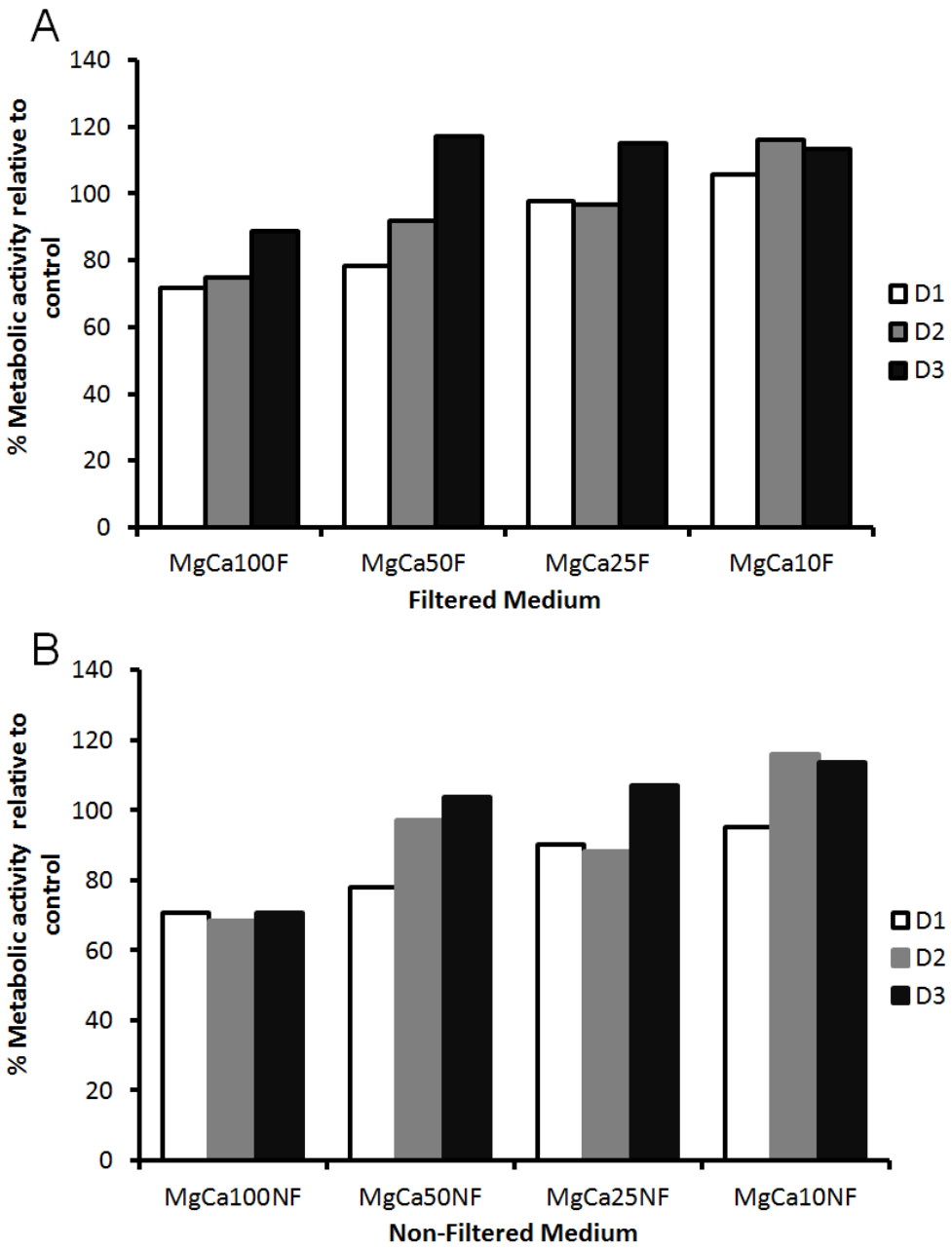

Fig.5-2. The effect of Mg-Ca conditioned medium on RAW cell metabolic activity was investigated using AlamarBlue assay. RAW cells were cultured in the presence of Mg-Ca conditioned medium at varying concentrations (**A**) without (filtered medium) or (**B)** with (non-filtered medium) the presence of corrosion granule over a period of 3 days. Metabolic activity was above the cytotoxic threshold for all the conditions. The data is presented relative to the control (100%).

5.3. Osteoclastogenesis related gene analysis on RAW cells after culture in Mg and Mg-Ca conditioned media

The effect of Mg conditioned media on the expression of osteoclast specific markers (NFATC-1 and TRAP) was performed using qRT-PCR. RAW cells were cultured in Mg conditioned media for a period of 5 days in the presence of RANK-L to allow for differentiation into mature osteoclast cells. The culture of RAW cells with Mg filtered and non-filtered medium did not alter TRAP and NFATC-1 gene expression (Fig.5-3). However, a significant reduction in osteoclast cell number was detected between the positive control and cells cultured in Mg conditioned media. The treatment with both Mg50 filtered and non-filtered medium significantly reduced ($p<0.01$) the number of osteoclasts formed compared to the positive control (5-4A). Furthermore, conditioned media concentration had an effect on osteoclast formation when cells were cultured in the presence of non-filtered medium. There was a significant increase ($p<0.05$) in osteoclast formation when cells were cultured in Mg25 non-filtered medium compared to Mg50 non-filtered medium. The presence of corrosion products (Mg50 non-filtered medium) resulted in the formation of smaller osteoclast cells compared to the positive control (Fig.5-4B). There was also a large population of undifferentiated cells when cells were treated with Mg50 non-filtered medium compared to the positive control. On the other hand, culture of cells in Mg25 filtered or non-filtered medium resulted in large multinucleated cells similar to those observed in the positive control condition.

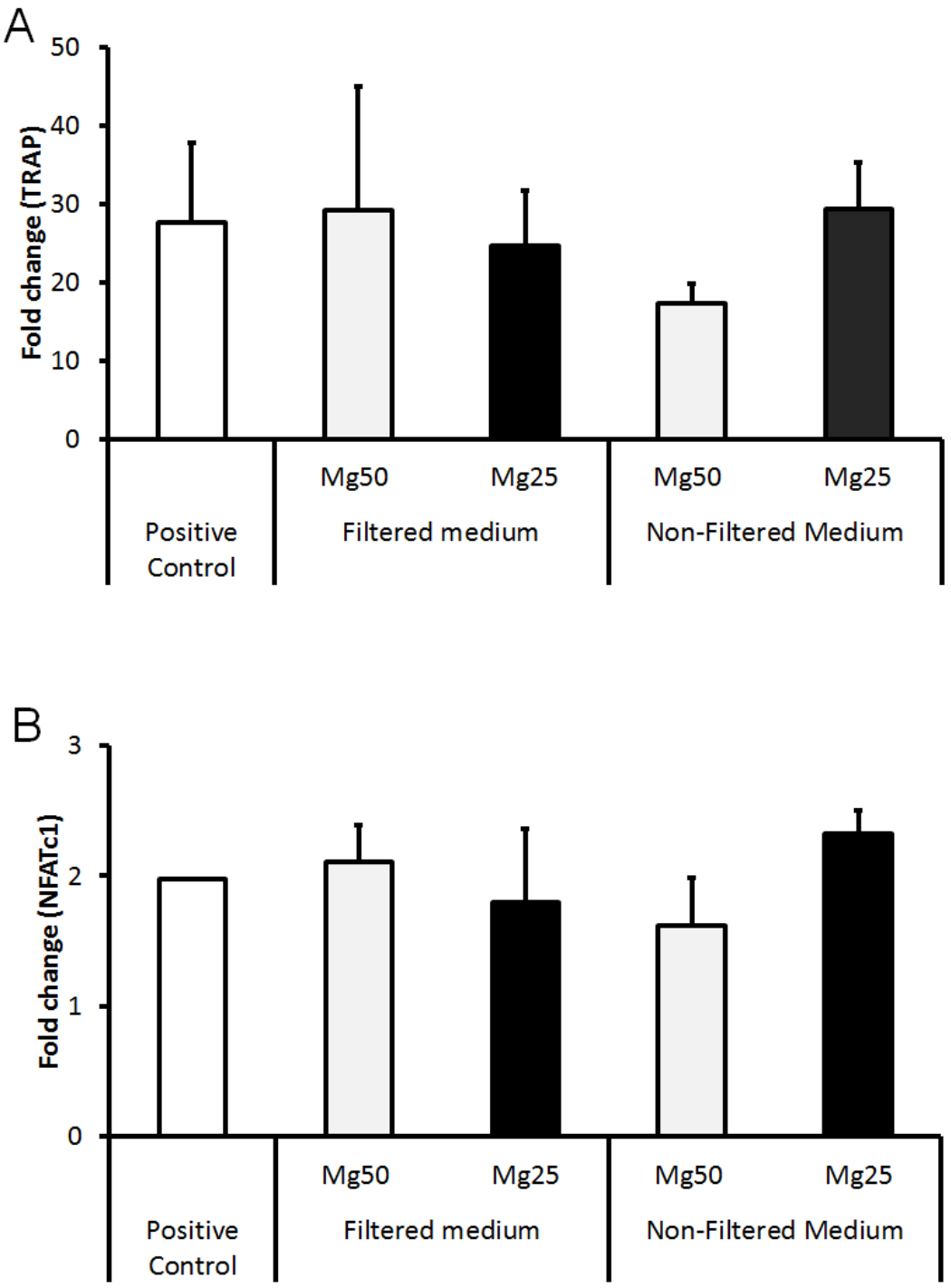

Fig.5-3. Effect of Mg conditioned media on osteoclast related genes was investigated using qRT-PCR. RAW cells were cultured in the presence of Mg conditioned medium at varying concentration with (non-filtered medium) or without (filtered medium) the presence of corrosion granule for a period of 5 days. RANK-L was also added to the culture to allow for

osteoclast differentiation. Fold change in the expression of (**A)** TRAP and (**B)** NFATC-1 after treatment with Mg conditioned medium is presented. The fold change is relative to the untreated sample (without RANK-L or Mg). Positive control represents RAW cells cultured in normal growth medium and then treated with RANK-L to induce differentiation. The bars represent the mean and standard deviation in the positive orientation of three independent experiments, each with n=3.

A

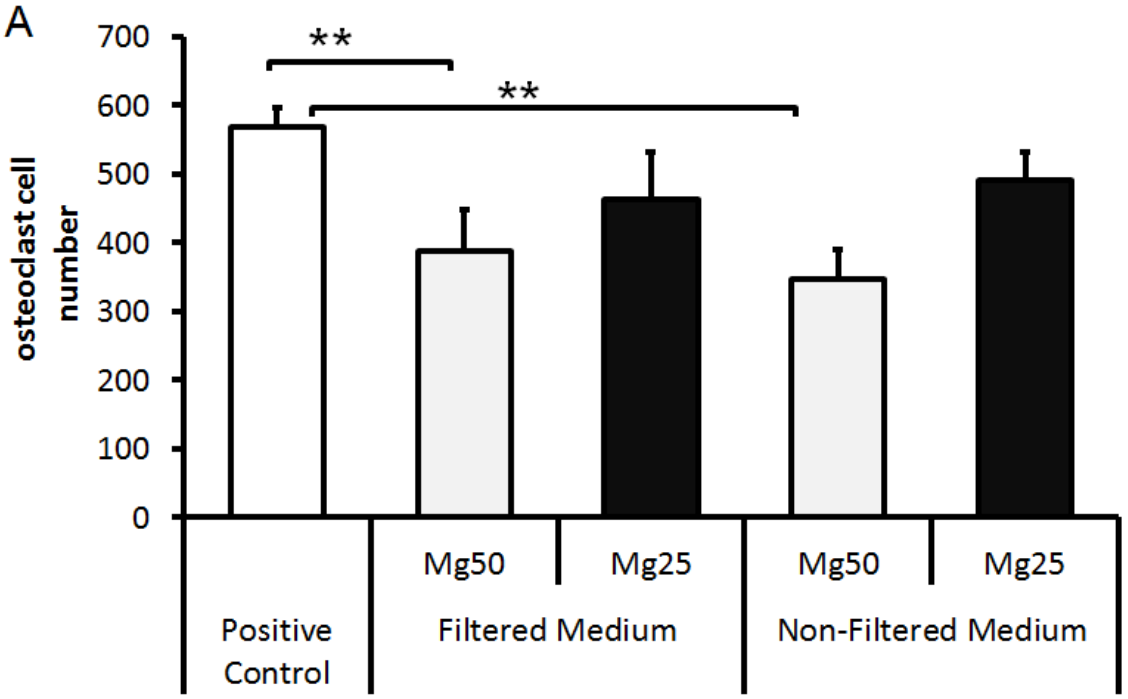

B

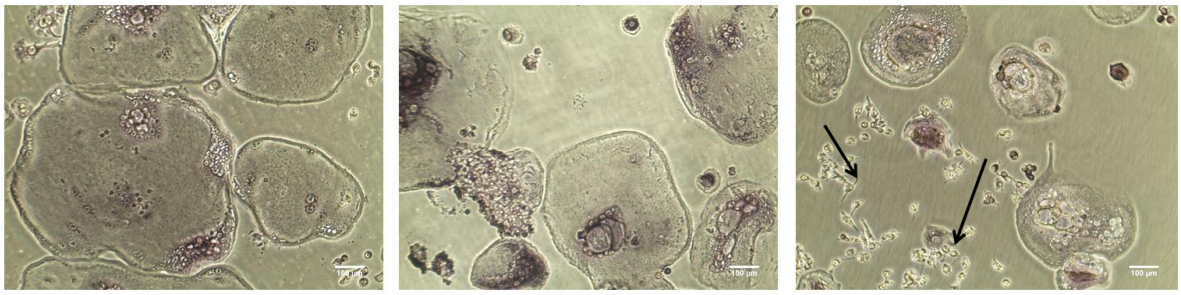

Positive Control

Mg50 Filtered Medium

Mg50 Non-Filtered Medium

Mg25 Filtered Medium

Mg25 Non-Filtered Medium

Fig.5-4. Effect of Mg conditioned media on osteoclastogenesis was investigated using the TRAP assay. RAW cells were cultured in the presence of Mg conditioned medium at varying concentrations with (non-filtered medium) or without (filtered medium) the presence of corrosion granule for a period of 5 days. (**A)** TRAP assay was performed following culture in Mg conditioned medium and RANK-L; all TRAP positive multinucleated cells in each well were counted for analysis. Culture in Mg50 filtered and non-filtered medium resulted in a significant reduction in cell number (**, $p<0.01$) compared to the positive control. (**B)** Representative images of TRAP positive multinucleated cells taken after 5 days of culture are presented. The arrows represent undifferentiated RAW cells. Positive control represents RAW cells cultured in standard growth medium and then treated with RANK-L to induce differentiation. The bars represent the mean and standard deviation in the positive orientation of three independent experiments, each with n=8.

A reduction in gene expression for both TRAP and NFaTC-1 were observed in the presence of Mg-Ca conditioned media compared to positive control; however no significant difference was detected (Fig.5-5). The gene expression data on the cells cultured in MgCa50 non-filtered medium is not shown. The corrosion behaviour of Mg-Ca used in this particular experiment was significantly higher than the other batches. When cells were cultured in the presence of MgCa 50 non-filtered medium the number of osteoclast cells formed was very low compared to the control and subsequently the RNA extracted was below the threshold required for qRT-PCR analysis. TRAP assay showed that the culture of cells in the presence of MgCa50 filtered and non-filtered medium resulted in a significant reduction ($p<0.001$) in osteoclast cell number. Similar to cells treated with Mg conditioned medium the presence of corrosion products reduced osteoclast number further. Culture in Mg-Ca50 filtered and non-filtered medium also resulted in a significant population of undifferentiated cells in the presence of corrosion granules (MgCa50 non-filtered medium) resulting in smaller osteoclast cells compared to the positive control (Fig.5-6B). When cells were cultured in the presence of both Mg and Mg-Ca conditioned media, many cells stained positive for TRAP staining, however only cells that had more than three nuclei and stained positive for TRAP were counted. Some cells were able to fuse but were not able to form large multinuclear cells as observed with the positive control.

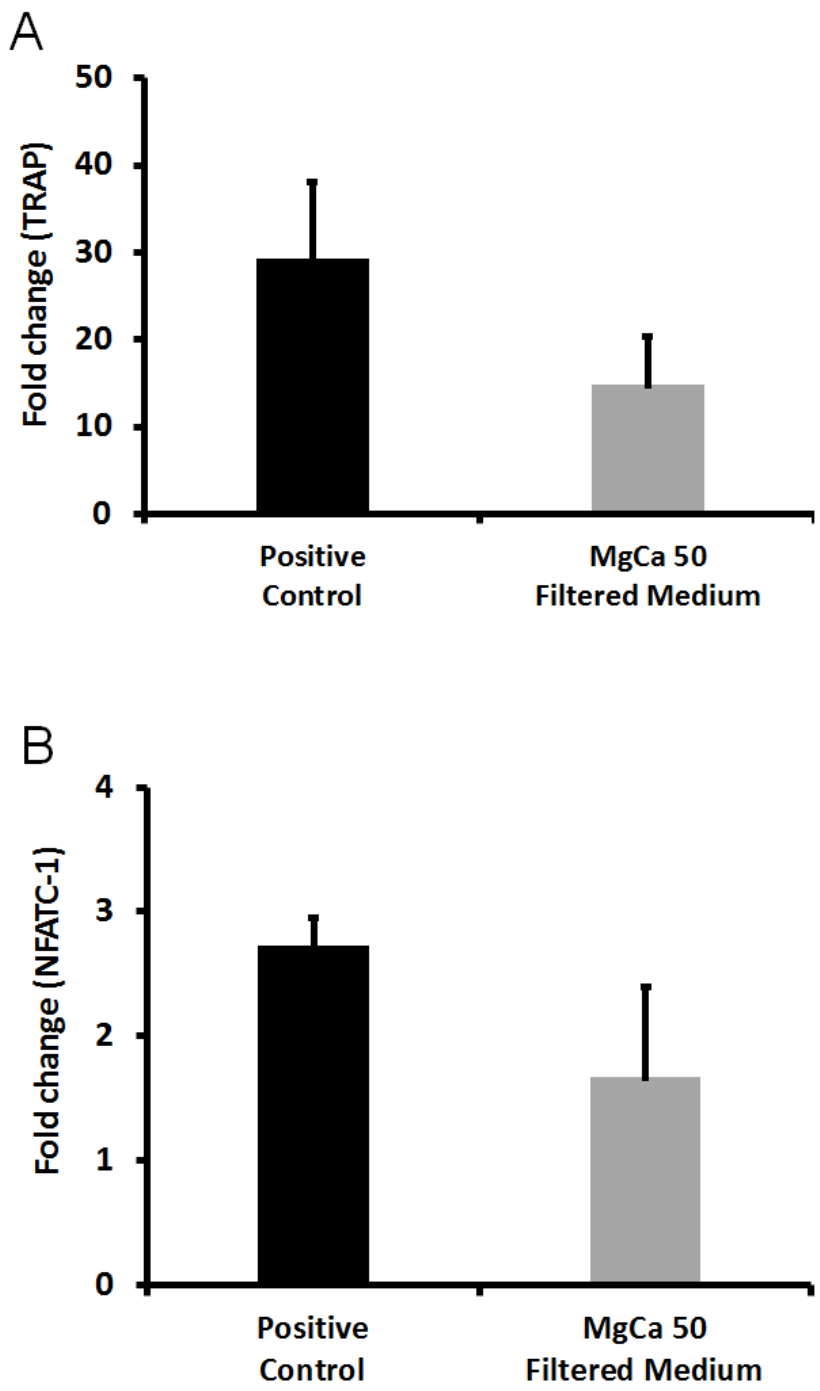

Fig.5-5. Effect of Mg-Ca conditioned media on osteoclast related genes was investigated using qRT-PCR. RAW cells were cultured in the presence of Mg-Ca conditioned medium at varying concentrations without (filtered medium) the presence of corrosion granule for a period of 5 days. RANK-L was also added to the culture to allow for osteoclast differentiation. Fold change in the expression of (**A**) TRAP and (**B**) NFATC-1 after treatment with MgCa50

filtered medium is presented. Fold change expression is relative to the untreated sample. Positive control represents RAW cells cultured in normal growth medium and then treated with RANK-L to induce differentiation. The bars represent the mean and standard deviation in the positive orientation of three independent experiments, each with n=3.

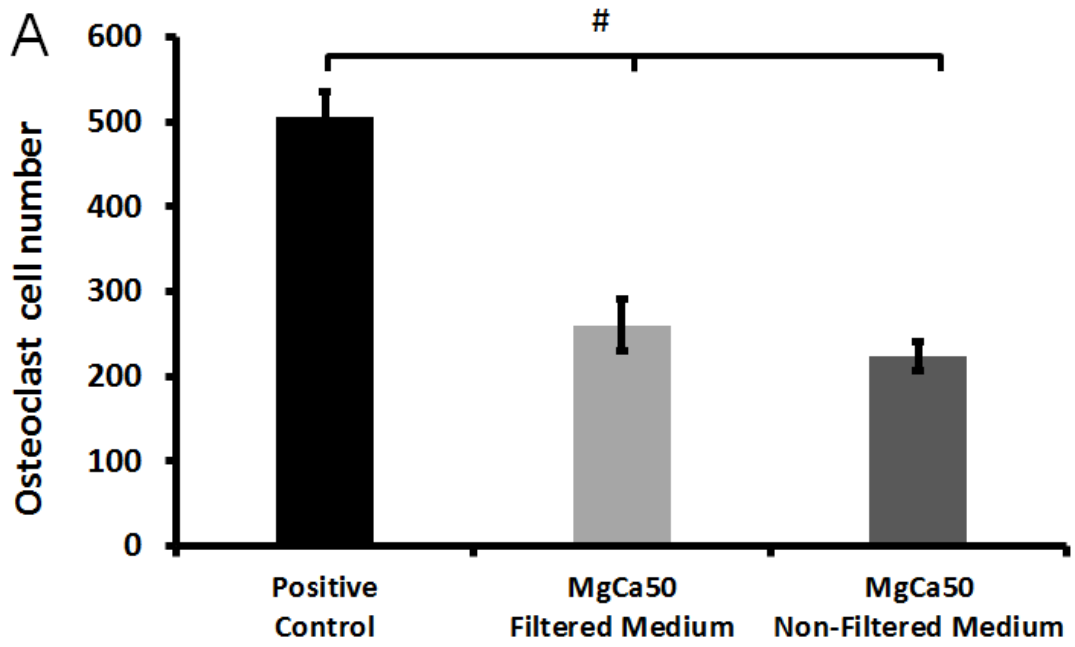

5-6A. Effect of Mg-Ca conditioned media on osteoclastogenesis investigated using the TRAP assay. RAW cells were cultured in the presence of Mg conditioned medium at varying concentration with (non-filtered medium) or without (filtered medium) the presence of corrosion granule for a period of 5 days. TRAP assay was performed following culture in Mg-Ca conditioned medium and RANK-L; all TRAP positive multinucleated cells in each well were counted for analysis. Culture in Mg-Ca50 filtered and non-filtered medium resulted in a significant reduction (#, $p < 0.001$) in osteoclast cell formation. Positive control represents RAW cells cultured in normal growth medium and then treated with RANK-L to induce differentiation. The bars represent the mean and standard deviation in the positive orientation of three independent experiments, each with n=8.

B

Positive Control

Mg-Ca50
Filtered Medium

Mg-Ca50
Non-Filtered Medium

5-6B. Effect of Mg-Ca conditioned media on osteoclastogenesis. Representative images of TRAP positive multinucleated cells taken after 5 days of culture. The arrows represent undifferentiated RAW cells. Positive control represents RAW cells cultured in normal growth medium and then treated with RANK-L to induce differentiation.

5.4. The response of mature osteoclast cells to Mg non-filtered conditioned media

Further investigation on the effect of Mg conditioned media on mature osteoclast resorption activity was performed. Fig.5-7 is showing the effect of Mg corrosion products on mature osteoclast cells; these cells were cultured on dentin bone slices and then treated with various concentrations of Mg non-filtered medium for 24 hours. Following treatment with Mg non-filtered medium, TRAP positive cells were counted and a reduction in osteoclast cell number was observed with Mg100 condition. However, following dilution (Mg50 and Mg25) osteoclast cell number increased. The treatment with calcitonin (sCT), an inhibitor of osteoclast activity did not affect cell number either. The data in Fig.5-7A shows that high Mg concentration and high pH did not have detrimental effects on mature osteoclast cell number. Since the cells were able to tolerate the various concentrations of Mg conditioned media, the resorption activity of these cells was also investigated. The presence of Mg non-filtered conditioned medium resulted in a reduction in osteoclast resorption activity. Even at low concentration (Mg25), the activity was very low compared to the control. The culture of cells in Mg100 non-filtered medium and the presence of calcitonin completely inhibited the activity of mature osteoclast cells.

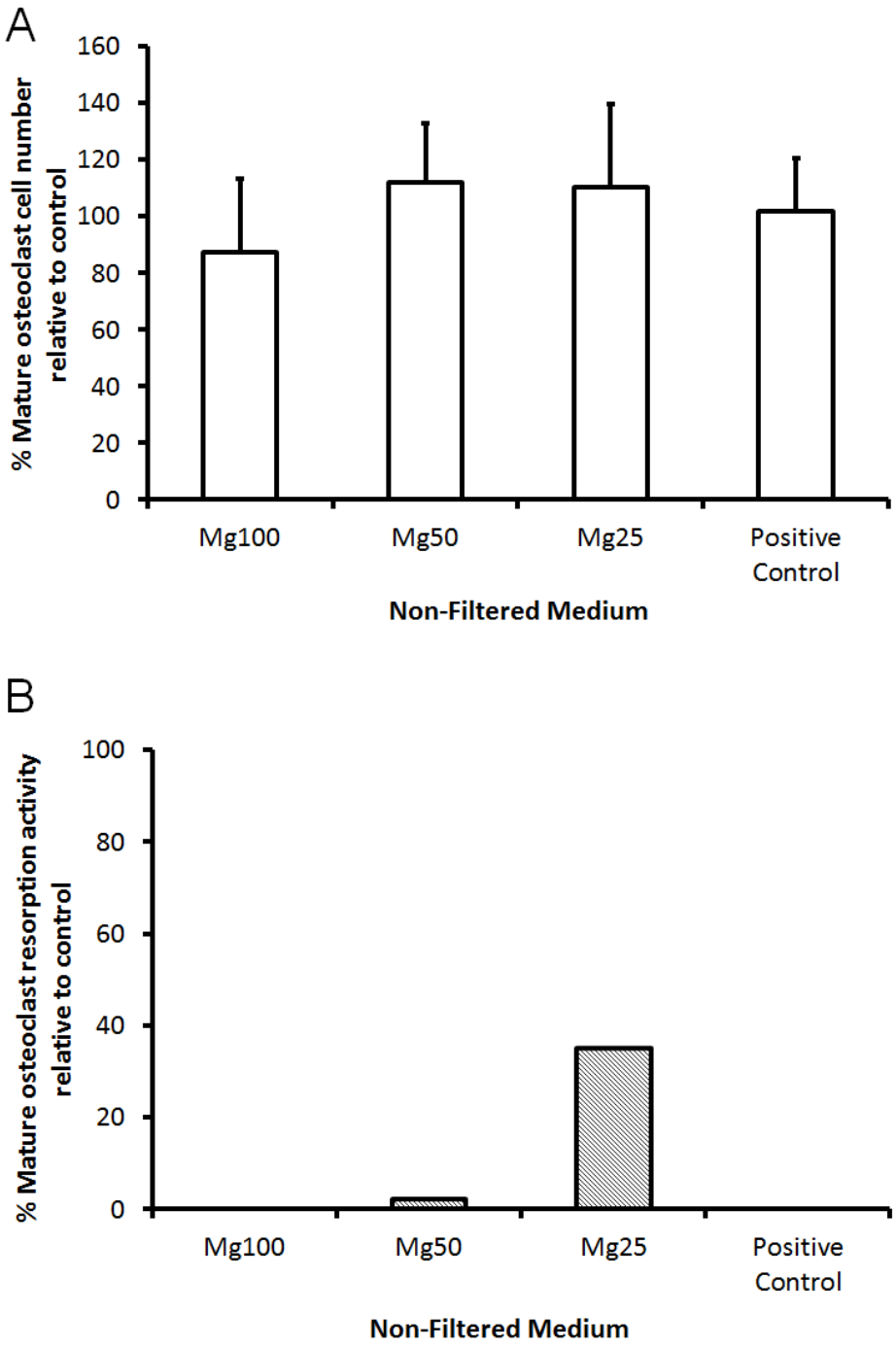

Fig.5-7. Effect of Mg non-filtered medium on mature osteoclast activity. (**A**) The number of TRAP positive mature osteoclast cells present on bone slices following a 24 hr treatment with various concentration of Mg non-filtered conditioned medium. Mature osteoclast cell number was normalised relative to the control (untreated sample). (**B**) Resorption pits formed by mature osteoclasts in the presence of Mg non-filtered medium were counted and

normalised to osteoclast cell number. Resorption activity was normalised relative to cells cultured in MO standard medium (control, 100%). Cells cultured in MO standard medium with the presence of sCT (inhibitor of resorption activity) were used as the positive control. The bars represent the mean and standard deviation in the positive orientation of three independent experiments, each with n=6.

5.5. The immune response of Mg and Mg-Ca biomaterials

The immune response of cells to Mg and Mg-Ca biomaterials was also investigated using cells involved in the immune response known as THP-1 cells. THP-1 cells were cultured in the presence of corroding Mg and Mg-Ca disks for a period of 24hours. The response of these cells to the presence of the disks was investigated at gene level (TNF-α, IL-1β and IL-8) (Fig.5-8). The absorbable suture material used was made from polyglycolic acid. This material is used routinely in clinic to hold tissue together following surgery or injury. This material is known to have minimal immune reaction (Bender & Brouwer, 1975). Untreated cells with no contact to biomaterial were used as the control. The expression of TNF-α was significantly reduced in the presence of both corroding Mg ($p<0.001$) and Mg-Ca ($p<0.01$) disks compared to the suture material. Similarly, the expression of IL-8 expression was also significantly reduced ($p<0.05$) in the presence of Mg compared to the suture material. On the other hand, in the presence of Mg-Ca alloy there was an 5x fold increase in the expression of IL-1β expression compared to suture material. 4x fold increase ($p<0.01$) in IL-1β expression was also observed in the presence of Mg-Ca compared to Mg.

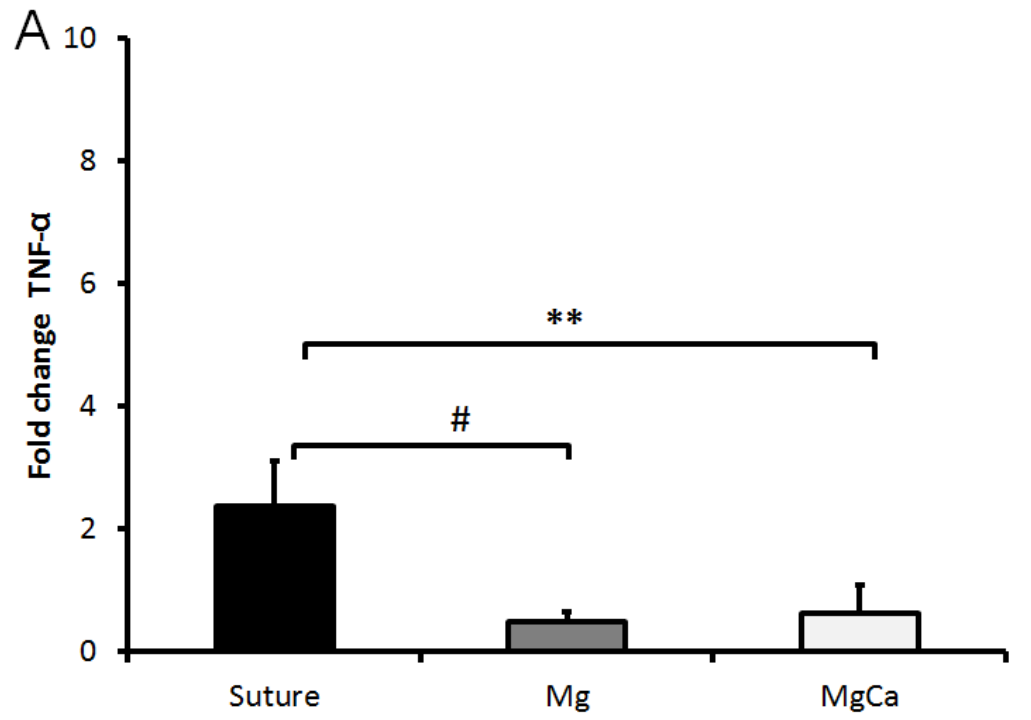
A
10
8
6
4
2
0
Fold change TNF-α
**
#
Suture
Mg
MgCa

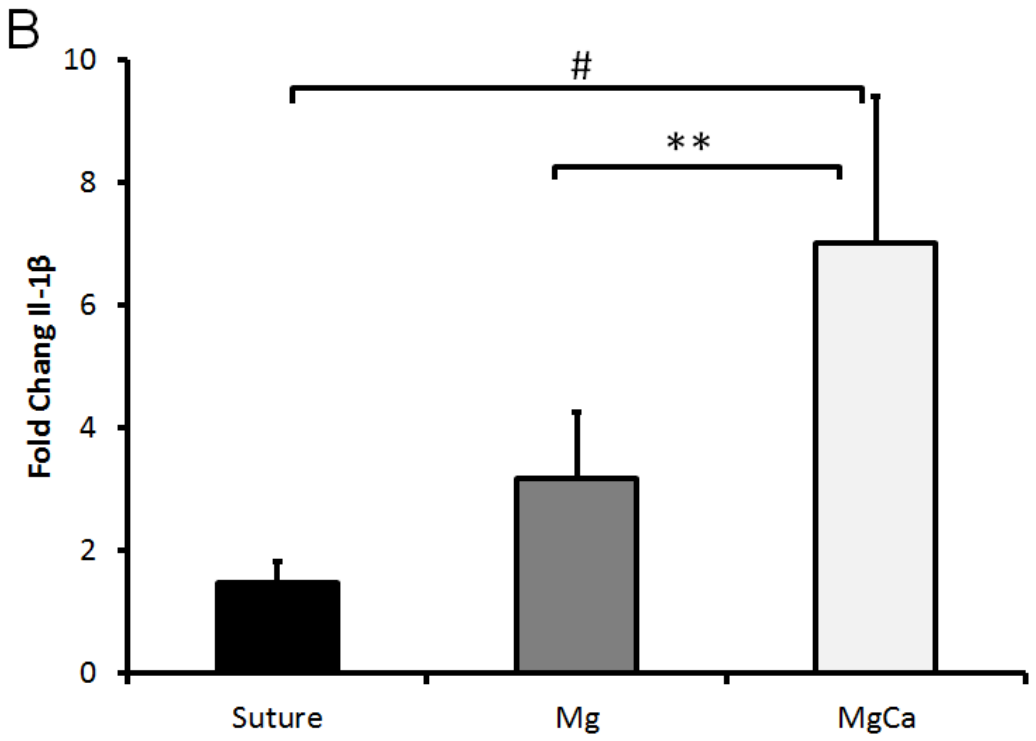
B
10
8
6
4
2
0
Fold Chang Il-1β
#
**
Suture
Mg
MgCa

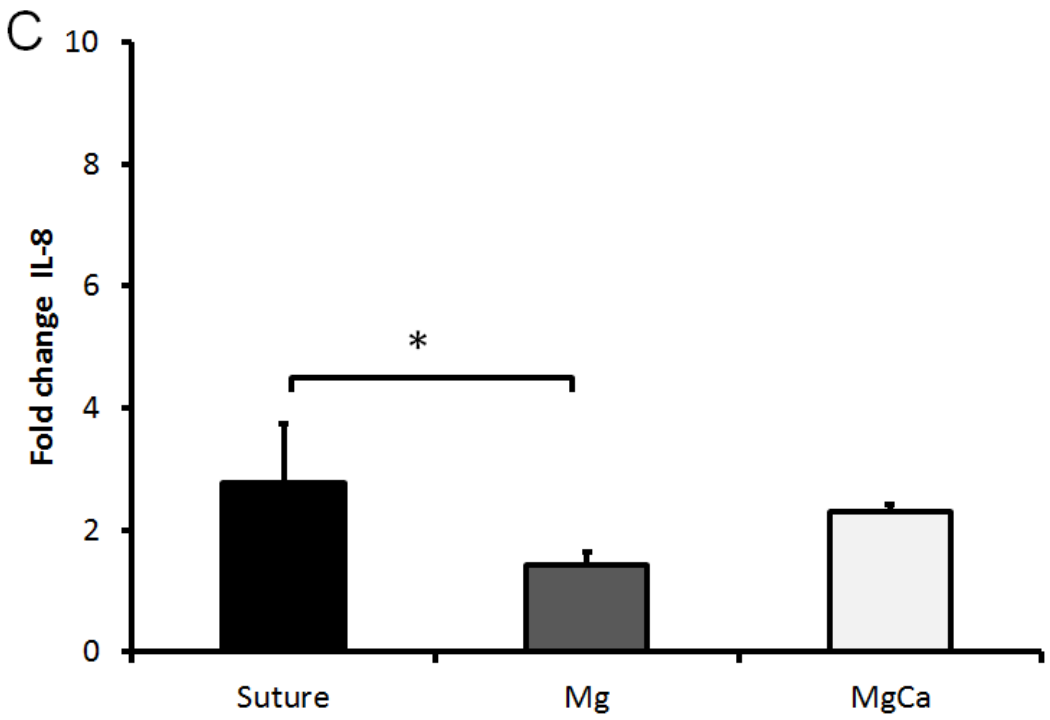

Fig.5-8. Immune response of Mg and Mg-Ca biomaterials investigated using qRT-PCR. (**A**) There was a significant reduction in the expression of TNF-α in the presence of both Mg (**, $p<0.01$) and Mg-Ca (#, $p<0.001$) disk compared to suture material. (**B**) The culture of cells in the presence of Mg-Ca disk resulted in a significant increase (#, $p<0.001$) and (**, $p<0.01$) in IL-1β expression compared to suture material and Mg disk respectively. (**C**) A significant reduction (*, $p<0.05$) in IL-8 expression was also observed when cells were cultured in the presence of Mg disk. Cells with no biomaterial contact (untreated condition) were used as the control. Gene expression data was normalised to the control. The bars represent the mean and standard deviation in the positive orientation of three independent experiments, each with n=3.

5.6. Summary

- RAW cells were highly sensitive to high concentrations of Mg and Mg-Ca conditioned medium.

- Even though metabolic activity was significantly reduced in the presence of Mg or Mg-Ca 100% filtered condition, cells were able to proliferate over time. RAW cells were able to overcome the initial shock and adapt to the change in environment created by the corroding disks.

- The presence of corrosion granules significantly affected metabolic activity and osteoclastogenesis. In the presence of corrosion granules (Mg or Mg-Ca non-filtered medium) the fusion of RAW cells into osteoclast cells was negatively affected resulting in a large number of undifferentiated cells, despite the fact that the cells were treated with RANK-L.

- Mature osteoclast cells were able to tolerate high concentrations of Mg conditioned medium. The culture of these cells with Mg100 non-filtered medium did not affect cell number; however the activity of these cells was significantly reduced.

- Mg was shown to downregulate inflammatory markers; however Mg-Ca corrosion induced the expression of IL-1β, a factor that stimulates osteoclast activity and proliferation.

CHAPTER 6: The effect of Magnesium corrosion products on myotubes formed by differentiated myoblasts

6.1. The response of myotubes to the presence of Mg conditioned media

C2C12 myoblasts were cultured on glass substrates, the cells were allowed to proliferate and differentiate into mature myotubes before treatment with Mg conditioned media. Following treatment with Mg conditioned media, metabolic activity of cells was investigated using the AlamarBlue assay. The metabolic activity of myotubes was significantly different over time following treatment with Mg conditioned media (filtered and non-filtered medium). A reduction in metabolic activity was observed on day 1 compared to day 2 and 3 when myotubes were treated with the various concentrations of filtered medium. On the other hand, the treatment of myotubes with non-filtered medium resulted in a reduction in metabolic activity when myotubes were treated with Mg25 and Mg 10 compared to Mg100 and Mg 50 (Fig.6-1). Even though a significant reduction in metabolic activity was observed on day 1, metabolic activity was still above 70% throughout the culture period, even at the highest concentration of 16.9mM (Mg100), suggesting no cytotoxicity effects for both filtered and non-filtered medium. The initial (day 1) treatment of cells with Mg conditioned media caused the greatest effect on mature myotube metabolic activity. Nevertheless, following the initial exposure to Mg conditioned media, myotubes were able to adapt to the environment overtime with or without the presence of corrosion granules.

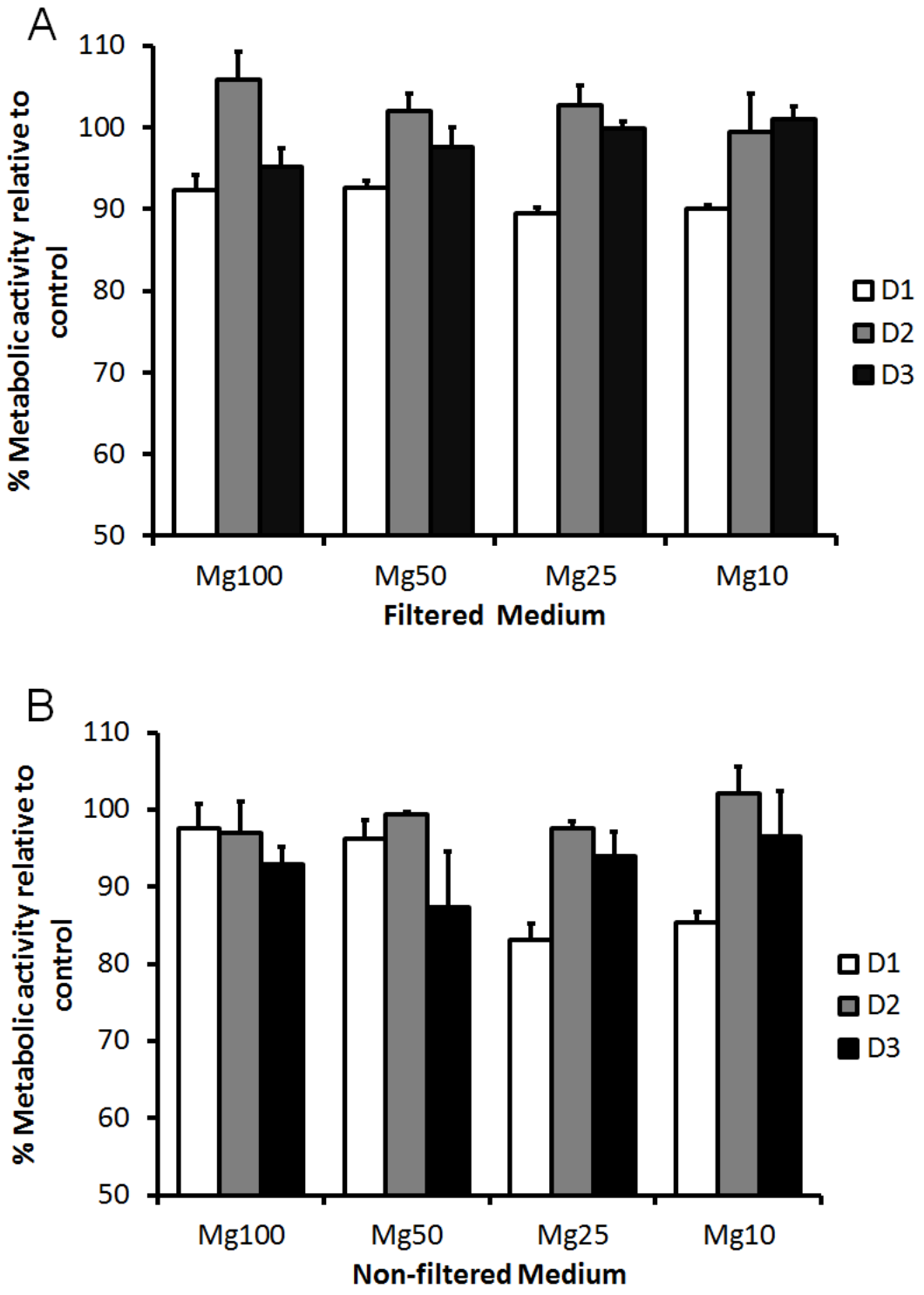

Fig.6-1. Effect of Mg conditioned media on mature myotubes metabolic activity was investigated using Alamar Blue assay. Myotubes were cultured in various concentrations of (A) Mg filtered medium and (B) Mg non-filtered medium over a period of 3 days. Metabolic actvity for all concentrations at all time points was above 70%, suggesting no cytotoxic effects.

100% metabolic activity represents the control. The bars represent the mean and standard deviation in the positive orientation of three independent experiments, each with n=3.

6.2. Morphological analysis of myotubes after treatment with Mg conditioned media

To further understand the effect of Mg conditioned media on myotubes, morphological analysis was performed on images captured on day 3 of treatment. Mature myotubes were cultured in Mg conditioned medium. After 3 days in culture, the myotubes were fixed with formalin and stained with phalloidin for analysis. Mg100 filtered and non-filtered media resulted in small sized myotubes (Fig. 6-2). These myotubes were smaller, thinner and shorter compared to the control, especially in the presence of the corrosion granule. However, dilution of the Mg conditioned media alleviated the effect observed with Mg100 concentration. In the control condition, (Fig.6-2I) thick, elongated multinucleated myotubes were observed. This was also similar when myotubes were treated with diluted concentrations (Mg50, Mg25, Mg10) of Mg filtered (B-D) and non-filtered medium (F-H).

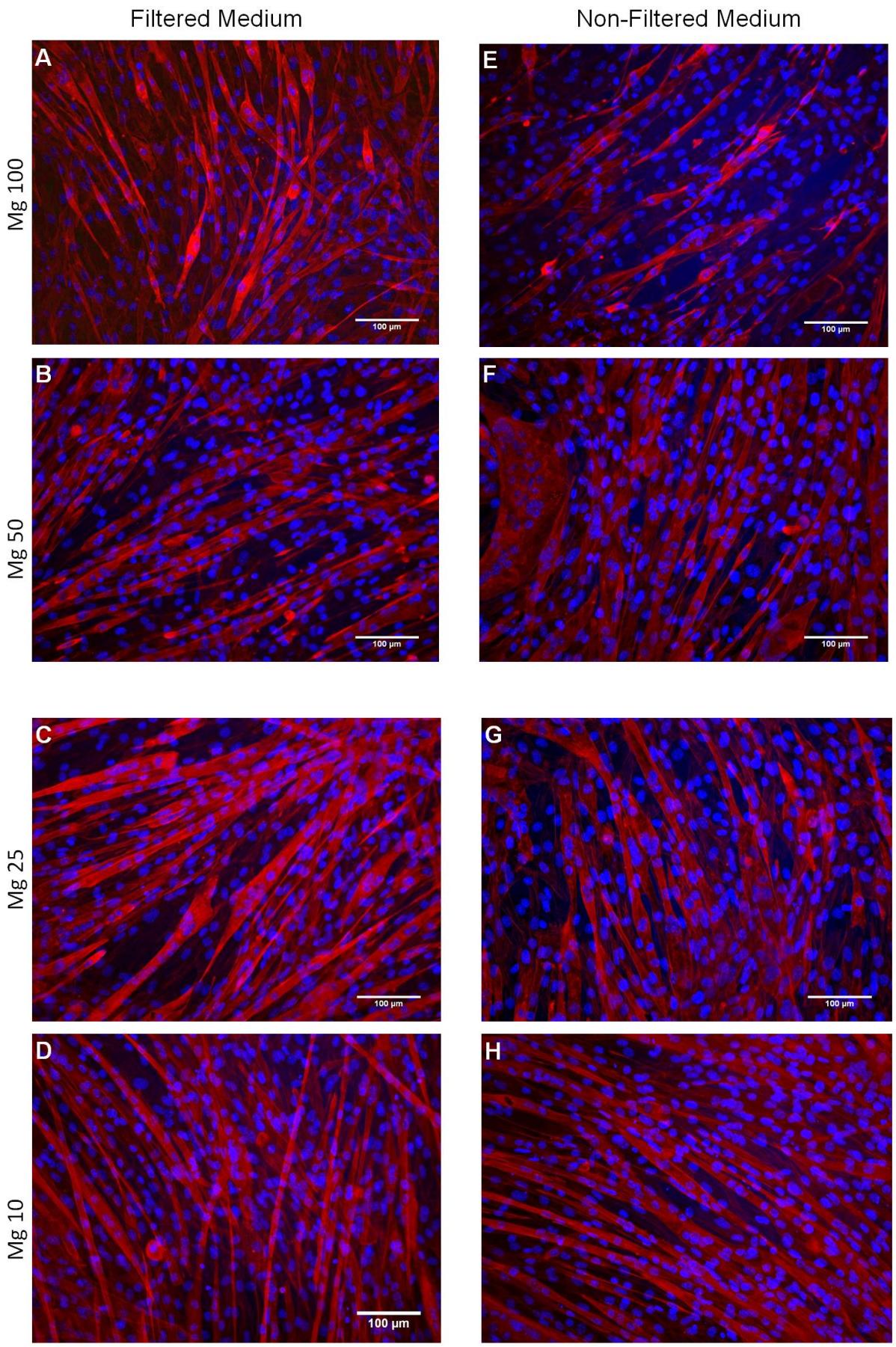
Filtered Medium
Non-Filtered Medium
Mg 100
Mg 50
Mg 25
Mg 10
A
B
C
D
E
F
G
H
100 µm

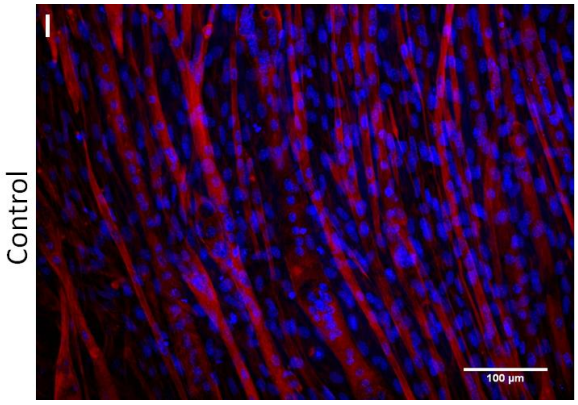

Fig.6-2. Representative images showing actin filament staining of myotubes after treatment with various concentrations of Mg conditioned media. (**A-D**) Images showing the effect of filtered medium on myotubes and (**E-H**) images showing the effect of non-filtered medium on myotubes. (**I**) Image showing cells cultured in standard growth medium (control). Scale bar= 100µm. Blue represent the nuclei and red represent the myotubes.

Further image analysis was performed to quantify the size distribution of myotubes presented in the field of view of randomly selected images. A multinucleated myotube is formed when myoblasts fuse together. The number of nuclei per myotube can be used as an indication of myotube size. The more myoblasts that fuse together the bigger the myotube and the higher the number of nuclei present per myotube. Image analysis of myotubes treated with both Mg filtered and non-filtered medium is illustrated in Fig.6-3. The data reflected quantitatively the influence of Mg conditioned media on myotube size as shown in the images of Fig.6-2. When cells were treated with Mg100 conditioned media (filtered and non-filtered medium) there was a significantly higher ($p<0.001$) percentage (80%) of smaller myotubes compared to the control (50%) (Fig.6-3). Myoblasts were allowed to proliferate and differentiate into mature myotubes in normal cell culture conditions before the myotubes were treated with Mg conditioned media. The presence of a higher percentage of smaller myotubes in Mg100 conditioned medium implies that treatment with the conditioned medium caused the myotubes to shrink in size. However, when the concentration of Mg conditioned media (filtered and non-filtered medium) was reduced by half; this effect on myotube size was reduced by at least 20%. Dilution of Mg100 filtered medium to Mg50, 25 and 10 concentrations resulted in myotube size distribution similar to the control. The dilution of Mg100 non-filtered medium to Mg50 and Mg25 concentrations also resulted in a myotube size distribution similar to control. However, treatment with Mg10 non-filtered medium resulted in a significantly lower ($p<0.05$) percentage of smaller myotubes and a significantly higher ($p<0.05$) percentage of medium sized myotubes in comparison to the control.

The treatment of cells with Mg50 and Mg25 non-filtered medium resulted in a significantly lower ($p<0.05$) myotube number per field of view compared to treatment with Mg100 and

Mg50 filtered medium (Fig. 6-3C). Smaller myotubes led to high cell number count per field of view, hence the high cell count observed with Mg 100 condition (Fig.6-3C).

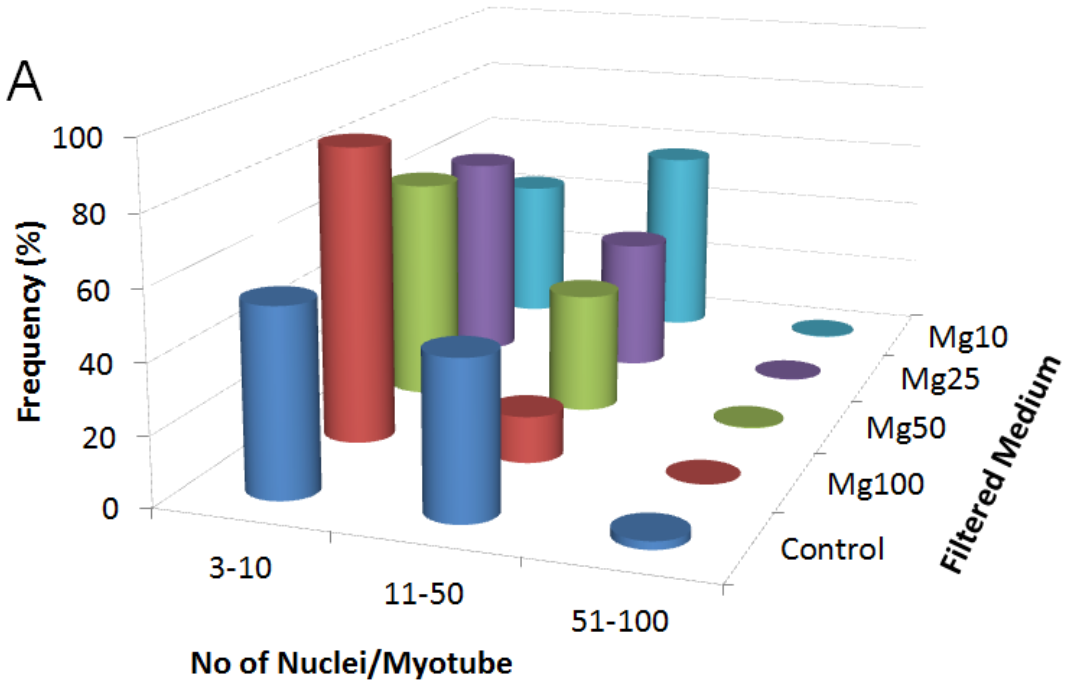

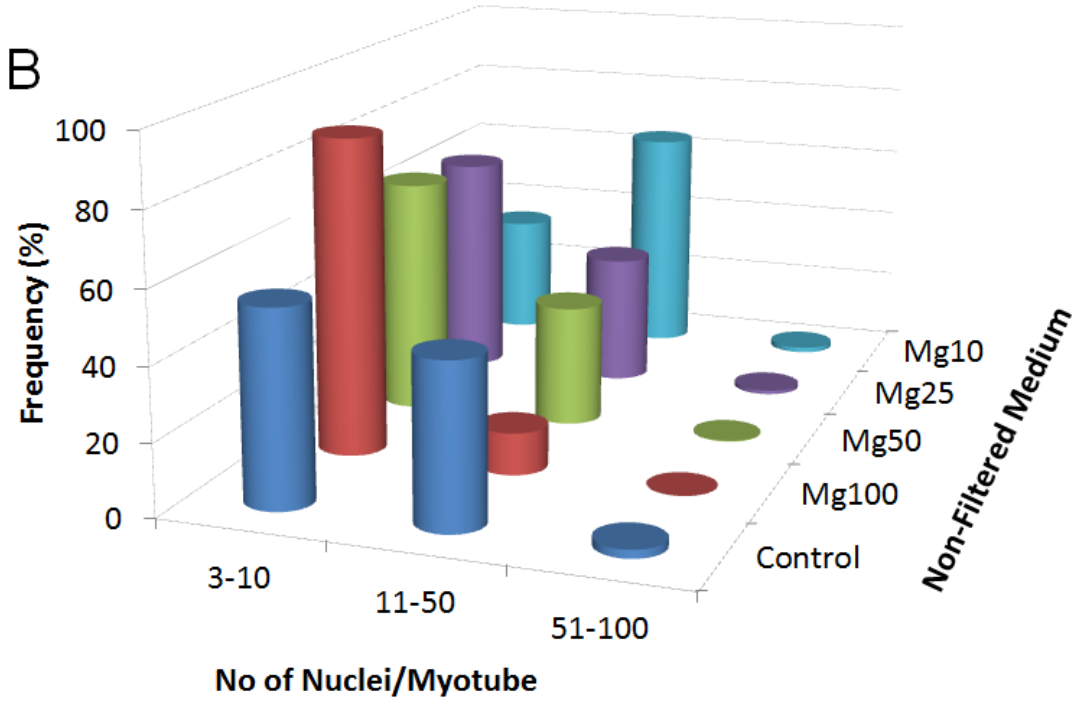

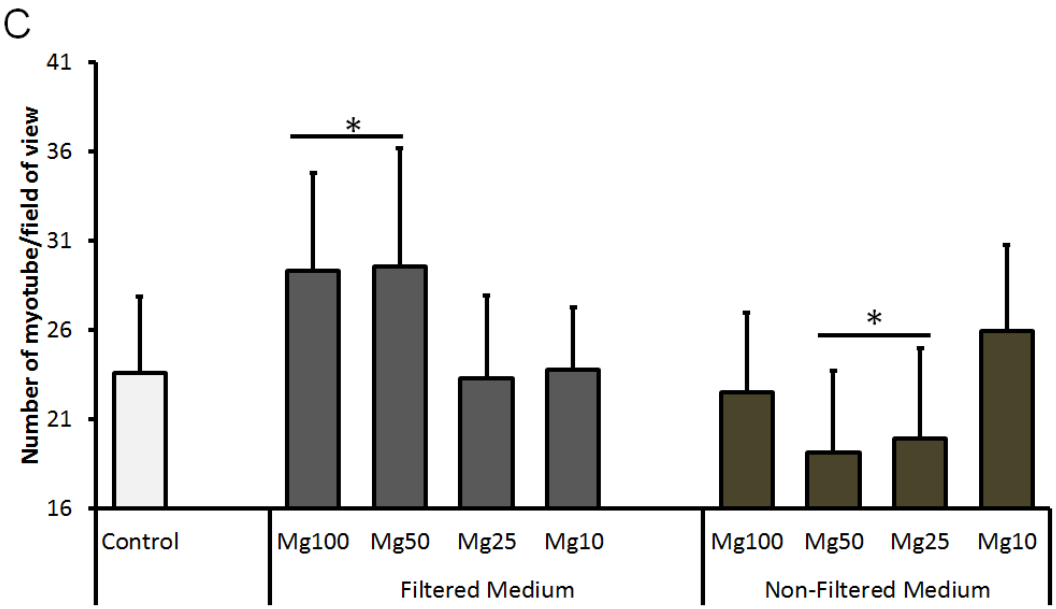

Fig.6-3. Image analysis of stained myotubes following treatment with Mg filtered and non-filtered medium. (**A**) and (**B**) Treatment with both Mg100 filtered and non-filtered medium resulted in a significantly high ($p<0.001$) percentage of smaller myotubes (3-10 nuclei/myotube) compared to control. (**C**) There was a significant increase (*, $p<0.05$) in the number of myotubes per field of view when myotubes were treated with Mg100 and Mg50 filtered medium compared to treatment with Mg25 and Mg10 non-filtered medium. The bars represent the mean and standard deviation in the positive orientation of three independent experiments, each with n=3.

6.3. The response of myotubes to the presence of Mg-Ca conditioned media

C2C12 myoblasts were cultured on glass substrates, the cells were allowed to proliferate and differentiate into mature myotubes before treatment with Mg conditioned media. Following treatment with Mg-Ca conditioned media, metabolic activity of cells was investigated using the AlamarBlue assay. Tthe treatment of myotubes in the presence of Mg-Ca conditioned media (filtered and non-filtered medium) resulted in an increase in metabolic activity when comparing the various concentrations to the control at each time point (Fig.6-4). The treatment of myotubes with Mg-Ca conditioned media resulted in a 1.5x increase at the most in metabolic activity. However, by day 3 a reduction in metabolic activity was observed compared to day 1 and 2, but activity was still above the control.

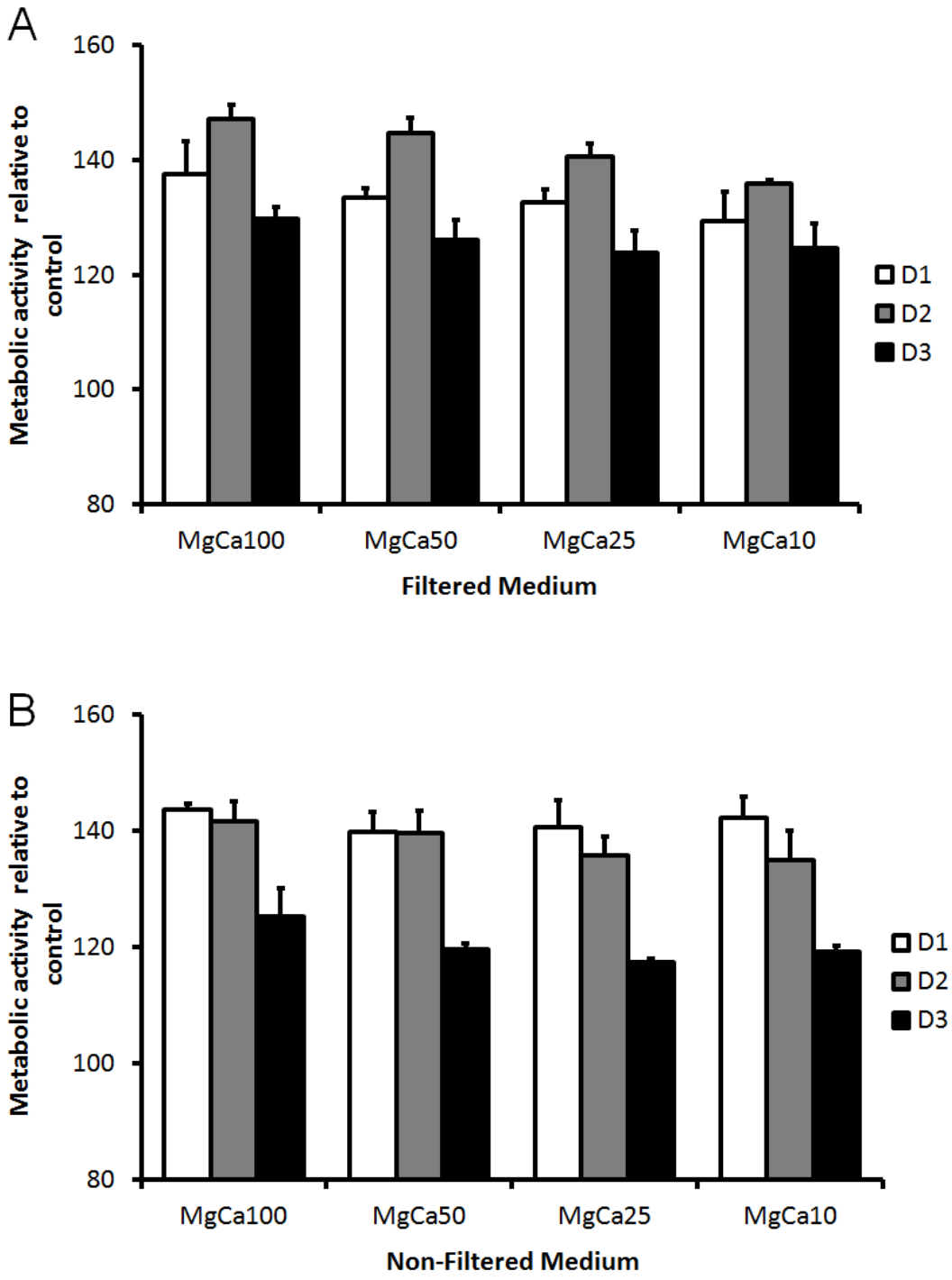

Fig.6-4. Effect of Mg-Ca conditioned media on mature myotubes metabolic activity was investigated using Alamar Blue assay. Myotubes were cultured in various concentrations of (A) Mg-Ca filtered medium and (B) Mg-Ca non-filtered medium over a period of 3 days. Treatment with Mg-Ca conditioned media resulted in enhanced metabolic activity. 100%

metabolic activity represents the control. The bars represent the mean and standard deviation in the positive orientation of three independent experiments, each with n=3.

6.4. Morphological analysis of myotubes after treatment with Mg-Ca conditioned media

Actin filament staining of myotubes treated with Mg-Ca conditioned media (filtered and non-filtered medium) revealed the formation of large myotubes.

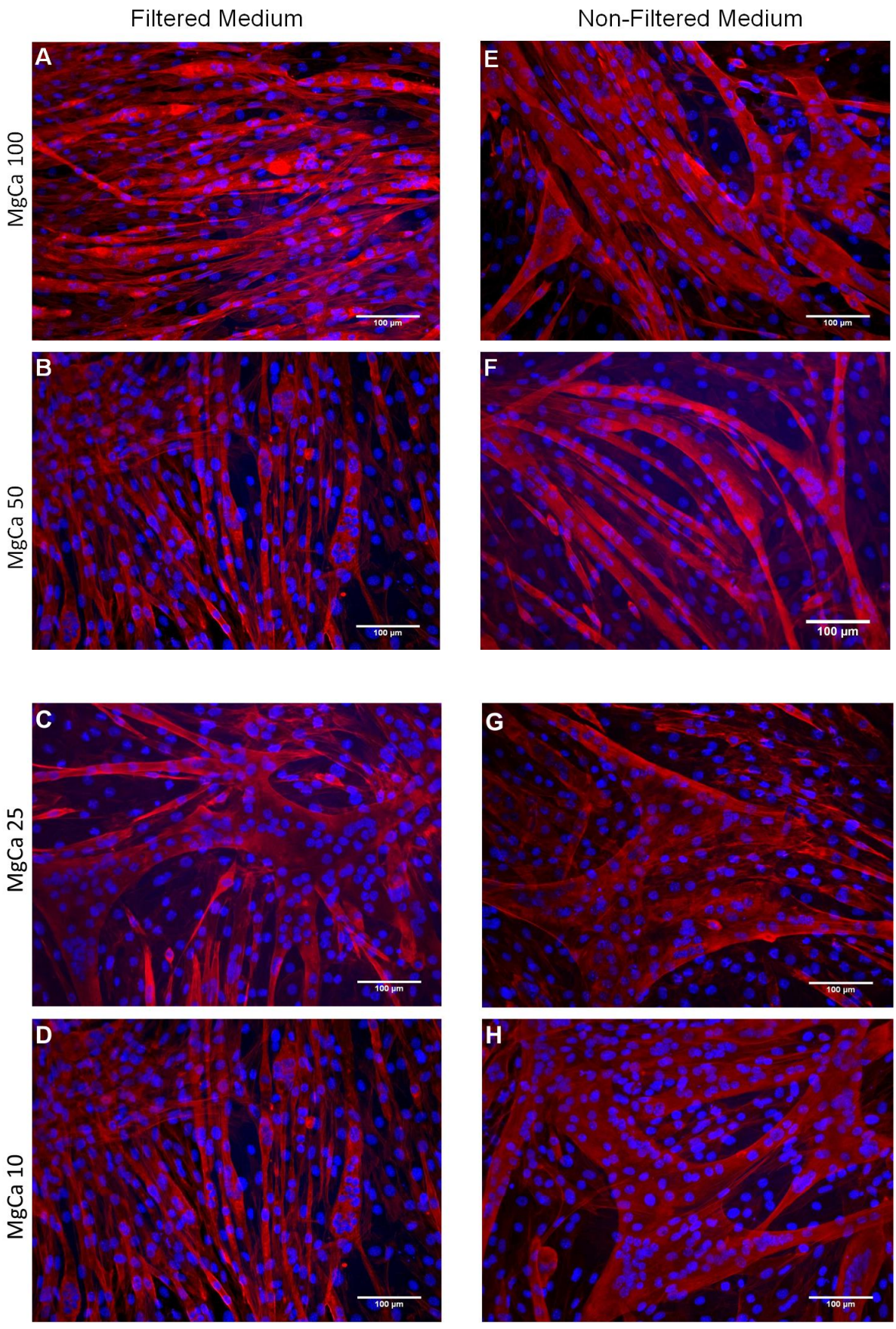
Filtered Medium
Non-Filtered Medium
MgCa 100
MgCa 50
MgCa 25
MgCa 10
A
B
C
D
E
F
G
H
100 µm

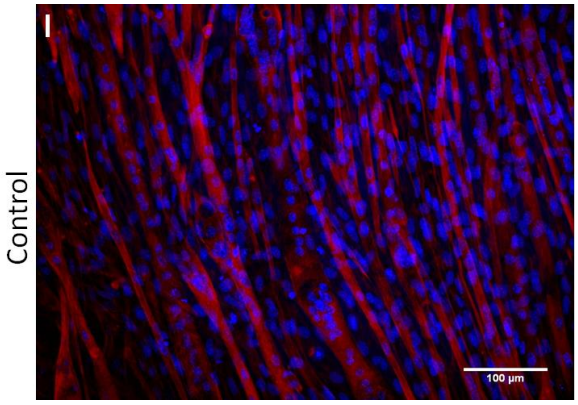

Fig.6-5. Representative images showing actin filament staining of myotubes after treatment with various concentrations of Mg-Ca conditioned media. (**A-D**) Images showing the effect of filtered medium on myotubes and (**E-H**) images showing the effect of non-filtered medium on myotubes. (**I**) Image showing myotubes cultured in growth medium (control). No adverse effects were seen when myotubes were treated with Mg-Ca conditioned medium; treatment with Mg-Ca resulted in the formation of large myotubes compared to the control. Scale bar= 100µm.

Image analysis of myotubes treated with both Mg-Ca filtered and non-filtered medium is illustrated in Fig.6. The data reflected quantitatively the influence of conditioned media on the size of myotubes as shown in the images of Fig.5. When myotubes were cultured in MgCa100 filtered medium there was a significantly higher percentage of smaller myotubes compared to MgCa10. Furthermore, treatment of myotubes with MgCa25 and MgCa10 filtered medium resulted in a higher percentage ($p < 0.01$) of extra-large myotubes compared to the control. When cells were cultured in Mg-Ca non-filtered conditioned medium, myotube size distribution was similar to control for all the concentrations.

The effect of Mg-Ca conditioned medium on myotube number was also investigated; treatment of cells with MgCa25 and MgCa10 filtered medium resulted in a significantly lower ($p < 0.01$) myotube number per field of view compared to treatment with MgCa100 non-filtered medium (Fig.6-6C). When cells were treated with Mg-Ca filtered medium, dilution of MgCa100 resulted in lower myotube number. A large myotube covers a large surface area; therefore lower numbers of myotubes were counted per unit surface area, significantly reducing total myotube count.

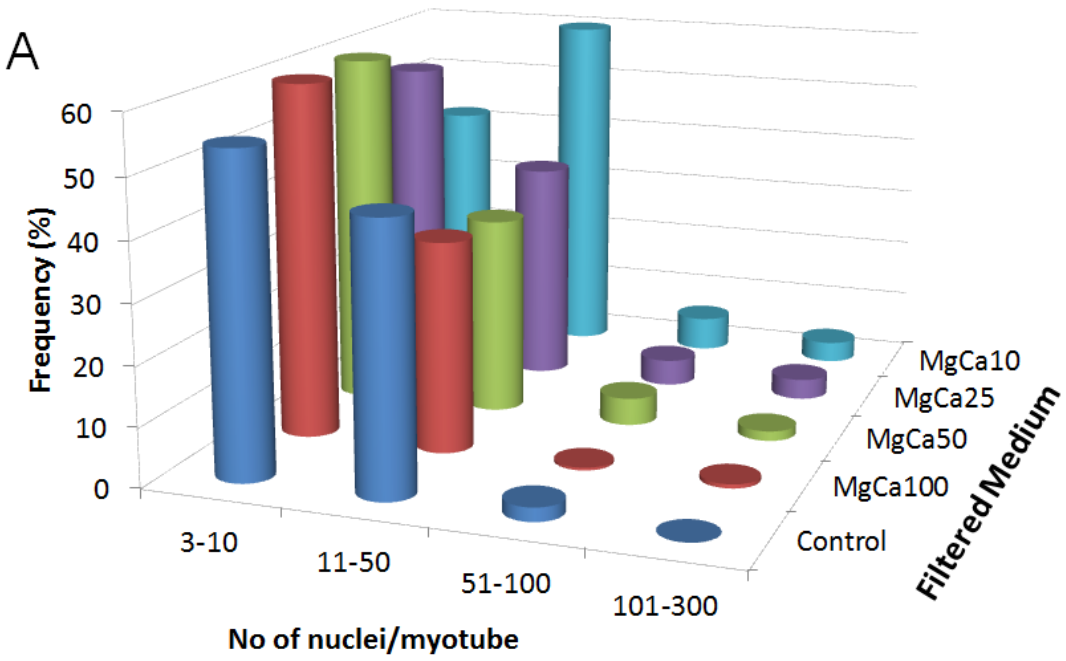
A
60
50
40
30
20
10
0
Frequency (%)
3-10
11-50
51-100
101-300
No of nuclei/myotube
MgCa10
MgCa25
MgCa50
MgCa100
Control
Filtered Medium

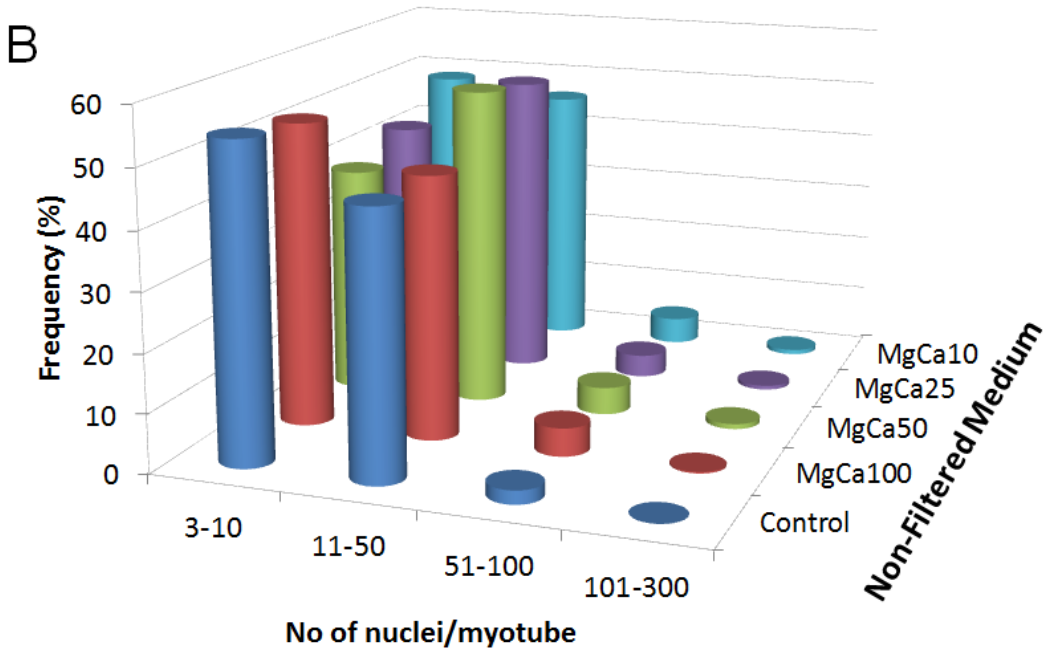
B
60
50
40
30
20
10
0
Frequency (%)
3-10
11-50
51-100
101-300
No of nuclei/myotube
MgCa10
MgCa25
MgCa50
MgCa100
Control
Non-Filtered Medium

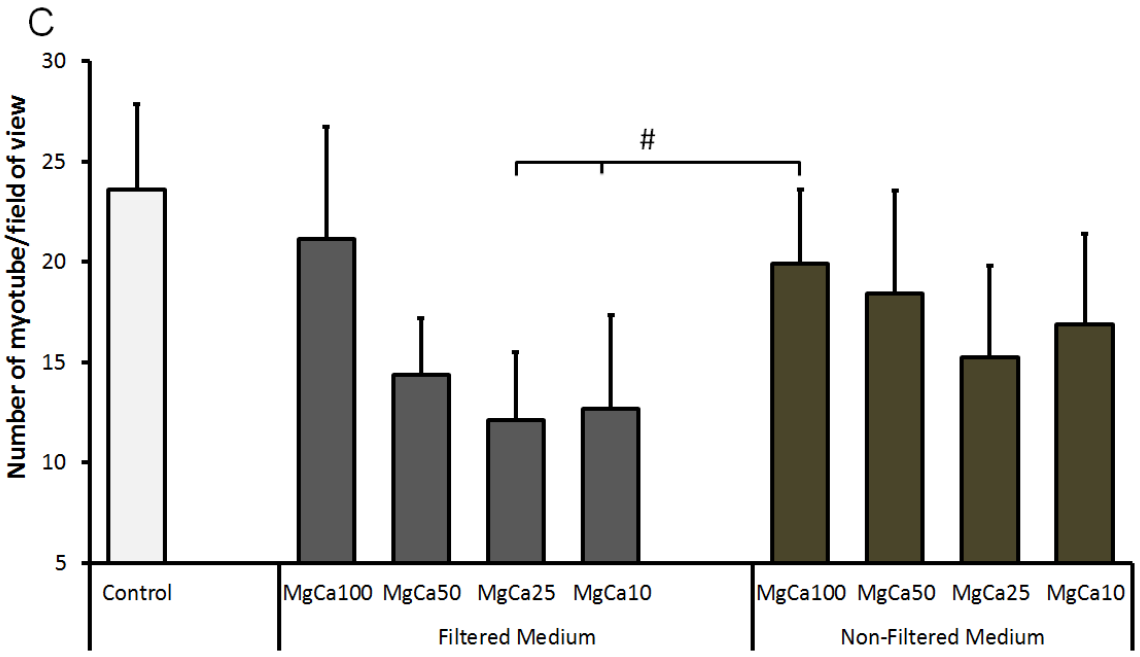

Fig.6-6. Image analysis of the stained myotubes following treatment with Mg-Ca conditioned media. (**A**)When myotubes were treated with filtered medium, myotube size distribution followed a trend similar to the control. However, treatment of myotubes with MgCa25 and MgCa10 filtered medium resulted in a higher percentage ($p<0.01$) of extra-large myotubes. (**B**) The treatment of myotubes with Mg-Ca non-filtered medium also resulted in a size distribution similar to control. (**C**) Treatment of cells with MgCa25 and MgCa10 filtered medium resulted in a significantly lower (#, $p < 0.001$) myotube number as measured per field of view compared to treatment with MgCa100 non-filtered medium. The bars represent the mean and standard deviation in the positive orientation of three independent experiments, each with n=3.

6.5. The effect of Mg and Mg-Ca conditioned media on myotubes at gene level

Gene analysis was performed to investigate the effects of high concentration of Mg corrosion products on myotubes. Gene expression analysis of myogenin, a muscle specific gene marker for myotube formation was performed following treatment with Mg conditioned medium. As observed earlier, high Mg^{2+} concentration caused adverse effects on myotube size, resulting in small sized myotubes. Therefore gene analysis was performed on cells treated with Mg concentration ≥10mM (Mg100 and Mg50). As shown in Fig. 6-7, expression of myogenin was slightly higher when myotubes were treated with Mg filtered medium compared to non-filtered medium.

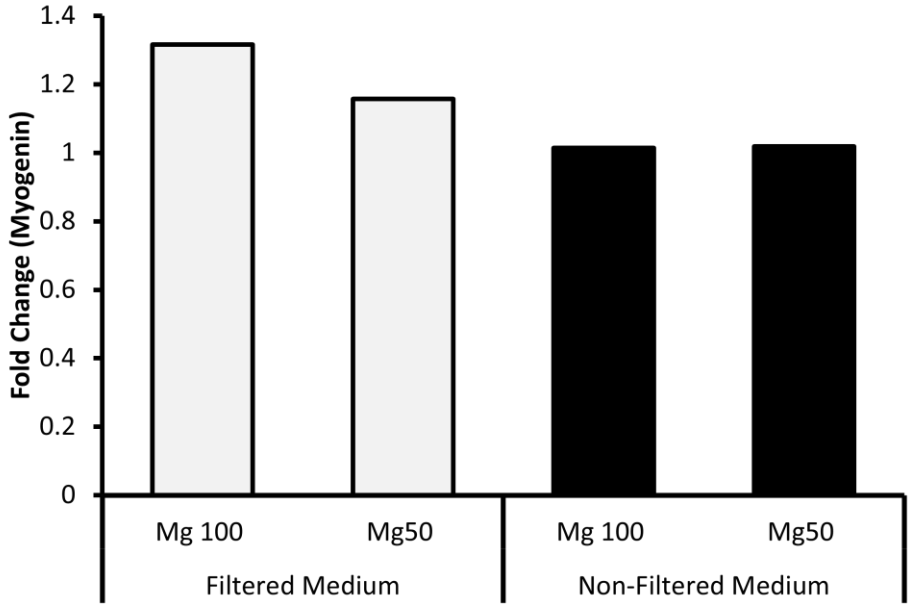

Fig.6-7. The effect of Mg conditioned medium at gene level on myotubes investigated using qRT-PCR. Following treatment with Mg conditioned media (filtered and non-filtered) for 3 days, gene expression analysis on myogenin was performed. Expression of myogenin was slightly higher in myotubes treated with filtered medium compared to non-filtered medium.

The fold change is relative to the control sample, represented by a fold change of 1. Target gene expression was normalised to the housekeeping gene (RP2-β).

Further investigation on gene expression analysis was performed; the expression of MurF1 and MAFbx was investigated following treatment with Mg conditioned media. MurF1 and MAFbx are muscle-specific ubiquitin ligases genes that are upregulated during skeletal muscle atrophy (Bodine & Baehr, 2014). The treatment of myotubes with Mg filtered and non-filtered medium downregulated MurF1 expression compared to the control (Fig.6-8A). On the other hand the expression of MAFbx was upregulated when myotubes were treated with Mg100 non-filtered medium compared to control; however, only a 0.4 fold change was observed (6-8B).

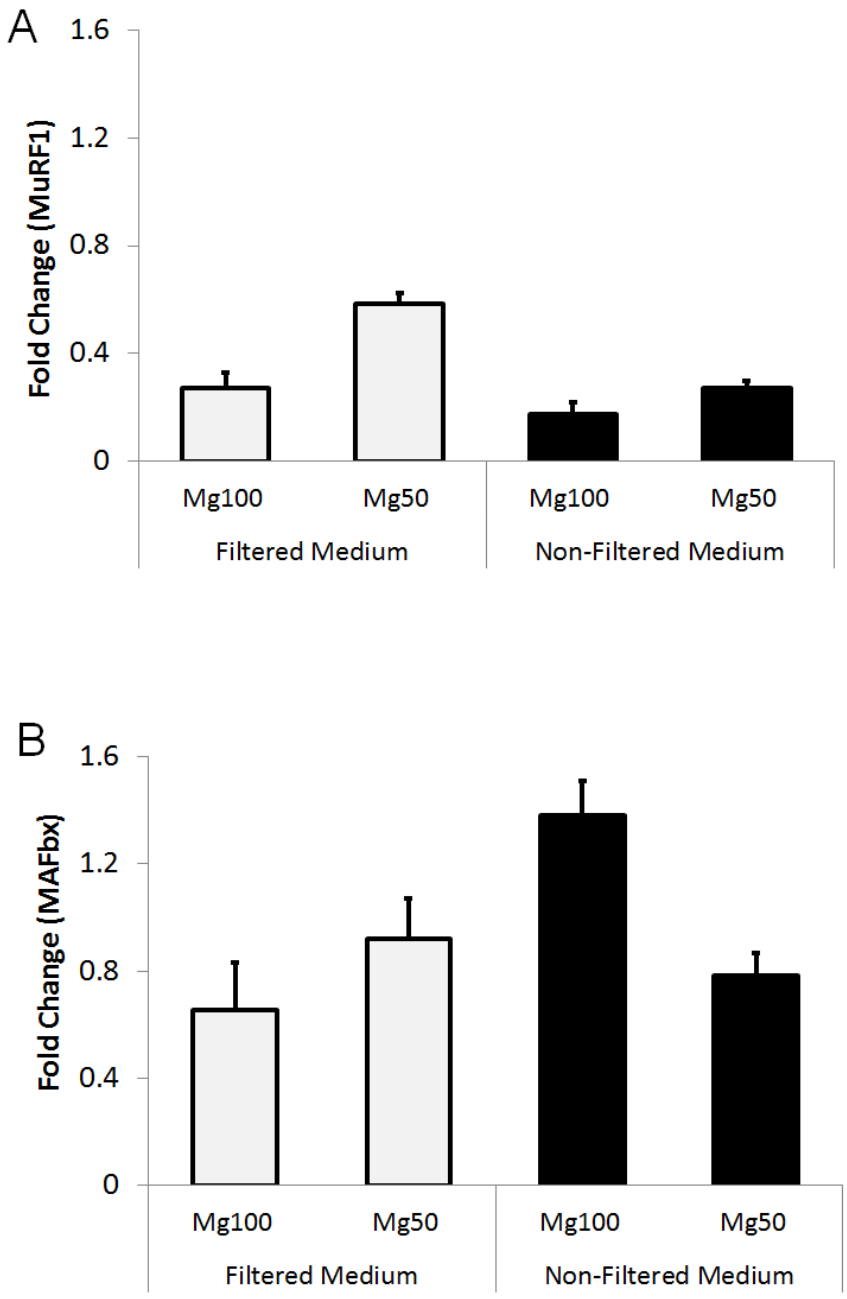

Fig.6-8. The effect of corrosion products at gene level on myotubes treated with Mg conditioned medium over a period of 3 days was investigated using qRT-PCR. (**A**) Fold change in the gene expression of MuRF1 following treatment with Mg conditioned medium. Treatment of myotubes with Mg conditioned medium resulted in the downregulation of MurF1. (**B**) T**r**eatment of myotubes with the presence of Mg100 non-filtered medium resulted in a 0.4-fold increase in the expression of MAFbx. The fold change is relative to the control

sample, represented by a fold change of 1. Target gene expression was normalised to the housekeeping gene (RP2-β). The bars represent the mean and standard deviation in the positive orientation of three independent experiments, each with n=3.

6.6. Summary

- Mg^{2+} and Ca^{2+} ions are important in the process of myogenesis, the concentration of these ions and the ratio of the ions to each other play a significant role in maintaining the cellular activities of myoblasts.

- Initial exposure of myotubes to high Mg corrosion product concentration reduced cell viability but over time the myotubes were able to adapt.

- Over the time period investigated, cells responded differently to Mg and Mg-Ca conditioned media.

- A high Ca/Mg ratio resulted in the formation of large myotubes and a low Ca/Mg ratio resulted in small sized myotubes..

- High Mg^{2+} concentration between 4-10mM can accelerate cell proliferation but the availability of Ca^{2+} is crucial for myotube formation

CHAPTER 7: Discussion

7.1. The *in vitro* corrosion conditions of Mg/Mg-Ca alloy

The corrosion of Mg/Mg-Ca alloys results in the release of Mg^{2+} into the media. The ions released are dependent on the corrosion rate; the higher the corrosion rate the higher the amount released in a unit of time. Secondly, the corrosion of Mg/Mg alloy results in calcium depletion from the media to form calcium phosphates. Thirdly, corrosion of Mg/Mg alloy results in an increase in pH, making the culture media alkaline. However, DMEM contains sodium carbonate and exposure of the conditioned medium to CO_2 during cell culture results in the formation of a CO_2/bicarbonate buffering system similar to that in blood (Willumeit et al., 2011). *In vivo* pH is tightly regulated not only through the CO_2/bicarbonate system but also through biochemical buffers such as proteins (Naddaf Dezfuli et al., 2014; Witecka et al., 2016). Therefore, the addition of FBS to the conditioned medium after the *in vitro* corrosion process could also provide further buffering capabilities. The presence of proteins in the corrosion medium has been reported to slow down corrosion rate of magnesium through adsorption into the corrosion layer. The adsorption of proteins into the corrosion layer makes it more dense, turning it into a more effective protective barrier against corrosion (Yamamoto & Hiromoto, 2009; Jian Zhang et al., 2014). *In vitro,* equilibrium is reached when the corrosion medium is saturated with Mg ions released through the corrosion process. However, under the dynamic *in vivo* environment, equilibrium is never reached and eventually the magnesium implant corrodes completely. The differences between *in vitro* and *in vivo* corrosion environment greatly affects the corrosion behaviour of magnesium based implants. The *in vivo* environment is complex. In addition to the organic and inorganic

components of the body fluids, interaction of cells with the proteins in the corrosion layer can cause desorption, disrupting the protective corrosion layer (Jian Zhang et al., 2014). Furthermore, fluid flow and location of the implant within the body all contribute to the corrosion behaviour of magnesium. This study aimed to emulate the *in vivo* environment as closely as practically possible by using corrosion medium that has similar composition to body fluids and performing the corrosion test in a humidified atmosphere at 37°C and 5% CO_2. Furthermore, corrosion products containing both insoluble and soluble ions were used to investigate the local biological response of cells in an effort to mimic the *in vivo* implantation site. The dilution of the corrosion products gave the understanding of the concentration effects simulating the concentration gradients in the surrounding tissue.

7.2. Effect of Mg/Mg alloy conditioned media on cell viability

7.2.1. Human Mesenchymal Stem Cells

hMSCs were able to tolerate Mg ion concentration of up to 17mM, which is 17 times greater than that typically found in serum (0.70-1.0mM), but metabolic activity (Fig.3-1) and proliferation (Fig.3-2) was enhanced at concentrations ≤10mM . When cells were cultured in the presence of Mg-Ca conditioned media metabolic activity was comparable to the control (Fig.3-5), the impact of Mg-Ca conditioned media was significantly less compared to Mg conditioned media. This is because the highest Mg ion concentration of the Mg-Ca conditioned media was 4mM, which is within the beneficial range (Table.2-11). The mere presence of corrosion granules resulted in reduced metabolic activity (Fig.3-1B) and proliferation (Fig.3-2B), and more so in the presence of high corrosion granules concentration (Mg100). The effect was also time dependent, with longer exposure to the corrosion granules

resulting in reduced cell viability. When cells were presented with Mg100 non-filtered medium, no change in cell number was observed as shown by the DNA concentration analysis (Fig.3-2B). It is possible that the presence of the corrosion granules in high concentration became a physical barrier for cell growth by limiting the surface area available for the cells to grow, but may not necessarily be toxic to the cells. Indeed, when corrosion granules were reduced (Mg50 non-filtered medium) proliferation capacity was improved and further reduction in corrosion granule concentration resulted in enhanced cell proliferation. This is further validated by the fact that cells cultured in Mg-Ca conditioned media (low corrosion granule) did not show significant alterations in metabolic activity/proliferation (Fig.3-5 & 3-6).

To further understand how each cell responded to the presence of the conditioned media, the metabolic activity/cell was also investigated. Culture in both Mg (Fig.3-3A) and Mg-Ca (Fig3-7A) filtered conditioned media resulted in the reduction of metabolic activity/cell with time, on day1 metabolic activity/cell was significantly above the control but by day 7, metabolic activity/cell was significantly below the control. The reduction in metabolic activity/cell over time could be attributed to a higher proliferation rate due to the presence of the mitogenic Mg ions, resulting in the cells reaching confluency earlier than the control. On the other hand, in the presence Mg (Fig.3-3B) and Mg-Ca (Fig.3-7B) non-filtered medium, the metabolic activity remained constant over time and levels were comparable to the control throughout the culture period except for Mg100 and Mg50 non-filtered medium on day 7. The high metabolic activity/cell observed on day 7 in the presence of Mg100 and Mg50 non-filtered medium could be attributed to the cells responding to the high amount of corrosion granules present. The presence of corrosion granules was not toxic to cells, as evidenced by the ability of treated cells (Mg100 and Mg50) to maintain metabolic activities similar to the

control by day 3 (Fig.3-3B). The detachment of nodules formed when cells were presented with the corrosion granules could also be seen as an *in vitro* coping mechanism to clear the high amount of corrosion granule. The images from the live imaging (Fig.3-4) further supports the assumption that higher cell metabolic activity of Mg100 and Mg50 at day 7 and the reduction of proliferation rate (Mg 50) or even stopping of growth (Mg100) as evidenced by the DNA concentration is attributed to cells metabolic activity being diverted to dealing with the high amount of corrosion granules (Fig.3-2). The mechanism *in vivo* would be different; other cells could be recruited to remove the high amount of corrosion granules. The exact mechanism of how cells cope with high levels of Mg corrosion products is not clear at this point, but it is clear that the presence of the corrosion granules significantly alters the cells' metabolic and proliferative activities.

TEM analysis was performed to understand the effect of corrosion granules at subcellular level. When cells were cultured in the presence of Mg or Mg-Ca non-filtered conditioned media, spontaneous cell aggregates were formed (Fig.3-4 & 3-8). Cell aggregates were formed when cells were presented with both high amount of corrosion granules (Mg50) (Fig.3-4) and low amounts of corrosion granules (Mg-Ca100) (Fig.3-8B). In the presence of corrosion granules changes in the structure and distribution of organelles was observed. The structure of the nucleus was irregular with deep invagination. The irregularity of the nucleus could be explained by how the images were obtained (Fig.3-10). TEM requires ultra-thin sections of cell samples and the images are presented in 2D format at high magnification. This reveals small irregularities that would otherwise seem insignificant when light microscopy is used with thicker sections. An alternative explanation could be inferred from some studies which say that this is a result of high metabolic activity; the irregularities increases the surface area

of the nucleus, resulting in an increased area for the nucleus to interact with the cytoplasm (Ghadially, 2013). However, it is also important to note that some control cells also appeared to have irregular nucleus with invaginations (Fig.3-9A). It is then most likely that the irregularities in nuclear structure were not related to treatment but rather related to the processing effects of the images. Examination of the treated cells also showed a trend that many mitochondria and organelles containing electron dense materials were distributed towards the surface of the cells at 24 and 48hours (Fig. 3-9 & 3-10). Considering the format of 2D cell culture, it would be reasonable to anticipate more transmembrane and subcellular activity for cell surface facing the corrosion products. This would explain the significant blebbing observed on part of the cell membrane where the corrosion granule was anticipated to be present (Fig.3-10A). Particle size was not controlled in this study, and therefore the cells would have experienced dual effects of both nano and micro-sized particles. In the presence of different sized particles it is reasonable to suggest that nano-sized particles were endocytosed and larger particles remained at the extracellular space interacting with the cell membrane. The interaction of corrosion products with the cells resulted in increased autolysosome activity. Indeed, cells with a lot of clear space were noted, presumably due to the large number of autolysosomes present (Fig.3-10 & 3-12). Autolysosomes are also present in normal cells to maintain homeostasis through removal of old and damaged organelles. However when the cell is under stress, autolysosomes are upregulated to help the cell survive (Mizushima & Komatsu, 2011). During starvation autolysosomes are upregulated and can produce amino acids that can be used to synthesize proteins that can adapt to starvation. Autolysosomes can also be useful for the maintenance of mitochondria and generation of energy in specific environments (Mizushima & Komatsu, 2011). Studies have shown that autophagy protects cells from apoptosis; it is believed that following stress

autophagy allows the cells to survive if the stress is not prolonged (Murrow & Debnath, 2013). The high number of autolysosomes seen in treated cells could have been working to prevent cell death during stressful times caused by large amounts of corrosion granules (Fig.3-11). When cells were presented with corrosion granules, autolysosomes were visible near altered cisternae and mitochondria (Fig.3-10B & 3-11A). This is evidence of autolysosome activity; interacting with altered organelles, digesting damaged organelles, allowing the cell to continue to function as normal.

Organelles containing concentric lamellar features were also seen scattered at the periphery of the cells amongst the autolysosomes (Fig.3-11). These concentric lamellar features are also known as myelin figures and they readily form in cells that have been fixed in glutaraldehyde (Ghadially, 2013). Because glutaraldehyde does not fix lipids, the lipids leak out and interact with the aqueous environment, leading to the formation of membranes that have affinity for osmium (myelinoid figures) (Ghadially, 2013). No myelinosomes were seen in the control sample, therefore it is believed that the presence of these myelinosomes was a consequence of the endocytosis of Mg corrosion granules. $MgCO_3$ and calcium phosphates readily degrade inside the lysosomes due to the acidic environment (Chowdhury et al., 2006). Since the corrosion granule is composed of $MgCO_3$ (Harrison *et al.*, 2014) and calcium phosphates (Li *et al*., 2008). it is believed the degradation of the corrosion granule also leads to the release of Ca^{2+}, Mg^{2+} and phosphate (PO_4^{3-}). All these ions are involved in cellular processes. Phosphates ions are known to influence osteoblastic cell differentiation, particularly the expression of osteopontin a middle stage marker of osteoblastic differentiation (Beck *et al*., 2000).

7.2.2. Osteoclast cells

RAW cells are from a murine macrophage/pre-osteoclast cell population. These cells can differentiate into osteoclast cells in the presence of RANK-L, and have cell characteristics similar to osteoclasts directly isolated from murine bones or from primary bone marrow precursor cells (Akchurin *et al.*, 2008; Collin-O9sdoby & Osdoby, 2012). In this study, it has been observed that RAW cells were highly sensitive to the high concentrations of Mg and Mg-Ca conditioned media, particularly in presence of corrosion granules (Fig.5-1 & 5.2). In the presence of corrosion granule metabolic activity was significantly reduced, similar to the observation with hMSCs. Even though metabolic activity was still significantly reduced in the presence of Mg concentration, cells were able to proliferate over time (Fig.5-1). RAW cells were able to adapt to the change in environment created by the corroding disks as it was observed here after 3 days of culture. It is important to note that cells responded better to Mg-Ca conditioned media compared to Mg conditioned media when metabolic activity of cells was investigated. Fig. 5.2 is a true representation of cell behaviour in the presence of Mg-Ca conditioned media.

Because of sample batch variation in this study, Mg-Ca displayed corrosion behaviour similar to Mg (Table.2-12). Previous studies using Mg-Ca have consistently showed a much slower (3x less) corrosion rate compared to Mg (Table.2-11). The new sample batch of Mg-Ca disks that was used for the subsequent experiments was significantly different from that used for the initial experiment (Fig.5.2). One of the aims of the study was to compare the effect of the different degradation behaviour of Mg and Mg-Ca on cells of the skeletal tissue. Therefore, the unexpected higher corrosion rate of Mg-Ca affected the interpretation of the data. Analysis of the corrosion of pure Mg and Mg-Ca alloy showed that the corrosion product

formed by these two metals was the same (Harrison et al., 2014). Another benefit for alloying with calcium is that the co-release of Mg and Ca would be beneficial for bone growth since calcium also plays important roles in cellular function. However the solubility of calcium is very low (Aljarrah & Medraj, 2008), the release of calcium from the corrosion process would require a longer immersion time *in vitro.* Even if there was any calcium released from the alloy, ICP-OES data showed that calcium was depleted from the conditioned media following degradation of both Mg and Mg-Ca disks (Table.2-10 & 2-12). The major difference between Mg and Mg-Ca is the amount of ions released into the media, even though Mg-Ca was degrading faster, the effects of high conditioned media concentration vs low conditioned media concentration were noticeable when the conditioned media was diluted.

7.2.3. Muscle cells

Overall muscle cells appeared to be more robust and therefore more able to cope when cultured in high concentrations of Mg conditioned media. The initial exposure of Mg conditioned medium to myotubes resulted in a decrease in metabolic activity. However, no effects of conditioned media concentration (Mg ion and corrosion granules) were observed and over time the cells (myotubes and myoblasts) were able to adapt to the conditioned media (Fig.6-1). Even though a reduction in metabolic activity was observed, this was still above 70% when compared to the control for all concentrations at all time points, suggesting no cytotoxic effects. In the presence of Mg-Ca conditioned medium, metabolic activity of myotubes was enhanced compared to the control (Fig.6-4), suggesting that a concentration of 4mM or less and higher Ca/Mg ratio was beneficial for myotube integrity.

7.2.4. Summary of cellular response

The degradation behaviour of the two metals (pure Mg and Mg-Ca alloy) resulted in two different media environments. The differences in these environments had a huge impact on cells of the skeletal tissue. The different cells types responded differently to these environments. A calcium deficient environment has been shown to increase cell permeability (Bowen-Pope *et al*., 1979), therefore the culture of cells in a calcium deficient media could result in the cells being more permeable to Mg^{2+}. The increase in cell permeability could also have an impact on the permeability of other important ions such as sodium and potassium, altering normal cell behaviour (Rubin *et al*, 1979; Rubin, 2005). Rubin *et al*., 1979 showed that calcium deprivation inhibited DNA synthesis, whereas high Mg^{2+} concentration reversed the effects of low Ca^{2+}. It is believed that Mg^{2+} plays a more direct role than calcium in influencing cell proliferation. High Mg^{2+} concentration increases $MgATP^{2-}$ and activates mTOR kinase; in turn mTOR phosphorylates proteins involved in the initiation of protein synthesis during the G1 phase of the cell cycle thereby accelerating cell proliferation (Rubin, 2005). Mg is also known to influence cell adhesion and differentiation (Kirchhofer *et al*., 1991; Yang *et al.*, 2010; Yoshizawa *et al.*, 2014). Collectively, findings in this study on cellular effects indicated that there is an optimum concentration of Mg that confers these beneficial effects, above which Mg concentrations have detrimental effects. The presence of CO_2 increases the solubility of $MgCO_3$. Therefore under *in vitro* cell culture conditions, the corrosion granules in the conditioned medium start to re-dissolve resulting in further release of ions into the medium, thereby maintaining Mg^{2+} concentration in the medium (Willumeit *et al.*, 2011). This means that in the presence of corrosion granules, i.e. in Mg non-filtered medium, cells were exposed to a continuous higher Mg^{2+} concentration for a prolonged period of time. This prolonged

exposure to high concentration of Mg^{2+} in combination with calcium depletion impacted further on the cell metabolic activities regardless of the cell type, as shown by the outcomes of the biochemical analysis. Moreover, the influence of the corrosion granules on hMSCs metabolic activity was further confirmed by the changes of sub-cellular characteristics. The reduced size/number of osteoclasts and myotubes observed could further imply the influence of Mg corrosion products on metabolic activities could also play a role in cell fusion/differentiation and tissue maturation.

7.3. The effect of Mg/Mg alloy on cell differentiation

7.3.1. Human Mesenchymal Stem Cells

The increase in expression of osteoblast related markers when cells were cultured in the presence of corrosion products could be related to the continuous supply of Mg ion afforded by the corrosion granules in the medium (Fig.4-1 & 4-4). Other studies (R. W. Li et al., 2014; Liu et al., 2016; Yoshizawa et al., 2014) have shown that the presence of Mg can influence osteogenic differentiation. Furthermore the presence of calcium phosphates such hydroxyapatite has been shown to enhance ALP expression (M. Zhao et al., 2016). Even though formation of calcium phosphates resulted in calcium depletion in the media, the presence of corrosion granules not only acted as a reservoir for Mg^{2+} but for Ca^{2+} and PO_4^{3-} as well. It is believed that the corrosion granule is a mixture of $MgCO_3$ (Harrison et al., 2014), and calcium phosphates (Li *et al.*, 2008). Calcium phosphates are known to have a role in regulating calcium dependent proteins. M. Zhao et al., 2016 showed that the presence of hydroxyapatite resulted in the upregulation of a number of proteins involved bone formation, this includes: 1) focal adhesion proteins, which are involved in cell proliferation and adhesion,

2) actin binding proteins, involved in cytoskeletal organization and cell differentiation and 3) Sarcoplasmic/endoplasmic reticulum calcium ATPase 2 (SERCA2), involved in osteoblast differentiation and osteoclastogenesis (M. Zhao et al., 2016). Shih et al., 2014 proposed a molecular mechanism of how calcium phosphates contribute to osteogenic differentiation. Their model suggests that the dynamic dissolution and precipitation of a calcium phosphate matrix on which cells are cultured on determines the concentration of Ca^{2+} and PO_4^{3-} available for the cells. The dissolution of calcium phosphates increases the concentration of PO_4^{3-}, which then enters the cell through a solute carrier family 20 phosphate transporter, member 1 (SLC20a1) and act as a substrate for ATP synthesis. The synthesized ATP is secreted into the extracellular space and converted into adenosine, which subsequently binds to the adenosine receptor on the cell surface, triggering osteogenic differentiation (Shih *et al*., 2014). Although there is an established understanding of the effects of Ca^{2+} and PO_4^{3-} on osteogenesis, it is anticipated that Mg^{2+} and $MgCO_3$ largely contributed to the cellular responses observed in this study.

The chemical composition of scaffolds or particles also affects cell behavior by influencing the differentiation of MSCs towards the osteogenic lineage. It has been reported (Pham et al., 2008) that the culturing of MSCs on a scaffold containing a mineralised ECM resulted in enhanced OC and ALP expression. Indeed, another study also showed that mineralized ECM had the ability to induce and sustain osteogenic differentiation of cells in the absence of osteogenic supplements such as dexamethasone (Thibault *et al*, 2010). In this study, the presence of corrosion granules induced mRNA and protein expression of osteoblast markers such OC and ALP (Fig.4-1 & 4-4). OC is primarily produced by committed osteoblasts and signifies a mature osteogenic phenotype. This is not typically observed in differentiating MSCs

until after at least 14 days of *in vitro* culture in the presence of osteogenic supplements (Birmingham et al., 2012). The supplements used for osteogenic differentiation include dexamethasone, ascorbic acid and β-Glycerophosphate. In confluent cultures dexamethasone promotes differentiation by regulating the expression of transcription factors such as Runx-2 (Langenbach & Handschel, 2013). Ascorbic acid acts a cofactor for the formation of functional collagen and it also increases the secretion of collagen type 1 into the extracellular matrix. β-Glycerophosphate provides phosphate component for the formation of hydroxyapatite (Langenbach & Handschel, 2013).

The early expression of OC combined with the presence of cell aggregates pointed towards early mineralisation for cells cultured in the presence of corrosion granule (non-filtered medium) (Fig.4-1B). The process of osteogenic differentiation *in vivo* is different from the process observed *in vitro.* However the prolife of gene expression is similar, for example the expression of Runx-2, ALP and collagen type 1 occurs during the early stages of differentiation and the expression of OC during the late stages of differentiation. It is reasonable to say that in the presence of corrosion granule composed of different bioactive ions the expression profile during differentiation would be different compared to the one seen with osteogenic supplements. Even though OC mRNA and ALP protein levels were upregulated when treated with Mg corrosion granule (Mg non-filtered medium), Runx-2 and COL1 expression were not significantly enhanced (Fig.4-1 & 4-2). Therefore, the assumption that early mineralisation was taking place was not fully supported by the profile of Runx-2 and COL1 during the culture period investigated. Hence it is believed that the presence of Mg corrosion granules induced the differentiation of MSCs into osteoblast cells with a particular function as evidenced by the immediate upregulation of OC expression by day 4 without any significant changes on the

other osteogenesis related genes. Even though OC is usually used as a marker of bone formation, studies have shown that OC may also be involved in the recruitment and differentiation of osteoclast precursors (Glowacki & Lian, 1987; Patti *et al.*, 2013). Indeed in the presence of the high amounts of corrosion products with similar properties to mineralized bone, OC expression may be a signal from differentiated MSCs for the need of phagocytosis and osteoclastogenesis to digest these materials rather than bone formation (Heinemann et al., 2000). In summary, the early expression of OC could be a coping mechanism for the cells in the presence of large amounts of corrosion granules.

7.3.2. Osteoclast cells

The corrosion of Mg and Mg alloys creates an environment that reduces the capability of pre-osteoclast cells to fuse into multinucleated cells. This reduction could be due to the presence of high magnesium ions (>6mM) or the alkaline environment (> pH 8). Mg25 filtered and non-filtered media did not have inhibitory effects on osteoclastogenesis (Fig.5-4). At this concentration (Mg25) the amount of Mg ions released was 2x less compared to Mg50. The reduction of Mg ion concentration (<3mM) and pH restored osteoclast cell formation to levels comparable to the control. The presence of corrosion granules significantly affected osteoclastogenesis. In the presence of corrosion granules (Mg or Mg-Ca non-filtered medium) the fusion of RAW cells into osteoclast cells was negatively affected resulting in many undifferentiated cells, even though the cells were treated with RANK-L. This implies that the lower number in TRAP positive cells in the presence of Mg50 filtered or non-filtered media was not due to cytotoxic effects. There was no correlation between the number of multinucleated TRAP positive cells and expression of osteoclast specific genes (TRAP, NFATc1) (Fig.5-3 &5-5) No significant differences in gene expression were observed between the

different Mg/Mg-Ca concentrations and positive control. This suggests that the low numbers of multinucleated cells was due to the inhibition of fusion at the cell surface and that Mg corrosion products did not affect cell differentiation at least at gene level as observed here. A potential mechanism for the formation of multinucleated osteoclast cells was reported by (Vignery, 2005). A transmembrane receptor, dendrocyte-expressed seven transmembrane protein (DC-STAMP) has been reported to be involved in the fusion of osteoclast precursor cells into multinucleated cells. In response to differentiation factors such as RANKL, osteoclast precursor cells express DC-STAMP. The cells expressing the DC-STAMP receptor become the master fusing cells that fuses with the DC-STAMP negative cell. The DC-STAMP master cell fuses directly with the negative cell via a DC-STAMP ligand. Some functions of integrins are dependent on Mg^{2+} and Ca^{2+} through metal ion dependent adhesion sites (MIDAS) (Leitinger, McDowall, Stanley, & Hogg, 2000), therefore it is possible that the presence of Mg^{2+} in high concentrations could inhibit the fusion of the cells by altering the structure of integrins required for cell fusion. The extracellular environment also plays an important role in the process of osteoclastogenesis; acidic environments have been reported to have the ability to induce or trigger fusion of macrophages (Vignery, 2000). Furthermore acidic environments increase osteoclast activity and inhibit osteoblast activity and alkaline environments increase osteoblast activity and reduce osteoclast activity (Bushinsky, 1996; Janning et al., 2010). Zhai *et al*., 2014 also showed that both high Mg concentrations and pH have an inhibitory effect on osteoclastogenesis.

Interestingly mature osteoclasts were able to tolerate high concentrations of Mg conditioned medium compared to RAW cells. The culture of these cells with Mg100 non-filtered medium did not affect cell number (Fig.5-7A). Calcitonin was used as positive control*, in vivo* it is

released from the thyroid in the presence of high calcium and acts as an inhibitor of osteoclast activity (Wu, Luthringer, Feyerabend, Schilling, & Willumeit, 2014). It was noticed that mature osteoclast cells were able to tolerate high Mg^{2+} concentration (Mg100); furthermore, the presence of calcitonin did not seem to affect mature osteoclast cell number. On the other hand, in the presence of Mg conditioned media, bone resorption activity of mature osteoclast cells was significantly reduced (Fig.5-7B).

To understand why resorption activity was significantly lower when cells were cultured in the presence of Mg conditioned medium, it is important to appreciate the mechanism of osteoclast-mediated resorption process. Activation of bone resorption requires polarization of the osteoclast cell membrane, formation of ruffled membrane on the osteoclast and a sealing zone which separates the resorptive environment from the extracellular space. Attachment of the osteoclast cells to the bone matrix is mediated by integrins and bone matrix proteins (osteopontin and bone sialoprotein). Integrin binding then triggers intracellular signalling that leads to cytoskeleton organization, cell spreading and polarization (Yamada *et al.*, 1997; Barrere et al., 2006; Yavropoulou & Yovos, 2008). In the resorbing compartment, osteoclasts release hydrogen ions resulting in an acidification of the environment. The mineral is removed in this acidic environment exposing the matrix to the activity of proteolytic enzymes thereby initiating the resorption process (Teitelbaum *et al* 1995; Bart Clarke, 2008).

Any significant alteration in Mg ion concentration will influence integrin binding to the bone matrix resulting in osteoclast dysfunction. Moreover, studies have shown that osteoclast-mediated bone resorption activity is pH dependant, with pH 6.8 regarded as the optimum pH (Arnett, 2008; Yuan et al., 2016)(Arnett, 2008; Yuan et al., 2016). The protocol for the

resorption assay includes the addition of hydrochloric acid to the culture medium to lower the pH. However, it should be noted that in this study, medium pH was not adjusted in order to emulate *in vivo* environment at the implantation site. At pH 7.4 osteoclast cells are reported to be inactive, the *in vitro* corrosion of Mg in culture medium resulted in a pH level > pH 8. The alkaline environment created by the corroding Mg disk inhibited osteoclast resorption. However, when the conditioned medium was diluted (thereby decreasing the pH), the activity of mature osteoclasts started to increase confirming that high pH had a negative impact on osteoclast activity. The combination of low pH and availability of pro-resorptive factors (e.g. RANK-L) is essential for osteoclast mediated activity. Acidosis plays an important role in initiating osteoclast activity and up regulating factors associated with bone resorption (TNF, NFTAC and TRAP) (Arnett, 2008). Treatment of osteoclast cells with high magnesium chloride concentration actually increased osteoclast cell activity (Wu et al., 2014) further confirming that the reduction in cell activity is likely due to the alkalinity of the conditioned medium rather than Mg ion concentration per se.

7.3.3. Muscle cells

The fusion of cells requires the disruption of two membranes that are in close proximity. This is then followed by content mixing of the two cells. The onset of fusion (i.e. the disruption of the lipid bilayers) depends on the amount of calcium bound on the membrane surface (Mondal Roy & Sarkar, 2011). During the fusion of lipid vesicles, Mg^{2+} or Ca^{2+} neutralizes the charge of the anionic lipid head groups. Vesicle aggregation and changes in membrane surface tension then lead to lipid bilayer destabilisation. Ca^{2+} induces fusion at a threshold concentration of 1mM and Mg^{2+} at 10mM (Mondal Roy & Sarkar, 2011).

When myoblasts are induced to differentiate not all of them form myotubes; a mixed population of myoblasts and myotubes exists. When myotubes were treated with Mg100 filtered medium, high magnesium concentration (17mM) and low calcium concentration (0.8mM) resulted in small sized myotubes (Fig.6-2 A & E). It is likely that the presence of high corrosion product concentration (Mg100) affected the stability of the myotubes that had formed prior to treatment, resulting in their detachment from the cell culture substrate. It would then appear that in the presence of high Mg^{2+} concentration the unfused myoblasts started to fuse; but due to concurrent low Ca^{2+} concentrations, the fusion process was ineffective resulting in the formation of smaller myotubes observed in this study. Even though magnesium has been reported to play a role in fusion, calcium is the key player as higher concentrations (10mM) of magnesium are required to compensate for calcium deficiency. Therefore a calcium deficient media will negatively impact myotube formation. Friday *et al*., 2000, suggested that there are three phases of myogenesis: commitment, phenotypic differentiation and fusion (Friday *et al*., 2000). For each of these phases, specific optimum concentrations of calcium are required. For commitment and phenotypic differentiation, Ca^{2+} concentration below 300µm is sufficient. However fusion phase requires Ca^{2+} concentration of 1.5mM. When cells were treated with Mg100 filtered media, calcium concentration was below the concentration required for fusion. Important proteins required for fusion such as calpains are calcium dependent. Calpain has a high affinity for $Ca^{2+}$and increase in intracellular Ca^{2+} results in the activation of calpain-induced proteolysis that destabilizes the cytoskeleton, thereby initiating fusion (Leitinger *et al.*, 2000; Horsley & Pavlath, 2004). As mentioned earlier integrin binding is an important part of the fusion process. A study has reported that the maximum binding of integrins to their ligands requires Mg^{2+} and Ca^{2+} concentrations of between 5 and 10mM, above 10mM threshold the binding capacity

decreases (Kirchhofer *et al*., 1991). Inhibition of integrin binding will have a negative impact on myotube formation; it has been shown that myoblast deficient in β1 integrins resulted in short myotubes and accumulation of unfused cells (Schwander et al., 2003). Furthermore, Kirchhofer *et al*., 1991 have reported that small changes in calcium concentration in the presence of Mg^{2+} can dramatically change integrin binding properties.

It is believed in this study that fusion process was impaired due to a low Ca/Mg ratio in the conditioned media. When myogenin expression was analysed the levels of expression for cells cultured in Mg filtered and non-filtered medium were comparable to the control (Fig.6-7), suggesting impairment in cell fusion was not caused by faults in the differentiation process. This is the same effect that was also observed during osteoclastogenesis. Studies have shown that muscle specific gene expression was not affected in myoblasts that were not able to fuse (Schwander *et al.*, 2003; Horsley & Pavlath, 2004), further confirming that impairment in fusion is related to calcium interaction at the surface of the cell. Loss of nuclei is related to atrophy. An increase in MAFbx was noticed when cells were exposed to Mg100 non-filtered medium (Fig.6-8B). However, this increase was not significant enough to provide strong evidence for muscle atrophy. On the other hand, MuRF1 was significantly downregulated in the presence of Mg100 filtered and non-filtered media (Fig.6-8A). Exposure to Mg-Ca conditioned media resulted in large or hypertrophic myotubes (Fig.6-5). Changes in myotube size are related to the number of nuclei/myotube. Fusion of myoblasts to myotubes or myotubes to myotubes results in a high rate of protein synthesis (Schwander et al., 2003). The increase in metabolic activity observed when cells were treated with Mg-Ca conditioned media (Fig.6-4) could be related to increase in protein synthesis and this increase could have subsequently led to the formation of large myotubes. A high Ca/Mg ratio is important in the

formation of large myotubes; calcium dependent signalling has been shown to be involved in the induction of hypertrophy (Dunn *et al*., 1999). A high Ca/Mg ratio resulted in the formation of large myotubes and a low Ca/Mg ratio resulted in myotube shrinking. High Mg^{2+} concentration is required for accelerating cell proliferation but the availability of Ca^{2+} is crucial for myotube formation.

7.4. Immune Response

The aim of the immune assay was to understand the response of cells to the corroding disks during the first 24 hours of contact. TNF-α , IL-8 and IL-1β are pro inflammatory cytokines that are released during the early stages of implantation *in vivo* (Refai, Textor, Brunette, & Waterfield, 2004). The corrosion of pure Mg did not elicit an immune response; all the inflammatory factors investigated in this study were significantly downregulated in comparison to the suture material. However Mg-Ca corrosion induced the expression of IL-1β, a factor that stimulates osteoclast activity and proliferation (Ziats *et al*., 1988; Lee *et al.*, 2010) When the disks were placed in culture medium in the presence of THP-1 cells the corrosion reaction of pure Mg was slightly more vigorous compared to Mg-Ca but cells were able to survive this reaction for 24 hours. 24hrs after the medium had been saturated, the vigorous reaction for both Mg and Mg-Ca had subsided. The increase in IL-1β expression observed in the presence of Mg-Ca cannot be due to the corrosion reaction as a similar response would be expected from pure Mg. A major difference between these two disks is the manufacturing process; pure Mg disk was commercially sourced. Commercially sourced Mg was then mixed with commercially sourced Ca to produce Mg-Ca1% alloy. The addition of Ca to Mg during the casting process could have increased the amount of impurities in the alloy. Impurities such as beryllium and nickel have been found in Mg alloys and if present in

high amounts, these could elicit an immune response when released during the corrosion process (Persaud-Sharma & McGoron, 2012). Studies have shown that the presence of soluble and insoluble metal corrosion products can elicit an immune response (Hallab & Jacobs, 2009). However *in vivo* studies with magnesium based implants have shown magnesium to be biocompatible with no significant immune response (Witte et al., 2007). There are no *in vitro* studies on the response of immune cells to Mg- based materials. What's also interesting is that IL-1β is also involved in the stimulation of osteoblast proliferation during bone healing (Y.-M. Lee et al., 2010). TNF-α has been shown to stimulate proliferation of osteoblast like cells but inhibit mineralization by downregulating the expression of OC and ALP (Lange et al., 2010). The induction of inflammatory cytokine expression by Mg-based implants may play a role in regulating bone formation by acting on both osteoclasts and osteoblasts.

7.5. Concluding Remarks

The presence of a degrading material during fracture healing is associated with local and systemic tissue response. The corrosion products formed have a huge impact on the behaviour of cells surrounding the corroding biomaterial. The *in vitro* studies presented here did not show direct evidence of granule endocytosis or pinocytosis into the cells. While interaction of the cells with the corrosion granules was at an intercellular level, there is a possibility that over time as the corrosion granules re-dissolved, the released smaller particles entered the cells through endocytosis as evidenced by the presence of myelinosomes. At the intercellular level, cells were dealing with the corrosion granule as evidenced by the formation of nodules and at the intracellular level cells were dealing with both the corrosion granules and ions released from the degradation of the endocytosed granules, resulting in high metabolic activities. The body is able to utilize the bioactive ions for cell growth and

proliferation but at high concentrations above a certain level the body is also working to remove the excess ions via the kidney. The presence of implant debris could excite an inflammatory response by recruitment of macrophages to the implantation site. These activated macrophages then release inflammatory factors such TNF-α, IL-8 and IL-1β which in turn stimulate the differentiation of pre-osteoclasts to into mature cells, thereby encouraging bone resorption activity. Evidence from this study has shown that Mg corrosion products do not elicit an inflammatory response, implying that the body does not recognize the corrosion granule as foreign. If the macrophages are not recruited to the implantation site to remove the corrosion granule how then does the body deal with the high corrosion granule concentration? It is anticipated that the MSCs that are recruited to the implantation site deal with the corrosion granule. High Mg corrosion products will stimulate MSC proliferation and differentiation into osteoblasts. Because the corrosion granule is similar in composition to mineralized matrix the osteoblasts release OC and RANK-L leading to the activation and recruitment of osteoclast cells to initiate digestion or removal of the corrosion granule. However, the presence of high Mg corrosion products and high pH could hinder the resorption activity of osteoclasts. Increased calcium levels result in the release of calcitonin which in turn inhibits osteoclast activity, high Mg^{2+} could also have the same osteoclast inhibiting effects as Ca^{2+}. Even though pH is tightly regulated within the body, the continuous corrosion of the implant could overload the buffering mechanisms and still result in pH higher than the physiological range. The presence of overactive osteoclasts at the implantation site would have explained the formation of cavities reported by (Zhang *et al*. 2010; Li *et al*. 2008) following degradation of Mg alloy implants. Since osteoclast activity is inhibited by the presence of Mg corrosion products the next reasonable explanation is that the presence of cavities is an indirect result of inhibition of osteoblast function. In the presence of corrosion

granules, MSCs differentiate into osteoblasts. However the osteoblast activity is diverted from bone formation and tissue regeneration to mopping the high concentration of corrosion granules. Janning *et al*., 2010 reported a temporary inhibition of osteoclast activity at the implantation site during the first 4 weeks of healing. Most likely over time the body is able to regulate the pH and this in turn restores osteoclast activity. Local alkalosis is the most likely reason for inhibited osteoclast activity. This *in vitro* study has shown that even in the presence of RANK-L, osteoclast differentiation was inhibited when cells were cultured in high Mg conditioned media concentration. It was also observed that the initial contact with conditioned medium reduced cell viability. This could be due to the high alkaline environment but overtime as the buffering mechanisms are activated the pH is lowered towards physiological range allowing cells to cope better.

The released Mg^{2+} can also diffuse away from the implantation site towards the periosteum where they activate the release of calcitonin gene-related polypeptide-a (CGRP) from the dorsal root ganglia (DRG). In turn CGRP activates osteogenic differentiation of MSCs derived from the periosteum (J. Wang et al., 2016). Moreover the exposure of muscle cells to Mg^{2+} could lead to muscle cell hypertrophy resulting in the release of osteogenic/chrondogenic factors and growth factors involved in bone regeneration (Abou-Khalil et al., 2015). The interaction of released Mg^{2+} with the periosteum and surrounding muscle could be the main reason for enhanced bone formation that is reported *in vivo*. The integrity of the muscle cells is important for normal bone healing, therefore the effect of Mg corrosion products on muscle cells also influences bone regeneration. *In vitro* studies presented here did not show strong evidence of atrophy in the presence of high Mg corrosion product concentration. However, there is evidence that the presence of corrosion products at specific concentrations (≤10mM)

downregulate the expression of markers related to muscle atrophy. Muscle cells are most sensitive to Mg ions during fusion where the presence of high Mg ions and low calcium ions results in small myotube formation. However, *in vivo* where ion concentration is tightly regulated this effect is eliminated by homeostasis; if low calcium ions are detected bone resorption might be initiated to release calcium ions. As the osteoblasts lay down new bone, the presence of Mg^{2+} might result in it being substituted into the mineral phase of bone, altering its crystallinity and this in turn could alter osteoclast activity. Osteoclast cells are able to resorb amorphous or less crystalline matrix more easily leading to increased release of calcium and phosphates ions (Overgaard et al., 1999). The calcium and phosphate ions would then initiate expression of bone related genes by activating specific signalling pathways involved in osteogenic differentiation. Activation of osteogenic differentiation would then lead to enhanced bone growth. Farther away from the implantation site the concentration of Mg corrosion products is within the beneficial range, therefore increased bone formation would be observed *in vivo.*

7.6. Conclusion

The effect of Mg corrosion products varied depending on the state of differentiation of cells, concentration and length of exposure. Mature cells were able to tolerate corrosion products up to a certain concentration; above this concentration they did not have the capacity to deal with corrosion products as well as stem cells. The presence of the corrosion granule significantly altered the cells' metabolic and proliferative activities. This influence on metabolic activities also affected cell fusion/differentiation and tissue maturation. Osteoclastogenesis and myotube formation were significantly affected by the presence of high Mg corrosion products, it was shown that a high Mg^{2+} concentration is required for accelerating cell proliferation but the availability of Ca^{2+} is crucial for cell fusion. High Mg corrosion products indirectly inhibited bone healing by interfering with the differentiation process of MSCs.

A model of *in vivo* behaviour was suggested in this study. It is anticipated that MSCs in direct proximity to the corroding Mg biomaterial experience a high concentration of the corrosion products, the cells respond by differentiating into osteoblast-like cells that act to clear the corrosion granule directly or indirectly by releasing OC which in turn recruits and activates osteoclasts to the implantation site. However, the activities of the recruited osteoclasts maybe temporally impaired due to the inhibiting action of the corrosion environment. Further away from the implantation site, as the concentration of the corrosion products decreases, the presence of the bioactive ions from the corrosion products induces the differentiation of MSCs to bone forming cells (osteoblasts) leading to enhanced bone formation.

7.7. Further Work

- An EDX analysis on the samples treated with Mg corrosion products would provide evidence of the presence of Mg^{2+}, Ca^{2+} and any other elements, following treatment with the corrosion products.

- Extend the differentiation studies by investigating gene expression at earlier and later time points (day 1 to 28). Furthermore, investigation of the effect of lower concentrations of Mg corrosion products on osteogenic differentiation would give clearer evidence of the concentration range that is optimum for bone formation. This information could then be correlated to the degradation rate of magnesium, informing better design of Mg implants that degrades at a rate that releases ions within the beneficial range.

- Following exposure to corrosion products, characterization of the hMSCs at the different stages of growth, looking at surface markers to investigate changes in cell phenotype and possibility of de-differentiation would be useful. This information would give a better understanding of the effect of Mg corrosion products on stem cells.

- The hMSCs used in this study came from the same donor; the behaviour observed could be related to cells obtained from this particular donor. Other factors such as donor age or sex could also have influenced the response of these cells. A library of different donor types or MSCs from different sources other than the bone marrow such as adipose tissue, placenta and umbilical cord could be set up. The response of cells from these different types of cells could be investigated and compared. Even though the use of cell lines could give reproducible results they may not represent the true *in vivo* reaction or response as they have been manipulated.

- A set up co-cultures could be established, it is known that muscle cells play an important role in bone formation. Osteoblasts or osteoclasts could be cultured in muscle cell conditioned media to look at the effect of factors released by muscle cells on bone cells. Furthermore, examination of the factors that are released by muscle cells in the presence of Mg ions could also be investigated.

- Confirmation of Mg ion uptake by the cells is important; the rate of Mg ion uptake by the cells could be correlated to the biological response.

- If the corrosion products were to be released into the blood stream how would they affect blood cells? Mg has been used as stents in cardiovascular related conditions and as such, an understanding of the effect of these corrosion products on the blood cells would be important.

- A 3D co-culture system of MSCs with endothelial cells could be developed to investigate the effect of vascularization on osteogenic differentiation in the presence of degrading Mg nanoparticles.

8.0. Appendix

8.1. Method optimization for the in vitro testing on the effect of Mg/Mg-Ca conditioned medium on hMSCs

One of the most important step in *in vitro* testing is the preparation of extracts from the implants, the current testing standards requires the removal of the corrosion granule formed during the corrosion process. However, in this study in order to test the effects of the complete products formed the conditioned medium contained both soluble products (Mg ions) and insoluble (corrosion granule). Other studies use a specific mass: volume ratio for the immersion test, however following degradation a large amount of corrosion products is released into the medium. This results in high amounts of Mg ions being released into the medium, high concentrations of Mg ions are toxic to cells. When high amounts (i.e. 50mM) are released into the medium during the immersion test, dilution of the conditioned medium is required. In this study, a different approach to the immersion test was adopted, to accommodate biodegradable materials and also to emulate the *in vivo* environment at the implantation site. Instead of immersing the Mg sample at a specific mass: volume ratio, the Mg samples were immersed in a 400ml of culture medium until the medium was saturated. For Mg samples the medium became saturated after 72hrs. For Mg-Ca samples the corrosion rate was much slower but the immersion time was kept at 72hrs to show the effect of corrosion rate between Mg and Mg-Ca samples on cellular activities. No other studies have reported the inclusion of corrosion granule in the conditioned medium for the biocompatibility testing of Mg based biomaterials. In the initial experiment hMSCs were seeded for 24 hours before culture with Mg/Mg-Ca conditioned medium. After 48 hours of culture in Mg/Mg-Ca non-filtered medium, analysis using a light microscopy showed random

areas in the monolayer were there were no cells. In an effort to understand how hMSCs responded to the corrosion products, live imaging was employed. Cells were cultured in a six well plate under live imaging for 48hrs. Cells were seen to interact with granules forming aggregates. After the aggregates were formed they would detach from the plate, accounting for the void space that was observed when using light microscopy. These cell aggregates that were formed closely resembled bone nodules. Bone nodules are usually formed following 4 weeks culture in osteogenic supplements. The presence of these nodules at 48hrs would mean early mineralization. Mineralization of *in vitro* osteogenic cultures can be assessed using stains such Alizarin red S (ARS). ARS is used to detect calcium phosphate formed by mature osteoblasts during mineralization. ARS reacts with calcium forming a complex that stains bright red. Alizarin red S is not specific for calcium, high Mg ion concentration can also interact with the dye. In a previous study (Harrison *et al.*, 2014), the corrosion products of Mg and Mg-Ca were shown to stain positive in the presence of the ARS, due to high Mg^{2+} content from the corrosion process and high Ca^{2+} content absorbed from the culture media. Since the cells were cultured in the presence of corrosion granule containing calcium phosphate, ARS staining was omitted in order to avoid false positive results. Instead RT-PCR was used to confirm mineralization by assessing the expression of markers associated with mineralization such as osteocalcin and collagen type 1. In order to assess the presence and effects of Mg at subcellular level TEM analysis was performed. Initially cells were grown on a clear film made from fluorinated-chlorinated resins. hMSCs were grown on the film and allowed to attached for 24 hours, after 24hrs the cells were treated with Mg non-filtered medium for 48 hours. After cell culture, cells were fixed and dehydrated using ethanol as previously mentioned in section 2.21. However, there were challenges with the embedding of the cells in resin, during the embedding process the cell aggregates formed detached from the film and therefore it

was not possible to analyse the samples. In order to overcome this issue cell suspension samples were used instead as mentioned in section 2.21. Cell pellets were formed and were

9.0. References

Abou-Khalil, R., Yang, F., Lieu, S., Julien, A., Perry, J., Pereira, C., … Colnot, C. (2015). Role of muscle stem cells during skeletal regeneration. *Stem Cells (Dayton, Ohio)*, *33*(5), 1501–11. https://doi.org/10.1002/stem.1945

Abou-Khalil, R., Yang, F., Mortreux, M., Lieu, S., Yu, Y. Y., Wurmser, M., … Colnot, C. (2014). Delayed bone regeneration is linked to chronic inflammation in murine muscular dystrophy. *Journal of Bone and Mineral Research*, *29*(2), 304–315. https://doi.org/10.1002/jbmr.2038

Aghion, E., Gueta, Y., Moscovitch, N., & Bronfin, B. (2008). Effect of yttrium additions on the properties of grain-refined Mg-3%Nd alloy. *Journal of Materials Science*, *43*(14), 4870–4875. https://doi.org/10.1007/s10853-008-2708-9

Agus, Z. S., & Morad, M. (1991). Modulation of cardiac ion channels by magnesium. *Annual Review of Physiology*, *53*, 299–307. https://doi.org/10.1146/annurev.ph.53.030191.001503 [doi]

Akchurin, T., Aissiou, T., Kemeny, N., Prosk, E., Nigam, N., & Komarova, S. V. (2008). Complex dynamics of osteoclast formation and death in long-term cultures. *PLoS ONE*, *3*(5). https://doi.org/10.1371/journal.pone.0002104

Aljarrah, M., & Medraj, M. (2008). Thermodynamic modelling of the Mg-Ca, Mg-Sr, Ca-Sr and Mg-Ca-Sr systems using the modified quasichemical model. *Calphad: Computer Coupling of Phase Diagrams and Thermochemistry*, *32*(2), 240–251. https://doi.org/10.1016/j.calphad.2007.09.001

Arnett, T. R. (2008). Extracellular pH Regulates Bone Cell Function 1 – 3, 415–418.

Astier, C., Rock, E., Lab, C., Gueux, E., Mazur, A., & Rayssiguier, Y. (1996). Functional

alterations in sarcoplasmic reticulum membranes of magnesium-deficient rat skeletal muscle as consequences of free radical-mediated process. *Free Radical Biology and Medicine*, *20*(5), 667–674. https://doi.org/http://dx.doi.org/10.1016/0891-5849(95)02180-9

Aubin, J. E., & Heersche, J. N. M. (2003). Bone Cell Biology Osteoblasts, Osteocytes, and Osteoclasts. *Pediatric Bone: Biology & Diseases*, 43–75. https://doi.org/10.1016/B978-012286551-0/50004-X

Barrere, F., van Blitterswijk, C. A., & de Groot, K. (2006). Bone regeneration: molecular and cellular interactions with calcium phosphate ceramics. *International Journal of Nanomedicine*, *1*(3), 317–332.

Bayliss, L., Mahoney, D. J., & Monk, P. (2012). Normal bone physiology, remodelling and its hormonal regulation. *Orthopaedics I: General Principles*, *30*(2), 47–53. https://doi.org/http://dx.doi.org/10.1016/j.mpsur.2011.12.009

Beck, G., Zerler, B., & Moran, E. (2000). Phosphate is a specific signal for induction of osteopontin gene expression. *Proceedings of the National Academy of Sciences*, *97*(15), 8352–7. https://doi.org/10.1073/pnas.140021997

Belluci, M. M., Schoenmaker, T., Rossa-Junior, C., Orrico, S. R., de Vries, T. J., & Everts, V. (2013). Magnesium deficiency results in an increased formation of osteoclasts. *The Journal of Nutritional Biochemistry*, *24*(8), 1488–1498. https://doi.org/10.1016/j.jnutbio.2012.12.008; 10.1016/j.jnutbio.2012.12.008

Bender, J., & Brouwer, J. (1975). Experience with the use of polyglycolic acid suture material (Dexon) in 500 surgical patients. *Archivum Chirurgicum Neerlandicum*, *27*(1), 53–61.

Berzina-Cimdina, L., & Borodajenko, N. (2012). Research of Calcium Phosphates Using Fourier Transform Infrared Spectroscopy. *Infrared Spectroscopy – Materials Science,*

Engineering and Technology, 123–148. https://doi.org/10.5772/36942

Beyenbach, K. W. (1990). Transport of magnesium across biological membranes. *Magnesium and Trace Elements*, *9*(5), 233–254.

Birmingham, E., Niebur, G. L., Mchugh, P. E., Shaw, G., Barry, F. P., & McNamara, L. M. (2012). Osteogenic differentiation of mesenchymal stem cells is regulated by osteocyte and osteoblast cells in a simplified bone niche. *European Cells and Materials*, *23*(353), 13–27. https://doi.org/vol023a02 [pii]

Bodine, S. C., & Baehr, L. M. (2014). Skeletal muscle atrophy and the E3 ubiquitin ligases MuRF1 and MAFbx/atrogin-1. *American Journal of Physiology. Endocrinology and Metabolism*, *307*(6), E469-84. https://doi.org/10.1152/ajpendo.00204.2014

Bowen-Pope, D. F., Vidair, C., Sanui, H., & Rubin, A. H. (1979). Separate roles for calcium and magnesium in their synergistic effect on uridine uptake by cultured cells: significance for growth control. *Proceedings of the National Academy of Sciences of the United States of America*, *76*(3), 1308–1312.

Brown, J. L., Kumbar, S. G., & Laurencin, C. T. (2013). Chapter II.6.7 - Bone Tissue Engineering. In B. D. Ratner, A. S. Hoffman, F. J. Schoen, & J. E. Lemons (Eds.), *Biomaterials Science (Third Edition)* (pp. 1194–1214). Academic Press. https://doi.org/http://dx.doi.org/10.1016/B978-0-08-087780-8.00113-3

Buehler, M. J. (2007). Molecular nanomechanics of nascent bone: fibrillar toughening by mineralization. *Nanotechnology*, *18*(29), 295102. Retrieved from http://stacks.iop.org/0957-4484/18/i=29/a=295102

Bushinsky, D. A. (1996). Metabolic alkalosis decreases bone calcium efflux by suppressing osteoclasts and stimulating osteoblasts. *American Journal of Physiology - Renal Physiology*, *271*(1), F216 LP-F222. Retrieved from

http://ajprenal.physiology.org/content/271/1/F216.abstract

Cao, J. D., Kirkland, N. T., Laws, K. J., Birbilis, N., & Ferry, M. (2012). Ca-Mg-Zn bulk metallic glasses as bioresorbable metals. *Acta Biomaterialia*, *8*(6), 2375–2383. https://doi.org/10.1016/j.actbio.2012.03.009; 10.1016/j.actbio.2012.03.009

Castellani, C., Lindtner, R. A., Hausbrandt, P., Tschegg, E., Stanzl-Tschegg, S. E., Zanoni, G., … Weinberg, A. M. (2011). Bone-implant interface strength and osseointegration: Biodegradable magnesium alloy versus standard titanium control. *Acta Biomaterialia*, *7*(1), 432–440. https://doi.org/10.1016/j.actbio.2010.08.020

Chen, Y., Zhang, S., Li, J., Song, Y., Zhao, C., & Zhang, X. (2010). Dynamic degradation behavior of MgZn alloy in circulating m-SBF. *Materials Letters*, *64*(18), 1996–1999. https://doi.org/10.1016/j.matlet.2010.06.011

Cho, T. J., Gerstenfeld, L. C., & Einhorn, T. A. (2002). Differential temporal expression of members of the transforming growth factor beta superfamily during murine fracture healing. *Journal of Bone and Mineral Research : The Official Journal of the American Society for Bone and Mineral Research*, *17*(3), 513–520. https://doi.org/10.1359/jbmr.2002.17.3.513 [doi]

Choi, M. G., Koh, H. S., Kluess, D., O'Connor, D., Mathur, A., Truskey, G. A., … Sung, K.-L. P. (2005). Effects of titanium particle size on osteoblast functions in vitro and in vivo. *Proceedings of the National Academy of Sciences of the United States of America* , *102*(12), 4578–4583. https://doi.org/10.1073/pnas.0500693102

Chowdhury, E. H., Maruyama, A., Kano, A., Nagaoka, M., Kotaka, M., Hirose, S., … Akaike, T. (2006). pH-sensing nano-crystals of carbonate apatite: Effects on intracellular delivery and release of DNA for efficient expression into mammalian cells. *Gene*, *376*(1–2), 87–94. https://doi.org/10.1016/j.gene.2006.02.028

Clarke, B. (2008). Normal bone anatomy and physiology. *Clinical Journal of the American Society of Nephrology : CJASN*, *3 Suppl 3*, S131-9. https://doi.org/10.2215/CJN.04151206 [doi]

Clarke, B. (2008). Normal bone anatomy and physiology. *Clinical Journal of the American Society of Nephrology : CJASN*, *3 Suppl 3*, 131–139. https://doi.org/10.2215/CJN.04151206

Collin-Osdoby, P., & Osdoby, P. (2012). RANKL-mediated osteoclast formation from murine RAW 264.7 cells. *Methods in Molecular Biology (Clifton, N.J.)*, *816*, 187–202. https://doi.org/10.1007/978-1-61779-415-5_13

Currey, J. (2004). Incompatible mechanical properties in compact bone. *Journal of Theoretical Biology*, *231*(4), 569–580. https://doi.org/10.1016/j.jtbi.2004.07.013

Cruess, R.L., Dumont, J., (1975). Healing of bone, tendon, and ligament. In Rockwood CA, Green DP (eds): Fractures, p 97. Philadelphia, JB Lippincott

Deckers, M. M., van Bezooijen, R. L., van der Horst, G., Hoogendam, J., van Der Bent, C., Papapoulos, S. E., & Lowik, C. W. (2002). Bone morphogenetic proteins stimulate angiogenesis through osteoblast-derived vascular endothelial growth factor A. *Endocrinology*, *143*(4), 1545–1553. https://doi.org/10.1210/endo.143.4.8719 [doi]

Deschaseaux, F., Sensébé, L., & Heymann, D. (2009). Mechanisms of bone repair and regeneration. *Trends in Molecular Medicine*, *15*(9), 417–429. https://doi.org/10.1016/j.molmed.2009.07.002

Dimitriou, R., Tsiridis, E., & Giannoudis, P. V. (2005). Current concepts of molecular aspects of bone healing. *Injury*, *36*(12), 1392–1404. https://doi.org/10.1016/j.injury.2005.07.019

Doblaré, M., García, J. M., & Gómez, M. J. (2004). Modelling bone tissue fracture and

healing: a review. *Engineering Fracture Mechanics*, *71*(13–14), 1809–1840. https://doi.org/http://dx.doi.org/10.1016/j.engfracmech.2003.08.003

Dunn, S. E., Burns, J. L., & Michel, R. N. (1999). Calcineurin is required for skeletal muscle hypertrophy. *The Journal of Biological Chemistry*, *274*(31), 21908–21912.

Erdmann, N., Angrisani, N., Reifenrath, J., Lucas, A., Thorey, F., Bormann, D., & Meyer-Lindenberg, A. (2011). Biomechanical testing and degradation analysis of MgCa0.8 alloy screws: a comparative in vivo study in rabbits. *Acta Biomater*, *7*. https://doi.org/10.1016/j.actbio.2010.10.031

Erdmann, N., Bondarenko, A., Hewicker-Trautwein, M., Angrisani, N., Reifenrath, J., Lucas, A., & Meyer-Lindenberg, A. (2010). Evaluation of the soft tissue biocompatibility of MgCa0.8 and surgical steel 316L in vivo: a comparative study in rabbits. *Biomedical Engineering Online*, *9*(1), 63. https://doi.org/10.1186/1475-925X-9-63

Fernandez-Tresguerres-Hernandez-Gil, I., Alobera-Gracia, M. A., del-Canto-Pingarron, M., & Blanco-Jerez, L. (2006). Physiological bases of bone regeneration I. Histology and physiology of bone tissue. *Medicina Oral, Patologia Oral Y Cirugia Bucal*, *11*(1), E47-51. https://doi.org/10489007 [pii]

Feyerabend, F., Fischer, J., Holtz, J., Witte, F., Willumeit, R., Drucker, H., … Hort, N. (2010). Evaluation of short-term effects of rare earth and other elements used in magnesium alloys on primary cells and cell lines. *Acta Biomaterialia*, *6*(5), 1834–1842. https://doi.org/10.1016/j.actbio.2009.09.024; 10.1016/j.actbio.2009.09.024

Flatman, P. W. (1991). Mechanisms of magnesium transport. *Annual Review of Physiology*, *53*, 259–271. https://doi.org/10.1146/annurev.ph.53.030191.001355 [doi]

Friday, B. B., Horsley, V., & Pavlath, G. K. (2000). Calcineurin Activity Is Required for the Initiation of Skeletal Muscle Differentiation. *The Journal of Cell Biology*, *149*(3), 657–

666. Retrieved from http://www.ncbi.nlm.nih.gov/pmc/articles/PMC2174840/

Furutani, Y., Funaba, M., & Matsui, T. (2011). Magnesium deficiency up-regulates Myod expression in rat skeletal muscle and C2C12 myogenic cells. *Cell Biochemistry and Function*, *29*(7), 577–581. https://doi.org/10.1002/cbf.1790

Gebert, A., Wolff, U., John, A., Eckert, J., & Schultz, L. (2001). Stability of the bulk glass-forming Mg65Y10Cu25 alloy in aqueous electrolytes. *Materials Science and Engineering: A*, *299*(1–2), 125–135. https://doi.org/http://dx.doi.org/10.1016/S0921-5093(00)01401-5

Gerber, H.-P., & Ferrara, N. (2000). Angiogenesis and Bone Growth. *Trends in Cardiovascular Medicine*, *10*(5), 223–228. https://doi.org/10.1016/S1050-1738(00)00074-8

Gerstenfeld, L. C., Cullinane, D. M., Barnes, G. L., Graves, D. T., & Einhorn, T. A. (2003). Fracture healing as a post-natal developmental process: molecular, spatial, and temporal aspects of its regulation. *Journal of Cellular Biochemistry*, *88*(5), 873–884. https://doi.org/10.1002/jcb.10435 [doi]

Ghadially, F. N. (2013). *Ultrastructural Pathology of the Cell and Matrix: A Text and Atlas of Physiological and Pathological Alterations in the Fine Structure of Cellular and Extracellular Components*. Elsevier Science. Retrieved from https://books.google.co.uk/books?id=8XjAAgAAQBAJ

Glowacki, J., & Lian, J. B. (1987). Impaired recruitment and differentiation of osteoclast progenitors by osteocalcin-deplete bone implants. *Cell Differentiation*, *21*(4), 247–254. https://doi.org/http://dx.doi.org/10.1016/0045-6039(87)90479-9

Grubbs, R. D., & Maguire, M. E. (1987). Magnesium as a regulatory cation: criteria and evaluation. *Magnesium*, *6*(3), 113–127.

Gu, X.-N., & Zheng, Y.-F. (2010). A review on magnesium alloys as biodegradable materials.

Frontiers of Materials Science in China, *4*(2), 111–115. https://doi.org/10.1007/s11706-010-0024-1

Gu, X., Zheng, Y., Zhong, S., Xi, T., Wang, J., & Wang, W. (2010). Corrosion of, and cellular responses to Mg–Zn–Ca bulk metallic glasses. *Biomaterials*, *31*(6), 1093–1103. https://doi.org/http://dx.doi.org/10.1016/j.biomaterials.2009.11.015

Guan, R. G., Johnson, I., Cui, T., Zhao, T., Zhao, Z. Y., Li, X., & Liu, H. (2012). Electrodeposition of hydroxyapatite coating on Mg-4.0Zn-1.0Ca-0.6Zr alloy and in vitro evaluation of degradation, hemolysis, and cytotoxicity. *Journal of Biomedical Materials Research - Part A*, *100 A*(4), 999–1015. https://doi.org/10.1002/jbm.a.34042

Gunde, P., Furrer, A., Hanzi, A. C., Schmutz, P., & Uggowitzer, P. J. (2010). The influence of heat treatment and plastic deformation on the bio-degradation of a Mg-Y-RE alloy. *Journal of Biomedical Materials research.Part A*, *92*(2), 409–418. https://doi.org/10.1002/jbm.a.32350 [doi]

Hallab, N. J., & Jacobs, J. J. (2009). Biologic effects of implant debris. *Bulletin of the NYU Hospital for Joint Diseases*, *67*(2), 182–188.

Hamrick, M. W. (2012). A Role for Myokines in Muscle Bone Interactions, *39*(1), 43–47. https://doi.org/10.1097/JES.0b013e318201f601.A

Hänzi, A. C., Gunde, P., Schinhammer, M., & Uggowitzer, P. J. (2009). On the biodegradation performance of an Mg–Y–RE alloy with various surface conditions in simulated body fluid. *Acta Biomaterialia*, *5*(1), 162–171. https://doi.org/http://dx.doi.org/10.1016/j.actbio.2008.07.034

Harrison, R., Maradze, D., Lyons, S., Zheng, Y., & Liu, Y. (2014). Corrosion of magnesium and magnesium-calcium alloy in biologically-simulated environment. *Progress in Natural Science: Materials International*, *24*(5), 539–546.

https://doi.org/10.1016/j.pnsc.2014.08.010

Heinemann, D. E., Lohmann, C., Siggelkow, H., Alves, F., Engel, I., & Koster, G. (2000). Human osteoblast-like cells phagocytose metal particles and express the macrophage marker CD68 in vitro. *The Journal of Bone and Joint surgery.British Volume*, *82*(2), 283–289.

Herman, B. C., Cardoso, L., Majeska, R. J., Jepsen, K. J., & Schaffler, M. B. (2010). Activation of bone remodeling after fatigue: Differential response to linear microcracks and diffuse damage. *Bone*, *47*(4), 766–772. https://doi.org/10.1016/j.bone.2010.07.006

Herzog, E. L., Chai, L., & Krause, D. S. (2003). Review in translational hematology Plasticity of marrow-derived stem cells. *Stem Cells*, *102*(10), 3483–3493. https://doi.org/10.1182/blood-2003-05-1664.Supported

Hong, D., Saha, P., Chou, D. T., Lee, B., Collins, B. E., Tan, Z., … Kumta, P. N. (2013). In vitro degradation and cytotoxicity response of Mg-4% Zn-0.5% Zr (ZK40) alloy as a potential biodegradable material. *Acta Biomaterialia*, *9*(10), 8534–8547. https://doi.org/10.1016/j.actbio.2013.07.001 [doi]

Hong, D., Saha, P., Chou, D. T., Lee, B., Collins, B. E., Tan, Z., … Kumta, P. N. (2013). In vitro degradation and cytotoxicity response of Mg-4% Zn-0.5% Zr (ZK40) alloy as a potential biodegradable material. *Acta Biomaterialia*, *9*(10), 8534–8547. https://doi.org/10.1016/j.actbio.2013.07.001

Horsley, V., & Pavlath, G. K. (2004). Forming a Multinucleated Cell: Molecules That Regulate Myoblast Fusion. *Cells Tissues Organs*, *176*(1–3), 67–78. https://doi.org/10.1159/000075028

Huehnerschulte, T. A., Angrisani, N., Rittershaus, D., Bormann, D., Windhagen, H., & Meyer-Lindenberg, A. (2011). In vivo corrosion of two novel magnesium alloys ZEK100 and AX30 and their mechanical suitability as biodegradable implants. *Materials*, *4*(6), 1144–

1167. https://doi.org/10.3390/ma4061144

Huehnerschulte, T. A., Reifenrath, J., von Rechenberg, B., Dziuba, D., Seitz, J. M., Bormann, D., … Meyer-Lindenberg, A. (2012). In vivo assessment of the host reactions to the biodegradation of the two novel magnesium alloys ZEK100 and AX30 in an animal model. *Biomedical Engineering Online*, *11*, 14. https://doi.org/10.1186/1475-925X-11-14; 10.1186/1475-925X-11-14

Hutchison, C., Pilote, M., & Roy, S. (2007). The axolotl limb: A model for bone development, regeneration and fracture healing. *Bone*, *40*(1), 45–56. https://doi.org/10.1016/j.bone.2006.07.005

Ilich, J. Z., & Kerstetter, J. E. (2000). Nutrition in Bone Health Revisited: A Story Beyond Calcium. *Journal of the American College of Nutrition*, *19*(6), 715–737. https://doi.org/10.1080/07315724.2000.10718070

Iskandar, M. E., Aslani, A., & Liu, H. (2013). The effects of nanostructured hydroxyapatite coating on the biodegradation and cytocompatibility of magnesium implants. *Journal of Biomedical Materials Research - Part A*, *101 A*(8), 2340–2354. https://doi.org/10.1002/jbm.a.34530

Iso, B. S. E. N. (2008). Biological evaluation of medical devices.

Janning, C., Willbold, E., Vogt, C., Nellesen, J., Meyer-Lindenberg, A., Windhagen, H., … Witte, F. (2010). Magnesium hydroxide temporarily enhancing osteoblast activity and decreasing the osteoclast number in peri-implant bone remodelling. *Acta Biomaterialia*, *6*(5), 1861–1868. https://doi.org/10.1016/j.actbio.2009.12.037

Johnson, I., & Liu, H. (2013). A study on factors affecting the degradation of magnesium and a magnesium-yttrium alloy for biomedical applications. *PloS One*, *8*(6), e65603. https://doi.org/10.1371/journal.pone.0065603; 10.1371/journal.pone.0065603

Johnson, I., & Liu, H. (2013). A Study on Factors Affecting the Degradation of Magnesium and a Magnesium-Yttrium Alloy for Biomedical Applications. *PLoS ONE*, *8*(6). https://doi.org/10.1371/journal.pone.0065603

Johnson, I., Perchy, D., & Liu, H. (2011). In vitro evaluation of the surface effects on magnesium-yttrium alloy degradation and mesenchymal stem cell adhesion. *Journal of Biomedical Materials research.Part A*. https://doi.org/10.1002/jbm.a.33290; 10.1002/jbm.a.33290

Johnson, I., Perchy, D., & Liu, H. (2012). In vitro evaluation of the surface effects on magnesium-yttrium alloy degradation and mesenchymal stem cell adhesion. *Journal of Biomedical Materials Research - Part A*, *100 A*(2), 477–485. https://doi.org/10.1002/jbm.a.33290

Kalb, S., Mahan, M. A., Elhadi, A. M., Dru, A., Eales, J., Lemos, M., & Theodore, N. (2013). Pharmacophysiology of bone and spinal fusion. *Spine Journal*, *13*(10), 1359–1369. https://doi.org/10.1016/j.spinee.2013.06.005

Kalfas, I. H. (2001). Principles of bone healing. *Neurosurgical Focus*, *10*(4), E1. https://doi.org/100401 [pii]

Karalaki, M., Fili, S., Philippou, A., & Koutsilieris, M. (2009). Muscle regeneration: cellular and molecular events. *In Vivo (Athens, Greece)*, *23*(5), 779–96. https://doi.org/23/5/779 [pii]

Kirchhofer, D., Grzesiak, J., & Pierschbacher, M. D. (1991). Calcium as a potential physiological regulator of integrin-mediated cell adhesion. *The Journal of Biological Chemistry*, *266*(7), 4471–4477.

Krause, A., Von Der Höh, N., Bormann, D., Krause, C., Bach, F. W., Windhagen, H., & Meyer-Lindenberg, A. (2010). Degradation behaviour and mechanical properties of

magnesium implants in rabbit tibiae. *Journal of Materials Science*, *45*(3), 624–632. https://doi.org/10.1007/s10853-009-3936-3

Kular, J., Tickner, J., Chim, S. M., & Xu, J. (2012). An overview of the regulation of bone remodelling at the cellular level. *Bone and Calcium*, *45*(12), 863–873. https://doi.org/http://dx.doi.org/10.1016/j.clinbiochem.2012.03.021

Kunert-Keil, C., Botzenhart, U., Gedrange, T., & Gredes, T. (2014). Interrelationship between bone substitution materials and skeletal muscle tissue. *Annals of Anatomy*, *199*, 73–78. https://doi.org/10.1016/j.aanat.2014.07.008

Lange, J., Sapozhnikova, A., Lu, C., Hu, D., Li, X., Miclau, T., & Marcucio, R. S. (2010). Action of IL-1β during fracture healing. *Journal of Orthopaedic Research : Official Publication of the Orthopaedic Research Society*, *28*(6), 778–784. https://doi.org/10.1002/jor.21061

Langenbach, F., & Handschel, J. (2013). Effects of dexamethasone, ascorbic acid and β-glycerophosphate on the osteogenic differentiation of stem cells in vitro. *Stem Cell Research {&} Therapy*. https://doi.org/10.1186/scrt328

Lee, J.-W., Han, H.-S., Han, K.-J., Park, J., Jeon, H., Ok, M.-R., … Mantovani, D. (2016). Long-term clinical study and multiscale analysis of in vivo biodegradation mechanism of Mg alloy. *Proceedings of the National Academy of Sciences of the United States of America*, *113*(3), 716–721. https://doi.org/10.1073/pnas.1518238113

Lee, Y.-M., Fujikado, N., Manaka, H., Yasuda, H., & Iwakura, Y. (2010). IL-1 plays an important role in the bone metabolism under physiological conditions. *International Immunology*, *22*(10), 805–816. Retrieved from http://dx.doi.org/10.1093/intimm/dxq431

Leitinger, B., McDowall, A., Stanley, P., & Hogg, N. (2000). The regulation of integrin function

by Ca(2+). *Biochimica et Biophysica Acta*, *1498*(2–3), 91–98.

Li, B., Han, Y., & Qi, K. (2014). Formation mechanism, degradation behavior, and cytocompatibility of a nanorod-shaped HA and pore-sealed MgO bilayer coating on magnesium. *ACS Applied Materials & Interfaces*, *6*(20), 18258–18274. https://doi.org/10.1021/am505437e

Li, R. W., Kirkland, N. T., Truong, J., Wang, J., Smith, P. N., Birbilis, N., & Nisbet, D. R. (2014). The influence of biodegradable magnesium alloys on the osteogenic differentiation of human mesenchymal stem cells. *Journal of Biomedical Materials Research - Part A*, *102*(12), 4346–4357. https://doi.org/10.1002/jbm.a.35111

Li, Z., Gu, X., Lou, S., & Zheng, Y. (2008). The development of binary Mg-Ca alloys for use as biodegradable materials within bone. *Biomaterials*, *29*(10), 1329–1344. https://doi.org/10.1016/j.biomaterials.2007.12.021

Liu, C., Fu, X., Pan, H., Wan, P., Wang, L., Tan, L., … Chu, P. K. (2016). Biodegradable Mg-Cu alloys with enhanced osteogenesis, angiogenesis, and long-lasting antibacterial effects. *Scientific Reports*, *6*(May), 27374. https://doi.org/10.1038/srep27374

Lu, W., Chen, Z., Huang, P., & Yan, B. (2012). Microstructure, corrosion resistance and biocompatibility of biomimetic HA-based Ca-P coatings on ZK60 magnesium alloy. *International Journal of Electrochemical Science*, *7*(12), 12668–12679.

Marsell, R., & Einhorn, T. A. (2011). The biology of fracture healing. *Injury*, *42*(6), 551–555. https://doi.org/10.1016/j.injury.2011.03.031 [doi]

Marieb, E.N., (2004) Bone and Skeletal tissues part A. Human anatomy and physiology, 6th edn.Pearson Education, New York, publishing as Benjamin Cummings

Mehta, M., Schmidt-Bleek, K., Duda, G. N., & Mooney, D. J. (2012). Biomaterial delivery of morphogens to mimic the natural healing cascade in bone. *Targeted Delivery of*

Therapeutics to Bone and Connective Tissues, *64*(12), 1257–1276. https://doi.org/http://dx.doi.org/10.1016/j.addr.2012.05.006

Miyamoto, T., Ohneda, O., Arai, F., Iwamoto, K., Okada, S., Takagi, K., … Suda, T. (2001). Bifurcation of osteoclasts and dendritic cells from common progenitors. *Blood*, *98*(8), 2544–2554. https://doi.org/10.1182/blood.V98.8.2544

Mizushima, N., & Komatsu, M. (2011). Autophagy: Renovation of cells and tissues. *Cell*, *147*(4), 728–741. https://doi.org/10.1016/j.cell.2011.10.026

Mondal Roy, S., & Sarkar, M. (2011a). Membrane fusion induced by small molecules and ions. *Journal of Lipids*, *2011*, 528784. https://doi.org/10.1155/2011/528784

Mondal Roy, S., & Sarkar, M. (2011b). Membrane fusion induced by small molecules and ions. *Journal of Lipids*, *2011*, 528784. https://doi.org/10.1155/2011/528784

Murrow, L., & Debnath, J. (2013). Autophagy As A Stress Response And Quality Control Mechanism—Implications for Cell Injury and Human Disease. *Annual Review of Pathology*, (2), 105–137. https://doi.org/10.1146/annurev-pathol-020712-163918.Autophagy

Naddaf Dezfuli, S., Huan, Z., Mol, J. M. C., Leeflang, M. A., Chang, J., & Zhou, J. (2014). Influence of HEPES buffer on the local pH and formation of surface layer during in vitro degradation tests of magnesium in DMEM. *Progress in Natural Science: Materials International*, *24*(5), 531–538. https://doi.org/10.1016/j.pnsc.2014.08.009

Nalla, R. K., Stolken, J. S., Kinney, J. H., & Ritchie, R. O. (2005). Fracture in human cortical bone: local fracture criteria and toughening mechanisms. *Journal of Biomechanics*, *38*(7), 1517–1525. https://doi.org/10.1016/j.jbiomech.2004.07.010

Newman, P., Minett, A., Ellis-Behnke, R., & Zreiqat, H. (2013). Carbon nanotubes: Their potential and pitfalls for bone tissue regeneration and engineering. *Nanomedicine:*

Nanotechnology, Biology, and Medicine, *9*(8), 1139–1158. https://doi.org/10.1016/j.nano.2013.06.001

Nguyen, T. Y., Liew, C. G., & Liu, H. (2013). An in vitro mechanism study on the proliferation and pluripotency of human embryonic stems cells in response to magnesium degradation. *PloS One*, *8*(10), e76547. https://doi.org/10.1371/journal.pone.0076547; 10.1371/journal.pone.0076547

Orbay, H., Tobita, M., & Mizuno, H. (2012). Mesenchymal stem cells isolated from adipose and other tissues: Basic biological properties and clinical applications. *Stem Cells International*, *2012*. https://doi.org/10.1155/2012/461718

Orimo, H. (2010). The mechanism of mineralization and the role of alkaline phosphatase in health and disease. *Journal of Nippon Medical School = Nippon Ika Daigaku Zasshi*, *77*(1), 4–12.

Ortega, N., Behonick, D. J., & Werb, Z. (2004). Matrix remodeling during endochondral ossification. *Trends in Cell Biology*, *14*(2), 86–93. https://doi.org/10.1016/j.tcb.2003.12.003

Overgaard, S., Bromose, U., Lind, M., Bünger, C., & Søballe, K. (1999). The influence of crystallinity of the hydroxyapatite coating on the fixation of implants. Mechanical and histomorphometric results. *The Journal of Bone and Joint Surgery. British Volume*, *81*(4), 725–731. https://doi.org/10.1302/0301-620X.81B4.9282

Patti, A., Gennari, L., Merlotti, D., Dotta, F., & Nuti, R. (2013). Endocrine actions of osteocalcin. *International Journal of Endocrinology*, *2013*. https://doi.org/10.1155/2013/846480

Persaud-Sharma, D., & McGoron, A. (2012). Biodegradable Magnesium Alloys: A Review of Material Development and Applications. *Journal of Biomimetics, Biomaterials, and*

Tissue Engineering, *12*, 25–39. https://doi.org/10.4028/www.scientific.net/JBBTE.12.25

Pham, Q. P., Kurtis Kasper, F., Scott Baggett, L., Raphael, R. M., Jansen, J. A., & Mikos, A. G. (2008). The influence of an in vitro generated bone-like extracellular matrix on osteoblastic gene expression of marrow stromal cells. *Biomaterials*, *29*(18), 2729–2739. https://doi.org/10.1016/j.biomaterials.2008.02.025

Rao, R. R., & Stegemann, J. P. (2013). Cell-based approaches to the engineering of vascularized bone tissue. *Cytotherapy*, *15*(11), 1309–1322. https://doi.org/10.1016/j.jcyt.2013.06.005

Refai, A. K., Textor, M., Brunette, D. M., & Waterfield, J. D. (2004). Effect of titanium surface topography on macrophage activation and secretion of proinflammatory cytokines and chemokines. *Journal of Biomedical Materials Research A*, *70*, 194–205. https://doi.org/10.1002/jbm.a.30075

Rho, J.-Y., Kuhn-Spearing, L., & Zioupos, P. (1998). Mechanical properties and the hierarchical structure of bone. *Medical Engineering & Physics*, *20*(2), 92–102. https://doi.org/http://dx.doi.org/10.1016/S1350-4533(98)00007-1

Ritchie, R. O. (2011). The conflicts between strength and toughness. *Nat Mater*, *10*(11), 817–822. Retrieved from http://dx.doi.org/10.1038/nmat3115

Ritchie, R. O., Buehler, M. J., & Hansma, P. (2009). Plasticity and toughness in bone. *Physics Today*, *62*(6), 41–47. https://doi.org/10.1063/1.3156332

Romani, A. M., & Scarpa, A. (2000). Regulation of cellular magnesium. *Frontiers in Bioscience : A Journal and Virtual Library*, *5*, D720-34.

Rubin, A. H., Terasaki, M., & Sanui, H. (1979). Major intracellular cations and growth control: correspondence among magnesium content, protein synthesis, and the onset of DNA synthesis in BALB/c3T3 cells. *Proceedings of the National Academy of Sciences of the*

United States of America, *76*(8), 3917–3921.

Rubin, C., & Rubin, J. (2006). Biomechanics and Mechanobiology of Bone. *Primer on the Metabolic Bone Diseases and Disorders of Mineral Metabolism*, 36–42. Retrieved from http://www.cber.udel.edu/oldsite/OA JCpapers/Rubin - Biomechanics and Mechanobiology of Bone.pdf

Rubin, H. (2005). The membrane, magnesium, mitosis (MMM) model of cell proliferation control. *Magnesium Research*, *18*(4), 268–274.

Ruwin, P. (2013). EM Sample Preparation. *Leica Microsystems*, 3–16. https://doi.org/10.1002/9780471980582.ch14

Saris, N.-E. L., Mervaala, E., Karppanen, H., Khawaja, J. A., & Lewenstam, A. (2000). Magnesium: An update on physiological, clinical and analytical aspects. *Clinica Chimica Acta*, *294*(1–2), 1–26. https://doi.org/http://dx.doi.org/10.1016/S0009-8981(99)00258-2

Schindeler, A., McDonald, M. M., Bokko, P., & Little, D. G. (2008). Bone remodeling during fracture repair: The cellular picture. *Bone Remodelling*, *19*(5), 459–466. https://doi.org/http://dx.doi.org/10.1016/j.semcdb.2008.07.004

Schwander, M., Leu, M., Stumm, M., Dorchies, O. M., Ruegg, U. T., Schittny, J., & Muller, U. (2003). Beta1 integrins regulate myoblast fusion and sarcomere assembly. *Developmental Cell*, *4*(5), 673–685.

Scully, J. R., Gebert, A., & Payer, J. H. (2007). Corrosion and related mechanical properties of bulk metallic glasses. *Journal of Materials Research*, *22*(2), 302–313.

Sen, M. K., & Miclau, T. (2007). Autologous iliac crest bone graft: Should it still be the gold standard for treating nonunions? *Injury*, *38*(SUPPL. 1), 2–7. https://doi.org/10.1016/j.injury.2007.02.012

Serre, C. M., Papillard, M., Chavassieux, P., Voegel, J. C., & Boivin, G. (1998). Influence of magnesium substitution on a collagen?apatite biomaterial on the production of a calcifying matrix by human osteoblasts. *Journal of Biomedical Materials Research*, *42*(4), 626–633. https://doi.org/10.1002/(SICI)1097-4636(19981215)42:4<626::AID-JBM20>3.0.CO;2-S

Shapiro, F. (2008). Bone development and its relation to fracture repair. The role of mesenchymal osteoblasts and surface osteoblasts. *European Cells & Materials*, *15*, 53–76. https://doi.org/vol015a05 [pii]

Shih, Y.-R. V, Hwang, Y., Phadke, A., Kang, H., Hwang, N. S., Caro, E. J., … Varghese, S. (2014). Calcium phosphate-bearing matrices induce osteogenic differentiation of stem cells through adenosine signaling. *Proceedings of the National Academy of Sciences of the United States of America*, *111*(3), 990–5. https://doi.org/10.1073/pnas.1321717111

Song, G., & Atrens, A. (2003). Understanding Magnesium Corrosion?A Framework for Improved Alloy Performance. *Advanced Engineering Materials*, *5*(12), 837–858. https://doi.org/10.1002/adem.200310405

Song, G. L., & Atrens, A. (1999a). Corrosion Mechanisms of Magnesium Alloys. *Advanced Engineering Materials*, *1*(1), 11–33. https://doi.org/10.1002/(SICI)1527-2648(199909)1:1<11::AID-ADEM11>3.0.CO;2-N

Song, G. L., & Atrens, A. (1999b). Corrosion Mechanisms of Magnesium Alloys. *Advanced Engineering Materials*, *1*(1), 11–33. https://doi.org/10.1002/(SICI)1527-2648(199909)1:1<11::AID-ADEM11>3.0.CO;2-N

Tagliaferri, C., Wittrant, Y., Davicco, M. J., Walrand, S., & Coxam, V. (2015). Muscle and bone, two interconnected tissues. *Ageing Research Reviews*, *21*, 55–70. https://doi.org/10.1016/j.arr.2015.03.002

Teitelbaum, S. L., Abu-Amer, Y., & Ross, F. P. (1995). Molecular mechanisms of bone resorption. *Journal of Cellular Biochemistry*, *59*(1), 1–10. https://doi.org/10.1002/jcb.240590102

Thibault, R. A., Scott Baggett, L., Mikos, A. G., & Kasper, F. K. (2010). Osteogenic differentiation of mesenchymal stem cells on pregenerated extracellular matrix scaffolds in the absence of osteogenic cell culture supplements. *Tissue Engineering. Part A*, *16*(2), 431–40. https://doi.org/10.1089/ten.TEA.2009.0583

Udagawa, N., Takahashi, N., Yasuda, H., Gillespie, M. T., Martin, T. J., & Higashio, K. (2014). Osteoprotegerin Produced by Osteoblasts Is an Important Regulator in Osteoclast Development and Function *. *Endocrinology*, *141*(9), 3478–3484.

Utting, J. C., Robins, S. P., Brandao-Burch, A., Orriss, I. R., Behar, J., & Arnett, T. R. (2006). Hypoxia inhibits the growth, differentiation and bone-forming capacity of rat osteoblasts. *Experimental Cell Research*, *312*(10), 1693–1702. https://doi.org/http://dx.doi.org/10.1016/j.yexcr.2006.02.007

Vaananen, H. K., & Horton, M. (1995). The osteoclast clear zone is a specialized cell-extracellular matrix adhesion structure. *Journal of Cell Science*, *108 (Pt 8*(Pt 8), 2729–2732.

Vignery, A. (2000). Osteoclasts and giant cells: macrophage–macrophage fusion mechanism: Current Status Review: Granulatomous Disease. *International Journal of Experimental Pathology*, *81*(5), 291–304. https://doi.org/10.1111/j.1365-2613.2000.00164.x

Vignery, A. (2005). Macrophage fusion: the making of osteoclasts and giant cells. *The Journal of Experimental Medicine*, *202*(3), 337–340. https://doi.org/10.1084/jem.20051123

von der Höh, N., von Rechenberg, B., Bormann, D., Lucas, A., & Meyer-Lindenberg, A. (2009). Influence of different surface machining treatments of resorbable magnesium

alloy implants on degradation ? EDX-analysis and histology results. *Materialwissenschaft Und Werkstofftechnik*, *40*(1–2), 88–93. https://doi.org/10.1002/mawe.200800378

Wacker, W. E., & Parisi, A. F. (1968). Magnesium metabolism. *The New England Journal of Medicine*, *278*(14), 772–6 concl. https://doi.org/10.1056/NEJM196804042781406 [doi]

Wan, Y., Xiong, G., Luo, H., He, F., Huang, Y., & Zhou, X. (2008). Preparation and characterization of a new biomedical magnesium-calcium alloy. *Materials and Design*, *29*(10), 2034–2037. https://doi.org/10.1016/j.matdes.2008.04.017

Wang, B., Gao, J., Wang, L., Zhu, S., & Guan, S. (2012). Biocorrosion of coated Mg-Zn-Ca alloy under constant compressive stress close to that of human tibia. *Materials Letters*, *70*, 174–176. https://doi.org/10.1016/j.matlet.2011.12.009

Wang, J., Witte, F., Zhang, Y., Xu, J., Ruan, Y. C., Yu, M. K., … Wise, H. (2016). Implant-derived magnesium induces local neuronal production of CGRP to improve bone- fracture healing in rats Implant-derived magnesium induces local neuronal production of CGRP to improve bone-fracture healing in rats, (October). https://doi.org/10.1038/nm.4162

Wang, L., & Nancollas, G. H. (2009). NIH Public Access, *108*(11), 4628–4669. https://doi.org/10.1021/cr0782574.Calcium

Weatherholt, A. M., Fuchs, R. K., & Warden, S. J. (2012). Specialized connective tissue: Bone, the structural framework of the upper extremity. *Journal of Hand Therapy*, *25*(2), 123–132. https://doi.org/10.1016/j.jht.2011.08.003

William Axelrad, T., Kakar, S., & Einhorn, T. A. (2007). New technologies for the enhancement of skeletal repair. *Scientific Basis of Fracture Healing: An Update*, *38*(1, Supplement), S49–S62. https://doi.org/10.1016/j.injury.2007.02.010

Willumeit, R., Fischer, J., Feyerabend, F., Hort, N., Bismayer, U., Heidrich, S., & Mihailova, B.

(2011a). Chemical surface alteration of biodegradable magnesium exposed to corrosion media. *Acta Biomaterialia*, *7*(6), 2704–2715. https://doi.org/10.1016/j.actbio.2011.03.004

Willumeit, R., Fischer, J., Feyerabend, F., Hort, N., Bismayer, U., Heidrich, S., & Mihailova, B. (2011b). Chemical surface alteration of biodegradable magnesium exposed to corrosion media. *Acta Biomaterialia*, *7*(6), 2704–2715. https://doi.org/10.1016/j.actbio.2011.03.004

Windhagen, H., Radtke, K., Weizbauer, A., Diekmann, J., Noll, Y., Kreimeyer, U., … Waizy, H. (2013). Biodegradable magnesium-based screw clinically equivalent to titanium screw in hallux valgus surgery: short term results of the first prospective, randomized, controlled clinical pilot study. *BioMedical Engineering OnLine*, *12*(1), 62. https://doi.org/10.1186/1475-925X-12-62

Witecka, A., Bogucka, A., Yamamoto, A., Máthis, K., Krajňák, T., Jaroszewicz, J., & Święszkowski, W. (2016). In vitro degradation of ZM21 magnesium alloy in simulated body fluids. *Materials Science and Engineering C*, *65*, 59–69. https://doi.org/10.1016/j.msec.2016.04.019

Witte, F., Kaese, V., Haferkamp, H., Switzer, E., Meyer-Lindenberg, A., Wirth, C. J., & Windhagen, H. (2005). In vivo corrosion of four magnesium alloys and the associated bone response. *Biomaterials*, *26*(17), 3557–3563. https://doi.org/10.1016/j.biomaterials.2004.09.049

Witte, F., Ulrich, H., Rudert, M., & Willbold, E. (2007). Biodegradable magnesium scaffolds: Part 1: appropriate inflammatory response. *Journal of Biomedical Materials Research. Part A*, *81*(3), 748–756. https://doi.org/10.1002/jbm.a.31170

Woolf, A. D., & Pfleger, B. (2003). Burden of major musculoskeletal conditions. *Bulletin of*

the World Health Organization, *81*(9), 646–656. https://doi.org/S0042-96862003000900007 [pii]

Wu, L., Luthringer, B. J. C., Feyerabend, F., Schilling, A. F., & Willumeit, R. (2014). Effects of extracellular magnesium on the differentiation and function of human osteoclasts. *Acta Biomaterialia*, *10*(6), 2843–2854. https://doi.org/10.1016/j.actbio.2014.02.010

Yamada, S., Heymann, D., Bouler, J. M., & Daculsi, G. (1997). Osteoclastic resorption of calcium phosphate ceramics with different hydroxyapatite/beta-tricalcium phosphate ratios. *Biomaterials*, *18*(15), 1037–1041.

Yamamoto, A., & Hiromoto, S. (2009). Effect of inorganic salts, amino acids and proteins on the degradation of pure magnesium in vitro. *Materials Science and Engineering C*, *29*(5), 1559–1568. https://doi.org/10.1016/j.msec.2008.12.015

Yang, C., Yuan, G., Zhang, J., Tang, Z., Zhang, X., & Dai, K. (2010). Effects of magnesium alloys extracts on adult human bone marrow-derived stromal cell viability and osteogenic differentiation. *Biomedical Materials (Bristol, England)*, *5*(4), 45005. https://doi.org/10.1088/1748-6041/5/4/045005

Yavropoulou, M. P., & Yovos, J. G. (2008). Osteoclastogenesis--current knowledge and future perspectives. *Journal of Musculoskeletal & Neuronal Interactions*, *8*(3), 204–216.

Yeni, Y. N., & Norman, T. L. (2000). Calculation of porosity and osteonal cement line effects on the effective fracture toughness of cortical bone in longitudinal crack growth. *Journal of Biomedical Materials Research*, *51*(3), 504–509.

Yoshizawa, S., Brown, A., Barchowsky, A., & Sfeir, C. (2014). Magnesium ion stimulation of bone marrow stromal cells enhances osteogenic activity, simulating the effect of magnesium alloy degradation. *Acta Biomaterialia*, *10*(6), 2834–2842. https://doi.org/10.1016/j.actbio.2014.02.002

Yuan, F.-L., Xu, M.-H., Li, X., Xinlong, H., Fang, W., & Dong, J. (2016). The roles of acidosis in osteoclast biology. *Frontiers in Physiology*, *7*(JUN), 1–8. https://doi.org/10.3389/fphys.2016.00222

Zberg, B., Uggowitzer, P. J., & Löffler, J. F. (2009). MgZnCa glasses without clinically observable hydrogen evolution for biodegradable implants. *Nature Materials*, *8*(11), 887–891. https://doi.org/10.1038/nmat2542

Zhai, Z., Qu, X., Li, H., Yang, K., Wan, P., Tan, L., … Dai, K. (2014). The effect of metallic magnesium degradation products on osteoclast-induced osteolysis and attenuation of NF-kappaB and NFATc1 signaling. *Biomaterials*, *35*(24), 6299–6310. https://doi.org/10.1016/j.biomaterials.2014.04.044

Zhang, J., Kong, N., Shi, Y., Niu, J., Mao, L., Li, H., … Yuan, G. (2014). Influence of proteins and cells on in vitro corrosion of Mg-Nd-Zn-Zr alloy. *Corrosion Science*, *85*, 477–481. https://doi.org/10.1016/j.corsci.2014.04.020

Zhang, J., Niu, X., Qiu, X., Liu, K., Nan, C., Tang, D., & Meng, J. (2009). Effect of yttrium-rich misch metal on the microstructures, mechanical properties and corrosion behavior of die cast AZ91 alloy. *Journal of Alloys and Compounds*, *471*(1–2), 322–330. https://doi.org/10.1016/j.jallcom.2008.03.089

Zhang, S., Zhang, X., Zhao, C., Li, J., Song, Y., Xie, C., … Bian, Y. (2010). Research on an Mg-Zn alloy as a degradable biomaterial. *Acta Biomaterialia*, *6*(2), 626–640. https://doi.org/10.1016/j.actbio.2009.06.028; 10.1016/j.actbio.2009.06.028

Zhao, D., Huang, S., Lu, F., Wang, B., Yang, L., Qin, L., … Li, J. (2016). Vascularized bone grafting fixed by biodegradable magnesium screw for treating osteonecrosis of the femoral head. *Biomaterials*, *81*, 84–92. https://doi.org/10.1016/j.biomaterials.2015.11.038

Zhao, D., Witte, F., Lu, F., Wang, J., Li, J., & Qin, L. (2017). Current status on clinical applications of magnesium-based orthopaedic implants: A review from clinical translational perspective. *Biomaterials*, *112*, 287–302. https://doi.org/10.1016/j.biomaterials.2016.10.017

Zhao, M., Li, H., Liu, X., Wei, J., Ji, J., Yang, S., … Wei, S. (2016). Response of Human Osteoblast to n-HA/PEEK—Quantitative Proteomic Study of Bio-effects of Nano-Hydroxyapatite Composite. *Scientific Reports*, *6*(February), 22832. https://doi.org/10.1038/srep22832\rhttp://www.nature.com/articles/srep22832#supplementary-information

Ziats, N. P., Miller, K. M., & Anderson, J. M. (1988). In vitro and in vivo interactions of cells with biomaterials. *Biomaterials*, *9*(1), 5–13.

Zreiqat, H., Howlett, C. R., Zannettino, A., Evans, P., Schulze-Tanzil, G., Knabe, C., & Shakibaei, M. (2002). Mechanisms of magnesium-stimulated adhesion of osteoblastic cells to commonly used orthopaedic implants. *Journal of Biomedical Materials Research*, *62*(2), 175–184. https://doi.org/10.1002/jbm.10270